FUNCTIONAL STUDIES OF PURIFIED RECOMBINANT BK_{CA} CHANNELS AND THE MECHANOSENSITIVE CHANNEL OF HIGH CONDUCTANCE (MSCL) RECONSTITUTED IN BILAYER LIPID MEMBRANES TETHERED TO A MICROELECTRODE ARRAY DEVICE

By

GEORGE ODHIAMBO OKEYO

A DISSERTATION PRESENTED TO THE GRADUATE SCHOOL
OF THE UNIVERSITY OF FLORIDA IN PARTIAL FULFILLMENT
OF THE REQUIREMENTS FOR THE DEGREE OF
DOCTOR OF PHILOSOPHY

UNIVERSITY OF FLORIDA

2009

To my Parents:

Zephaniah Jura Okeyo
and
Peres Atieno Jura

ACKNOWLEDGMENTS

I would first like to extend my utmost appreciation to Dr. Gail Fanucci for taking over the responsibility of being my advisor after the departure of Dr. Randolph Duran from the University of Florida. Additionally, her support, encouragement and technical advice over the years cannot go unnoticed, and for that I will always be grateful. I also thank Dr. Duran for taking me into his group when I joined the University of Florida and for his support while there.

Special thanks also go to Dr. Peter Anderson for his commitment, advice and the special interest he took to make sure that I succeeded in all my work. I thank him too for facilitating all those trips to the Whitney Laboratory for Marine Bioscience and his technical advice, which I always asked for in short notice, but received promptly, courtesy of his sacrificed time. I thank Dr. Joanna Long for her encouragement and for letting me in her laboratory to learn from Dr. Chris Williams whom I also thank. I appreciate the support of the rest of my committee members; Dr. Nicole Horenstein for her encouragement and Dr. Benjamin Smith for making all challenges seem easily manageable.

My experiences in the Chemistry department over the years were enriched by past members of the Duran group, Dr. Martin Andersson, Dr. Maria Stjerndahl, Dr. Henk Keizer, Dr. Firouzeh Sabri, Jorge Chavez, Eric Greeley, Brian Dorvel and all the others that I interacted with, whom I thank for their friendship and support. I'd like to thank those at the Whitney Laboratory who made my life easier, especially Becky Price and Dr. Christelle Brouchard. I thank Mandy Blackburn and all members of the Fanucci research group who offered constructive criticism and support.

Finally, I would like to thank my family for their love and support. I thank my wife Janetricks Chebukati for her unconditional love, the scientific discussions and for putting up with me. I thank my daughters Lavender and Subi for brightening my life. I also thank my parents and siblings who helped to shape me into the man I am today.

Above all else, I thank God through whom I have all that I have and in whom all things are possible. Glory be to God!

TABLE OF CONTENTS

page

LIST OF TABLES

LIST OF FIGURES

LIST OF ABBREVIATIONS

AFM	Atomic force microscopy
BK_{Ca}	High-conductance, calcium-activated potassium (maxi-K) channel
BLM	Bilayer lipid membranes
ChTX	Charybdotoxin
DLS	Dynamic light scattering
DPhPE	1, 2-diphytanoyl-sn-glycero-3-phosphoethanolamine
DPhPC	1, 2-diphytanoyl-sn-glycero-3-phosphocholine
DPTL	2,3-di-*O*-phytanyl-s*n*-glycero-1-tetraethylene glycol-DL-α-lipoic acid ester
IbTX	Iberiotoxin
Kcps	Kilocounts per second
pS	Picosiemens
PE	Phosphatidylethanolamine
PC	Phosphatidylcholine
mRFP	Monomeric red fluorescence protein
PIPES	1,4-Piperazinebisethanesulfonic acid
OG	Octyl-β-glucoside
MLV	Large multilamellar vesicles
LUV	Large unilamellar vesicles
MEA	Microelectrode array
MOPS	3-morpholinopropanesulfonic acid
RCK	Regulator of potassium conductance
RT	Room temperature
Rpm	Revolutions per minute
SAM	Self-assembled monolayers

SDS-PAGE	Sodium dodecyl sulfate polyacrylamide gel electrophoresis
SUV	Small unilamellar vesicles
sBLM	Supported bilayer lipid membranes
tBLM	Tethered lipid bilayer membrane
TEA	Tetraethyammonium
TEM	Transmission electron microscopy
TEVC	Two-electrode voltage clamp

Abstract of Dissertation Presented to the Graduate School
of the University of Florida in Partial Fulfillment of the
Requirements for the Degree of Doctor of Philosophy

FUNCTIONAL STUDIES OF PURIFIED RECOMBINANT BK_{CA} CHANNELS AND THE MECHANOSENSITIVE CHANNEL OF HIGH CONDUCTANCE (MSCL) RECONSTITUTED IN BILAYER LIPID MEMBRANES TETHERED TO A MICROELECTRODE ARRAY DEVICE

By

George Odhiambo Okeyo

December 2009

Chair: Gail E. Fanucci
Major: Chemistry

The measurement of single-channel activity of the high conductance calcium-activated potassium (BK_{Ca}) channels incorporated in tethered bilayer lipid membranes is a major step towards the development of biosensors based on ion channels. Recombinant BK_{Ca} channels were expressed with hexa-histidine fusion tags and isolated from *Xenopus laevis* oocyte membranes by detergent solubilization. The histidine tag was included to facilitate purification of the desired channels by immobilized metal-ion affinity chromatography, which provided a convenient purification protocol that yielded high purity BK_{Ca} channels which in turn were successfully reconstituted in vesicles consisting of phytanoyl phospholipids.

Biophysical characterization of vesicular and solid-supported bilayer lipid membrane assemblies of two different phytanoyl lipids, 1,2-diphytanoyl-*sn*-glycero-3-phosphocholine (DPhPC) and 1,2-diphytanoyl-*sn*-glycero-3-phosphoethanolamine (DPhPE) were performed. These studies revealed the appropriate physical conditions and optimal lipid concentrations required to form stable membranes suitable for both reconstitution of proteins and for tethering on solid substrates to form electrically stable

membranes. Results showed that the most stable biomimetic model membranes were formed using a combination of DPhPC and DPhPE lipids in a 7:3 ratio; these were then interfaced to microelectrode array devices for incorporation of channels for functional studies. Formation of the tethered bilayer lipid membrane on a gold substrate and the successful incorporation of BK_{Ca} channels in this membrane system were verified with surface plasmon resonance-enhanced ellipsometry.

Functional studies of incorporated channels were performed using a modified patch clamp electrophysiology technique and single-channel events were recorded. Results indicate that the IMAC purified BK_{Ca} channels were functional and that their electrical properties in the tBLM system had similarities with channels investigated under conventional patch-clamp conditions. However, conductance levels were lower in the tBLM and channels in this membrane system exhibited slower gating kinetics. Pharmacological studies of tBLM incorporated BK_{Ca} channels showed that these channels were sensitive to tetraethylammonium compounds at micromolar concentrations, just like wild type channels investigated by patch clamp techniques.

The mechanosensitive channel of large conductance (MscL), a stretch-activated ion channel isolated from E. coli was also studied in this experimental set-up. This study represents the first documented report on the investigation of MscL in a supported bilayer membrane. Results obtained here demonstrate that the MscL channel can be activated by voltage and that the channel is gated in response to stress in the lipid membrane as opposed to pressure across it. Furthermore, these findings show the possibility of using MscL as a release valve for engineered membrane devices; one step closer to mimicking the true function of the living cell.

CHAPTER 1
INTRODUCTION TO ION CHANNELS AND BIOMIMETIC MODEL MEMBRANE SYSTEMS

Ion channels are integral membrane proteins that form aqueous pores in cell membranes through which selected ions and other small molecules can translocate from one side to the other. The permeation of ions across ion channels usually occurs very rapidly at nearly diffusion limited rates *ca*. 10^8 ions s^{-1} per channel.[1] According to electron microscopy and X-ray crystallography studies, typical aqueous pores within ion channels have lengths of approximately 3 nm and radii which vary along the pore length but which may be as low as 0.2 nm in places. Typically, channel pores have comparable dimensions to the sizes of transported molecules or ions.

Many types of cells from diverse organisms including bacteria, viruses, plants and animals have ion channels responsible for the regulation of numerous cellular and physiological functions. Ion channels regulate their physiological roles by switching between open and closed states to allow ion flow in a process of gating which can occur on a wide range of timescales through conformational changes of the channel interior. The gating action can be driven by allosteric modulation of conformation due to ligand binding, depolarizing membrane potentials and mechanical stimuli such as membrane tension, as happens with mechanosensitive channels. Mutations in ion channel genes result in alteration of gating properties, resulting in either excessive or diminished activity thereby causing a number of diseases referred to as channelopathies. Ion channels are therefore drug targets and are being studied for the development of therapeutic options for the correction of these disorders which include epilepsy, myotonia, arrhythmias and migraines.[2-4]

Most ion channels exhibit great selectivity for different ions and show a high level of recognition of specific compounds. For that reason, ion channels make ideal candidates as sensor elements in the rapidly growing field of biosensor development for chemical and biological analytes.[5-7] Nature has produced subfamilies of channels selective for each of the principal species of ions in living tissues: potassium, sodium, calcium and chloride ions. In each of these subfamilies, there are many differences in functional properties associated with the types of ions allowed through channels. These functional properties are voltage-dependence, gating kinetics and modulation by intracellular factors, for instance calmodulin and calcium.[8] Conductance is a signature functional property that varies between ion channels by at least two orders of magnitude, and it gives a measure of the current that can pass through a single open channel at a given membrane potential.[9]

Potassium Ion Channels

Potassium channels are responsible for a diversity of physiological processes in cells such as hormone secretion, cell volume regulation and electric impulse formation in electrically excitable cells. Because potassium channels are the only ion-selective cation channels that have an equilibrium potential near the typical cellular resting potential, they play a vital role in determining the resting potential of most cells.[10] The classification of potassium channels is broadly defined by transmembrane topology, as reflected in primary sequence: the six-transmembrane-helix voltage-gated (K_v) and the two-transmembrane-helix inward-rectifier (K_{ir}) subtypes.[11, 12] Fully assembled K^+ channels of the two transmembrane and six transmembrane architectures are formed by homo- or heterotetramers of principal subunits, often supplemented by auxiliary β-subunits. BK_{Ca} channels have an extra transmembrane domain, the S0 which leads to

an external NH_2 – terminus, therefore they possess the seven transmembrane architecture. A highly conserved segment is found between the two most carboxy-terminal transmembrane helices in all potassium channels, bearing the unique sequence of amino acids TMxTVGYG commonly referred to as the "K+ signature sequence".[13] A few variations in the signature sequence are known to exist as can be observed in Figure 1-1, which shows sequence alignments of several different ligand-gated and voltage-gated K^+ channels with the characteristic selectivity filter portion of the signature sequence highlighted.

```
hBK:    YLLMVTMSTVGYGDVYAKTTLGRLFMVFFILGGLAMFASYVPEIIELIGN
Shaker:WWAVVTMTTVGYGDMTPVGFWGKIVGSLCVVAGVLTIALPVPVIVSNFNY
KcsA:   WWSVETATTVGYGDLYPVTLWGRLVAVVVMVAGITSFGLVTAALATWFVG
MthK:   YWTFVTIATVGYGDYSPSTPLGMYFTVTLIVLGIGTFAVAVERLLEFLIN
Dradio:YWAVVTVTTVGYGDISPKTGLGKFIATLAMLSGYAIIAVPTGIVTVGLQQ
Ecoli: YFSIETMSTVGYGDIVPVSESARLFTISVIISGITVFATSMTSIFGPLIR
hDRK1: WWATITMTTVGYGDIYPKTLLGKIVGGLCCIAGVLVIALPIPIIVNNFSE
hGIRK2:LFSIETETTIGYGYRVITDKCPEGIILLLIQSVLGSIVNAFMVGCMFVKI
hIRK1:  LFSIETQTTIGYGFRCVTDECPIAVFMVVFQSIVGCIIDAFIIGAVMAKM
hSK3:   WLISITFLSIGYGDMVPHTYCGKGVCLLTGIMGAGCTALVVAVVARKLEL
hERG2:  YFTFSSLTSVGFGNVSPNTNSEKIFSICVMLIGSLMYASIFGNVSAIIQR
```

Figure 1-1. Sequence alignment showing the conserved region known as the selectivity filter in members of the potassium channel family.

Numerous positively charged amino acid residues are found in a conserved region on the fourth transmembrane segment of Kv type channels.[14] This region undergoes an outward conformational movement which is energetically favored by depolarizing voltage, and constitutes the central event which initiates channel opening. Potassium channels open to allow the rapid permeation of K^+ into cells while rejecting the biologically abundant potential competitors Ca^{2+}, Na^+ and Mg^{2+}. The exceptionally high ion selectivity and the high throughput rate of K^+ channels is made possible by a precise coordination of dehydrated K^+ by the protein and multiple ion occupancy within the

permeation pathway of the channel.[15] The mechanism of ion selectivity depends on the arrangement of backbone carbonyl groups of the "K^+ signature sequence" of the channel in which a dehydrated K^+ exactly fits (Figure 1-2). The smaller Na^+ ion would fit so loosely in this region; therefore it energetically favors being in aqueous solution.[16]

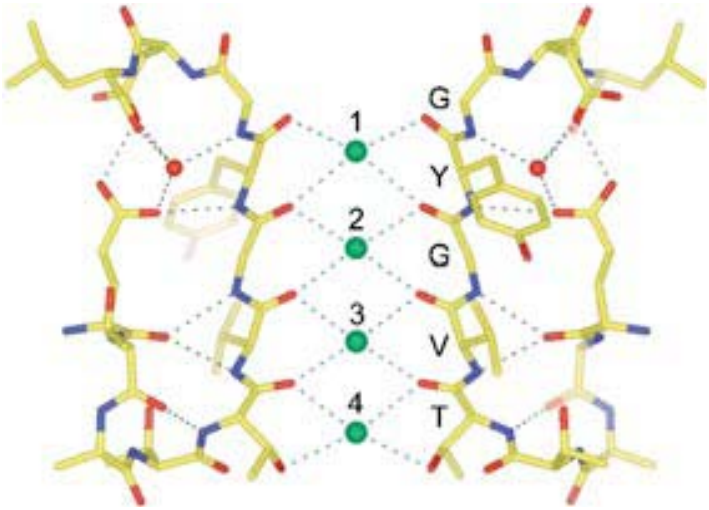

Figure 1-2. The structure of the K+ selectivity filter and single letter amino acid code of the signature sequence.

Calcium-Activated Potassium Channels

Calcium-activated potassium channels are a large family of potassium channels responsible for translocation of K^+ across membranes in response to the binding of Ca^{2+} at intracellular receptor sites. They are gated by increase in cytoplasmic calcium concentrations which occurs largely in response to calcium influx via voltage-gated calcium channels that open during action potentials.[17] Calcium-activated potassium channels are classified into three broad families based on their biophysical and pharmacological properties. These families are the large or high conductance calcium-activated potassium (BK_{Ca}) channels,[18] small conductance calcium-activated potassium (SK) channels[19, 20] and the intermediate conductance calcium-activated potassium (IK) channels.[21, 22] Table 1-1 summarizes the properties of calcium-activated channels.

Table 1-1. Summary of functional characteristics defining vertebrate calcium-activated potassium channels

Property	Channel Type		
	BK_{Ca}	IK_{Ca}	SK_{Ca}
Intracellular Ca^{2+} needed for activation	1-10 nM (at -50 mV)	50-900 nM	50-900 nM
Voltage dependence	e-fold/ 9 to 15 mV	None	None
Single-channel conductance	90-250 pS	20-80 pS	4-20 pS
Blockers	Charybdotoxin (nM) Iberiotoxin (nM) TEA (nM)	α-KTx (nM) Clotrimazole (nM)	Apamin (nM) Scyllatoxin (nM)
Mammalian clones	slo1 (slo2,3)	IK1/SK4	SK1,2,3

Functional properties of the three subtypes of calcium-activated ion channels differ markedly. BK_{Ca} channels are highly selective for potassium ions, have single-channel conductances of 90 pS to 300 pS and require both calcium and membrane depolarization to initiate gating. SK channels on the other hand have a single-channel conductance of 2 to 20 pS and unlike BK_{Ca} channels, are voltage insensitive. The activity of SK channels following action potentials leads to much longer lasting currents than those mediated by BK_{Ca} channels, owing to their higher affinity for calcium at hyperpolarized membrane potentials. IK channels show conductances of 20 to 100 pS and are also voltage insensitive.[22] Other differences in functional properties between calcium-activated potassium channels are in their response to modulatory agents. Both IK and SK channels are unaffected by BK_{Ca} channel blockers isolated from scorpion toxins.[19] However, SK channels are potently blocked by the bee venom apamin, amongst other compounds.[20] IK channels are distinctly separable from BK and SK channels since they show no response to scorpion toxins or apamin. They are poorly

studied due to their sparse distribution in different cell types. Figure 1-3 illustrates the topology maps of BK and SK channels.

A

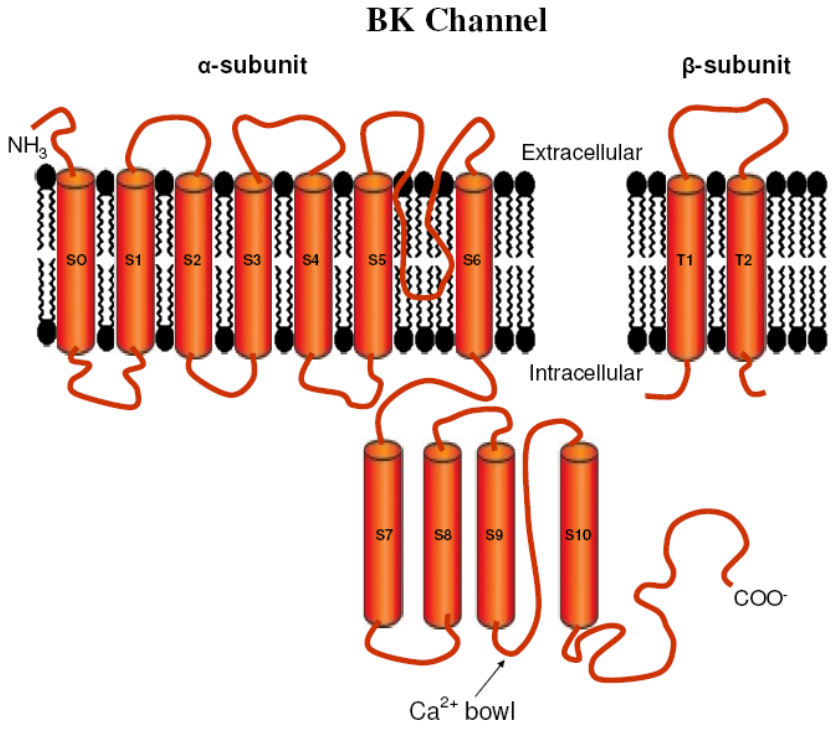

B

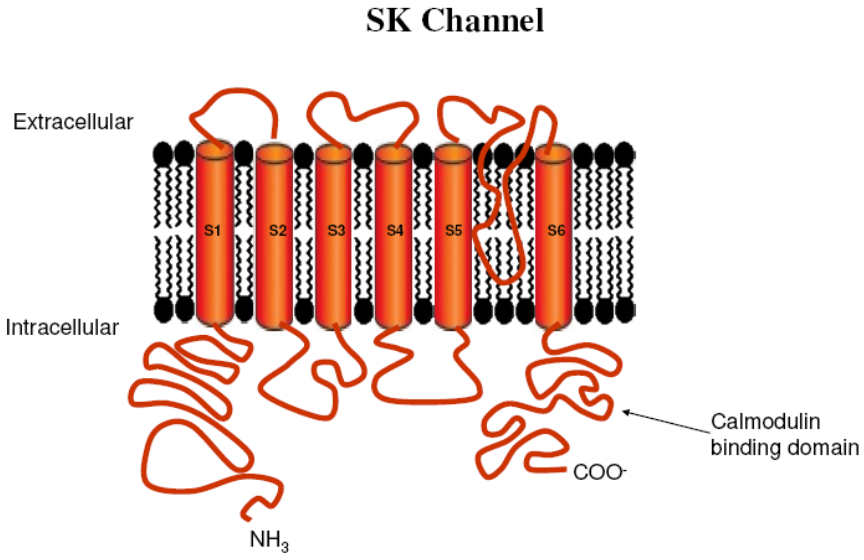

Figure 1-3. Topology maps of calcium-activated potassium channels showing the position of helices and locations of the N- and C-termini. A) High conductance calcium-activated potassium (BK) channel. B) Small conductance calcium-activated potassium (SK) channel.

High conductance calcium-activated potassium channels

High conductance calcium-activated potassium (BK_{Ca}) or maxi-K channels which are the main subjects of this study were the first calcium-activated channels to be identified. They are also called SLO family channels, a name derived from the conserved *slowpoke* gene that encodes this channel, which was first cloned in *Drosophila melanogaster.*[23, 24] Structurally, BK_{Ca} channels comprise a pore-forming tetrameric α domain made of seven putative transmembrane segments and a β domain comprising two α-helical transmembrane domains connected by a large glycosylated extracellular loop, with intracellular amino and carboxy termini.[25, 26] The α-and β-subunits are associated with each other noncovalently in the form of an octameric complex in a 1:1 stoichiometry.[27-29] BK_{Ca} channels have an extracellular N-terminus on the α-subunit, which distinguishes them from other potassium channels, and this comes as a result of the extra transmembrane segment they possess, relative to the other potassium channels.[26] They also have a large cytoplasmic C-terminal domain which controls different functional properties of the channel. In the C-terminal domain region, two regulators of potassium conductance (RCK) domains have been identified on each α subunit and these connect to the pore region by a short linker.[30, 31] The RCK domains have been proposed to form a “gating ring”, where calcium binding causes a conformational change that promotes channel opening by pulling the linker connecting the gating ring to the pore region.[32, 33]

BK_{Ca} channel modulation

BK_{Ca} channels are activated by both depolarizing membrane potentials as well as elevated concentrations of cytosolic calcium. The calcium dependence for the gating of these channels relies on membrane potential,[34] the Kd for calcium being in the

micromolar range at resting membrane potentials (~ -60 mV) but in the nanomolar range at depolarized potentials (+20 to +40 mV).[35] Interestingly, some BK_{Ca} channels can open in the absence of calcium and it appears that the effects of calcium and membrane potential are independent processes.[36] Depolarization causes a conformational change in the voltage sensor regions S0 through S4 perhaps involving a twisting outward motion of the positively charged S4 helix. The voltage sensitivity of the channel is conferred by acidic residues in the S2 and S3 segments, along with basic residues at every third position in the S4 segment.[37] Each of four voltage sensor movements is coupled to the opening of the conduction pathway, lined by the loop connecting the S5 and S6 regions, driving the concerted gating transition toward the open state. Likewise, Ca^{2+} binding causes conformational changes at the cytoplasmic Ca^{2+} sensors and these changes are coupled to the opening transition that is optimally driven forward when all voltage sensors and Ca^{2+} sensors are activated (Figure 1-4).[38]

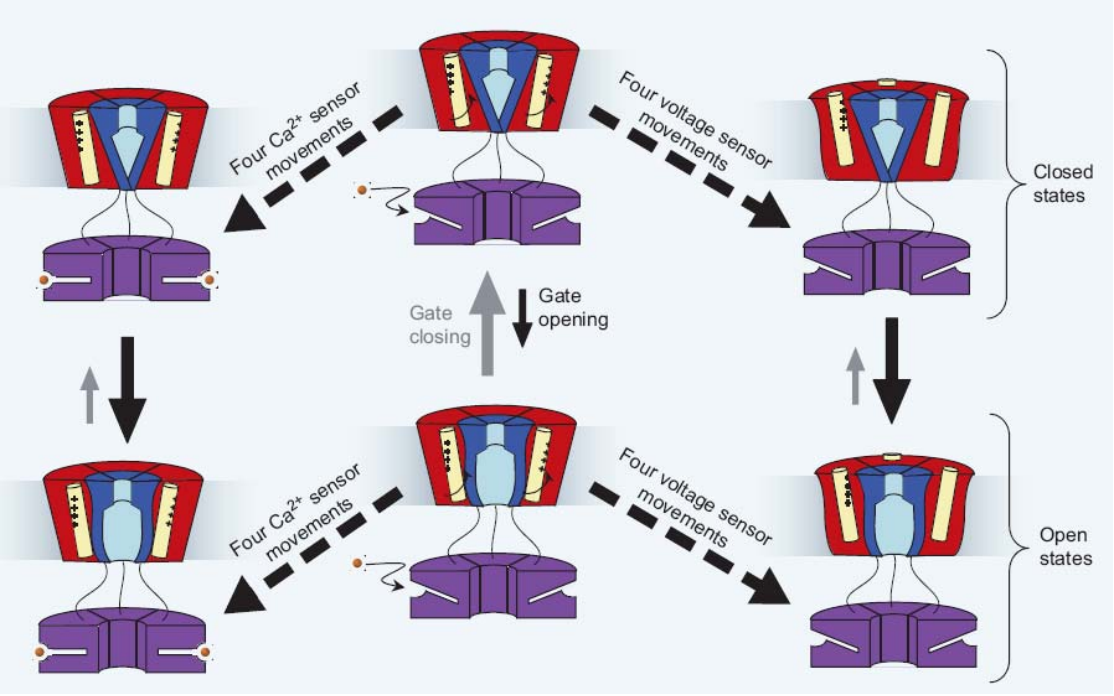

Figure 1-4. BK_{Ca} channel modulation by voltage and calcium. (Adopted from Ref. 38)

An understanding of the structural implications of the BK_{Ca} channel to modulation by voltage and bound calcium ions would explain the observations made during functional studies of C-terminally deleted recombinant channels in this study. The C-terminal region of the BK_{Ca} channel contains multiple regulatory sites which include the bulky region in the transmembrane domain referred to as the "Ca^{2+} bowl" located just before the S10 segment, implicated in Ca^{2+} regulation.[39] Changes in Ca^{2+} concentration that regulate channel opening span a range of 0.5 mM to 50 mM, the wide range explained by the existence of multiple independent calcium binding sites. Advances in understanding the regulation of BK_{Ca} channels reveal that both the calcium bowl located within the S9-S10 peptide, and the RCK domain around the S7-S8 segments play a role in the regulation of channel opening by Ca^{2+}.[40, 41] A study comparing the Ca^{2+} sensitivity of wild-type BK_{Ca} currents arising from α-subunits to that arising from α-subunits with a mutation abolishing the function of the Ca^{2+} bowl, show currents from the mutant channel still exhibiting substantial regulation by Ca^{2+}, albeit with less channel activation at low [Ca^{2+}] relative to wild-type currents.[42] Piskorowski and Aldrich performed studies documenting Ca^{2+} dependent gating of BK_{Ca} channels with completely truncated C-termini, suggesting the existence of an additional undefined Ca^{2+}-activation site different from that located in the RCK domain and the one within the calcium bowl.[43]

Besides the conventional modulatory mechanisms of depolarizing membrane potentials and elevated concentrations of intracellular calcium, BK_{Ca} channels can be modulated by post-translational modifications. Glycosylation is known to affect both cell-surface expression and channel activity of BK_{Ca} channels.[28, 44, 45] N-linked glycosylation sites on the β-subunits of these channels provide a means by which modifications can

be done and these influence modulation of channel activity as a result of the β-subunit regulatory effect or an alteration of the interaction between the α- and β-subunits.[45] Other known post-translational modifications that affect channel modulations include phosphorylation and oxidative reduction.[46-48] The effects of post-translational modifications on channel function arising from using oocytes as an expression system were observed during the study documented in this dissertation.

Pharmacology

The well understood signature responses of BK_{Ca} channels to agonists (activators) and antagonists (blockers) can provide useful information that makes these channels ideal for development of ion channel based biosensors, which is the long term goal of this project. Located between the S5 and S6 segments of the α-subunit is the pore loop (P-loop) which is part of the pore-forming motif of BK_{Ca} channels and bears the receptor site for the binding of the pore blockers: iberiotoxin (IbTX) and charybdotoxin (ChTX).[49] IbTX possesses several acidic residues and has an overall lower net positive charge than ChTX which may explain its selective inhibition of the BK_{Ca} channel. IbTX is therefore a better functional probe for BK_{Ca} channel pharmacology unlike ChTX which is less selective and blocks other potassium channels as well. The sequence alignment comparing the amino acid residues of these peptidyl blockers is shown in Figure 1-5.

```
ChTX: FTNVSCTTSKECWSVCQRLHNTSRGKCMNKKCRCYS
IbTX: FTDVDCSVSKECWSVCKDLFGVDRGKCMGKKCRCYQ
```

Figure 1-5. Sequence alignment for Charybdotoxin (ChTX) and Iberiotoxin (IbTX) with non-homologous residues highlighted.

The mechanism for IbTX inhibition of the BK_{Ca} channel is the same as that of ChTX, but the dissociation rate of IbTX is much slower.[50, 51] These inhibitors are useful not only as agents for investigations of the pharmacology of recombinant BK_{Ca} channels

in this study, but can also give an understanding of the channel's orientation in the tethered bilayer membrane. Both IbTX and ChTX work by binding to residues in the external pore of the channel through a freely reversible bimolecular reaction driven by electrostatic and hydrophobic interactions. In the tethered bilayer membrane, modulation of current through channels in response to ChTX and IbTX binding should only be observed if channel incorporation into the membrane occurs with the N-terminus facing outwards. Other structural types of small molecule compounds such as glycotriterpenes possess BK_{Ca} channel agonist activity. Dehydrosoyasaponin 1 (DHS-1) inhibits ChTX binding to BK_{Ca} channels through an allosteric mechanism and it reversibly increases the open probability of channels at concentrations as low as 10 mM.[52] Quaternary ammonium compounds such as tetraethylammonium (TEA) are known pharmacological blockers of the BK_{Ca} channel used in this study.[53]

Table 1-2. Summary of BK_{Ca} Channel modulatory molecules

Blockers	Peptide Blockers: Iberiotoxin, Charybdotoxin, Slototoxin
	Non-peptide Blockers: Paxilline, Penitrem, Tetrandrine
	Non-specific Blockers: Tetraethylammonium, Tetrabutylammonium, Clotrimazole
Openers	Maxikdiol, Dihydrosoyasaponin-1, Estradiol, Primaric acid, NS004, NS619, NS88 Mefenamic acid, Niflumic acid, Flufenamic acid

Voltage-Gated Potassium Channels

The simplest member of the voltage-gated potassium channel family is homotetrameric in structure, with each subunit surrounding the water-filled conduction pathway and bearing a voltage sensor. Unlike BK_{Ca} channels, voltage-gated K^+ channels have intracellular amino and carboxy termini and six transmembrane regions.[54] Each subunit has these six subunits (S1-S6) with the voltage sensor located

on the S4 subunit and the pore located between S5 and S6. Permeability of ions is regulated by channel opening and closing which involves two main mechanisms, a conformational constriction of the permeation pathway, or a conditional plugging of the pore by an auto-inhibitory part of the channel protein.[55] The closing of the channel occurs when the intracellular entrance pinches shut and the S6 segment obstructs the entrance from the cytoplasmic surface to the water-filled core of the conduction pathway.[56] The second mechanism responsible for the closing of voltage-gated potassium channels is the "N-terminal peptide block" which involves a tethered peptide blocker attached to the N terminus (N-type inactivation) that gave this mechanism the name "ball and chain" mechanism.[57, 58] A third mechanism is postulated to occur via a pinching shut of the pore at the narrowest part of the selectivity filter.[59] This inactivation mechanism is thought to regulate repetitive electrical activity and may also determine a physiological response to accumulation of extracellular potassium ions.

Membrane Lipids

Biological membranes are complex bilayer structures that form boundaries between different cell compartments and are composed of a diversity of lipids, sterols and membrane proteins. This general membrane composition is found in most organisms, however, a few exceptions are known, for instance, prokaryotes which lack sterols in their membranes.[60] Lipids can be broadly classified into two groups; saponifiable lipids, which upon hydrolysis contain salts of fatty acids, and the non-saponifiable which do not contain fatty acids. Saponifiable lipids are categorized based on their backbone structure to which fatty acids are covalently attached. Fatty acids are categorized based on their hydrocarbon chain lengths (C_4-C_{36}) and degree of saturation; and these determine the physical properties of membranes formed by these

lipids. Membrane lipids play numerous designated roles such as storage of energy reserves, provision of a matrix to help maintain correct protein folding and stability, and therefore maintain optimal cellular function,[61, 62] and signal transduction.[63, 64] The most abundant membrane lipids are phospholipids, which are derived from glycerol or sphingosine, though phosphoglycerides are the most commonly found phospholipids. Sterols are also a major component of biological membranes where they play important functional and structural roles. Cholesterol is the best studied sterol, and is known to influence phase transitions of phospholipid bilayers, cause a space effect within membrane phospholipids, and affect lateral diffusion of lipids in membranes among other roles.[65]

Phosphoglycerides

Phosphoglycerides constitute the major component of structural lipids and are characterized by a terminal hydroxyl group of glycerol esterified to phosphoric acid, with the other two hydroxyl groups esterified to fatty acids, resulting in phosphatidic acid illustrated in Figure 1-6. Phosphoglycerides are amphiphilic and are classified into groups based upon the identity of the moiety attached to the phosphate. This moiety is referred to as the headgroup.

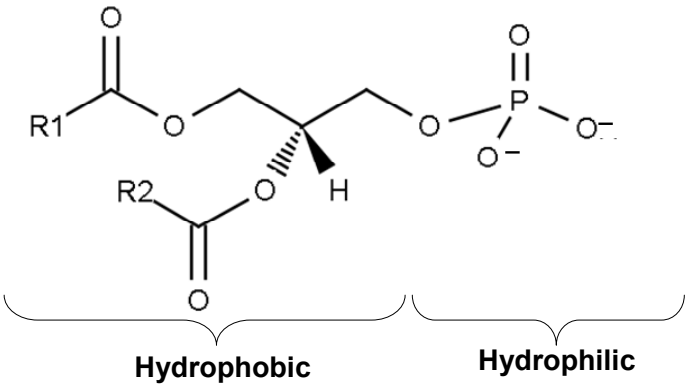

Figure 1-6. Structure of phosphatidic acid showing its polar and hydrophilic domains.

Phosphoglycerides can also be categorized by the number of carbon atoms present in the acyl chains whose carbonyl groups are esterified to the hydroxyl groups on the first and second carbon groups on the glycerol backbone. Glyceride nomenclature is often in terms of the stereospecific numbering (*sn*) system with most phosphoglycerides having the phosphate located at the *sn*-3 position of the glycerol. The long-chain hydrocarbons attach to the *sn*-1 and *sn*-2 positions of the glycerol through ester linkages.[66]

Biological membranes differ in terms of their lipid compositions based on the different environmental conditions within which they are found. A variety of ratios of individual 1, 2-diacylphosphoglycerides or phospholipids are found among different strains of organisms based on ecological factors. Phosphatidylcholine (PC) is a bilayer-forming lipid found in a majority of eukaryotic and prokaryotic membranes, but not archaebacteria.[67] Biological membranes have both bilayer and nonbilayer-forming lipid components combined together in different ratios which ensure optimal function of cells in which they are localized. Under physiological conditions, the nonbilayer-forming lipid components are represented by phosphatidylethanolamine (PE) and/or monogalactosyl or monoglucosyl diacylglycerol. The latter neutral lipids are usually found in chloroplasts. The anionic lipids phosphatidylserine (PS), phosphatidylglycerol (PG), cardiolipin (CL) and phosphatidic acids (PA) confer negative charge to membranes. CL and PA can form nonbilayer structures in the presence of special divalent cations. The strength of interactions of glycerophospholipids with cholesterol increases in the following order: phosphatidylethanolamine, phosphatidylserine and phosphatidylcholine respectively.[68]

Table 1-3. Major Phosphoglycerides and their head groups.

Phosphoglyceride	Formula	Headgroup
Phosphatidylcholine (PC)	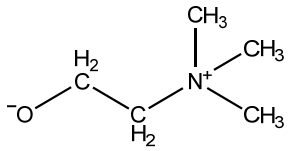	Choline
Phosphatidylethanolamine (PE)	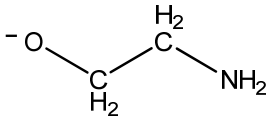	Ethanolamine
Phosphatidylinositol (PI)	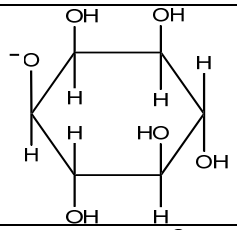	Inositol
Phosphatidylserine (PS)	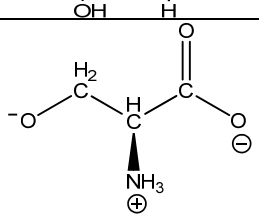	Serine
Phosphatidylglycerol (PG)	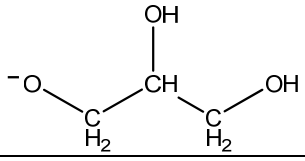	Glycerol
Diphosphatidylglycerol (DPG)	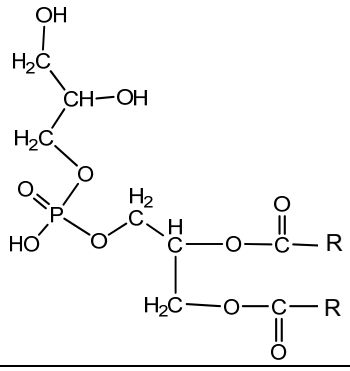	Phosphatidylglycerol

Cholesterol

Cholesterol is a type of membrane lipid that belongs to the class of compounds known as steroids, which includes saponins and bile acids. The common feature of steroids is the cyclopentanophenanthrene fundamental ring system or the

perhydrogenated form of this ring structure.[69] Cholesterol is the most common sterol and is found in mammalian plasma membranes comprising about 30% of the total lipid mass. It is an unsaturated alcohol with the cholestane structure consisting of an acyclic 4-ring system with three fused six-membered rings and one five-membered ring. The ring fusions in cholesterol are all *trans*, conferring a compact and relatively flat molecular arrangement with the stereochemistry of each of its atoms or groups defined with respect to the plane of the ring system as illustrated in Figure 1-7.

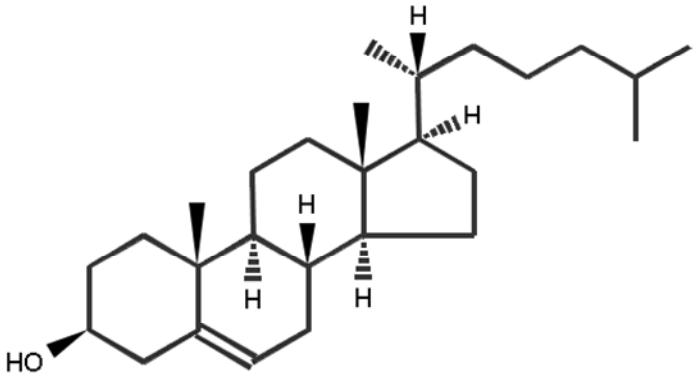

Figure 1-7. The molecular structure of cholesterol.

Cholesterol modulates membrane structure, dynamics and function in cells through sterol-protein interactions and also plays the role of altering the lateral distribution of components in the cell membrane. Cholesterol is quite rigid in membranes, exhibiting only axial diffusion about an axis perpendicular to the membrane surface therefore causing a condensing effect resulting in ordering of membrane lipids. Another major role played by cholesterol is the inhibition of permeation of small molecules through membranes. Normally, a disordering of the lipid bilayer causes defects in the bilayer structure which would allow small molecules to occupy small voids in the membrane and permeate across the bilayer. Bilayer ordering by cholesterol reduces incidences of these defects therefore reduces the membrane permeability.

Biomimetic Membrane Systems

Lipids adopt a bilayer assembly structure in biological membranes and this structure provides a barrier that defines the structural components within the cell and also separates the cell interior from the external environment. The complexity of natural membrane systems as regards the delicate balance of lipids and different types of integral and peripheral membrane proteins makes the in situ study of any single cell membrane component a major challenge. Hence there is need to develop simpler membrane mimics that can be used to study cellular structures in isolation.

Vesicles

The simplest model membrane system is that of lipid bilayers which form when amphiphilic lipid molecules dissolved in aqueous solution spontaneously aggregate to form multilamellar vesicles (MLVs) in a process partly driven by the hydrophobic effect.[70] The closure of bilayers to form vesicles is related to curvature induced by the constituent lipids, and is dependent on the size of the hydrophilic head groups relative to the hydrocarbon backbone.[66] Multilamellar vesicles can be mechanically disrupted through sonication, or forced through polycarbonate membrane pores in a process of extrusion to form unilamellar vesicles which vary in size ranging from few nanometers to tens of microns as summarized in Table 1-4.

Table 1-4. Classification of liposomes by size.

Liposomal structure	Small Unilamellar Vesicles (SUV)	Large Unilamellar Vesicles (LUV)	Very Large Unilamellar Vesicles (VLUV)	Giant Unilamellar Vesicles (GUV)
Size Range	4 – 50 nm	50 – 500 nm	500 – 5000 nm	> 5000 nm

Small unilamellar vesicles (SUV's) have less symmetry in lipid distribution between the inner and outer bilayer leaflets, and have high surface curvature therefore are less

stable thermodynamically and tend to fuse to form larger vesicles.[71] As a result, large unilamellar vesicles are more favored as model membranes to avoid these lipid packing problems associated with SUV's and because of the significant LUV interior volume.

The traditional method involving use of vesicular lipids has been as free suspensions in solution, but in recent years, several groups have developed systems whereby vesicles are tethered to supports using a number of recognition elements such as biotin-streptavidin coupling, or tethering by DNA hybridization (Figure 1-8).[72]

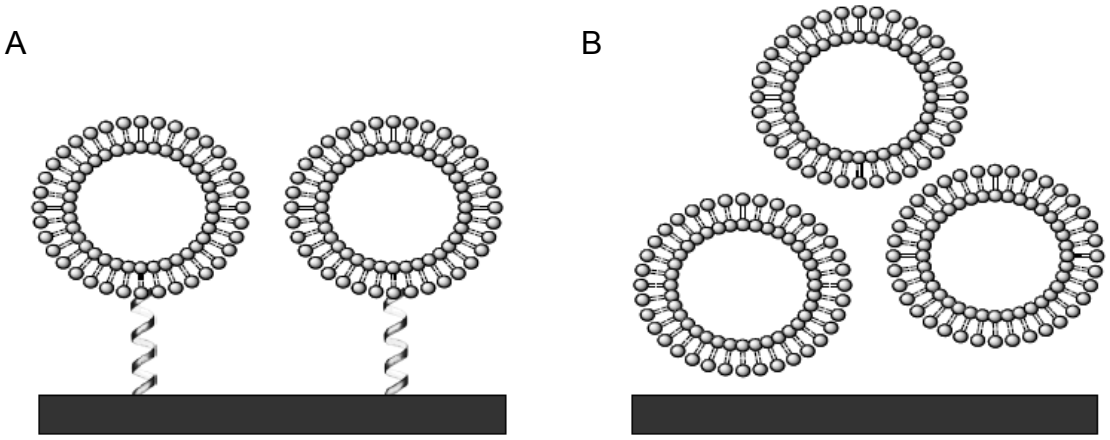

Figure 1-8. Vesicular model membranes. A) Vesicles tethered to solid supports. B) Free vesicle suspensions in solution.

Supported Lipid Bilayers

The formation of lipid bilayers supported on substrates was physically characterized for the first time by Tamm and McConnell when they deposited lipids on glass, quartz and oxidized single-crystal silicon wafers via Langmuir-Blodgett transfer.[73] The McConnell group demonstrated the lateral diffusion of lipid molecules in such supported membranes as being identical to diffusion in conventional multilayer systems as facilitated by the 1 – 2 nm thick water-filled space between the bilayer and the hydrophilic substrate. Later it was shown that SUVs deposited on glass cover slips

could spontaneously fuse to form supported bilayer membranes.[74] Subsequent work on supported lipid bilayers explained that fusion of phospholipid vesicles to substrates is dependent upon buffer pH, ionic strength as well as hydration and steric forces.[75] Electrostatic attractions and van der Waals forces had for a long time also been known to play a significant role in substrate bilayer interactions.[76]

Since the initial studies, planar lipid systems on solid supports proved valuable as suitable mimics to the natural lipid environment for immobilization of proteins for functional studies.[77] A variety of substrates are currently used with supported BLMs and include glass or silica substrates,[78-81] and unfunctionalized metal surfaces.[82-84] Surface sensitive characterization techniques such as ellipsometry, surface plasmon resonance spectroscopy (SPR), quartz crystal microbalance with dissipation (QCM-D), atomic force microscopy (AFM) and many others, are often used to characterize SLB's as model membranes.[85-87] Studies done by the combination of QCM-D and AFM have revealed mechanisms through which the self-organization of lipids occurs during the formation of the SLB, a process which has been determined to involve adhesion and rupture of vesicles on the support followed by the evolution of the supported bilayer patches which aggregate to form a continuous bilayer.[88]

The rupture of vesicles that have adhered to the surface for the formation of SLBs depends on a threshold surface density of vesicles that has to be overcome, and is further enhanced by proximity to other adhered vesicles.[89] Upon vesicle rupture, the resultant bilayer patch exposes an edge which due to the hydrophobicity of the hydrocarbon acyl chains is energetically unfavorable, therefore interacts with neighboring adhered or vesicles in solution depending on overall density of vesicles.

Eventually, a cascade of rupture events leads to extended bilayer patches that are continuous over the whole surface.[90]

A characteristic of supported lipid bilayers is the proximity between the membrane and substrate. This close contact is associated with loss of function and lateral mobility of transmembrane proteins incorporated in SLBs; therefore modifications were made to increase the space beneath the membrane by integration of polymer supports into the SLB.[91] Other modifications to the original SLB include efforts to mimic the biological membrane as closely as possible by the Tamm group through use of Langmuir transfers and vesicle fusion to create hybrid polymer-cushioned bilayers with an asymmetry of lipid compositions between the two leaflets.[92] The supported lipid bilayer membranes that can currently be assembled are illustrated in Figure 1-9.

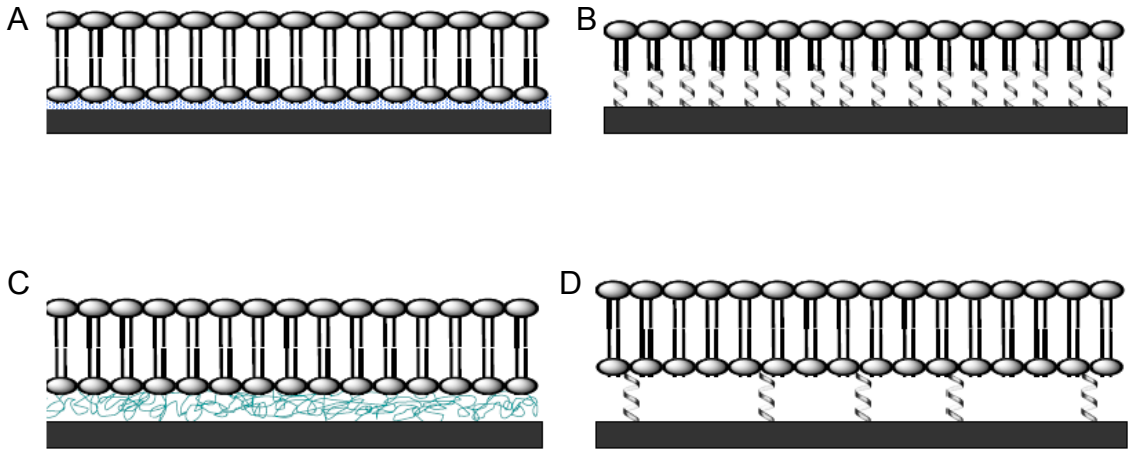

Figure 1-9. Immobilization methods for supported membranes. A) Membrane adsorbed on support with a separating thin water film. B) Formed on monolayer of alkanethiols or alkanesilanes on Au or Si/SiO2 substrates. C) Supported on a polymer matrix containing hydrophobic chains. D) Tethered through anchoring molecules.

Despite the advances made in the development of supported bilayers suitable for the integration of membrane proteins for functional studies, SLBs still lack a well-defined ionic reservoir on both sides of the membrane.[93] The limited volume below the SLB is a

deterrent to reconstitution of proteins with bulky extramembranous domains due to concerns about protein denaturation and sub-optimal function as a result of hydrophobic mismatch in the proteins therefore limiting the possible applications for such systems. Additionally, the exposed regions of transmembrane proteins may interact with substrates upon which the bilayer is supported with a pinning effect thereby inhibiting lateral mobility and proper function of proteins.[94] Attempts to address the problem of the limited volume below the membrane using polymer supports yielded patchy bilayers with defects which were unsuitable for reconstitution of integral membrane proteins.[77]

Tethered Bilayer Lipid Membranes

Generally, the tBLM is characterized by a proximal layer divided into three parts to include the bilayer forming lipids, a spacer group and an anchoring group (Figure 1-10).

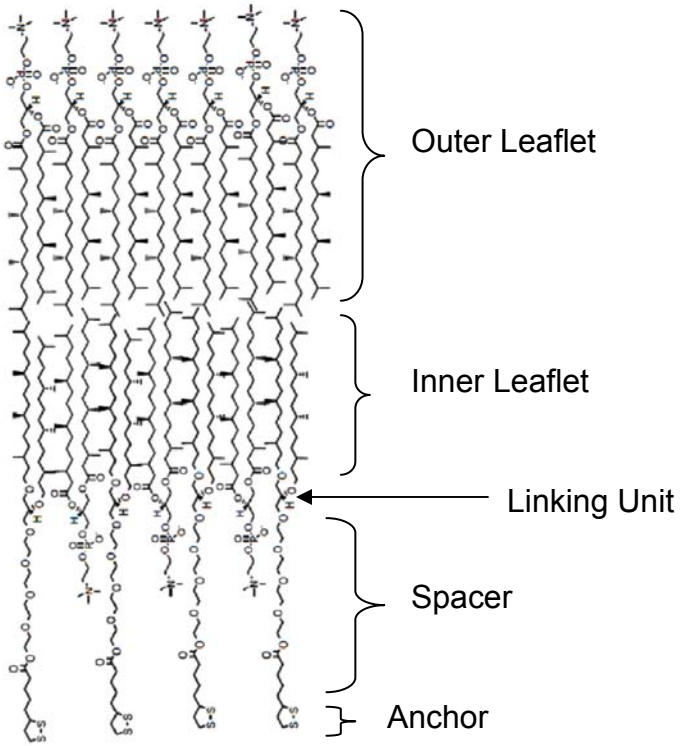

Figure 1-10. The tethered bilayer lipid membrane (tBLM). Shown are the spacer, linking unit, bilayer forming lipids and the anchor group by which the membrane is tethered onto a solid substrate.

Tethered bilayer lipid membranes (tBLMs) are emerging to be useful structural and functional mimics of biological membranes offering greater chemical, electrical and mechanical stability than other model membrane systems.[93] To date, gold and silica are the most commonly used substrates for the formation of tBLMs each of which is used depending on the desired applications.[93, 95] Applications for tBLMs so far is in drug discovery, basic research towards the better understanding of membrane dynamics and protein-lipid interactions or biosensing.[96] Gold substrates can be used as electrodes and therefore allow for electrical characterization of the system as well as for electrical measurements of ion channels incorporated within tBLMs .[97-99] The planar configuration of tBLMs allows for application of a number of powerful surface or intersurface-sensitive techniques similar to those used in SLB studies for the characterization of structural and dynamic organization, as well as order in these systems.[100]

The spacer group on the tBLM creates an ionic reservoir below the membrane therefore allows the lateral mobility critical for optimal function of incorporated integral proteins.[95] The quality of the ionic reservoir could be improved by increasing the volume of the reservoir by increasing the length of the hydrophilic region of the tethering molecules or by laterally spacing the reservoir forming lipids.[93] Anchor groups form covalent attachments by gold-sulfur interactions on the substrate[7, 101, 102] or by the bonds formed by lipid-polymer conjugates on silica substrates.[95]

The first step of formation of the tBLM typically involves self-assembly of thiols, disulfides, thiophenols and other organosulfur monolayers which serve as the tethering moiety onto the substrates.[103] After the disposition of the self-assembled monolayer (SAM), different lipids can be applied to complete the formation of the tBLM and this is

done either by vesicle fusion of SUVs to form tethered bilayers on the SAM or by a layer by layer transfer of lipid monolayers through Langmuir-Blodgett or Langmuir Schäfer techniques.[95] For the work documented in this dissertation, tBLMs were formed on a gold substrate using a SAM covalently attached by gold-sulfur interactions. The SAM is based on the archaea analogue 2,3-di-O-phytanyl-sn-glycerol-1-tetraethylene glycol-D,L-α-lipoic acid ester lipid (DPTL) which bears two phytanoyl chains bound to a spacer through a chiral glycerol unit, illustrated in Figure 1-11.

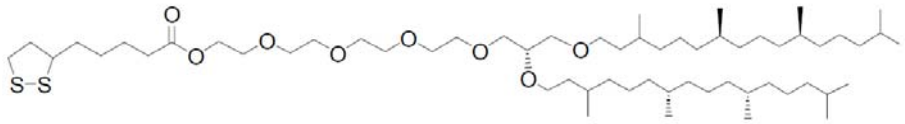

Figure 1-11. Structure of the 2,3-di-O-phytanyl-sn-glycerol-1-tetraethylene glycol-D,L-α-lipoic acid ester lipid (DPTL)

Phytanoyl lipids associated with archaea bacteria and other extremophiles are then used to prepare liposomes for fusion to the SAMs for the formation of tethered bilayer membranes. These lipids are characterized by their acyl chains composed of the phytanoyl functionality which consists of a highly branched 3,7,11,15-tetramethylhexadecyl group that confers thermal stability and fluidity to membranes.[104] Phytanoyl lipids have also been demonstrated to have electrical stability that makes them more suitable for use in the incorporation of ion channels and other pore-forming proteins during recordings of electrophysiological measurements. Two phytanoyl lipids were used for the preparation of vesicles for this study and these are 1,2-diphytanoyl-sn-glycero-3-phosphoethanolamine (DPhPE) and 1,2-diphytanoyl-sn-glycero-3-phosphocholine (DPhPC) illustrated in Figure 1-12 and used in various ratios that would provide optimal electrical and mechanical stability .

DPhPE

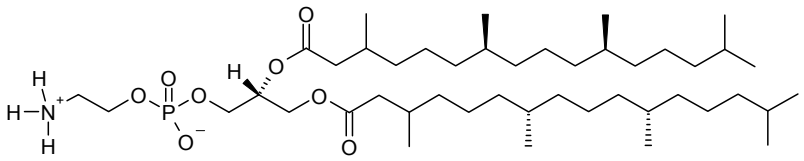

DPhPC

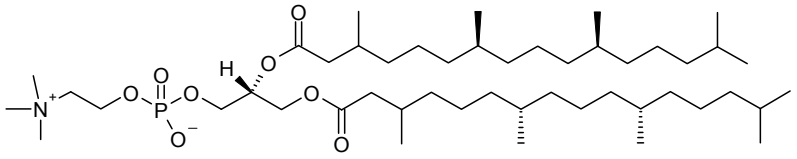

Figure 1-12. Structures of 1,2-diphytanoyl-sn-glycero-3-phosphoethanolamine (DPhPE) and 1,2-diphytanoyl-sn-glycero-3-phosphocholine (DPhPC) lipids

Electrical Properties of Membranes

Electrochemical forces on cell membranes are involved in facilitation of the regulation of chemical exchanges within cells and the surrounding environment. Membranes are semipermeable and therefore allow ionic interchange across the cell. The predominant ions within and around cells include Na^+, K^+, Ca^{2+} and Cl^- and are found in markedly different extracellular and intracellular concentrations. Voltage and concentration gradients drive ions across membranes with a net flux from regions of higher concentration to lower concentrations.[1]

The potential difference (voltage) is a measure of how much electrical work is required to move a charge in a frictionless manner from one point to another. The equilibrium potential is the membrane potential at which there is no net flux of ions from one side of the membrane to the other. The equilibrium potential for a single ion species across a membrane separating two regions of unequal concentration is described by the Nernst potential (E_{eq}):

$$E_{eq} = (RT/zF)\ln\{C_{(out)}/C_{(in)}\}$$

$$= 2.303\,(RT/zF)\log_{10}\{C_{(out)}/C_{(in)}\} \text{ in volts} \qquad (1\text{-}1)$$

Where *R* is the gas constant (8.314 V C K^{-1} mol^{-1}), *T* is the absolute temperature, z the charge of the ion, *F* is Faraday's constant (9.648 × 10^4 C mol^{-1}), and $C_{(out)}$ and $C_{(in)}$ are the ionic concentrations outside and inside the cell respectively. Assuming room temperature is 20˚C, 2.303(RT/zF) = 58 mV for a univalent ion.[1]

For a system with more than one permeable ionic species, the equilibrium voltage will depend on the concentration and relative permeability of the individual ions. The Goldman-Hodgkin-Katz (GHK) equations define absolute ion permeabilities in terms of flux measurements, and ion permeability ratios in terms of zero-current potential measurements without the contributions of ion channels.[105] The GHK equation therefore can define resting potentials and in a cell with K^+, Na^+ and Cl^- as the permeant ions, the equation would be:

$$V_{\text{rest}} = \frac{RT}{F} \ln \frac{P_{Na}[Na+]_e + P_K[K+]_e + P_{Cl}[Cl-]_i}{P_{Na}[Na+]_i + P_K[K+]_i + P_{Cl}[Cl-]_e} \quad (1\text{-}2)$$

Where E_{rev} is the resting potential, $[K^+]_e$ the outside K+ concentration, $[Na^+]_e$ the outside Na^+ concentration, $[Cl^-]_e$ the outside Cl^- concentration. In the case of only one permeant ion, E_{rev} becomes the Nernst potential for that ion.

Conductance (G) and resistance (R) are used to quantify the ease or difficulty of current (I) flow between two points and they are defined by the Ohm's law:

$$I = GV \text{ or } I = (1/R)\ V \quad (1\text{-}3)$$

Conductance varies with the salt ionic concentration and is affected by the viscosity of solutions on either side of the membrane. The bilayer lipid membrane acts as a barrier to the flow of ions and therefore increases the resistance of the system. Two conducting electrodes can be used to measure the conductance of a system if each is positioned on either side of the membrane. Because the membrane is a dielectric insulator

between two conductors, charge can build up at either interface. Capacitance is a measure of how much charge separation is required to create a given voltage difference and it is measured in farads and can be defined by the following equation:

$$C=Q/E \quad (1\text{-}4)$$

Where Q is the charge transferred, E is the potential difference and C is the capacitance. The rate of change of potential due to current flow, Im, at the membrane is given by:

$$dE/dT = I_m/C \quad (1\text{-}5)$$

Capacitance depends on the distance between the two charged surfaces (d) and the dielectric constant (ε) of the membrane in between. The dielectric constant is a measure of the polarizability of the material and the degree to which any permanent electric dipoles which may be present in the material respond to the voltage difference. The capacitance for a bilayer is given by the equation:

$$C = \varepsilon\varepsilon_0 A/d \quad (1\text{-}6)$$

Where ε is the dielectric constant and ε_0 is a constant of the permittivity of free space with the value 8.85×10^{-12} coulomb $V^{-1}m^{-1}$. The specific capacitance is the capacitance per unit area which depends on the charge separation per unit area of the membrane and for phospholipids and biomembranes has similar values of around 1μfarad/cm^2, which corresponds to a dielectric constant of 2 and distance of about 25 Å.[106-108]

The general effect of membrane capacitance is to slow down the response to any current by a time, τ that depends on the resistance and capacitance of the membrane. The discharge rate of the membrane capacitor can be expressed by the equation:

$$dE/dt = I_m/C = -E/RC = -E/\tau \quad (1\text{-}7)$$

When this equation is solved, it gives an expression for the potential across the membrane as a function of time, t.

If the initial potential is given as E_0, the relationship is expressed as:

$$E = E_0 \exp(-t/RC) = E0 \exp(-t/\tau) \quad (1\text{-}8)$$

Due to the great variation in time constants for different biological membranes the resting membrane resistances can vary broadly from 10 to 10^6 ohms.[109] The equivalent circuit in Figure 1-13 can be used to represent the electrical properties of the bilayer membrane and how they are related to each other.

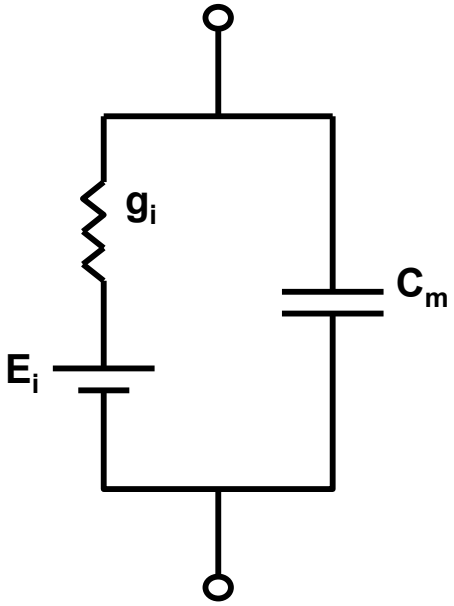

Figure 1-13. Equivalent circuit diagram of a membrane. The electrical properties of a membrane can be modeled using the conductance, g_i of ions, crossing the membrane with a membrane potential, E_i in series. These are in parallel with the capacitance, C_m.

Subsequent to the formation of a solid supported lipid bilayer or a tethered bilayer lipid, membrane capacity does not vary significantly since the bilayer determines its value. On the other hand, membrane resistance may vary over several orders of magnitudes in response to the lipid composition, preparative factors and experimental

parameters indicating whether a membrane is electrically dense or not.[66] Electrostatic interactions between the lipid bilayer and the surface of the supporting substrate as well as the membrane compressibility are key parameters determining formation of electrically dense supported or tethered bilayer lipid membranes.[110]

Stochastic Sensing

Stochastic sensing is a technique which relies on single-molecule detection and is usually based on transmembrane pores developed as sensing elements with binding sites for analytes. The first known example of a single-molecule experiment on a functional biomolecule was the observation of current flow through a single ion-conducting channel formed by the peptide gramicidin in a planar lipid bilayer.[111] Single-channel currents passing through a transmembrane pore can be modulated by channel blockers or antagonists reversibly bound within the pore as illustrated in Figure 1-14.

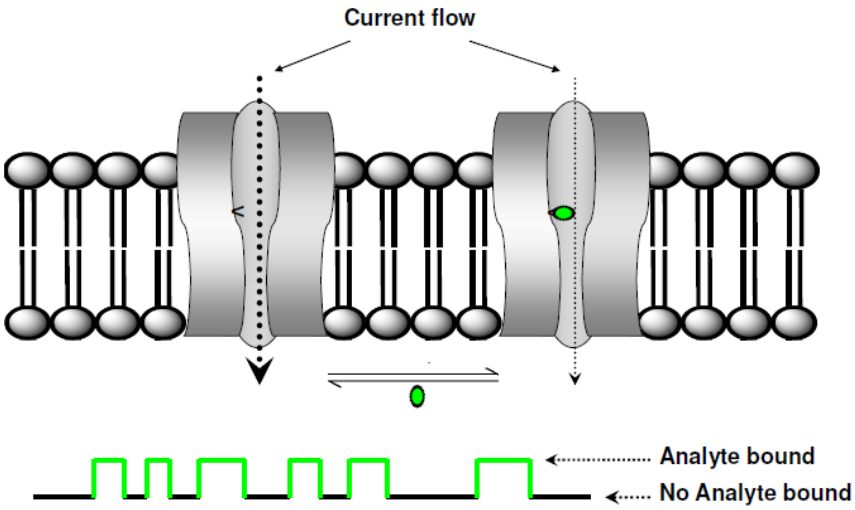

Figure 1-14. Schematic of stochastic sensing by an engineered pore in a planar bilayer.

Stochastic sensing monitors individual binding events and can reveal the concentration of analytes and based on structure specific current signatures, for instance the mean duration and amplitude of events, the identity of the analyte can be

deduced.[112] Quantitative kinetic information can be obtained about the interaction of an analyte to its binding site. In a simple case, the sensor element has two states; the state where the binding site is occupied by the analyte and another where the binding site is unoccupied, each giving a different output.[113]

In a simple equilibrium, $\tau_{off} = 1/K_{off}$ where τ_{off} is the mean dwell time of the analyte and K_{off} is the dissociation rate constant , and $\tau_{on} = 1/K_{on}[A]$ where τ_{on} is the mean time between binding events , K_{on} is the association rate constant and [A] is the analyte concentration.[113] If the support onto which the bilayer membrane is tethered is a conducting substrate, for example, the work documented in Chapter 5 in this dissertation, where the bilayer lipid membrane is tethered to a gold substrate, an alternating potential can be applied to allow impedance measurements. Advances have been made to engineer channel-forming peptides and proteins to detect a myriad of chemical analytes with potential applications in high throughput pharmaceutical screening, detection of heavy-metal contaminants in water and many others.[114] Chapter 5 of this dissertation documents single-channel recordings representing functional activity of the BK_{Ca} channel in a bilayer membrane tethered on gold, as well as pharmacological aspects of bound tetraethylammonium compounds.

CHAPTER 2
EXPERIMENTAL PROCEDURES AND TECHNIQUES

Introduction

Chimeric BK_{Ca} channels with a red fluorescent protein (mRFP1) tag were heterologously expressed in *Xenopus laevis* oocyte membranes. The approach used for expression involved *in vitro* transcription followed by microinjection of complementary RNA into oocytes.[115] Translation of RNA occurred followed by trafficking of functional channels to the oocyte membrane. The success of expression was quantified by two-electrode voltage clamping of oocytes. Membrane extracts containing channels were detergent solubilized and these were then purified by immobilized metal ion affinity chromatography. Purification was determined by SDS-PAGE and the identity of the protein verified by immunoblotting.

Protein reconstitution into liposomes was mediated by dialysis and the followed negative-staining transmission electron microscopy imaging to visualize the formed proteoliposomes. It was important to demonstrate functional activity of reconstituted channels, and this was done in a tethered bilayer lipid membrane (tBLM) by use of a modified patch clamp electrophysiology technique. The insertion process of channels into the membrane was analyzed by surface plasmon resonance-enhanced ellipsometry. Quartz crystal microbalance with dissipation (QCM-D) and atomic force microscopy (AFM) were used to characterize the formation of model membranes by phytanoyl lipids on solid substrates. Cryo-transmission electron microscopy imaging of lipid dispersions was performed at the Center of Chemistry and Chemical Engineering, Lund University, Lund, Sweden. Cryo-TEM provided us with images which allowed for the determination of the structural morphology of vesicle mesophases and analysis of

vesicle sizes. For a further characterization of the sizes of vesicles we used dynamic light scattering (DLS) and NMR diffusion. Briefly described below is the methodology of the experimental work as well as the basic principles of the techniques used for the characterization studies.

Techniques and Methods

Immobilized Metal Ion Affinity Chromatography (IMAC)

Theory

IMAC is a protein purification technology that makes use of specific binding relationships between the side chains of certain amino acids, in most cases, histidine and Lewis metal ions such as Cu^{2+}, Ni^{2+} and Zn^{2+}. A chelating agent attached to a stationary support combines with metal ions to form a metal ion complex referred to as the immobilized metal chelate complex (IMCC) thereby capturing of the metal ion. The earliest applications of IMAC made use of surface histidines that occur naturally in the target protein, however, advances to the technique allowed the inclusion of a hexahistidine tail or “tag” on the target protein thereby allowing for more specific and stronger binding affinities for use in more selective purification.[116-118]

Because IMAC relies on affinity interactions between amino acids and metal ions rather than biological function, it can function under denaturing conditions and has become a popular method for the purification of proteins expressed in inclusion bodies. Systems have been developed which bear capability to specifically detect histidine-tagged proteins by relying on anti-hexahistidine antibody for secondary antibody–reporter enzyme conjugate detection, or a reporter enzyme (horseradish peroxidase and alkaline phosphatase) linked to a chelator for direct metal chelate complex

detection. Samples can then be queried by either method for the presence of the histidine tag in an immunoblotting assay format.

Experimental settings

The instrument used for automated purification was the ÄKTA prime plus (GE Healthcare Life Sciences) using Unicorn PrimeView software and equipped with a UV and conductivity monitor. Supernatants obtained after solubilization of membrane extracts are loaded onto the Histrap FF (GE Healthcare Life Sciences, PA, USA) columns pre-packed with Ni^{2+} Sepharose media made from highly cross-linked agarose matrix. Elution is performed through columns equilibrated with binding buffer (10 mM β-octyl glucoside, 20 mM Tris buffer, 500 mM KCl and 20 mM imidazole, adjusted to pH 7.5) at a flow rate of 1 mL min^{-1} and washed with the same buffer. Unbound material is washed off using 5 column volumes of binding buffer, and then the samples eluted with an elution buffer containing 500 mM imidazole and all other components of the binding buffer at pH 7.4 and a flow rate of 1 mL min^{-1}.

Patch Clamp Electrophysiology

Theory

The patch clamp electrophysiological technique allows the recording of macroscopic whole-cell or microscopic single-channel currents flowing across biological membranes through ion channels. The technique allows the experimental control and manipulation of the voltage of membrane patches or the whole cell, thus allowing the study of voltage dependence of ion channels and recordings of very low electrical currents amounting to a picoampere (10^{-12} A).[119]

The development of the gigaseal led to the establishment of various recording configurations such as the cell attached, inside-out, outside-out or whole-cell and these

have allowed the possibility of making patch recordings from the cell surface or cell-free membrane patches as well as intracellular recordings. However, the basis of all patch clamp recordings began with the “cell attached” method. In this method, a glass micropipette tip containing the reference electrode and electrolyte solution is micromanipulated into the cell’s surface, isolating a “patch” of the membrane. Suction is next applied to create a seal which indicates that a significant amount of electrical resistance was obtained between the patch containing the ion channels and the tip. This electrical resistance is needed to measure ion channel currents free of background noise. The current flow is reflective of all the ion channels within this patch and measured with a specific patch clamp amplifier. The amplified current transitions are then recorded and analyzed with a data acquisition program. Each channel exhibits a unique amplitude threshold, lifetime profile, and conductance parameters which relates to the single channel activity of the ion channel.

In recent years, variations of the patch-clamp technique have been developed making this a powerful technique capable of providing answers to questions that previously could not be addressed. Information that can be obtained from patch clamp recordings include the conductance, voltage dependence, selectivity, open probability, dwell times, resistance of the membrane, and pharmacological profile of the ion channels.[120]

Two-electrode voltage clamping: Two-electrode voltage clamping is a high throughput measurement configuration which allows measurement of current through channels in cells using a pair of electrodes while controlling the membrane potential. The voltage electrode measures membrane voltage (V_m) while clamping the membrane potential at

a desired level (V_h) by injecting current via a second electrode. Any change in membrane current caused by opening or closure of ion channels is immediately followed by a change in the current equal in amplitude but opposite in sign at the output of the amplifier connected to the current electrode. The experimental set-up is illustrated in Figure 2-1.

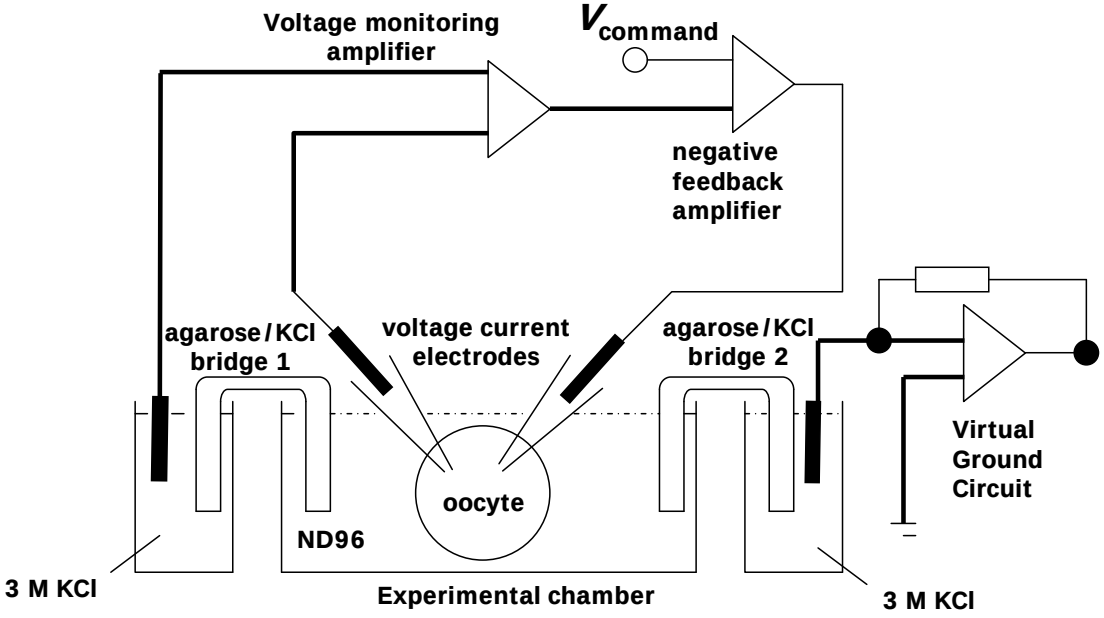

Figure 2-1. Principal scheme of a typical TEVC recording arrangement. Bold lines denote Ag/AgCl electrodes. The oocyte is placed in the middle of an experimental chamber filled with ND96 recording solution.

The amplifier output is monitored on a computer. Because it makes use of two electrodes, TEVC is especially useful for the recording of measurements in cells with large dimensions such as oocytes. We used TEVC for the analysis of the success of expression of the BK_{Ca} channels. Oocytes that were injected with complementary RNA encoding for BK_{Ca} channels were incubated for three days after which the oocytes were analyzed for the activity of ion channels. Oocytes were placed in a 1 ml plexiglass experimental chamber, impaled with two 0.3 to 2 megohm electrodes and the

membrane potential clamped at -90 mV using a Warner OC725C oocyte clamp. The clamping was done after a brief duration of 0.5 min to 2 minutes to allow for a partial recovery of the oocyte from the injury produced by the electrodes. Data was collected and analyzed using pClamp 8.0 software. Current-voltage relationships were obtained by stepping to voltage clamp to -70 mV and then increasing in 10 mV steps of 100ms duration to +120 mV. The maximum current at each voltage was recorded.

Specialized patch clamping on tethered bilayers: In recent years biomimetic membrane systems have been developed based on supported bilayers on solid substrates. Chapter 1 of this dissertation discusses the different types of systems that are currently in use. The studies documented here involve use of the tethered bilayer lipid membrane (tBLM), a system composed of a gold substrate with two interconnected pads; the sensor pad within which is the tBLM with incorporated ion channels, and a probe pad which serves as the ground electrode. In this modified patch clamp technique, a thiol-modified monolayer is covalently attached to a gold substrate by self assembly, forming the leaflet of the membrane proximal to the substrate, and the outer leaflet is deposited via vesicle fusion on top of the monolayer to form a complete hybrid bilayer. Alternatively, instead of fusing vesicles of different lipid mixtures, the bilayer can be formed by direct fusion of proteoliposomes containing ion channels or other pore-forming peptides of interest, thereby achieving both bilayer membrane formation as well as ion channel incorporation in one process. A buffer or water droplet is added onto the sensor pad in order to maintain hydration of the tethered bilayer and ion channel. A conventional patch microelectrode filled with the same buffer solution is then dipped into the bulk solution on the sensor pad by micromanipulation and a potential of 3 mV

pulsed to measure the electrical resistance of the tBLM. It is imperative that resistances in the giga-ohm range be observed before any electrical measurements can be recorded using this system to ensure that any currents passing across the membrane be those traversing through the ion channel during ion translocation rather than through membrane defects.

Experimental Settings

The experimental setup for the specialized patch clamping of tethered bilayers consisted of a patch-clamp amplifier (Axopatch 200B, Molecular Devices), data acquisition and digitizer (Digidata 1322A, Molecular Devices), a micromanipulator, two electrodes, a data recording system, an anti-vibration table, and a Faraday cage with a dust cover. A noise and dust free environment for the recording systems was established with an anti-vibration or vibration isolation table surrounded by a Faraday cage. A piezoelectric anti-vibration table provided the stage for patch clamp recording. To reduce the amount of electrical noise a copper mesh was placed around the stage thereby shielding the set-up from all external electrical signals and electrical noise. The seal resistance between both the reference and ground electrode must be at least 1 GΩ in order to observe single ion channel activity and ideally create an electrical stable bilayer.[69] A high resistance enables the complete electrical isolation of the membrane patch, and reduces the current noise. Experiments were not done if the resistance was not in the giga-ohm range. The discrepancy of the current noise is related to Johnson voltage noise S_i:

$$S_i^2 = 4kTf_c/R \qquad (2\text{-}1)$$

Where k is the Boltzmann's constant, T is temperature (in Kelvins), f_c is the low pass filter (Hz), and R is the resistance. The Johnson noise for a 1 GΩ resistance at 298

K, with a 1 kHz filter is 0.1 pA, and a 10 GΩ resistance results in current noise of 0.04 pA. Now if the resistance is 100 MΩ under the same conditions as the first seal, the noise becomes 0.4 pA. Therefore the higher the seal resistance, the less noise observed. This resistance in electrophysiology is termed the gigaseal.

A strong gigaseal depends on the pipette material used, the size of the tip, and a sample area free of microscopic debris. Both soft (thin wall CEE BEE glass) and hard glass pipettes may be used for patch clamp measurements. However, hard glass like borosilicate can establish greater resistance because it has thicker walls. The diameter of the tip depends on the pulling technique and can range form 0.5 to 5 μm.[70] In the tethered bilayer system, the resistance measured depends on the complete coverage of the sensor pad by the membrane thereby creating a barrier between the two electrodes. Software used during experiments included Axon Instrument's Clampex 8.0 or 9.0 for data collection and Clampfit 9.0 for data analysis. "Episodic" and "gap-free" were the two main software protocols involved in characterizing the bilayer and the single channel activity. The Episodic protocol was used to determine the conductance of the bilayer. During these experiments automated potentials from negative 200 mV to positive 200 mV were applied to the system for several seconds. From these studies, we determined the stability of the bilayer system. The gap free protocol gave us a chance to observe the ion channel's activity over a long period of time with different potentials. With the gap free protocol, we controlled the change in potential manually. Therefore a number of experiments were conducted using the gap-free protocol. The recording filter was 5 kHz low pass 8-pole Bessel.

Data analysis was done using the event detection for single channel statistics within the Clampfit program. From the event detection, we obtained statistics on the channel's average current during open and closed states, dwell time (average time spent at one level during the duration), and current transitions. We also determined the probability to which the channel was in an open and closed state. In order to conduct this analysis, signals were first filtered at 1 kHz by an 8-pole low-pass Bessel filter to reduce the high frequency noise during recording. Once the signal was filtered, the baseline was manually adjusted to zero, for the closed state and event detection was performed.

Event detection: Event detection for single channel analysis goes through a single trace and counts the number of events at different amplitude levels. An event is a continuous section of the trace at one level. In the event viewer, we manually set the different levels that are detected. Level zero accounts for when the channel is closed or not conducting and level one, or two correspond to the open states of the channel. This opening is called a threshold. Each change in amplitude to a different level must meet a maximum threshold in order to be counted as an event. The maximum amplitude $A_{max}/A_{0,}$ threshold depends on the error function erf, the frequency of the filter recording system, and the duration of the event w.

$$A_{max}/A_0 = \text{erf}\,(2.668\, f_c w) \qquad (2\text{-}2)$$

Because this value varies, we set a 10% level contribution within the software in which the changes in amplitude contributing to a new event have to be within 10% of that level's amplitude. For instance, if the existing open level is 5 pA and a new event begins at 5.5 pA, the 10% contribution setting will reduce the transition to 5.05 pA.

(0.9 x 5.0 pA) + (0.1 x 5.5) = 5.05pA (2-3)

Rapid deviations of the trace that are not within the range of the current level were ignored. Due to the possibility of the channel being open or closed upon entering the event detection, the first and last events were also excluded from the statistics. Once a count of all the different events at both the open and closed levels was obtained, single channel analysis of the recombinant BK_{Ca} channel was performed.

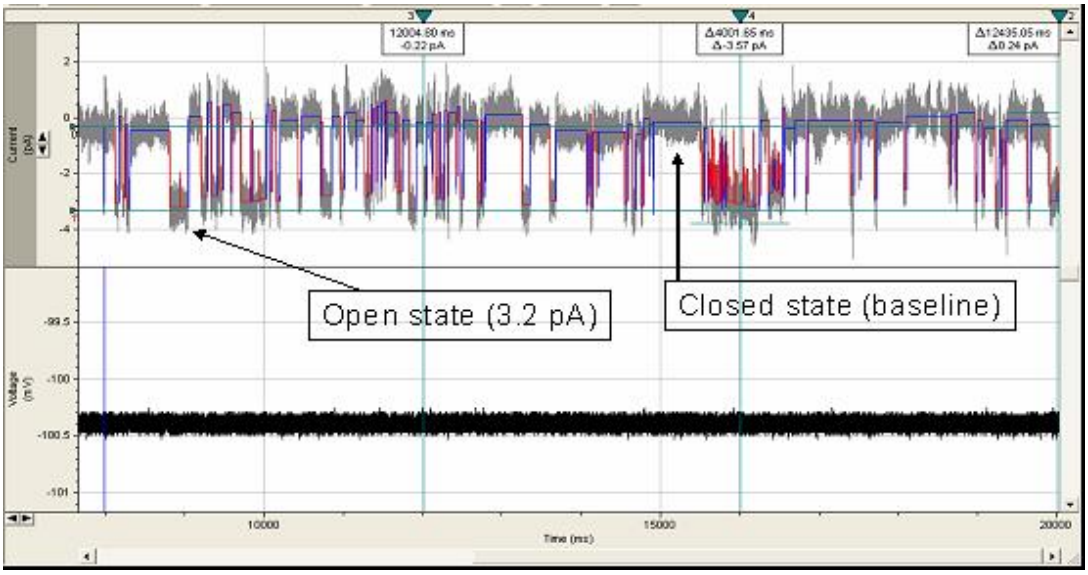

Figure 2-2. Event detection occurring at level zero and level one. Level zero indicates the closed state of the channel or the non-conducting level and it is adjusted to fit the baseline. Level one is roughly at -3.0-3.3 pA. Events are highlighted in red and accounts for the open state of the channel.

Single ion channel activity: Single ion channels exhibit stochastic activity. Theoretically the durations of events and the order in which they occur are random variables. The channel has no memory system of opening or closing at a given time, and behaves independently of specific potentials, and lipid environment. For this reason, parameters representative of single channel activity, and the information contained in each event are measured from statistical distributions. There are two main objectives for analyzing single ion channel activity of channels: First, amplitude studies

to understand ion permeation through open channels at different ionic compositions, and different membrane potentials, and secondly, the duration of open and shut times or the dwell time for lifetime and kinetic studies.

Point amplitude histograms: The conductance of biological ion channels is restricted by the channel's topology including its maximum pore expansion, length and structure in the lipid bilayer membrane. Because of this restriction, there is a specific range in which channels will conduct. For instance, the conductance of the wild type, full-length BK_{Ca} channel is between 90 pS to 200 pS. The large range is also due in part to the calculation of conductance and the method used for recording single channel activity. Conductance can be calculated by stationary fluctuation using voltage clamp measurements on large ensembles of channels or measurements of unitary current analysis using patch clamp. Variance calculations are used for stationary fluctuations to calculate N, the number of the independent and identical channels open and contributing to macroscopic current I from single channel conductance i:

$$\sigma_I^2 = iI - I^2/N \qquad (2\text{-}4)$$

Where σ_I^2 is the variance from each channel.

Patch clamp techniques require a gigaseal which allows the isolation of single ion channels resulting in direct measurements of unitary current. The conductance is calculated from the slope of current-voltage curves derived from Ohm's law. Unitary conductance is calculated from point amplitude histograms at given potentials.

All digitized current can be plotted as a histogram with a peak for each closed and open level. The area under the peak is proportional to the time spent at that level as shown in Figure 2-3. Point-amplitude histograms for each experiment at a known

potential were plotted from information obtained from the single channel event detection. A statistical frequency count with a minimum bin width of 0.05 mm was performed and fitted by the maximum likelihood with a continuous Gaussian curve using Origin software as in Figure 2-3.

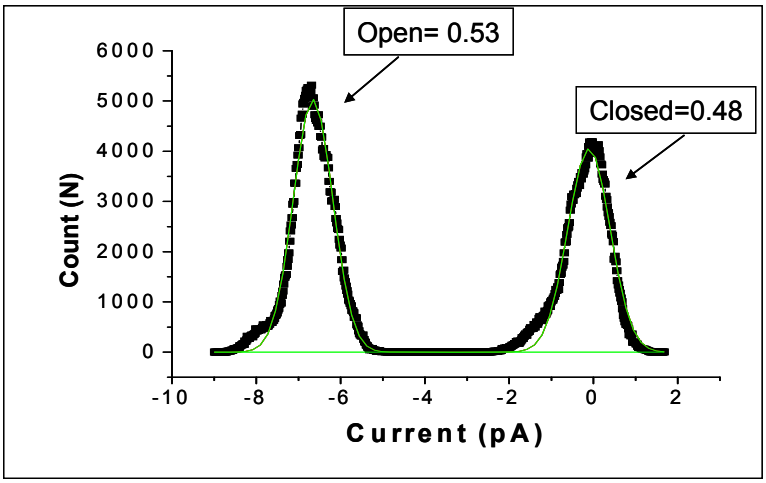

Figure 2-3. Histogram fitted by the maximum likelihood with a continuous Gaussian curve representing open and closed event distributions.

The open P_{open} /close P_{close} probability and the unitary conductance γ, are calculated from this distribution. Both probabilities were estimated as a fraction of the time the channel remained in the respective state, divided by the overall recording time. Unitary conductance is calculated by dividing the average amplitude from the amplitude histograms by the applied potential. Pore forming proteins must reproducibly conduct in a specific range to be considered as ion channels. Kinetic calculations of lifetime are determined by using a probability density function (pdf).

Probability density function: As mentioned throughout this chapter, single channel activity exists in at least two states: the open and closed state. Considering the simplest kinetic model of just two states, the transition mechanism from one state to the other is denoted by:

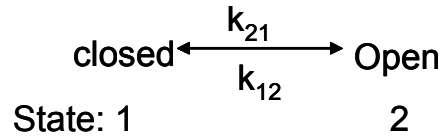

Where k_{21} is the transition from closed to the open state, and k_{12} is the transition from open to the closed state. This unimolecular transition reaction involves conformational changes of the ion channel from one state to the other.[121] Random thermal movements allow the bonds of the protein to vibrate, bend, and stretch in the correct rapid transition on the picosecond scale. This unsystematic motion leads to the randomness in the lifetime of the open and closed state.[122] The probability p that the channel will overcome the energy barrier holding the channel open and fail to close is (1-p) p. The probability that it will succeed in the next attempt r is independent of the first attempt:

$$P(r) = (1-p)^{r-1}p, \quad r = 1, 2, 3, \infty \tag{2-5}$$

The lifetime is therefore a probability distribution and is expressed by a probability density function (pdf) where the area under the curve represents the probability that the lifetime is less than the specified time t.[123] The exponential density of a time interval with mean of $\tau = 1/\lambda$, and equals:

$$f(t) = \tau_i^{-1} e^{-t/\tau} \qquad t>0 \tag{2-6}$$

The area under the curve for any pdf must equal unity. Therefore an ensemble of ion channels will lead to a corresponding number of exponential distributions *a*, and the total area of the *i*th component, will also have to equal unity when τ_i is mean.[123]

$$f(t) = \Sigma\, a_i \tau_i^{-1} e^{-t/\tau} \tag{2-7}$$

Data obtained from pdf are displayed in multi-component histograms where they are usually characterized by three different time values. These time values are representative of the different open and closed levels exhibited by the ion channel.

Dynamic Light Scattering

Theory

The principle of the dynamic light scattering technique is that the scattering of light can be viewed as a result of microscopic heterogeneities within the illuminated volume. When a volume of a homogeneous sample is illuminated with a beam of light, the scattered waves will have the same amplitude and interfere destructively in all directions, except in the direction of the incident beam. If a heterogeneous sample is being analyzed, the index of refraction would differ from the average value at some location, as a consequence, the wave that is scattered at this location would not be compensated for and some light would be observed in directions other than the incident light and light scattering occurs, as shown in Figure 2-4.

There are two ways to approach the phenomenon of light scattered by particulate matter in solution. The one is to consider the suspension as a homogeneous medium and ascribe light scattering to the spatial fluctuations of the solute. This is appropriate for solutions of small molecules in which the average distance between the center of the scatterers is small compared to the wavelength of light. The second is to consider each individual solute particle as a heterogeneity and therefore as a source of light scattering. The latter is more appropriate for solutions of large macromolecules and colloids, where the average distance between particles centers is comparable to the wavelength of light.

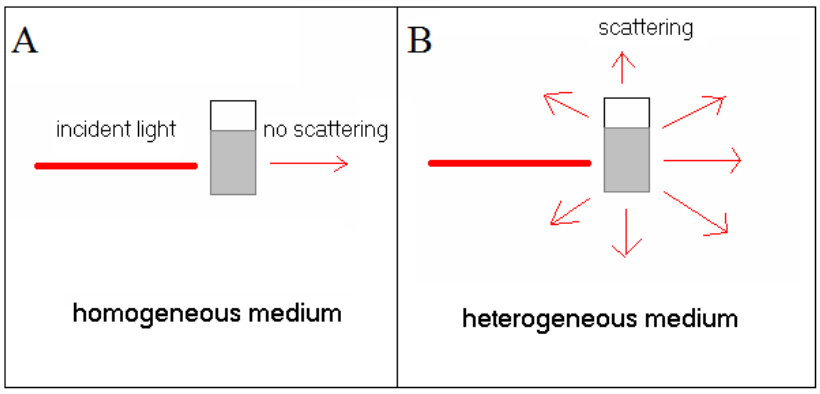

Figure 2-4. Possibilities for the interaction of a laser beam with a liquid sample. In a homogeneous medium, waves of the scattered light interact destructively, producing no scattering (A); while in a heterogeneous medium scattering is produced (B).

In cases in which the size of the scatterers is not small compared to the wavelength of light, the interference of the electromagnetic waves scattered by the solute is not all constructive and the phases of these waves must be taken into account. If the phase of a wave scattered at the origin is used as a reference, the phase of a wave scattered at a point with radius vector ***r*** is ***q.r***. The vector ***q*** is called the "scattering vector", which is a fundamental characteristic of any scattering process. The length of the vector is indicated in equation 2-1.[124]

$$q = |q| = \frac{4\pi\eta}{\lambda}\sin\frac{\Theta}{2} \qquad (2\text{-}7)$$

where η is the refractive index of the medium
λ is the wavelength of light
Θ is the scattering angle

The essence of the DLS technique is to measure the temporal correlations in the fluctuations in the intensity of the scattered light and to reconstruct from these data the physical characteristics of the scatterers. In a suspension of particles, the scatterers are randomly distributed within the scattering volume. Since the size of the scattering

volume is much larger than $\boldsymbol{q}^{-1}$ (with the exception of nearly forward scattering, where $\boldsymbol{q}\sim \Theta = 0$), the phases of the waves scattered by different particles vary dramatically. As a result, the average amplitude of the scattered light is proportional to $N^{1/2}$, where N is the number of scatterers, and the average intensity is simply N times the intensity scattered by an individual particle. The local intensity, however, fluctuates from one point to another around its average value. As the scattering particles move, the interference pattern changes in time resulting in temporal fluctuations in the intensity of light detected at the the observation point.[125]

In a DLS measurement, the instrument detects a random signal. The information is contained in the correlation function of this signal *i(t)*, which in the case of DLS is the photocurrent, defined as in equation 2-8

$$G^2(\tau) = \langle i(t) \bullet i(t+\tau) \rangle \qquad (2\text{-}8)$$

The notation $G^2(\tau)$ is introduced to distinguish the correlation function of the photocurrent from the correlation function of the electromagnetic field $G^1(\tau)$ (which is the Fourier transform of the light spectrum):

$$G^1(\tau) = \langle E(t) \bullet E^*(t+\tau) \rangle \qquad (2\text{-}9)$$

The angular brackets denote an average over time *t*. This time averaging, an inherent feature of the DLS method, is necessary to extract information from the random fluctuations in the intensity of the scattered light.

In the majority of practical cases, the scattered light is a sum of waves scattered by many independent particles and therefore displays Gaussian statistics. This being the case, there is a relation between the intensity correlation function $G^2(\tau)$ and the electromagnetic field correlation function $G^1(\tau)$:

$$G^2(t) = I_o{}^2(1+\gamma\left|g^1(\tau)\right|^2 \qquad (2\text{-}10)$$

Here $g^1(\tau) = G^1(\tau)/ G^1(0)$ is the normalized field correlation function, I_o is the average intensity of the scattered light and γ is the intensity factor.[125]

Temporal fluctuations of the intensity of the scattered light are caused by the Brownian motion of the scatterers. The speed of the particles is related to the size, small particles move faster than large particles. Though each particle moves randomly; in a unit time more particles leave regions of high concentration than region of low concentration. This results in a net flux of particles along the concentration gradient. Brownian motion is then responsible for the diffusion of the solute, and is quantitatively characterize by the diffusion coefficient, *D*. Rigorous mathematical analysis of the process of light scattering by Brownian particles leads to the following expression for the correlation function of the scattered light:

$$\left|g^1(\tau)\right| = \exp(-Dq^2\tau) \qquad (2\text{-}11)$$

The diffusion coefficient in an infinitely dilute solution is determined by particle geometry. For spherical particles, the relation between the radius *R* and its diffusion coefficient *D* is given by the Stokes-Einstein equation:

$$D = \frac{k_b T}{6\pi\eta R} \qquad (2\text{-}12)$$

where: k_b is the Boltzman constant
η is the viscosity of the solution
T is the absolute temperature

Hence, from equation 2-11 the diffusion coefficient can be obtained from the correlation function $g^1(\tau)$. Assuming that the scatterers are spherical, Equation 2-12 can be used to obtain the hydrodynamic radius of the particles. We used the imaging techniques to investigate whether the shape of the particles matched this requirement.

In this study, the suspensions obtained where not monodisperse but rather, made of particles a range of sizes. This made the analysis of the data obtained more complicated. In the case of polydispersed samples, a different analysis of the correlation function is required. For a continuous distribution of scattering particle size, the correlation function is obtained from the following equation

$$\left|g^{(1)}\right|(\tau) = \frac{1}{I_o}\int I(D)\exp\left(-Dq^2\tau\right)dT \qquad (2\text{-}13)$$

where $I(D)dD = N(D)I_o(D)dD$ is the intensity of light scattered by particles having their diffusion coefficient in the interval $[D,D+dD]$, $[N(D)dD]$ is the number of these particles in the scattering volume, $I_o(D)$ is the intensity of light scattered by each of them.[126]

The main goal of the software is to reconstruct as precisely as possible the distribution function $I(D)$ from the experimentally measured function $G^2_{exp}(\tau)$.The main problem encountered is that dramatically different distributions $I(D)$ lead to nearly identical correlation functions of the scattered light and therefore are equally acceptable fits of the experimental data. There are three typical approaches to solve this problem:

i) the direct fit method, in which a functional form of $I(D)$ is assumed *a priori* and the parameters that lead to the best fit of $G^2_{theor}(\tau)$ to $G^2_{exp}(\tau)$ are determined,

ii) the method of cumulants. This approach focuses on the "stable" characteristics of the distribution, which are the moments of the distribution, or closely related quantities called cumulants. The first cumulant of the distribution that gives the average diffusion coefficient D^*, can be determined from the initial slope of the field correlation function, as shown below

$$\frac{-d}{d\tau}\ln\left|g^{(1)}(\tau)\right|_{\tau\to o} = \frac{1}{I_o}\int I(D)Dq^2dD = D^*q^2 \qquad (2\text{-}14)$$

The second cumulant, the width of the distribution, is obtained from the curvature of the initial part of the correlation function

iii) regularization, a combination of the first previous methods mentioned assumes that the distribution $I(D)$ is a smooth function and seeks a non negative

> distribution producing the best fit to the experimental data. This method is used in different approaches used to reconstruct the scattering particle distribution from DLS data. The key point is the selection of the smoothness of the distribution. If the smoothing is too strong, the distribution will be stable but will lack details. If the smoothing is too weak, false spikes will appear in the distribution. The moments of the distribution reconstructed by the regularization procedure gives unbiased (apart from smoothing) information on the shape of the distribution.[126]

DLS was used as the primary technique to determine the sizes of the prepared lipid vesicles due to its ease of operation and the small amount of samples needed. As shown in Figure 2-4, the difference in size between different species can be visualized qualitative by a comparison of the normalized correlation function obtained. Our lipid samples were extruded through polycarbonate membranes with different pore sizes to manipulate the final sizes of vesicles. Extrusion also served to eliminate dust or aggregated particles that could not be separated by sonication. This is especially important due to the dependence of the intensity of the light scattered by a particle to the sixth power of its radius, which would result on the signal of the particles being obscured by the aggregates, producing an overestimation of their diameter.

Experimental settings

Throughout this work two instruments were used, a PDDLS/CoolBatch 90T detector with a PD2000DLSplus correlator, manufactured by Precision Detectors Inc, and a 90 Plus/BI-MAS detector with a BI 9000AT digital correlator manufactured by Brookhaven Inc. In both cases the detector was placed at 90 °from the incident beam. Each instrument works with its own software for size determination, the Precision Deconvolve 32 in the first case, and the BI-ISDAW advanced size distribution software, in the second case.

The vesicles prepared were sonicated for approximately 5 minutes and filtered through 0.45 μm filters before DLS analysis. Sonication was intended to break any

aggregates that were not hydrated from the dry lipid film obtained after removal of chloroform from lipids. These aggregates were especially observed in samples with greater than 50% molar concentrations of DPhPE vesicles. The samples needed to be diluted to avoid multiple scattering. The extent of dilution differed from sample to sample due to the differences in sizes and, as a consequence, on the intensity of light they scattered. As indicated by the manufacturers of the instruments, a total intensity of the scattered light between 100 to 300 kilocounts per second (kcps) was used; being the concentration of scatterers adjusted until these values were reached. Subsequently, the sample time was adjusted after a quick examination of the correlation function. The sample time is directly related to the size of the particles, so it can be adjusted to obtain the proper fit of the correlation function. After these setting were adjusted, the measurements were performed in 3 minute runs. This time was observed to be optimal to obtain a good signal to noise ratio, resulting in stable and reproducible results. The final results reported were obtained by the average of three measurements.

Negative Staining Transmission Electron Microscopy

Theory

Transmission electron microscopy is particularly useful in analyzing particles with diameters similar to the wavelength of the light. The transmission electron microscope uses a beam of electrons instead of light, resulting in better resolution, due to the shorter wavelength of the electrons, compared to photons (Figure 2-5).

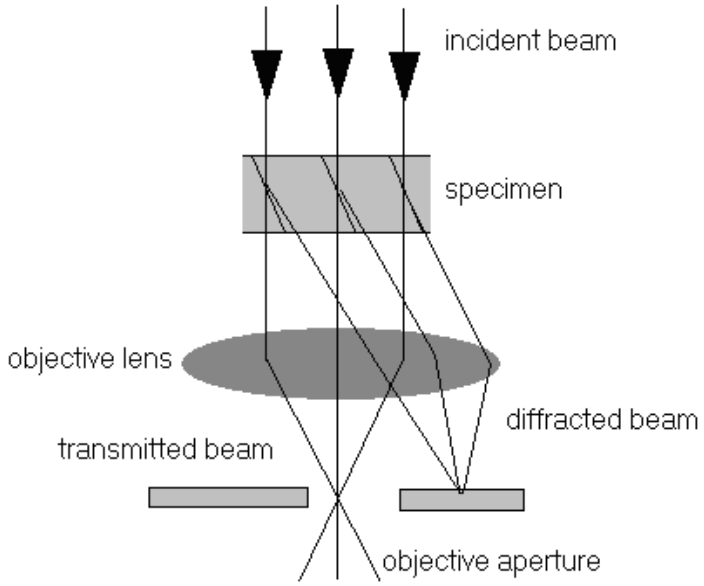

Figure 2-5. A simple representation of the basic concept of a transmission electron microscope operating in the bright field mode.

In the electron microscope, electromagnetic lenses are used to focus the beam of electrons into a tight coherent beam, which is then focused on the sample. Data is collected after the beam has passed through the sample. Our imaging has been performed in the bright field mode, meaning that after the beam of electrons has passed the sample deposited on the substrate, an objective aperture has been inserted. This aperture allows the electrons in the transmitted field to pass and contribute to the resulting bright field image, rejecting the electrons that had been scattered by the sample as shown in Figure 2-5. The lack of electron density with our samples necessitated the use of staining with the dye of choice being uranyl acetate which stains hydrophilic parts of the vesicle samples.

Experimental settings

The instrument used in this study was a Hitachi H-7000, with a maximum resolution of 0.2 nm and a maximum acceleration voltage of 125 kV. Imaging the

vesicles was made more challenging due to the low electron density, as explained above. Moreover, due to their size, especially the templates, getting a decent focus that can be used to measure the size of the particles was difficult. Images of our vesicle samples were taken with a voltage of 100 kV. We used this technique to image our vesicle samples before and after the dialysis procedure we use for the formation of proteoliposomes.

Similarly to what was observed with DLS, the particles needed to be diluted before loading them on the grids. If the concentration was too high, the particles were deposited as multilayer, making impossible their visualization. It was determined that a concentration of about 0.1 mg/mL was optimal in most of the cases to load the grids. Before insertion of the samples containing the grids in the microscope, the samples were stained with a methanolic solution of uranyl acetate (UA) for 1 minute. This is a common staining agent for biological samples, used primary to stain hydrophilic regions. Images were taken at different spots of the same grid to confirm that the species observed were present in most of the suspension and that they were not an unusual finding. Size analysis was performed by comparison of the diameter of the particles and the scale bar in the image. This was done in the Adobe photoshop® software.

Atomic Force Microscopy

Theory

Atomic force microscopy, since its introduction in 1986, has been used in many different applications, especially because of the improved resolution compared to other microscopy techniques. In case of the study documented here, the main reason to use this technique is the ability of AFM to obtain information on three dimensions without the need of any coatings or stains, an advantage over negative staining TEM. Additionally,

AFM enabled the obtaining of information on the surface morphology before and after vesicle fusion, thereby clearly observing changes in the lipid assemblies as they interacted with solid substrates.

The technique is based on the interaction of the tip of a cantilever with the sample deposited on a substrate. The instrument measures the forces between the tip of the flexible cantilever and the sample. The basic idea is that the local or attractive forces between the tip and the sample are converted into a bending, or deflection, of the cantilever. The key feature is that the force between the probe and the sample is maintained constant while the probe is raster scanned across the surface. In order to detect the probe bending, a laser beam is reflected from the back of the cantilever onto a detector, in such a way that a small change in the bending angle of the cantilever is converted to a measurable large deflection in the position of the reflected spots. The deflection observed then is converted into an electrical signal, to produce an image of the surface. A simple representation of the instrument setup is shown in Figure 2-6. In order to avoid any non desired interaction between the probe and the particles the instrument was used in the tapping mode. In this mode, the cantilever is oscillated close to its resonance frequency and the tip taps the surface only periodically, reducing significantly the lateral force. This means that the probe is free to oscillate up and down at its resonance frequency as a consequence of the interaction with the substrate when it comes extremely close to it. In tapping mode, the image is obtained by imaging the force of the oscillating contacts of the tip with the sample surface.[127, 128]

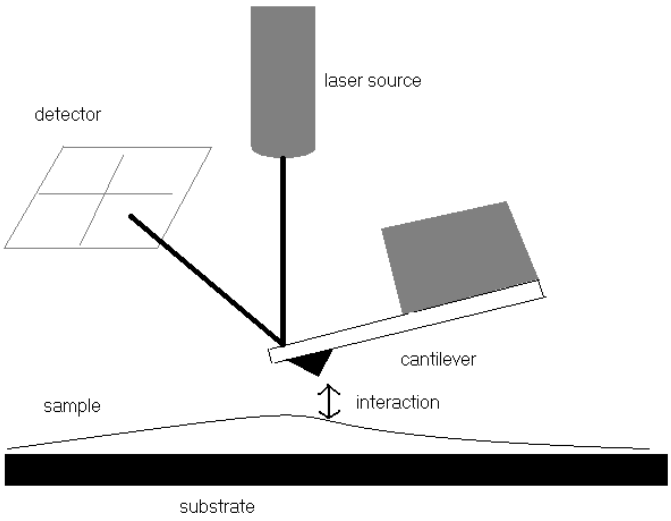

Figure 2-6. A simple representation of the basic setup of the atomic force microscope.

Experimental settings

The instrument used in this study was a Nanoscope III, manufactured by Digital Instruments, Inc. Imaging was performed in tapping mode, using silicon probes (Nanosensors, with dimensions: T=3.8-4.5 μm, W= 26-27 μm, L= 128 μm). The z-calibration was performed with a silicon grating (TGZ01, Mikromash), with a step height of 20 nm (accuracy 1 nm). Images were analyzed with the Nanoscope III software provided by the manufacturer.

To determine how accurate the z-measurements were in the instrument, analysis was done of a silicon grating calibration grid with a step height of 19.66 +/- 1 nm, as reported by the manufacturer. The instrument was used in contact mode. The area was scanned at 2.44 Hz and at 256 samples per line. The image was flattened with a first order fit, as suggested by the instrument manual. Figure 2-7 shows the bearing analysis, in which the software determines the distribution of data points in the Z-axis. The two spikes in the histogram correspond to two elevations on the surface: the bottom and top surface. The red box (Hist rel depth) indicates the distance between the two

cursors on the histogram (19.93 nm), which represent the height determined by the instrument. The result showed that the height was measured with an accuracy of 1.4 %, which confirmed that the measurements performed were accurate.

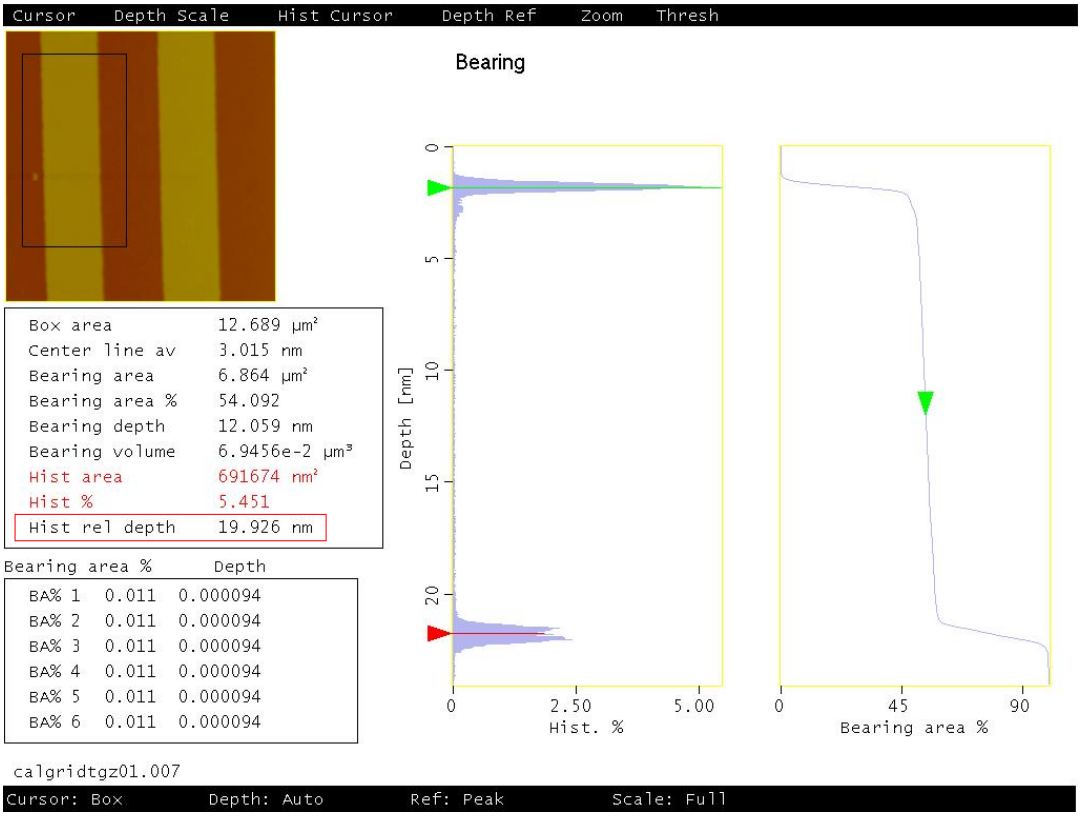

Figure 2-7. Data analysis of a Z-axis calibration grid performed in contact mode.

The samples were deposited on gold substrates by adding a couple of drops of the suspension and the solvent left to evaporate at room temperature. No other treatment was performed before analysis. The images were obtained with the scanner E, which offers a maximum imaging area of 15 x 15 μm. The exact conditions for the different parameters used varied from sample to sample, although average values or ranges can be reported. To image the samples, first, a fast scan was performed to identify areas were the sample was deposited, after which the tip was taken to one of this spots to zoom in and acquire an image of proper quality. Typically, we used 512 samples per

line, the best quality possible with our instrument. Next, the amplitude setpoint was decreased slightly to optimize the force use to scan the surface. This was stopped when the trace and retrace profiles in the section analysis looked similar. The scan rate was adjusted based on the dimension of the image, for areas between 2 x 2 to 2.5 x 2.5 μm, a typical scan rate between 1-1.5 Hz was used, and this value had to be increased for smaller areas scanned, typically to 2-2.5 Hz. This was done to maintain good track of the tip on the z-axis, which allowed the visualization of the changes in the height profile. Finally, the integral and proportional gains were adjusted to improve the quality of the images, with typical values of 0.35-0.45 and 0.4-0.6, respectively.

The section analysis was performed then with the images without any post-treatment. The particles used to measure the diameter and height profile were selected from each image taken after zooming in the area of interest and confirmation that both dimensions were possible to determine without ambiguities. Unless otherwise stated, the height images were used for the characterization of the types of assemblies obtained when lipid vesicles at different concentrations interact with gold substrates. Because lipid bilayer membranes are very thin unless deposited as multi-layers, it was easily discernible whether deposition of vesicles occurred rather than rapture and fusion to form bilayers. Vesicles being spherical would naturally have a much greater height profile in comparison to bilayer membranes.

Experimental Procedures

Molecular Biology

DNA manipulation

The murine BK_{Ca} channel (*mSlo*) gene was provided by the laboratory of Lawrence Salkoff, Washington University, St. Louis, MO. The maxi-K gene is contained

in the plasmid: pcDNAOX, a pcDNA3 derivative which contains flanking 5'- and 3'-UTR sequence from *Xenopus* Beta-globin. Site-directed-mutagenesis was performed with the QuickChange II XL kit (Stratagene). The competent *E.coli* cells used were purchased from Stratagene (XL-10gold), Invitrogen (Top-10, INV-110, BL21 (DE3), or Novagen/EMD Bioscience (BL21 (DE3), Rosetta-2 (DE3). Restriction enzymes were purchased from New England Biolabs (NEB), Calf intestinal alkaline phosphatase was either from Promega or NEB, and T4 DNA-ligase was from NEB. Gel extraction and purification was done with the QIAquick gel extraction kit (Qiagen) from agarose gels. Other media and reagents were from Sigma or Fisher Scientific. Sequencing was performed by the fluorescent dideoxy terminator method at either the Whitney Laboratory for Marine Bioscience, St. Augustine, FL or at the ICBR sequencing core, University of Florida, Gainesville, FL. All deoxyoligonucleotide primers were synthesized and PAGE purified by Integrated DNA Technologies, Coralville, IA. To allow deletion of the maxi-K C-terminal domain and fusion with mRFP1 in pcDNAOX, an insertion coding for a BamHI site flanked by a BstBI site was added in place of the BK_{Ca} stop codon by site directed mutagenesis. A second BamHI site was added by site directed mutagenesis in a position such that digest with BamHI followed by gel purification and re-ligation would result in the deletion of the C-terminal domain encoded between the two BamHI sites. As there was no stop codon added at this point of truncation, an additional 12 amino acid residues (ALRTPRRPELFF^{347}-stop) are coded for at the C-terminus of maxi-K mSlo CTD construct.

The monomeric red fluorescent protein gene was provided by the laboratory of Roger Tsien, University of California, San Diego, CA. The mRFP1 gene was contained

in the plasmid pRSET-B. Initially, the mRFP1 gene was cut away from the pRSET-B plasmid with BamHI and BstBI enzymes, then purified by gel extraction ("mRFP1-insert", above). XT-PCR was used to modify the mRFP1 gene by addition of a C-terminal extension containing a hexa-histidine tag, a new stop codon, BstBI restriction site, and unique SpeI restriction site. The following primers were utilized for XT-PCR: (extension sequence is underlined) "RFPhis-forward": (5'TAAGGATCCGATGGCCTCCTCCGAGG)

"RFPhis-reverse": (5'TATTTCGAACTAGAGATGGTGGTGATGATGTGC-GGCGCCGGTGGAGTGGCG). This C-terminally His-tagged mRFP1 gene ("mRFP1His") was subsequently fused to the C-terminally deleted BK_{Ca} in the pcDNAOX vector resulting in the preparation of the "CTD2-mRFP1His" construct. "CTD2-mRFP1His" gene cassettes were annealed and ligated to a linearized pRSET-M vector to complete the directional cloning. The ligated vector was transformed into competent cells (*E.coli* Top-10, Invitrogen), and grown on selective agar. Plasmid DNA purified from transformed colonies was screened by double restriction digest with an enzyme unique to the His-tag sequence (SpeI) and an enzyme unique to BK_{Ca} channels (PmlI). Positive subclones were confirmed by sequencing.

RNA synthesis and injection into oocytes

Plasmid DNA was transcribed using the Ambion mMessage mMachine T7 Ultra kit. RNA was precipitated with lithium chloride, washed and centrifuged in 70% ethanol, and then dissolved in diethylpyrocarbonate (DEPC) treated water (RNase free). Stage V or VI oocytes were harvested from adult *Xenopus laevis* (Xenopus Express, Florida) and their follicular layer removed by exposure to 2mg/ml collagenase for 45min.The transcribed RNA was injected with a Drummond Nanoject microinjector at a volume of

46nl per oocyte (approximately 50ng RNA) and the oocytes were incubated at 19 degrees in ND96 media consisting of 96 mM NaCl, 2 mM KCl, 1 mM $MgCl_2$, 10 mM HEPES, 1.8 mM $CaCl_2$, adjusted to pH 7.4 with NaOH, enriched with 2.5% sodium pyruvate, 1% penstrep, and 5% horse serum. Functional channel expression was determined by use of two-electrode voltage clamping within 3 days for recombinant BK_{Ca} channels.

Sodium dodecyl sulfate polyacrylamide gel electrophoresis

SDS-PAGE is a technique used to separate proteins according to their electrophoretic mobility which is a function of the length of the polypeptide chain or molecular weight as well as higher order protein folding, posttranslational modifications and other factors. SDS is an anionic detergent which denatures secondary and non–disulfide–linked tertiary structures, and applies a negative charge to each protein in proportion to its mass. Dissolved molecules in an electric field migrate within polyacrylamide gel at a speed determined by their charge: mass ratio upon the application of an electric field resulting in separation by size. Smaller proteins travel faster through the pores of the gel while larger proteins move slower. Ladders with known protein molecular weights are used to identify the target protein. The molecular weight of the recombinant BK_{Ca} channel with a truncated C-terminus and mRFP1 and hexahistidine fusion tags is around 70 kDa. After the purification process, samples were analyzed by SDS-PAGE in a 4-20% gradient Tris-HCl polyacrylamide gel (Bio-Rad Hercules, CA) in Tris-glycine running buffer. Each well was loaded with 13 µl of Laemmli sample buffer, 2.0 µl of Dithiothreitol (DTT) reducing agent and 10 µl of the protein sample and the gel was run for 1 hour with power supply settings at 100 mV and 100

mA. Staining of the gel was done using SYPRO Ruby Coomassie dye and imaging by a Biorad GelDoc system.

Western blotting

Western Blot was performed after gel fractionation of the BK_{Ca} channel to visualize the protein and therefore confirm that the histidine-tagged BK_{Ca} channel was eluted from chromatography columns. This immunological technique attaches antibodies to the target protein in a given sample. The proteins fractionated by SDS-PAGE are transferred to a membrane sheet. Primary-antibodies are next added to the membrane sheet to bind the specific proteins followed by enzyme-tagged antibodies that attach to the primary-antibody. Binding a substrate to the enzyme allows visualization of the selected protein by either colorimetric or fluorimetric detection.

In this study, BK_{Ca} channels were electro-transferred to Immobilon Polyvinylidene Fluoride (PVDF) membranes (Millipore Corporation, MA) at 105 mV for 70 minutes. Blots were blocked in 2 % milk/TBS for an hour at room temperature. Western Blot analysis was performed using the: primary-antibodies penta-His-tag antibody or HRP-His-Probe (Thermo Fisher Sic. Pierce Protein Research, Rockford, IL) against the BK_{Ca} channel C-terminally fused histidine-tag. The secondary antibody used for the channel was Goat-anti-Rabbit HRP (BioRad). When protein expression was too low for recognition with the penta-His-antibody, we used the HRP-His-Probe (HRP-His-Probe was used for the majority of the study). The HRP-His-probe uses a Ni-chelating group that binds to the hexa-histidine tag present on the protein. The HRP-His-probe reacts with the substrate giving off a chemiluminescent signal that was quantified using X-ray sensitive film (Kodak). The film was developed using the dipping method whereby the film was submerged in each of the following for 90 second intervals: developer, water,

and fixer (Developer and Fixer purchased from Kodak). The film was then rinsed under running water for 2 minutes and quantified.

Vesicle Formation Using DPhPC and DPhPE Lipids

Archaea analogue phospholipids 1,2-diphytanoyl-*sn*-glycero-3-phosphocholine (DPhPC) and 1,2-diphytanoyl-*sn*-glycero-3-phosphoethanolamine (DPhPE) in chloroform were purchased from Avanti Polar Lipids Inc. (Alabaster, AL, USA), and were used without further purification. Chloroform solutions of the lipids (50 mg/mL) were mixed to a 7:3 molar ratio (DPhPC/DPhPE) followed by rotary evaporation until a dry lipid film was obtained at the bottom of the vessel. The dry lipid film was then placed under vacuum in a dessicator overnight to eliminate any residual chloroform. The lipids were then lyophilized before hydration for 1 hour at 50 ˚C in buffer (5 mM MOPS, 250 mM KCl, 0.1 mM $CaCl_2$, pH 7.4) to a final concentration of 2 mg/mL. After being cooled to room temperature the suspension was sonicated for 5 min, and extruded (21 passes) through a 100 nm polycarbonate membrane in a mini-extruder (Avanti Polar Lipids Inc.).

Reconstitution of Recombinant Proteins in Liposomes

A detergent-mediated procedure was used for reconstitution of BK_{Ca} channels into lipid vesicles. A 1 ml suspension of pre-formed liposomes prepared using DPhPC:DPhPE lipids in a 7:3 molar ratio as detailed above were solubilized by the addition of a 1 ml solution of 10 mM β-octyl glucoside. A 500 µl sample of protein solubilized in 10 mM β - OG detergent that was eluted from the AKTA protein purifier is added to the solubilized liposomes resulting in co-micellization. The final mixture is composed of purified membrane proteins in an excess of liposomes and β-octyl glucoside detergent, forming a solution of mixed lipid-protein-detergent and lipid-detergent micelles. The next step involves removal of detergent from these micellar

solutions which leads to a progressive formation of closed lipid bilayers in which the proteins eventually incorporate. We remove the detergent by injecting the micellar solutions in 10,000 kDa membrane MW cut-off dialysis cassettes (Pierce) and these are immersed in 1 liter dialysis buffer (5 mM MOPS, 250 mM KCl, 0.1 mM $CaCl_2$, pH 7.4) for 2 hours at room temperature, the dialysis buffer is changed and dialysis continued for another 2 hours at room temperature and then a final change of dialysis buffer made and this is let to continue for 18 hours at 4 ˚C. All dialysis buffers have pre-cleaned polystyrene beads outside the dialysis bags and the process proceeds with constant stirring.

CHAPTER 3
BK_{CA} CHANNEL EXPRESSION, PURIFICATION AND FUNCTIONAL RECONSTITUTION IN LIPID VESICLES

Introduction

The demand for high yields of mammalian proteins for routine *in vitro* applications necessitates the use of heterologous systems, which are non-native systems for protein expression as compared to isolation from native tissue. In 1971 Gurdon and his co-workers established that upon injection with complementary RNA (transcribed from complementary DNA coding for the protein of interest) and after a brief incubation period for translation, oocytes extracted from the South-African clawed frog *Xenopus laevis* could appropriately express the RNA encoded proteins with high efficiency.[115] Since then, *Xenopus* oocytes have become very popular for electrophysiological analysis of channels, receptors and transporters, although several alternative expression systems for ion channels have been discovered over the years, including mammalian cells,[129, 130] insect cells e.g. *Spodoptera frungiperda* (Sf9 cells),[24, 131] yeast [132-134] and bacterial cell lines.[135, 136] The criteria for selection of the most appropriate expression system are based on factors such as the desired level of protein expression, presence of homologous endogenous receptors in the host cell, the experimental design in use, among others.

Heterologous expression of proteins in oocytes can be achieved by two methods. The most commonly used approach involves *in vitro* transcription, followed by the microinjection of complementary RNA coding for the protein of interest into the oocyte cytoplasm where translation occurs. Subsequently, docking and functional insertion of the protein into the oocyte plasma membrane is effected. An alternative approach involves a direct injection of complementary DNA into the oocyte nucleus. The two

methods of introducing genetic material into the oocyte are summarized in Figure 3-1. Insertion of cDNA into the nucleus is less favored because of the potential risk of damaging the nuclear membrane during the microinjection process. Furthermore, a visual localization of the nucleus is required, making direct injection of cDNA technically challenging and less efficient.

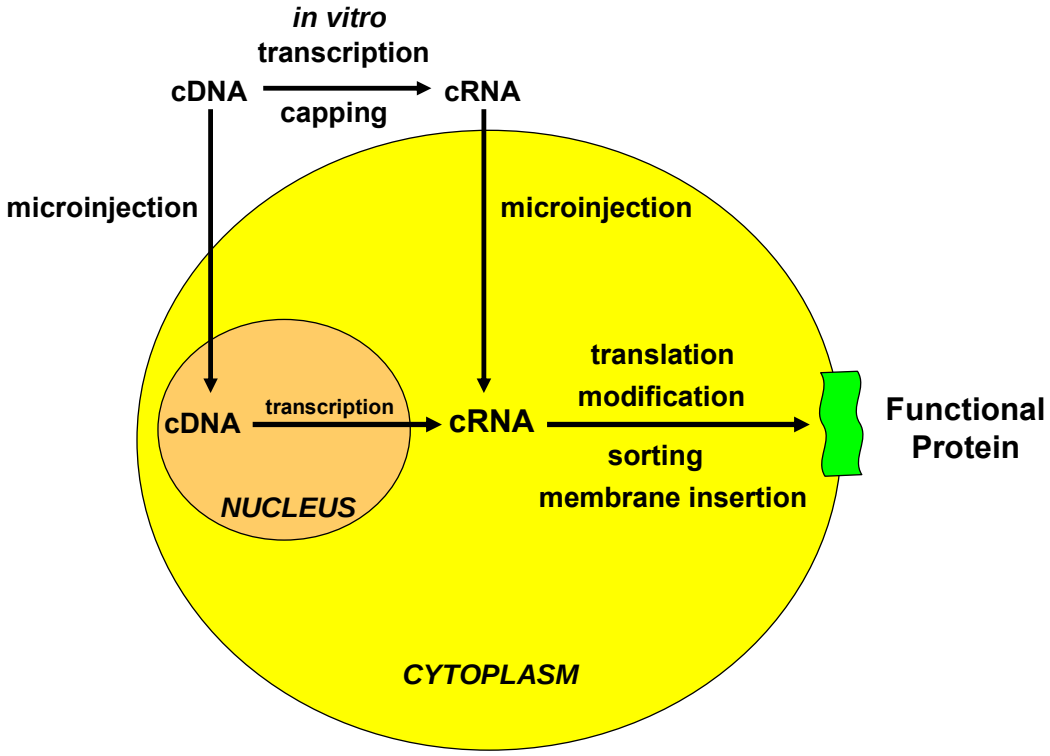

Figure 3-1. Summary of the approaches used to introduce genetic material into oocytes.

In this study, *Xenopus* oocytes were used for the expression of BK_{Ca} channels because oocytes express a low number of endogenous membrane transporters and channels, and they are virtually independent from exogenous nutrients.[137] The downstream application for the expressed BK_{Ca} channels here involves the incorporation of reconstituted channels in a bilayer lipid membrane that is tethered to a gold substrate. The overall goal of the project is the development of a biosensor based

on the direct interfacing of the sensor element – the BK_{Ca} channel – to the microelectronics of a detector, thereby creating a real-time sensory platform. The gold substrate onto which the bilayer membrane is tethered serves as an electrode which can be used to make electrical measurements. The tethered region of the tBLM is limited in terms of ionic mobility, therefore, in order to optimize on the ionic reservoir in the tethered region beneath the tBLM, a genetic modification of the channels to be incorporated is necessitated. The full-length BK_{Ca} channel is tetrameric in structure with each of the four domains having 1200 amino acid residues, majority of which are located intracellularly towards the C-terminus, forming a bulky structure referred to as the "calcium bowl" as illustrated in Figure1-3. For ease of incorporation into the tBLM, C-terminally deleted constructs were prepared, with truncations after the amino acid residue at position 347 located just after the S6 transmembrane segment, thus eliminating most of the intracellular domain as illustrated in Figure 3-2.

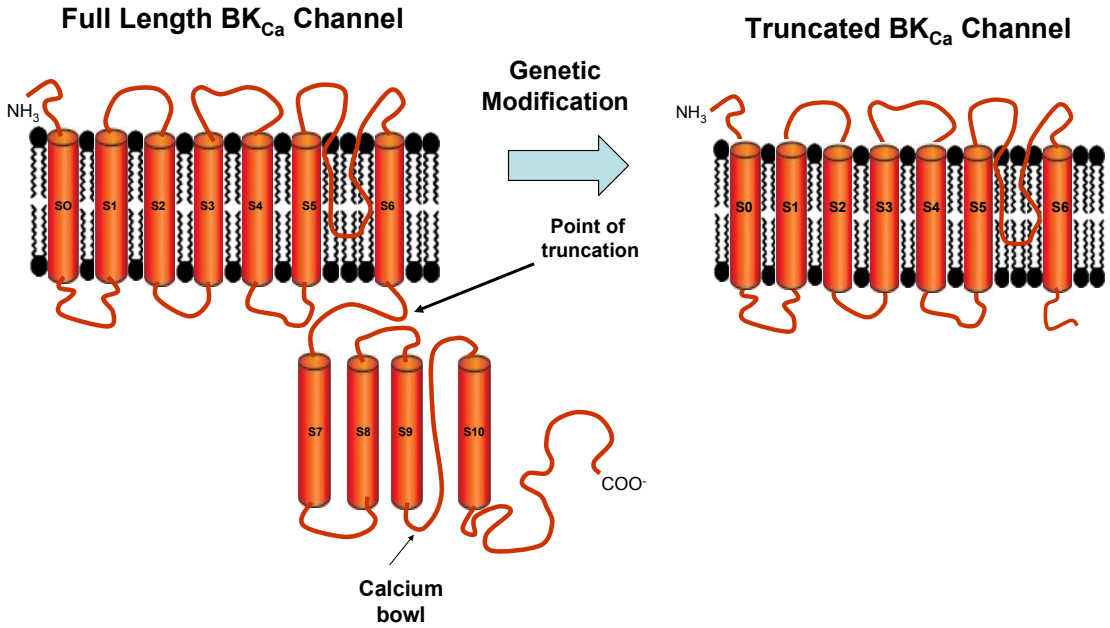

Figure 3-2. Illustration of the full length BK_{Ca} channel showing the point of truncation and the truncated product.

Fusion tags constitute a valuable component for the expression of biologically active recombinant proteins and they are useful for enhancing solubility of proteins, detection, aiding of purification and for many other roles. Two different tags were fused to the BK_{Ca} channel, a hexa-histidine tag and the monomeric red fluorescent protein (mRFP1) derived from *Discosoma* species. The hexa-histidine tag was added to facilitate a simple, one-step affinity purification of the ion channels based on the high selective affinity of the histidine-tagged protein to the Ni^{2+} chelated as an affinity ligand in the chromatography columns used. The mRFP1 on the other hand was used as a localization marker, to allow visualization of channels in oocytes for monitoring expression, and in vesicles to confirm successful reconstitution. The excitation and emission peaks for mRFP1 are 584 nm and 607 nm respectively and these confer spectral separation from autofluorescence and other fluorescent proteins.[138] Other features that make mRFP1 suitable as a fluorescent fusion protein are its rapid maturation relative to other fluorescent fusion proteins, and minimal emission when excited at wavelengths optimal for the more commonly used green fluorescent protein (GFP) from the jellyfish *Aequorea Victoria*; mRFP1 can therefore be used for multicolor labeling in combination with GFP.[139] Figure 3-3 shows the chimeric BK_{Ca} channel construct expressed for this study with the numbers of amino acid residues as well as positions of fusion tags.

Figure 3-3. Illustration depicting the chimeric C-terminally deleted BK_{Ca} channel with positions of fusion proteins and numbers of amino acid residues.

In general, the purification of membrane proteins involves removal from the membrane, using methods such as sonication, use of organic solvents, chemical modifications of proteins, extraction using chaotropic reagents, alkaline or Ethylene-diaminetetraacetic acid (EDTA) treatment, fractional digestion, solubilization with acetic acid, treatment with urea or by detergent solubilization.[140] The procedure utilized with the greatest success for isolation of active transport proteins from the plasma membrane is detergent solubilization, though the conditions needed to solubilize functionally active transport proteins have to be found empirically for each transport system.[141]

Detergents can generally be classified into different groupings based on their charge into nonionic, anionic and cationic detergents and the zwitterionic detergents. Although some detergents have specific interactions with membrane proteins, some general principles of detergent solubilization can be outlined. Foremost, detergents bind to membrane proteins and partition between the lipid bilayer and the aqueous phase to mimic the lipid bilayer of biological membranes. Incorporation of detergents into the lipid bilayer may perturb the structure and function of transport proteins. The binding of detergents may occur at charged protein residues if ionic detergents are employed or to hydrophobic protein groups if ionic or nonionic detergents are used.[142] After incubation of the membrane with sufficiently high detergent concentrations exceeding the critical micelle concentration (CMC), the biological membranes are lysed and detergent-protein-lipid mixed micelles form. Excessive amounts of detergents are usually used for complete dissolution of the membrane and to provide for a large number of micelles to give one protein per micelle molecule.

A common problem during solubilization and purification is the tendency of hydrophobic membrane proteins to form complexes after solubilization. Ionic detergents are more efficient in dissociating these complexes but in many cases they lead to denaturation and cannot be used when purification is done by ion exchange chromatography and by isoelectric focusing. Nonionic detergents are known to better solubilize membrane proteins while retaining native characteristics in comparison to ionic detergents or bile salts.[143]

For further characterization of membrane proteins and other downstream applications especially those involving incorporation into lipid membranes, it is often necessary to remove unbound detergents. Detergents with high CMC can be readily removed from protein-lipid-detergent mixed micelles by dialysis or gel filtration, whereas low CMC detergents dialyze slowly and are oftentimes insufficiently eliminated. The detergent CMC is therefore a major consideration to be made when choosing solubilization detergents depending on final use of proteins. In this study, the nonionic detergent octyl glucoside was used for solubilization and purification of BK_{Ca} channels.

Materials and Methods

Lipids and Chemicals

Archaea analogue phospholipids 1,2-diphytanoyl-*sn*-glycero-3-phosphocholine (DPhPC) and 1,2-diphytanoyl-*sn*-glycero-3-phosphoethanolamine (DPhPE) whose structures are illustrated in Figure 1-12, were purchased in an already diluted form in chloroform from Avanti Polar Lipids Inc. (Alabaster, AL, USA), and were used without further purification. 2,3-di-*O*-phytanoyl-*sn*-glycerol-1-tetraethylene glycol-$_{D,L}$-α-lipoic acid ester (DPTL) was obtained from the Schiller group (Max Planck Institute, Mainz Germany). NaCl, $MgSO_4$, $Ca(NO_3)_2$, $NaHCO_3$, $CaCl_2$, NaOH, KCl, $MgCl_2$, HEPES,

$CaCl_2$ and sodium pyruvate were purchased from Thermo scientific (Waltham, MA). Penicillin, Streptomycin and horse serum were purchased (Sigma-Aldrich, St. Louis, MO). All buffers were prepared in ultrapure water filtered in a Milli-Q water purification system (Millipore Corporation, Billerica, MA).

Oocytes

Adult *Xenopus laevis* frogs were purchased from Xenopus Express, Tampa, Florida. The surgical removal of oocytes from the frogs has been previously described.[144] Briefly, frogs are anesthetized by putting them in a solution of tricaine methanesulfonate (MS222) anesthetic, placed on ice to prolong the anesthetic effect and then a small incision of between 5-10 mm made in lower quarter of abdomen and oocytes can be pulled out in their fascia from the ovarian lobes. Oocytes are placed in a 2 mg/ml collagenase in divalent ion-free OR-2 solution (82.5 mM NaCl, 2 mM KCl, 5 mM HEPES, 1 mM $MgCl_2$ adjusted to pH 7.4 using NaOH) at room temperature for 45 minutes to dissolve the follicular layer and then the largest oocytes of the stage V and VI developmental stage selected under a light microscope. The oocytes are then washed in Barth solution (88 mM NaCl, 1.68 mM $MgSO_4$, 10 mM HEPES, 0.47 mM $Ca(NO_3)_2$, 2.4 mM $NaHCO_3$, 0.41 mM $CaCl_2$ adjusted to pH 7.4 using NaOH) to stop the enzymatic digestion. Oocytes are kept at 19 ˚C in ND96 oocyte culture medium (96 mM NaCl, 2 mM KCl, 1 mM $MgCl_2$, 5 mM HEPES buffer, 1.8 mM $CaCl_2$, 2.5 mM Sodium pyruvate, 100 µg/ml Penicillin, 100 g/ml Streptomycin, 5 % horse serum).

Plasmids

The gene encoding the murine (*mslo*) BK_{Ca} channel was provided by the laboratory of Lawrence Salkoff, Washington University, St. Louis, MO. The BK_{Ca} channel (*mslo*) gene is contained in the plasmid: pcDNAOX, a pcDNA3 derivative which

contains flanking 5'- and 3'-UTR sequence from *Xenopus* Beta-globin. The gene encoding the monomeric red fluorescent protein was provided by the laboratory of Roger Tsien, University of California, San Diego, CA. The mRFP1 gene was contained in the plasmid pRSET-B prior to fusion with maxi-K in the pcDNAOX vector. The pXOOM vector, used for co-expression of a target gene and (non-fused) green fluorescent protein in either *Xenopus* oocytes or mammalian tissue culture, was provided by the laboratory of Demitri Budko, The Whitney Laboratory for Marine Bioscience, St. Augustine, FL. The bacterial expression plasmid, pET46 EK/LIC, was purchased from Novagen/EMD Biosciences.

DNA Preparation and Manipulation

All site-directed-mutagenesis was performed with the QuickChange II XL kit (Stratagene). Competent *E.coli* cells were from Stratagene (XL-10gold), Invitrogen (Top-10, INV-110, BL21 (DE3), or Novagen/EMD Bioscience (BL21 (DE3), Rosetta-2 (DE3). Restriction enzymes were purchased from New England Biolabs (NEB), Calf intestinal alkaline phosphatase was either from Promega or NEB, and T4 DNA-ligase was from NEB. Gel extraction and purification was done with the QIAquick gel extraction kit (Qiagen) from agarose gels. Other media and reagents were from Sigma or Fisher Scientific. Sequencing was performed by the fluorescent dideoxy terminator method at either the Whitney Laboratory for Marine Bioscience, St. Augustine, FL or at the ICBR sequencing core, University of Florida, Gainesville, FL. All deoxyoligonucleotide primers were synthesized and PAGE purified by Integrated DNA Technologies, Coralville, IA. To allow deletion of the maxi-K C-terminal domain and fusion with mRFP1 in pcDNAOX, an insertion coding for a *Bam*HI site flanked by a *Bst*BI site was added in place of the maxi-K stop codon by site directed mutagenesis. A

second *Bam*HI site was added by site directed mutagenesis in a position such that digest with *Bam*HI followed by gel purification and re-ligation would result in the deletion of the C-terminal domain encoded between the two *Bam*HI sites. As there was no stop codon added at this point of truncation, an additional 12 amino acid residues (ALRTPRRPELFF^{347}-stop) are coded for at the C-terminus of BK_{Ca} *mSlo* CTD construct.

Initially, the mRFP1 gene was digested away from the pRSET-B plasmid with *Bam*HI and *Bst*BI enzymes, then purified by gel extraction ("mRFP1-insert", above). XT-PCR was used to modify the mRFP1 gene by addition of a C-terminal extension containing a hexa-histidine tag, a new stop codon, *Bst*BI restriction site, and unique *Spe*I restriction site. The following primers were utilized for XT-PCR: (extension sequence is underlined) "RFPhis-forward": (5'TAAGGATCCGATGGCCTCCTCCGAGG)

"RFPhis-reverse": (5'TATTTCGAACTAGAGATGGTGGTGATGATGTGC-GGCGCCGGTGGAGTGGCG). This C-terminally His-tagged mRFP1 gene ("mRFP1His") was subsequently fused to the C-terminally deleted maxi-K in the pcDNAOX vector resulting in the preparation of the "CTD2-mRFP1His" construct. "CTD2-mRFP1His" gene cassettes were annealed and ligated to a linearized pRSET-B vector to complete the directional cloning. The ligated vector was transformed into competent cells (*E.coli* Top-10, Invitrogen), and grown on selective agar. Plasmid DNA purified from transformed colonies was screened by double restriction digest with an enzyme unique to the His-tag sequence (*Spe*I) and an enzyme unique to BK_{Ca} (*Pmi*I). Positive subclones were confirmed by sequencing.

Expression in Oocytes

After harvesting of the oocytes, oocytes were selected that were in either maturation stage IV which show separation into animal and vegetal poles or stage V

oocytes which are used for microinjection of the cRNA. *In vitro* transcriptions were performed to obtain cRNA coding for the desired recombinant BK_{Ca} channels. The mMessage mMachine T7 Ultra kit (Ambion, Austin, TX) was used for in vitro transcriptions as follows; 2 hour incubation at 37 ˚C was done of a mixture of 4 µL BK_{Ca} channel miniprep DNA, 2 µL 10× transcription buffer, 10 µL ribonucleotide mix, 2 µL 10× enzyme mix and 2 µL 30 mM GTP. 30 µL of RNAse-free water and 25 µL of lithium chloride were added and the mix chilled for 30 min at -20 ˚C to terminate the reaction. The cRNA was pelleted by centrifugation at 14,000 rpm for 15 min and a temperature of 4 ˚C. The supernatant solution was removed, 90 µL of cold 70% ethanol added and spun again at 14,000 rpm for 5 min at 4 ˚C and the final supernatant removed. The cRNA pellet was resuspended in 20 µL of RNAse-free water. A microinjector (Drummond Nanoject, Drummond scientific Co., Bromall, USA) attached to a three dimensional micromanipulator was used to inject 46 nl (approximately 50 ng) of cRNA into the oocyte cytoplasm. Injected oocytes were incubated at 18˚ Celsius for 72 hours in ND-96 oocyte culture medium for translation, expression of BK_{Ca} channels and trafficking of functional channels to the membrane surface of oocytes.

Analysis of Expression: Electrophysiological Recordings

A variety of techniques can be used to analyze the levels of expression including biochemical techniques, physical and electrophysiological techniques. Analysis of the successful expression of functional ion channels by electrophysiological recording is significantly more sensitive than either of the other approaches. For analysis of expression by two-electrode voltage clamping, oocytes were placed in a 1ml plexiglass chamber, impaled with two electrodes fire polished to resistances of 0.3 to 2 megaohm (MΩ) fabricated from Corning 7052 borosilicate glass (Warner, Hamden, CT, USA) and

the membrane potential was clamped at -90 mV using a Warner OC725C oocyte clamp. Data was collected and analyzed using pClamp 8.0 software (Molecular Devices Corporation, Union City, CA, USA). Current/voltage relationships were obtained by stepping to voltage clamp to -70 mV and then increasing in 10 mV steps of 100ms duration to +120 mV. The maximum current at each voltage was recorded.

Membrane Extraction of Expressed Channels

The expressed BK_{Ca} channels from *Xenopus laevis* oocyte membranes were solubilized using the nonionic detergent β-octyl glucoside (β-OG). B-OG was chosen because it has a high CMC of 25 mM at 20-25°C and low molecular weight 292.4 g/mol, properties that facilitate rapid removal from mixed micellar complexes by dialysis or gel filtration after solubilization. For our purposes, a mild, easily removable detergent was necessary because the isolated and purified BK_{Ca} channels were to be reconstituted into lipid membranes for functional analysis. Ground oocytes were solubilized using a buffer solution at a final concentration of 10 mM β-octyl glucoside containing 20 mM Tris buffer, 500 mM KCl and 20 mM imidazole, equilibrated to pH 7.5 using KOH, and the mixture gently agitated at 200 rpm for 10 minutes at 4° C or in ice. The α-subunit of BK_{Ca} channels is known to be prone to protease degradation;[44] therefore 5 µL of mammalian protease inhibitor cocktail (Sigma-Aldrich, St. Louis, MO) was added to the solubilization buffer. The suspension was then agitated gently for 1 hour at 200 rpm on a platform shaker followed by centrifugation at 14,000 rpm at 4 °C to separate the solubilized mixed micelles from cellular debris. The supernatant containing the lipid-protein-detergent mixed micelles was collected and a portion of it assayed by SDS-PAGE followed by Coomassie staining.

Immobilized Metal Ion Affinity Chromatography

Supernatant solutions at volumes of 2 mL were obtained after solubilization by OG and loaded onto 1 mL Histrap FF (GE Healthcare Life Sciences, PA, USA) columns pre-packed with Ni^{2+} Sepharose media made from highly cross-linked agarose matrix. Elution was performed with columns equilibrated with binding buffer (10 mM β-octyl glucoside, 20 mM Tris buffer, 500 mM KCl and 20 mM imidazole, adjusted to pH 7.5 using KOH) at a flow rate of 1 mL min^{-1} and washed with the same buffer. Unbound material was washed off using 5 column volumes of binding buffer, and then fractions of 1.5 mL eluted in a stepwise manner with an elution buffer containing 500 mM imidazole and all other components of the binding buffer at pH 7.4 and a flow rate of 1 mL min^{-1}. IMAC purification was performed both manually in the cold room (4 ˚C), using syringes for applying pressure and under automation using the ÄKTA prime system (GE Healthcare Life Sciences, PA, USA).

Western Blot Analysis

Immunoblotting was used to determine the identity of purified protein samples and the procedure is described in greater detail in Chapter 2. SDS-polyacrylamide gel electrophoresis and Western blotting were performed by standard techniques.[145] Briefly, samples were loaded on 4-20% gradient Tris-HCl polyacrylamide gels followed by electrophoretic separation, and then by tank electro-transfer, proteins were transferred to Immobilon Polyvinylidene Fluoride (PVDF) membranes (Millipore Corporation, MA) at 105mV for 70 minutes. After transfer, membranes were blocked with 2% nonfat dry milk (NFDM) in tris-buffered saline (TBS) with 0.1% Tween 20 (TTBS) for 1 hour at room temperature. Hexa-histidine tag primary antibodies were diluted with 1% NFDM in TTBS and incubated with membranes overnight at 4 °C. This

was followed by three washes in TTBS and re-blocking of membranes with 1% NFDM in TTBS. The goat-anti-rabbit HRP secondary antibodies (Bio-rad) were diluted in 2 % NFDM (1:100,000) and applied to membranes for 1 hour at room temperature. The membranes were washed in TTBS prior to incubation with Immobilon Western Chemiluminescence HRP substrate (Millipore). The blots were exposed to X-ray sensitive film (Kodak). When the signal was weak or protein expression too low for distinct recognition by the hexa-His-antibody, we used the HRP-His-Probe (Pierce, Rockford, IL, USA). The HRP-His-probe uses a Ni-chelating group that binds to the 6His-tag present on the protein. The HRP-His- probe reacts with the substrate giving off a chemiluminescent signal that was quantified using X-ray sensitive film (Kodak).

Lipid Vesicle Formation

Chloroform solutions of the lipids (50 mg/mL) were mixed to a 7:3 molar ratio (DPhPC/DPhPE) followed by rotary evaporation until a dry lipid film was obtained at the bottom of the vessel. The dry lipid film was then placed under vacuum in a dessicator overnight to eliminate any residual chloroform. The lipids were then hydrated for 1 hour at 50 ˚C in buffer (5 mM MOPS, 250 mM KCl, 0.1 mM $CaCl_2$, pH 7.4) to a final concentration of 2 mg/mL. After being cooled to room temperature, the suspension was bath sonicated for 5 min, and extruded (21 passes) at room temperature through 100 nm polycarbonate membranes in a mini-extruder (Avanti Polar Lipids Inc.). The vesicle size profile was determined by the use of a dynamic light scattering (DLS) instrument (Brookhaven Instruments Corporation, Holtsville, New York, USA). Typically vesicle sizes of (140±30) nm were obtained as computed by the BI-DLSW Dynamic light scattering software.

Reconstitution of Recombinant Proteins in Artificial Liposomes

A detergent-mediated procedure was used for reconstitution of BK_{Ca} channels into lipid vesicles. A 1 ml volume suspension of pre-formed large unilamellar vesicles (LUVs) of 2 mg/mL DPhPC:DPhPE lipids in a 7:3 molar ratio extruded through 100 nm membranes prepared as detailed above, were solubilized by the addition of a 1 ml solution of 10 mM β-octyl glucoside. A 500 µl sample of protein solubilized in 10 mM β - OG detergent that was eluted from the Ni^{2+} chelated purification column was added to the solubilized liposomes resulting in protein mixed micelles. The final mixture composed of purified membrane proteins in an excess of liposomes and β-octyl glucoside detergent was incubated for 30 min at room temperature, forming a solution of mixed lipid-protein-detergent and lipid-detergent micelles. The next step involved removal of detergent from these micellar solutions which led to a progressive formation of closed lipid bilayers in which the proteins would eventually incorporate. Detergent was removed by dialysis when the micellar solutions were placed in 10,000 kDa membrane MW cut-off dialysis cassettes (Pierce) immersed in 1 liter dialysis buffer (5 mM MOPS, 250 mM KCl, 0.1 mM $CaCl_2$, pH 7.4) for 2 hours at room temperature. The dialysis buffer was changed and the dialysis process continued for another 2 hours at room temperature and then a final exchange of dialysis buffer made and this was let to continue for ~18 hours at 4 ˚C. All dialysis buffers had pre-cleaned polystyrene beads added outside the dialysis bags to reduce on the number of buffer exchanges necessary for complete removal of detergent. The polystyrene beads absorb octyl glucoside as it is removed from the mixed micelle solution in the dialysis bag. The whole process of dialysis proceeds with constant stirring.

Negative-Staining Transmission Electron Microscopy

Negative-staining TEM was used to image the proteoliposome products of the dialysis reconstitution and to characterize their morphologies. The instrument used was a Hitachi H-7000 transmission electron microscope with a maximum resolution at 0.2 nm with a magnification range of 110× to 600,000× operated at 75-100 kV with a Soft-Imaging System MegaViewIII with AnalySIS digital camera (Lakewood, CO). Prior to imaging, samples required negative staining using 2 % uranyl acetate. A detailed staining procedure is provided in Chapter 2 of this document. Briefly, portions of sample solution obtained from the dialysis bags were incubated for 2 minutes and allowed to dry for an additional 2 minutes on a 400-mesh formvar-coated copper grid (Electron Microscopy Sciences, PA). 2 % uranyl acetate was added to the dry sample for staining for 2 minutes before drying for another 2 minutes, followed by insertion onto the TEM specimen holder for imaging.

Results and Discussion

Expression of Recombinant BK_{Ca} Channels

The use of a C-terminal mRFP1 fusion tag provided an easy means by which to confirm expression of fluorescently tagged recombinant BK_{Ca} channels through bright field microscopy. A major advantage of using mRFP1 is that intact cells can be imaged without significant preparative procedures, therefore allowing for the possibility of further incubation of imaged oocytes in case expression is not satisfactory. Oocytes expressing the chimeric protein exhibited a bright red glow emanating from the mRFP1 fusion tag on the BK_{Ca} channels when observed under the microscope as can be seen in panel A of Figure 3-4. Control experiments of oocytes not injected with cRNA encoding for the recombinant BK_{Ca} channel show autofluorescence characteristic of oocytes when

exposed to transmitted light. However, a significant difference in the contrast and brightness can be observed, clearly differentiating oocytes expressing BK_{Ca} channels from those that do not express channels as observable in panel B of Figure 3-4.

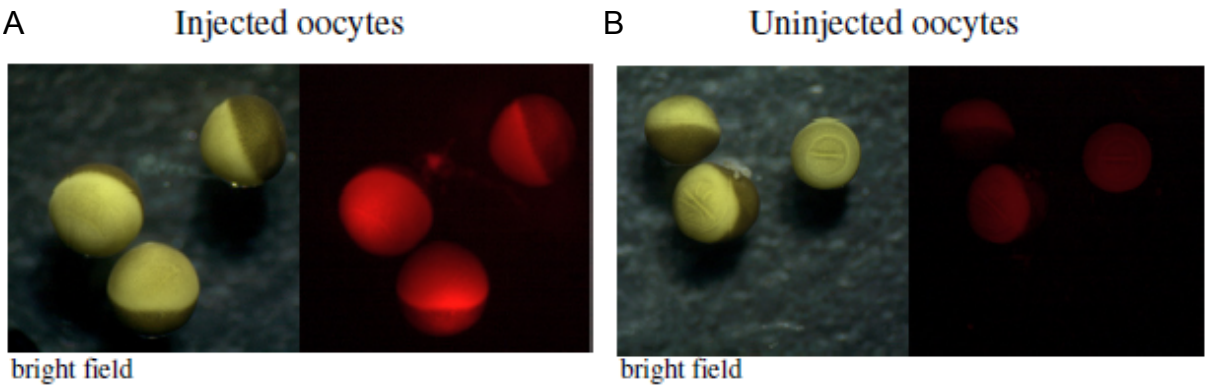

Figure 3-4. Bright field microscopy images of oocytes for analysis of expression. A) Oocytes injected with cRNA coding for recombinant BKCa channels showing brightness of fused mRFP1. B) Uninjected oocytes without the characteristic fluorescence observed from mRFP1.

A major limitation of bright field microscopy when used to analyze expression in oocytes is that it does not provide unequivocal information regarding the localization of the fluorescent-tagged proteins. Proteins localized in the cytoplasm which have undergone complete translation but have not yet trafficked to the oocyte membrane still fluorescence, although the signal would not correspond to functional BK_{Ca} channels. Hence, function is tested by the two-electrode voltage clamping (TEVC) electrophysiology technique that has the capability to detect membrane expressed ion channels. TEVC is used in combination with the bright field microscopy to demonstrate expression of functional chimeric mRFP1-tagged BK_{Ca} channels.

Analysis of Expression by Two-Electrode Voltage Clamping

TEVC is a method capable of detecting as few as 10^5 channel molecules on a single oocyte (less than 10^{-18} mol) as compared to biochemical techniques which have

a detection limit of 10 $^{-12}$ mol, a value dependent upon experimental parameters. Uninjected oocytes (without the cRNA coding for channels) were voltage clamped as a control for comparison with oocytes expressing BK_{Ca} channels as shown in Figure 3-5.

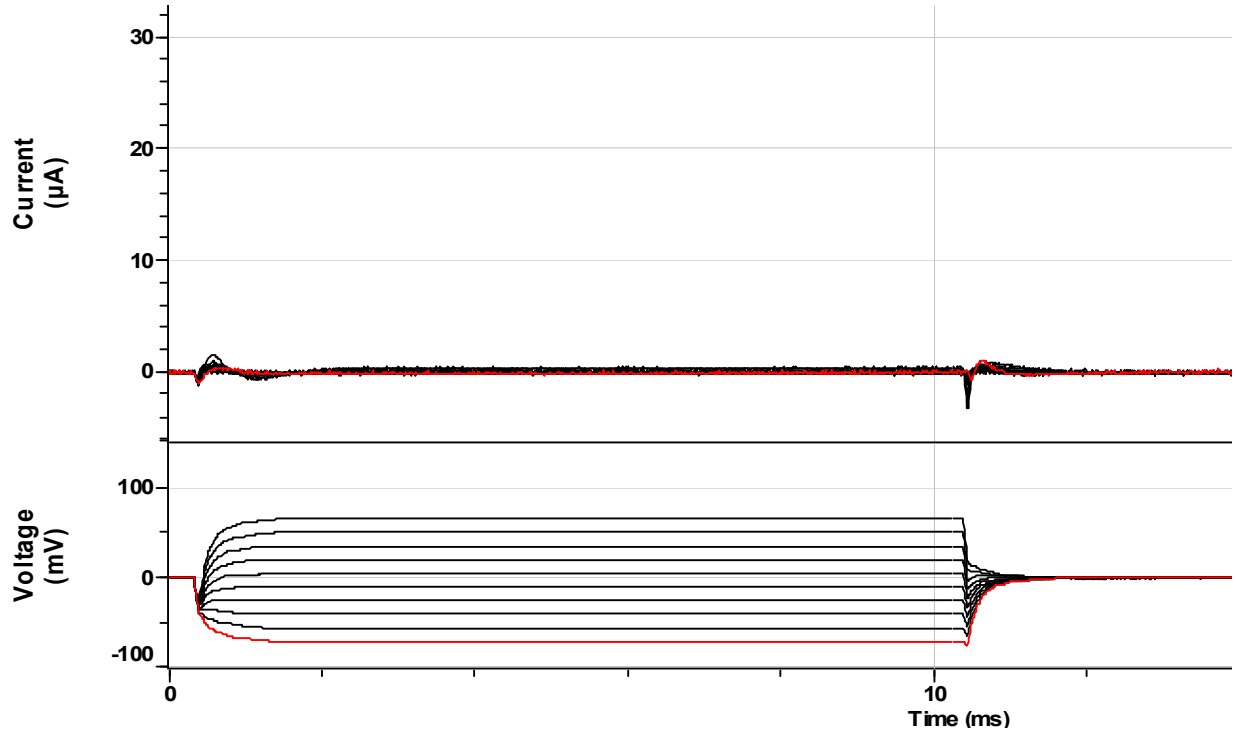

Figure 3-5. TEVC of uninjected oocytes as a control for monitoring expression levels of BK_{Ca} channels. Potentials applied in steps from -60 mV to 60 mV.

Potentials were applied stepwise from – 60 mV to + 60 mV in 10 mV increments and any current flow recorded. The control experiment showed no discernable current flow as can be observed in the upper panel on Figure 3-5 showing the recorded current levels in microamperes (µA). Ion channels expressed on the oocytes would typically be expected to allow current flow across the oocyte membrane, and because cRNA coding for BK_{Ca} channels was not injected into these oocytes, the obtained results were not surprising. *Xenopus laevis* oocytes are known for their endogenous expression of BK_{Ca} channels which exhibit gating behavior that is quantitatively similar to murine (*mslo*) BK_{Ca} channels and *hslo* channels cloned from the human brain.[146] However, because of

the low expression levels of endogenously expressed channels, currents through them are usually in the picoampere range, therefore negligible and cannot be accounted for in the recording shown in Figure 3-5 above. Oocytes injected with cRNA coding for the mRFP1-tagged BK_{Ca} channel and incubated for expression were analyzed for expression in a similar experiment as the control. The data of the voltage clamping of these injected oocytes is shown in Figure 3-6.

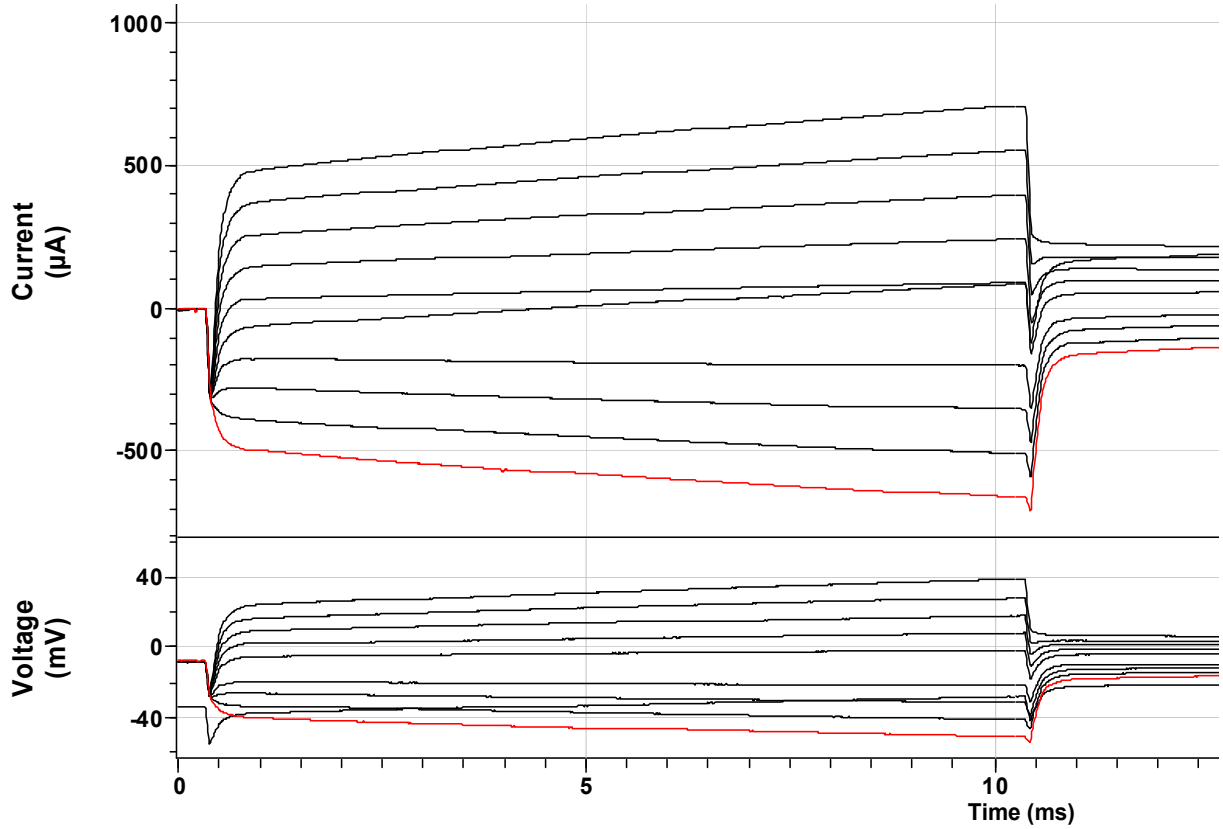

Figure 3-6. TEVC currents showing expression of mRFP1-tagged BK_{Ca} channels. Potentials were applied stepwise between -40 mV and 40 mV.

Potentials were applied in steps just like in the control clamping of uninjected oocytes, however, voltage was reduced and the steps in this case ranged from -40 mV to + 40 mV as can be observed in the lower panel in Figure 3-6 showing applied voltage in millivolts (mV). Current flowing through the expressed mRFP1-tagged BK_{Ca} channels

ranged between -700 µA to 700 µA as can be observed in the upper panel in Figure 3-6 showing current amplitudes in microamperes (µA). Such current amplitudes are associated with high levels of expression of the expressed channels, in this case, that of BK_{Ca} channels encoded for by the injected cRNA. Expression associated with the observed currents in the microampere range is generally acceptable as being from heterologous origins,[147] and reflects on the success of expression in this study. All the macroscopic currents observed in the recordings of the injected oocytes shown in Figure 3-6 are assigned to those passing through the heterologously expressed mRFP1-tagged BK_{Ca} channels and were not from any other source.

Figure 3-7 shows currents elicited when oocytes injected with cRNA encoding the mRFP1-tagged BK_{Ca} channel were voltage clamped to test for voltage dependence of expressed channels and analyzed by TEVC.

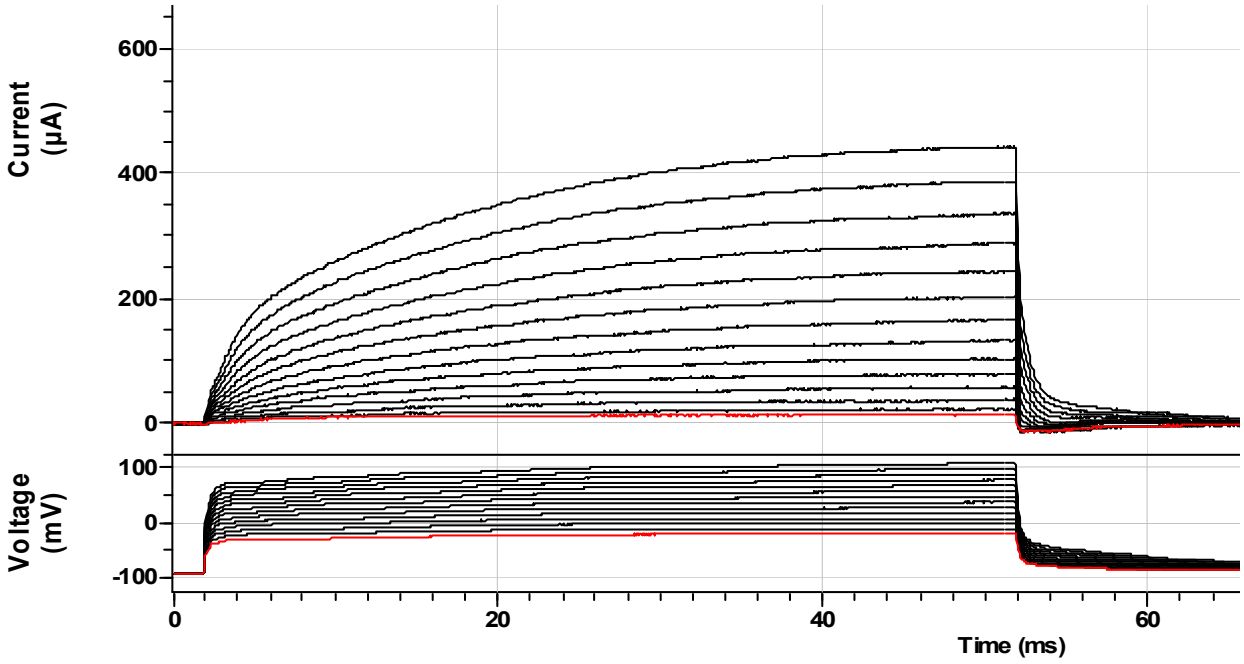

Figure 3-7. Currents recorded from mRFP1-tagged BK_{Ca} channels to test for voltage dependence of expressed channels. Potentials were applied stepwise from -20 mV to + 120 mV.

It was imperative to demonstrate the voltage dependence of the channels expressed in this study, to unequivocally show that currents observed during analysis of expression by TEVC were indeed from mRFP1-tagged BK_{Ca} channels because *Xenopus* oocytes are known to endogenously express stretch-activated channels with non-selective permeability to K^+ and Na^+.[148, 149] The current flow observed through expressed channels in Figure 3-7 was elicited in response to voltages ranging from -20 mV to + 120 mV in 10 mV increments from a holding potential of -80 mV as shown in the voltage panel. Current at levels of up to + 450 µA show the high levels of the expression of mRFP1-tagged BK_{Ca} channels achieved during this study. Increased membrane depolarization results in greater current amplitudes, and vice versa, as can be noted in Figure 3-7, a characteristic behavior of voltage dependent channels. The data attests to the success of expression of mRFP1-tagged BK_{Ca} channels.

Investigations were performed to analyze the expressed mRFP1-BK_{Ca} channels in comparison to native proteins (full-length BK_{Ca} channels) to determine whether the C-terminally deleted constructs tagged with fusion proteins maintained functional integrity. A plot was made relating voltage across the oocyte membrane (membrane potentials) against current flow elicited by ions traversing the membrane for the expressed mRFP1-BK_{Ca} channels. The current-voltage relationship or *I-V* curve as plotted in Figure 3-8 can be used to determine if the clamped channels exhibit their characteristic conductances, hence optimal functional activity by the equation:

$$\gamma = I / (V - V_{rev}) \qquad (3\text{-}1)$$

Where γ is the single channel conductance, *I* the unitary current for a single channel, *V* is the membrane potential, and V_{rev} is the reversal potential.

Unitary current was measured from the first current step from the basal level off the macroscopic currents. Figure 3-8 below is the current-voltage (I-V plot) relationship for mRFP1-BK_{Ca} channels.

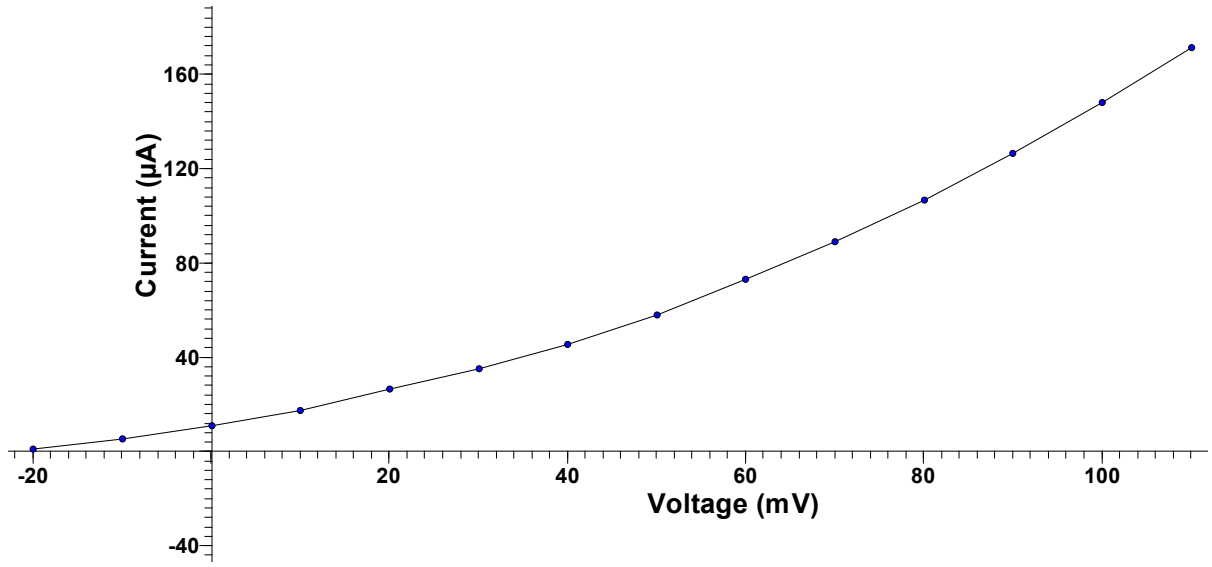

Figure 3-8. The current-voltage curve for the expressed mRFP1-tagged BK_{Ca} channel showing the voltage-dependence of this channel in oocytes.

The *I-V* curve in was obtained from macroscopic currents flowing through clamped mRFP1-BK_{Ca} channels at a holding potential of -80 mV and applied membrane potentials ranging from -20 mV to + 120 mV in 10 mV increments. As expected the expressed channels were voltage-dependent, a characteristic feature of BK_{Ca} channels indicated by the non-linearity of the *I-V* curve. Furthermore, the single channel conductance obtained by linear approximation using Equation 3-1 was within the expected range for fully functional BK_{Ca} channels. The unitary conductance derived from TEVC macroscopic currents and calculated as described above for the expressed mRFP1-tagged BK_{Ca} channels was 129 pS, a value which was within the expected conductance range for full-length BK_{Ca} channels. BK_{Ca} channels have been shown in literature to have a conductance range between 90 pS to 300 pS.

Isolation and Solubilization of Expressed mRFP1-BK_{Ca} Channels

After the screening process to determine expression levels, oocytes expressing the functional mRFP1-BK_{Ca} channels were isolated and aliquots made containing 100 oocytes each. These were ground up for storage as described in the materials and methods section in this chapter. Prior to purification, the expressed channels were isolated from the oocyte membrane by detergent solubilization and centrifugation. Two detergents were tested for solubilization and these were the non-ionic detergents β-octyl glucoside (OG) and dodecyl maltoside (DDM). Both these detergents are well documented and have been extensively used for solubilization of membrane proteins over the years.

Dodecyl maltoside is known to enhance protein delipidation during the solubilization of membrane-associated proteins, as well as improve protein mobility when performing electrophoretic assays.[150] Dodecyl maltoside solubilized membrane extracts were run through chromatography columns for purification but DDM could not be removed sufficiently by dialysis to allow incorporation into lipid membranes. In this study, it was necessary to remove the detergents, because the expressed mRFP1-BK_{Ca} channels were to be incorporated in synthetic lipid bilayer membranes. DDM is known to form large micelles of greater than 50 kDa at low concentrations of 0.17 mM (sub-optimal for the present study) which makes it difficult to remove by dialysis of gel filtration;[151] therefore, Octyl-β-glucoside a high critical micellar concentration (CMC) detergent, was used because it could be easily and conveniently removed by dialysis.

Octyl-β-glucoside concentrations ranging from 10 mM to 30 mM were tested on trial and error basis to find the optimal concentration for solubilization without wastage, and a 10 mM concentration was settled for. Solubilized membrane extracts were then

centrifuged to pelletize and remove cellular debris and separate these from the supernatant containing mRFP1-BK_{Ca} channels for purification.

Immobilized Metal Ion Affinity Chromatography

Purification of the mRFP1-tagged BK_{Ca} channel proteins was performed under non-denaturing conditions by immobilized metal ion affinity chromatography using 1 mL Histrap FF (GE Healthcare Life sciences) pre-packed columns charged with Ni^{2+} affinity resin. Figure 3-9 summarizes the purification scheme used for these his-tagged recombinant mRFP1-BK_{Ca} channels.

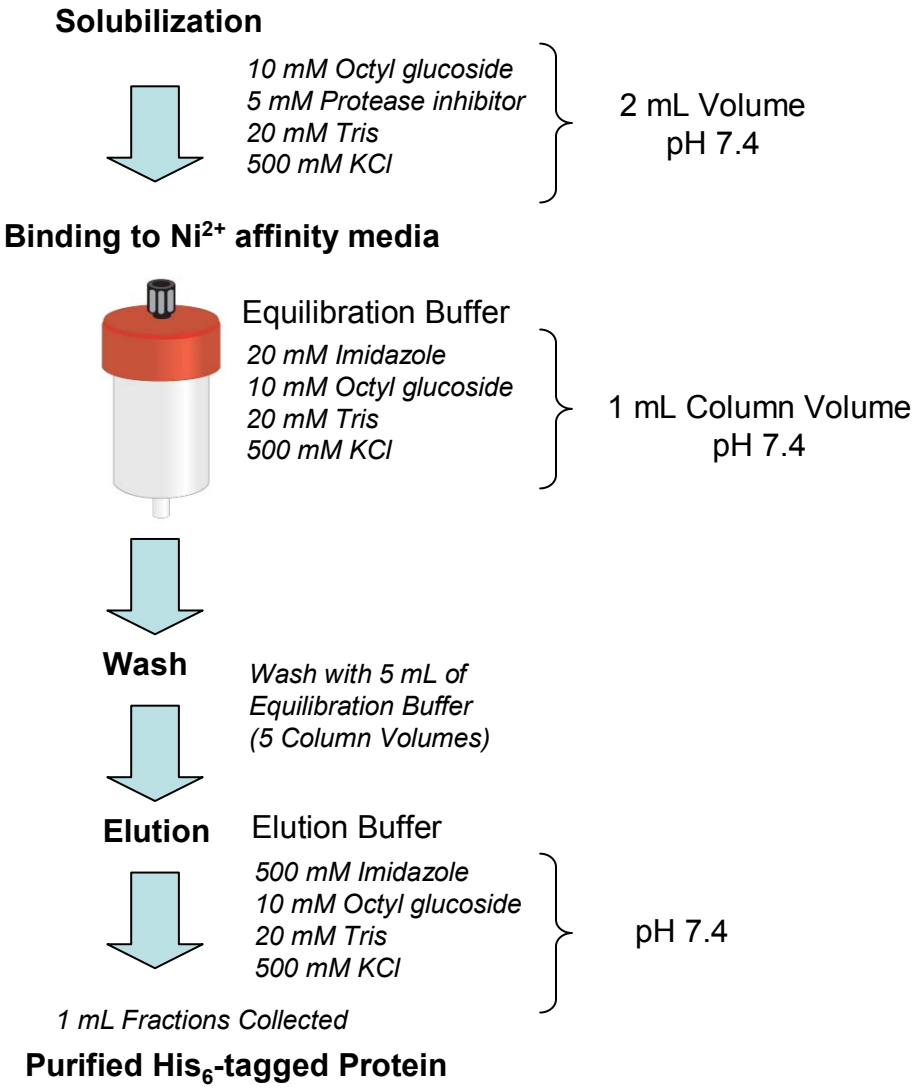

Figure 3-9. Purification scheme for the histidine-tagged mRFP1-BK_{Ca} channel.

The octyl glucoside used for solubilization helped to maintain the conformational integrity of mRFP1-tagged BK_{Ca} channels after de-lipidation. Volumes of 2 mL of supernatants from solubilized and centrifuged oocyte membrane extracts were loaded on Ni^{2+} affinity chromatography columns for adsorption of the histidine-tagged protein sample; unbound material was allowed to flow through the column. For the removal of unbound material, including proteins that may have been non-specifically bound, the Ni^{2+} column was washed with 5 mL of equilibration buffer (5 column volumes) at a flow rate of 1 ml/min. For the gravity (manual) purification, a flow rate of 1 mL/min was equivalent to an elution of 30 drops per minute. The desired his-tagged protein was eluted in one step with buffer containing 500 mM imidazole, a competitive ligand to Ni^{2+}. In all buffers, 10 mM octyl glucoside was present to provide a micellar environment for the membrane proteins. Three 1 mL volume fractions were collected after the manual purification and analyzed by UV absorbance 280 nm and data plotted in Figure 3-10.

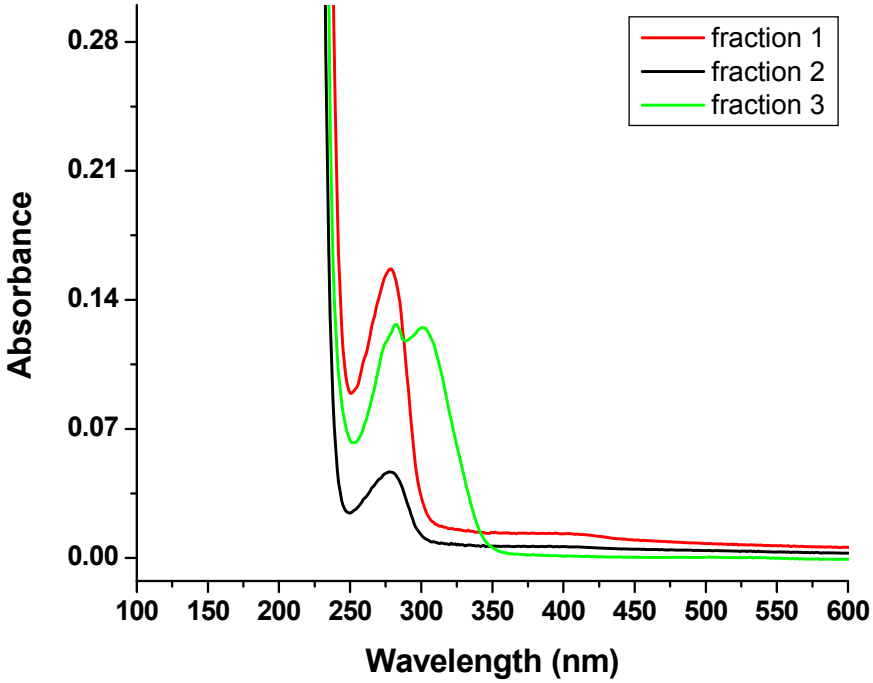

Figure 3-10. UV spectra of fractions from manual mRFP1-BK_{Ca} channel purification.

The three eluted fractions were loaded in 1 cm pathlength cuvettes and into a UV-VIS spectrometer followed by the collection of absorbance readings. The three fractions all yielded spectra with protein peaks at a wavelength of 280 nm corresponding to purified mRFP1-BK_{Ca} channels as can be observed from the spectra in Figure 3-10 and as expected of proteins. For the determination of the molecular weights of the proteins corresponding to the peaks observed, therefore confirm purification of the correct protein, an SDS-PAGE gel was run. Figure 3-11 shows the image obtained from the gel documentation system.

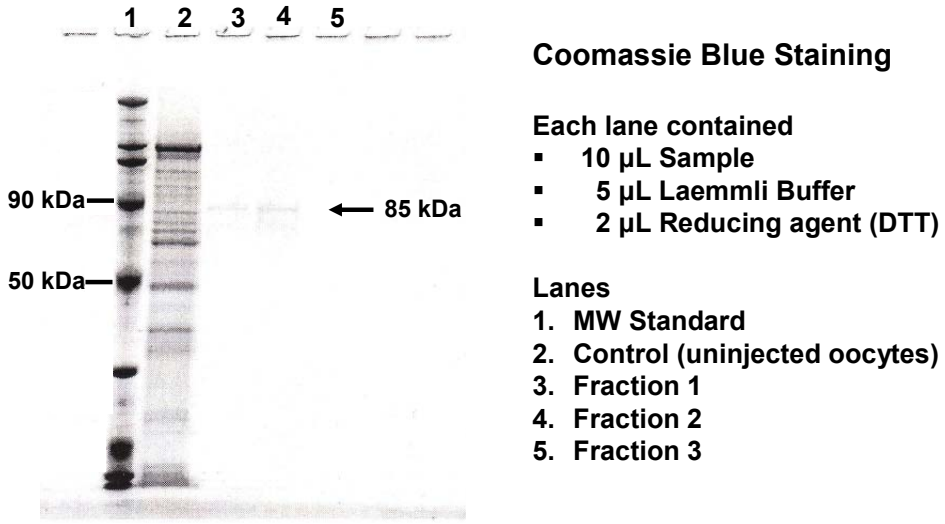

Figure 3-11. Image of a 4-20% gradient Tris-HCl gel stained with Coomassie Blue showing lanes with purified fractions of mRFP1-BK_{Ca} channels from the Ni2+ affinity column.

The protein fractions were analyzed by SDS-PAGE in a 4-20% gradient Tris-HCl polyacrylamide gel and imaged using a UV transilluminator as described in the materials and methods section in this Chapter. Lane 1 on the gel was loaded with a molecular weight ladder, lane 2 loaded with control membrane extracts isolated from oocytes which were not injected with cRNA of the mRFP1-BK_{Ca} channel, and lanes 3-5 were loaded with the purified fractions 1-3 respectively, eluted from the Ni^{2+} column. All

the lanes were loaded with sample volumes of 20 µL, 5 µL Laemmli buffer and 2 µL of the reducing agent dithiothreitol (DTT). As expected, the lane with uninjected controls had no band at 70 kDa corresponding to the molecular weight of mRFP1-BK_{Ca} channels. Lane 3 with fraction 1 and lane 4 with fraction 2 both have discernible bands appearing below the 90 kDa band corresponding to purified mRFP1-tagged BK_{Ca} channels. Fraction 3 yielded a very faint band that is not very clearly visible on the gel image. Most of the protein purification in this study was performed manually; however, the AKTA prime automated system was also used under similar conditions as the manual purification to give a comparison of results obtained from the two methods. The chromatogram obtained from the AKTA purifier is shown in Figure 3-12.

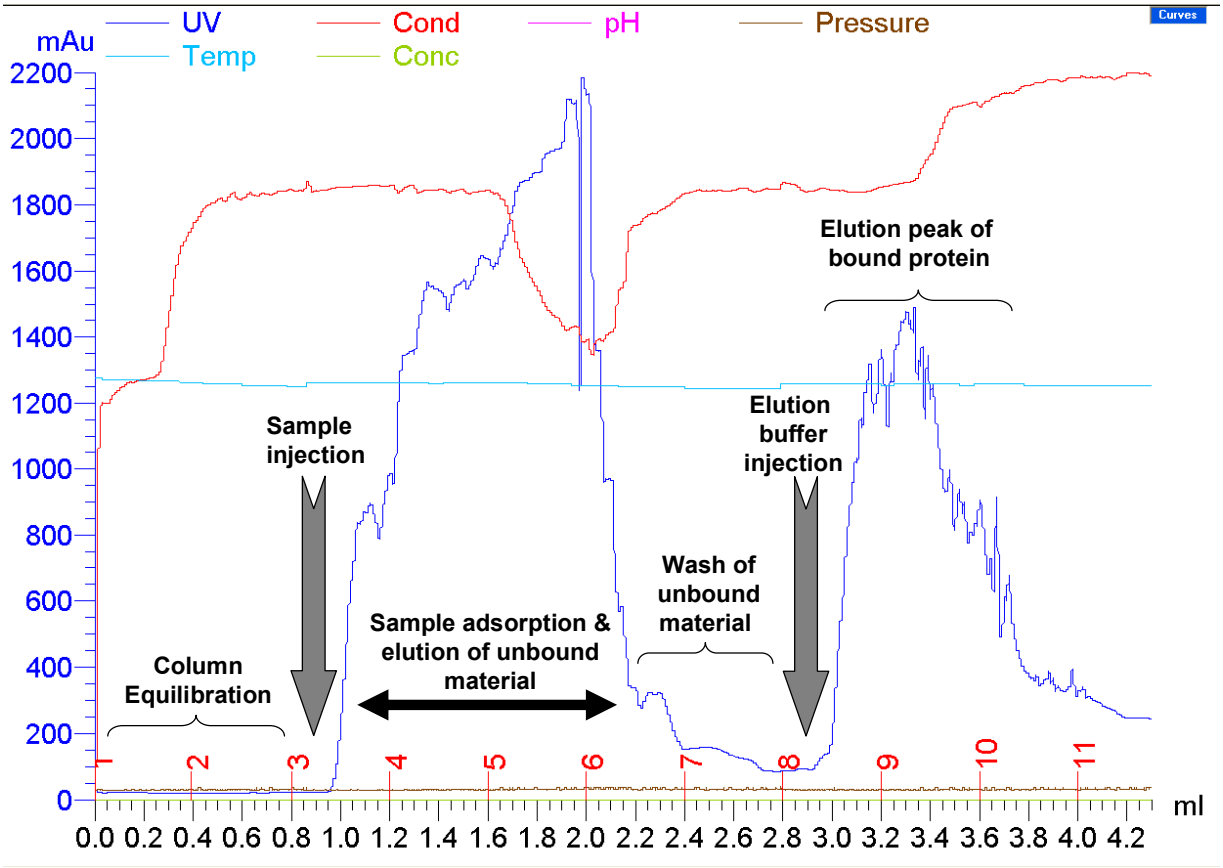

Figure 3-12. Chromatogram showing the purification stages of mRFP1-BK_{Ca} channels on the AKTA Prime automated protein purification system

The process of automated purification on the AKTA prime system performed in this study is described in great detail in Chapter 2 of this document. The separation of the target protein from other oocyte membrane components and the progression of the purification were tracked by the detection of UV-Vis absorbance at 280 nm, which is represented by the blue peaks on the chromatogram in Figure 3-12. Fractions 3-6, each 0.4 ml in volume, contained the flow through after the supernatant containing the solubilized mRFP1-tagged BK_{Ca} channels was loaded on the column. Wash of the column was performed in the next step in the purification with fractions 7 and 8 containing all the unbound oocyte membrane components. Fractions 8, 9 and 10 were obtained after injection of the elution buffer for desorption and these fractions contained the histidine-tagged BK_{Ca} channels. Aliquots of each fraction were analyzed by SDS-PAGE and western blotting to verify protein purification and for identification of the his-tagged constructs. Figure 3-13 shows images of the protein gel and western blot film.

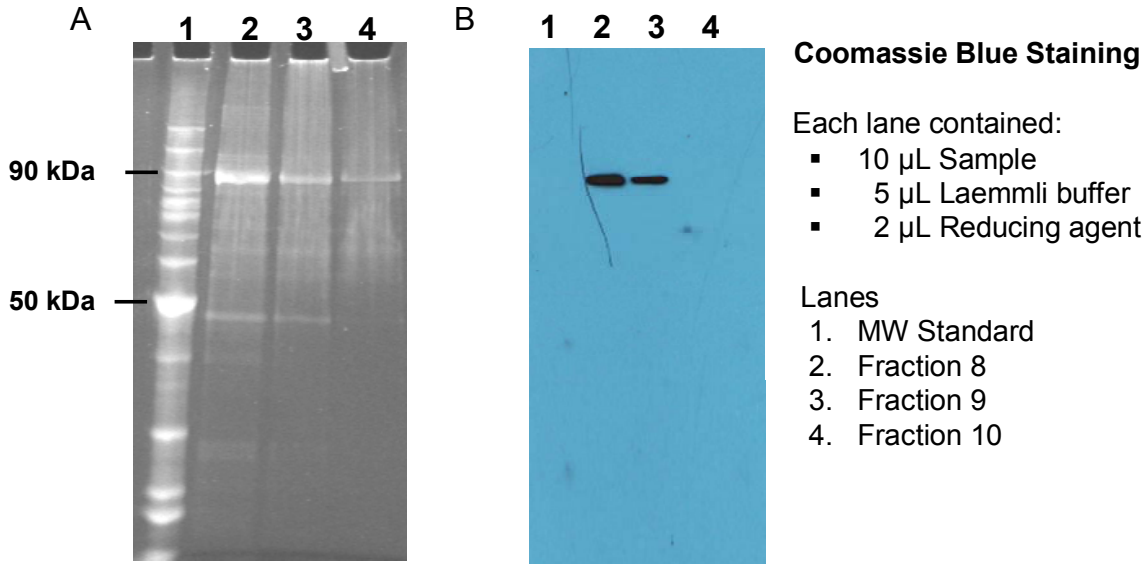

Figure 3-13. Electrophoresis and immunoblotting of purified BK_{Ca} channels. A) SDS-PAGE using 4-20% Tris-HCl polyacrylamide gels. B) Western blot on PVDF membrane.

Panel A in Figure 3-13 shows the image of the SDS-PAGE gel loaded with protein aliquots from fractions 8-10 collected from the AKTA Prime purifier. The lane assignments are indicated in the figure and were as follows; lane 1 was loaded with the molecular weight ladder and lanes 2-4 loaded with fractions 8-10 respectively. Each of the lanes was loaded with 10 µL of the protein sample, 5 µL of Laemmli sample buffer and 2 µL of the reducing agent dithiothreitol (DTT). The protein gel image is expected to show a band corresponding to a molecular mass of 70 kDa for the recombinant BK_{Ca} channel with a C-terminal truncation at position 347 and attachment of a 225 amino acid mRFP1 fusion tag and a six residue histidine tag. However, analysis of the gel image in panel A indicates that the BK_{Ca} channel protein migrated on the SDS/Tris-glycine gel at a molecular mass represented by a band observed at approximately 85 kDa. Additionally, an unidentified band with a molecular mass of approximately 45 kDa can be observed. This unidentified band is attributable to non-specifically bound oocyte membrane components with amino acid residues that had greater affinity for Ni^{2+} than the 20 mM imidazole which was added to the wash buffer. The apparent discrepancy of 15 kDa between the expected and actual molecular weights of the recombinant BK_{Ca} channel is probably as a result of post-translational modifications of the protein during expression, specifically N-linked glycosylation resulting in higher molecular weight of the glycosylated protein than the wild type channel.

It has been demonstrated that protein expression in *Xenopus laevis* oocytes is associated with glycosylation, and that inhibition of N-glycosylation blocks the incorporation of channels into the surface membrane of oocytes.[152-154] It is known that the electrophoretic mobility of glycosylated proteins is anomalous when analyzed by

SDS-PAGE and that migration of these proteins occurs with an apparent molecular weight greater than the actual protein molecular weight. The effect is not simply due to the additional mass contributed by the oligosaccharide, but due to the interference of the carbohydrate with the SDS-protein association (alteration of the mass-to-charge ratio) and effects of the glycan moieties on the migration of the denatured protein through the separating gel.[155]

Panel B in Figure 3-13 shows the image of the western blot film obtained when the SDS-PAGE gel in panel A was transferred to a PVDF membrane and targeted by antibodies specific to the hexa-histidine tag. Bands can be observed corresponding to those associated with the mRFP1-tagged BK_{Ca} channel on the protein gel. Western blotting provided confirmation that the correct protein was purified. Fractions 8, 9 and 10 eluted from the purifier were pooled together and the total protein yield quantified by the Coomassie (Bradford) method, a well known dye-binding method for determining protein concentrations. The method is based on the alteration of the absorption spectrum of the Coomassie Brilliant Blue G-250 dye when it binds to proteins in acidic media. Coomassie G-250 dye binds primarily to the basic (mainly lysine, arginine and histidine) and aromatic amino acid residues and generates a color change of the solution in response to various concentrations of the protein. Hydrophobic interactions and Van der Waals forces also participate in the binding of the dye by the protein. The absorbance maximum of the dye shifts from a wavelength of 465 nm to 595 nm when binding to the protein occurs. The number of Coomassie dye ligands bound to each protein molecule is approximately proportional to the number of positive charges found on the protein. Increase in the protein concentration results in a linear increase and

decrease in the absorbance of light at 595 nm and the absorbance of Coomassie Blue dye at 595 nm is proportional to the amount of protein bound. Protein standards were prepared from bovine serum albumin (BSA) to establish a correspondence between absorbance values and known BSA concentrations. The absorbance spectra for the protein standards are plotted in Figure 3-14.

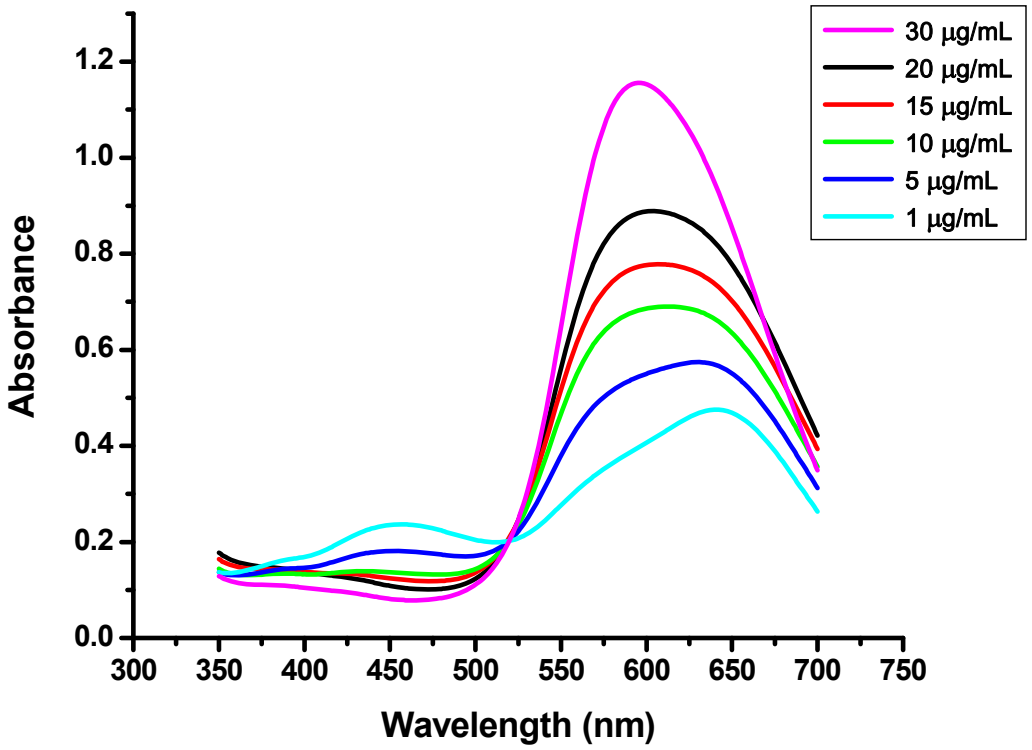

Figure 3-14. Absorbance spectra for bovine serum albumin standards in Coomassie blue G-250. Inset is a color code for the spectra representing different protein concentrations in µg/ml.

The BSA standards prepared were of concentrations of 30 µg/mL, 20 µg/mL, 15 µg/mL, 10 µg/mL, 5 µg/mL and 1 µg/mL. A spectral shift was observed in the absorbance maximum from 465 nm to 595 nm upon binding to the protein as expected. As can be observed in Figure 3-14, there is an inverse relationship between protein concentration and absorbance below 525 nm and this inverse relationship has an absorbance maximum at about 465 nm. There are possibilities of interfering substances

such as surfactants to results obtained from the Bradford assay, but these were a non-factor in this study since all protein standards and samples were treated under identical buffer conditions. A standard curve was constructed of absorbance at 595 nm as a function of the known protein content of each standard. The standard curve was used to estimate the amount of the purified recombinant BK_{Ca} channel proteins corresponding to the measured absorbance values. Figure 3-15 illustrates the standard curve constructed from the absorbance of BSA standards.

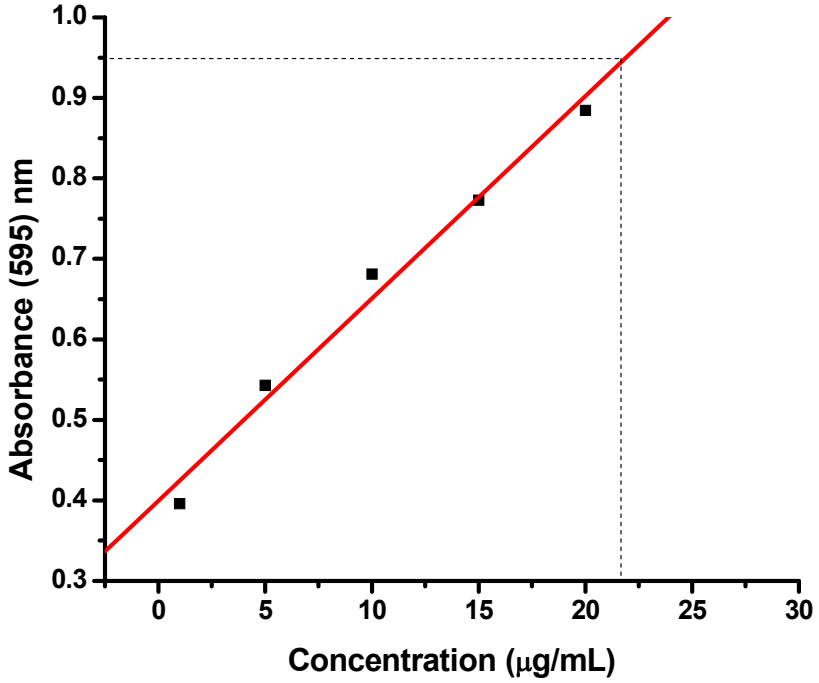

Figure 3-15. Standard curve plotted from A595 nm values from BSA for the estimation of protein concentration. The dotted line represents the absorbance of the extracts of the purified recombinant mRFP1-tagged BK_{Ca} channel.

The relationship between concentration and absorbance was best described by a straight line; therefore, a linear regression line was plotted through the set of standard points to estimate the concentration of purified mRFP1-BK_{Ca} channel proteins. The test sample resulted in an absorbance of 0.95 interpolated by the dotted line in Figure 3-15

and this yielded the concentration of the purified samples. A value of 23 μg/mL was determined to represent the concentration of the mRFP1-tagged BK_{Ca} channels purified and quantitated as described above based on the plotted standard curve.

Reconstitution of BK_{Ca} Channels into Liposomes

After purification, channels were incorporated into model membranes for further functional studies. The mechanism of octyl glucoside-mediated reconstitution involves, first, a direct incorporation into detergent-saturated liposomes, followed by a gradual removal of detergent.[156] Because of the relatively high CMC of octyl glucoside and its high monomer solubility, it was depleted from the protein sample by dialysis. The m-RFP1-tagged BK_{Ca} channels were reconstituted in 7:3 DPhPC: DPhPE liposomes at a lipid-protein ratio of 10:1 (w/w). The reconstitution procedure is detailed in the methods section of this chapter. Figure 3-16 shows negative-staining TEM imaging of DPhPC: DPhPE lipid dispersions prepared by hydration in 5 mM MOPS buffer at pH 7.4.

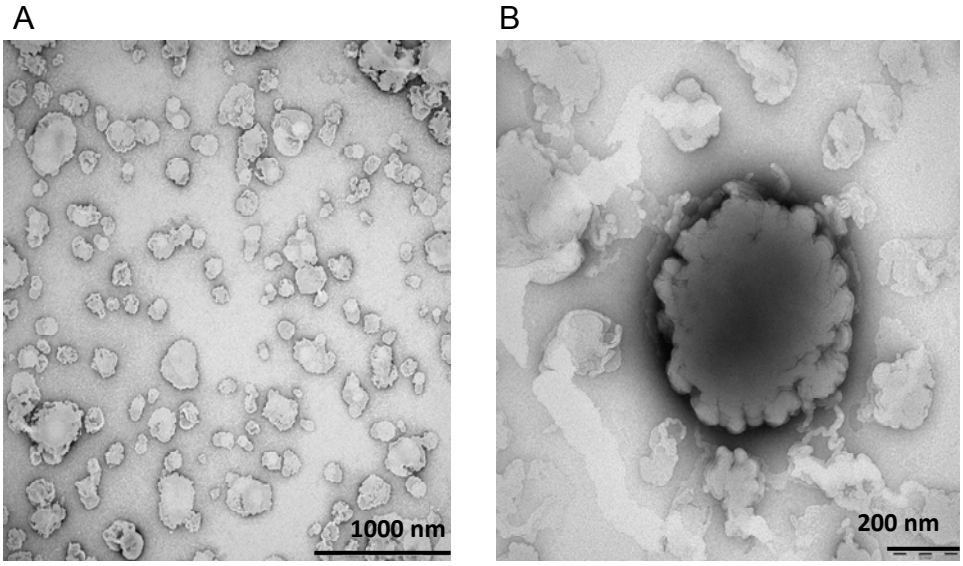

Figure 3-16. Negative-staining of 100 nm extruded DPhPC: DPhPE lipid vesicles at a 7:3 molar ratio. A) Image of dispersions of the lipid sample. B) Magnification of one of the vesicular structures observed from panel A.

TEM shows that the formed structures were not spherical, and had an average diameter size of 200 nm as can be observed in panel A of Figure 3-16. Magnification of the image shown in Figure 3-15 panel B reveals an apparent aggregation of vesicles that would explain why the objects had larger sizes than the ~100 nm diameter expected for liposomes extruded though 100 nm polycarbonate membranes. Polystyrene beads were added in the dialysis tank outside the dialysis bags to keep the external concentration of dialyzed detergent at a minimum, thus decreasing the time of dialysis by reducing on the number of required buffer changes. Figure 3-17 shows negative-staining TEM images of proteoliposomes obtained after completion of dialysis.

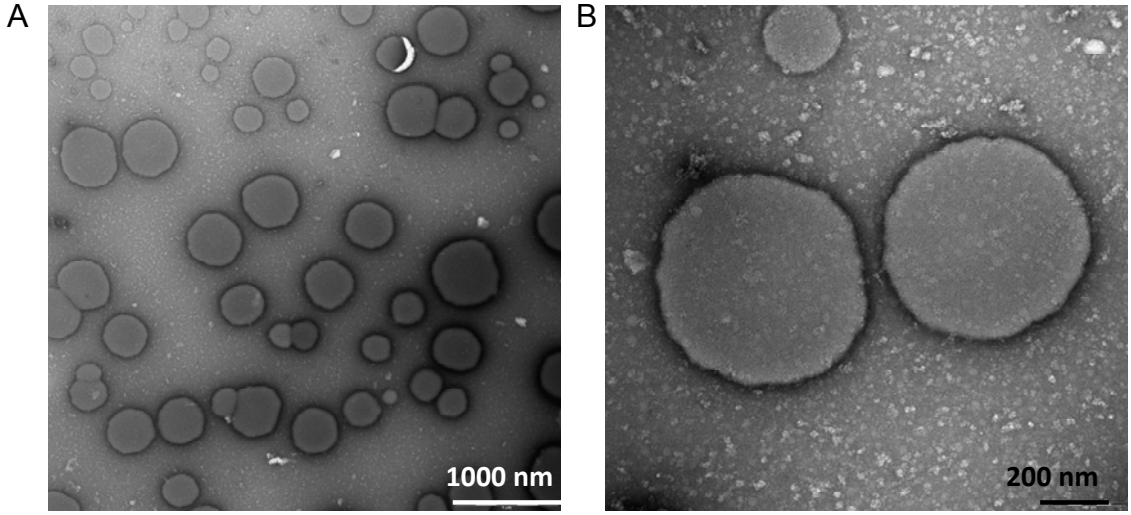

Figure 3-17. Negative-staining TEM images after dialysis of octyl glucoside for proteoliposome formation. A) Proteoliposomes of a homogenous size distribution representing the whole dialyzed batch. B) Magnification of TEM image to provide details of surface morphology.

It can be observed in Figure 3-17 panel B that the resultant proteoliposomes obtained after dialysis had homogenous sizes of approximately 400 nm diameters. These proteoliposomes were morphologically very spherical with ample internal volume in which incorporated BK_{Ca} channels could accumulate ions. The confirmation of

successful insertion of channels into liposomes and functional analysis of the reconstituted mRFP1-tagged BK_{Ca} channels is investigated in Chapter 5 of this study.

Conclusions

This chapter details the heterologous expression, purification and reconstitution of recombinant BK_{Ca} channels in *Xenopus laevis* oocytes. Successful expression of the desired ion channels was demonstrated by TEVC in two ways. Foremost, the voltage clamping of oocytes injected with mRFP1-tagged BK_{Ca} channel cRNA showed a flow of macroscopic currents which are consistent with those produced by voltage-dependent ion channels expressed on oocyte membranes and not the stretch-activated channels that are typically expressed endogenously in oocytes. Secondly, the possibility of the currents originating from endogenously expressed BK_{Ca} channels was ruled out by the currents observed of 10^{-6} picoampere (pA), 6 orders of magnitude higher, compared to the 10^{-12} picoampere (pA) currents obtained from the expression of endogenous BK_{Ca} channels in oocytes.[146] The red glow of fluorescencing oocytes observed under a bright field microscope originated from the mRFP1 fusion tag incorporated in the heterologously expressed BK_{Ca} channels, further supporting the conclusion that the expressed channels were translated from the injected cRNA.

The TEVC results suggest that the incorporation of mRFP1 and histidine fusion tags to form the chimeric BK_{Ca} channel does not prevent function. Additionally, the results demonstrate that the C-terminal truncation yields channels that produce macroscopic currents and electrical properties characteristic of BK_{Ca} channels.[38] SDS-PAGE reveals that C-terminally deleted recombinant *mslo* mRFP1-tagged BK_{Ca} channels expressed in *Xenopus laevis* oocytes have a molecular weight of 85 kDa which is approximately 15 kDa greater than expected, however, Western blotting using

antibodies specific for histidine-tag fusion proteins confirmed that the expressed and purified channels were indeed the chimeric BK_{Ca} channels. The higher than expected molecular weight is associated with probable N-glycosylation of the channels, since use of *X. laevis* oocytes as an expression system requires glycosylation which facilitates the effective trafficking of expressed channels to the oocyte membrane.[153] Glycosylation alters the mass-to-charge ration of the SDS-protein complex resulting in an apparently greater molecular weight of proteins analyzed by SDS-PAGE. The expressed mRFP1-tagged BK_{Ca} channels were successfully reconstituted in model membranes for functional analysis. Analysis by electrophysiology is investigated in Chapter 5 of this study and it served as a confirmation of successful reconstitution and also allowed investigations into whether the functional integrity of expressed channels was retained after purification.

CHAPTER 4
DIPHYTANOYLPHOSPHATIDYLCHOLINE AND -ETHANOLAMINE LIPID MIXTURE CHARACTERIZATION OF VESICLES AND PLANAR BILAYER FORMATION

Introduction

Lipid molecules form the bilayer structures that constitute the primary component of biological membranes. Biological membranes are highly complex with regard to their constituents and the study of any single membrane component in isolation typically involves removal from the membrane and reconstitution in simple synthetic bilayer lipid matrices. Lipids can be used to form synthetic bilayers as cell membrane mimics in different model membrane configurations for a diversity of applications such as membrane protein studies,[77, 94] pharmaceutical drug discovery,[157-159] biosensor development[97, 98, 160] membrane dynamics studies[161, 162] and studies of protein-lipid interactions.[163, 164] There is a great diversity of membrane lipids, each with specific designated roles in cells in which they are localized. The most commonly found membrane lipids are glycerophospholipids, most of which have one of the glycerol hydroxyls linked to a polar phosphate-containing group. Each of the other two hydroxyls is attached to a hydrophobic group through ester or ether linkages, with the phosphate group being at the sn-3 position of glycerol as illustrated in Figure 1-6.[66]

However, in *archaebacteria* that live in areas of extreme environmental conditions such as high temperatures, high acidity or high alkalinity, are found lipids with the stereoconfiguration of glycerophospholipids reversed such that the phosphoryl groups are in the sn-1 position of glycerol.[67] Lipids in many of these bacteria have hydrophobic constituents that are branched, saturated isopranyl glycol ethers rather than fatty acid esters.[165] These branched chains referred to as phytanoyl chains have unique acyl

chain packing properties which confer bilayer stability to membranes, as well as low permeability to water and other small ionic and nonionic molecules.[166]

Phytanoyl lipids exhibit high mechanical and chemical stability, and are therefore ideal for the formation of model membranes for protein reconstitution. Translational and rotational motions of headgroups are slower in lipids with branched acyl chains resulting in a reduction of conformational and wobbling motions of these lipids, and dynamics that are similar to those observed when cholesterol molecules are added to lipid bilayers.[167] Phytanoyl lipids form model membranes with high resistivity to permeation by electrical currents, making them suitable for electrophysiological applications involving ion-conduction measurements through reconstituted pore-forming peptides and ion channels.[168] The data for electrophysiological measurements of ion channels reconstituted in model membranes containing phytanoyl lipid mixtures are discussed in Chapters 5 and 6 of this dissertation.

This chapter focuses on the characterization of the formation of model membranes of the phytanoyl lipids, 1,2-diphytanoyl-*sn*-glycero-3-phosphocholine (DPhPC) and 1,2-diphytanoyl-*sn*-glycero-3-phosphoethanolamine (DPhPE), as well as specific mixtures of the two. The chemical structures of the two lipids are presented in Figure 1-12. Choline and ethanolamine lipids are generally the most abundant in the membranes of a majority of organisms. When a small amount of pure DPhPE is added to pure DPhPC, the average size of the headgroup becomes smaller while the acyl chain cross section remains the same, making it easier to accommodate membrane proteins in lipid mixtures of the two. Pure DPhPC, as well as DPhPC mixed with DPhPE in a 7:3 molar ratio, have previously been studied in our laboratory and shown to form

vesicles, which upon fusion with modified self-assembled monolayer (SAM) surfaces formed tethered bilayers, creating a suitable environment for fully functional ion channels.[99, 169, 170]

For the study documented here, particular emphasis was placed on how these lipids behave when hydrated in aqueous media and the assemblies they form when they interact with solid substrates. The specific conditions and compositions that favor bilayer formation were also analyzed. As a platform for electrophysiology studies, lipid bilayers can be used either as thin barriers separating two aqueous solutions across small apertures [171] or supported on solid substrates. The reconstitution of purified recombinant BK_{Ca} channels as documented in this dissertation is performed in model membranes prepared from PC: PE lipids in a 7:3 molar ration, which is closely related to the native composition of the two lipids in *Xenopus laevis* oocytes, used here as the expression system for these ion channels. The percentage of total phospholipids in oocyte membranes includes 65 % PC and 19 % PE while the rest is composed of phosphatidyl inositol (PI), phosphatidyl serine (PS), sphingomyelin and cholesterol.[172] Evidence shows that specific phospholipid headgroups and structural features of sterols play a more essential role in functional protein-lipid interactions than the effects of bulk lipid components.[60]

Dynamic light scattering (DLS), diffusion nuclear magnetic resonance (NMR-D), and cryogenic transmission electron microscopy (cryo-TEM) were used to characterize the lipid assemblies formed by different compositions of DPhPC and DPhPE mixtures in aqueous solution. Each technique gave insight into the physical properties of lipid assemblies, and these properties include size, phase, and diffusivity. The lipid

compositions that formed vesicles in aqueous solution were further investigated in terms of the interactions of their vesicles with solid surfaces. The interactions between plasma-treated gold and silica with lipids were examined using quartz crystal microbalance with dissipation monitoring (QCM-D). The effects of lipid concentrations on either vesicle fusion or vesicle adsorption were monitored by atomic force microscopy (AFM) to give visual analysis of the resulting structures formed on solid substrates. Furthermore, studies were performed to examine the temperature effects on sizes of formed vesicles of different lipid compositions of DPhPC and DPhPE.

Materials and Methods

Lipids and Chemicals

Archaea phospholipids, 1,2-Diphytanoyl-sn-Glycero-3-Phosphocholine (DPhPC) and 1,2-Diphytanoyl-sn-Glycero-3-Phosphoethanolamine (DPhPE), purity >99%, were used as purchased from Avanti Polar Lipids (Alabaster, AL). Buffer solutions were prepared with 5 mM 3-Morpholinopropanesulfonic acid, MOPS, (>99.5%, ultra grade, from Fluka), 250 mM potassium chloride (ACS certified grade), and 0.1 mM calcium chloride (ACS certified grade). The buffer was titrated to pH 7.4 using potassium hydroxide (ACS certified grade). All the salts were purchased from Fisher Scientific and used as received. Milli-Q filtered water (>18 MΩ·cm) was used for all sample preparations and studies.

Gold Surfaces

For the AFM investigations, ultra smooth gold surfaces were prepared on silicon wafers by evaporation of a 3 nm thick layer of Ti followed by deposition 500 nm thick layer of 60% Au to 40% Pd alloy. A 200 nm gold layer was finally deposited on top of the alloy. The gold surfaces were cleaned by rinsing with hexane, acetone, ethanol and

water respectively then dried under a continuous stream of nitrogen. This was followed by UV/ozone treatment of the gold surface in a Harrick PDC-32 G plasma cleaner/sterilizer at high radio-frequency power for 20 minutes under a flow of oxygen for oxidation, and for the removal of both chemical and organic contaminants.

Vesicle Preparation

The vesicles were prepared by mixing lipid solutions (2 mg/ml in chloroform) of DPhPC and DPhPE lipids in the desired molar ratios. The chloroform was evaporated under vacuum and the resultant film of lipid mixtures hydrated in water or buffer at the desired concentration, and then heated at 50°C for one hour under vigorous stirring until a clear solution was obtained. After allowing the suspension to cool to room temperature, it was bath sonicated for 5 min, followed by extrusion through an 80 nm polycarbonate membrane (21 times) using a mini-extruder from Avanti Polar Lipids. Extrusion was performed no longer than 24 hours prior to any investigation.

Cryogenic Transmission Electron Microscopy (Cryo-TEM)

Cryo-TEM was performed on a Phillips CM120 BioTWIN cryo electron microscope operated at 120 kV using an Oxford CT3500 cryo-holder. Specimens were kept in the microscope and imaged at a temperature of about 93.5 K using liquid nitrogen cooling. Images were recorded digitally with a CCD camera (Gatan MSC791), and under focus conditions to improve the phase contrast. Specimens for electron microscopy were prepared in a controlled environment vitrification system (CEVS)[173] to ensure a fixed temperature (26-28°C) and high humidity in order to minimize evaporation. In brief, a drop of sample was put on a glow discharge pretreated Pelco grid (lacy carbon film, supported by a copper grid). Then, excess solution was removed by blotting with filter paper, leaving a thin meniscus of the solution in the holes of the carbon film. The

blotting was done first on the side opposite to the sample drop and then gently on the same side as the placed sample. The grid was then rapidly plunged into liquid ethane at its melting temperature. The vitrified specimens were stored under liquid nitrogen.

Dynamic Light Scattering (DLS)

DLS measurements were performed on a Precision Detectors PDDLS/CoolBatch+90T instrument and the data were analyzed using the Precision Deconvolve32 Program. The measurements were performed using a 683 nm laser source and a 90 degree scattering angle, set at 20° C. When necessary, additional dilutions were performed until the count rate was between the recommended 200 and 400 k counts per second. CONTIN analysis was used for calculating the size distributions.[174, 175]

NMR Diffusion

The NMR diffusion experiments were performed on a Bruker 750 MHz (17.6 T) instrument equipped with a diffusion probe with 24 T/m actively-shielded gradients (Diff60). A Bruker 10 mm diffusion probe was used but with 5 mm NMR tubes. All NMR experiments were performed at 25 °C. Stimulated Echo with Pulsed Field Gradients (PFG-STE) was used. Diffusion time (Δ) of 100 ms and gradient time (δ) of 1.1 ms were used and the gradient strength (g) was arrayed in 32 steps with 16 scans in each step. To monitor the diffusion of the vesicles, a small amount (less than 1% of the lipids) of hexamethyl-disiloxane (HMDS) was added. HMDS is essentially insoluble in water, so the characteristic HMDS signal (0 ppm) will arise from HMDS that is dissolved into the lipid membrane. The echo-decays obtained from the vesicles gave curved plots in a Log Y-axis of signal intensity vs. k, k= $\left(\gamma^2 g^2 \delta^2 \left(\Delta - \delta/3\right)\right)$, where γ is the gyromagnetic

constant. Echo-decays were fitted to a Log Normal distributed function, which can be described by:

$$P(D) = \frac{1}{D\sigma_{\ln}\sqrt{2\pi}} \exp\left(- \frac{\left[\ln(D) - \ln(D_m)\right]^2}{2\sigma_{\ln}^{\ 2}} \right) \tag{4-1}$$

where D_m is the mass weighted median diffusion coefficient and $\sigma_{\ln}$ is the standard deviation of the logarithmic distribution of diffusion coefficients. A mean diffusion coefficient, $\langle D \rangle$, can be calculated from:

$$\langle D \rangle = D_m \exp\left(\sigma_{\ln}^{\ 2}/2\right) \tag{4-2}$$

and the normal standard deviation, σ_D, of the diffusion coefficients with

$$\sigma_D^{\ 2} = \langle D \rangle^2 \left(\exp\left(\sigma_{\ln}^{\ 2}\right) - 1\right) \tag{4-3}$$

The diameters of the vesicles were obtained through the Stokes-Einstein relation.[176]

Quartz Crystal Microbalance with Dissipation Monitoring (QCM-D)

The QCM-D measurements were performed on a QCM-Z500 from KSV Instruments (Helsinki, Finland) equipped with a temperature control unit from Oven Instruments. AT-cut crystals, coated with either an evaporated silica or gold layer, had a resonance frequency of 5 MHz and were also purchased from KSV. Prior to the measurements, the crystals were cleaned using either piranha solution for the gold-coated crystals (3:1 concentrated sulphuric acid to 30% hydrogen peroxide solution) or an SDS solution for the silica-coated crystals, followed by rinsing with water and ethanol, and drying with a gentle stream of nitrogen gas. All rinse cleaning procedures were followed by UV-oxygen plasma cleaning for 20 min. This sequence of pre-treatment led to clean and oxidized surfaces that had contact angles of less than 6 degrees. The instrument was calibrated using the standard procedure as described by

the instrument provider.[99] The fluids were introduced batch-wise via a reservoir, and then proceeded to a bypass chamber (500 µl volume), located above the crystal. After loading the instrument with the crystal, it was allowed to stabilize in the buffer solution for approximately 30 min until a stable baseline was obtained. The measurements were recorded at the fundamental frequency, the 3rd overtone, and the 5th overtone. The measured resonant frequency, *f*, depends on the mass of the oscillating crystal including any adsorbed species. For rigid films there is a relation between the change in frequency $\triangle f$ and the adsorbed mass, *m,* according to the Sauerbrey equation

$$\Delta m = -\frac{C}{n}\Delta f \tag{4-4}$$

where C is the mass sensitivity constant (17.7 ng•cm^{-2}•Hz^{-1}) at f=5 MHz and n is the overtone number. The dissipation factor, *D*, is related to the energy lost (E_{lost}) to the surroundings in relation to the stored energy (E_{stored}) upon oscillation and is defined as

$$D = \frac{E_{lost}}{2\pi E_{stored}}\Delta f = \frac{R}{\omega L} = \omega RC \tag{4-5}$$

where ω is the angular frequency, *R* is the resistance, *L* is the inductance, and *C* is the capacitance of the crystal.

Atomic Force Microscopy (AFM)

AFM analysis was performed in buffer solution using a Nanoscope III MultiMode Scope (Veeco) equipped with a 13 µm E-scanner. The instrument was calibrated in the z-direction using a silicon grating (TGZ01, Mikromash), with a step height of 20 nm (accuracy 1 nm). A fluid cell was used, which was cleaned in ethanol and water prior to use. The cell was used without o-ring. Images were obtained using silicon cantilevers (Nanosensors, Neuchatel, Switzerland with dimensions: T = 3.8-4.5 µm, W = 26-27 µm,

and L = 128 μm). The cantilevers were mounted in the fluid cell and a drop of the solvent solution was placed on the tip to ensure wetting. The solution was placed on the sample surface, followed by attachment of the fluid cell. No addition or removal of liquid through the hoses that are attached to the sample holder was performed. Prior to the measurements, the sample was left undisturbed for ~20 min to let the solution equilibrate. AFM analysis was performed by scanning in contact mode and the images were processed using a second-order parameter flattening.

Results

Cryogenic Transmission Electron Microscopy (Cryo-TEM)

To visualize the mesophases of vesicles, cryo-TEM was utilized. In Figure 4-1, TEM micrographs of the vesicles are presented for the different lipid compositions.

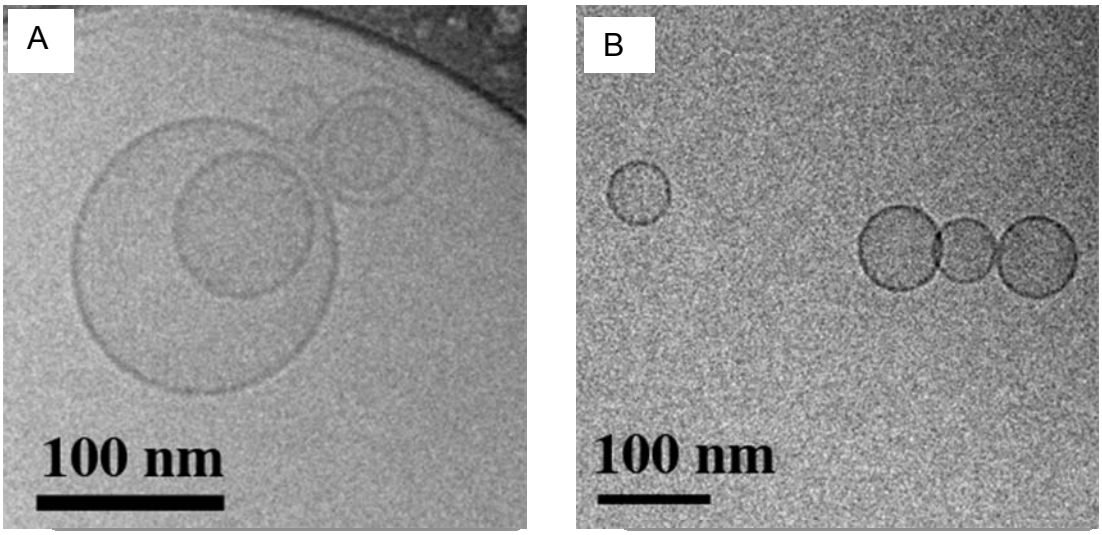

Figure 4-1. TEM micrographs of hydrated dispersions composed of extruded vesicles. A) Pure DPhPC and B) 7:3 DPhPC: DPhPE. The lipid concentration was 0.2 g/l in 5 mM MOPS buffer at pH 7.4. All scale bars correspond to 100 nm.

In the sample containing pure DPhPC, unilamellar vesicles were observed (Figure 4-1A). The mean diameter of these vesicles was 92 nm (n=8) and they were often found

adhered to each other. In Figure 4-1 panel B, a micrograph of vesicles composed of 7DPhPC:3DPhPE is presented. These vesicles were also unilamellar, though slightly smaller in size compared to the pure DPhPC (diameter ~ 60 nm (n=7)). Micrographs of samples of 5DPhPC:5DPhPE are shown in Figure 4-2 panels A, B, and C.

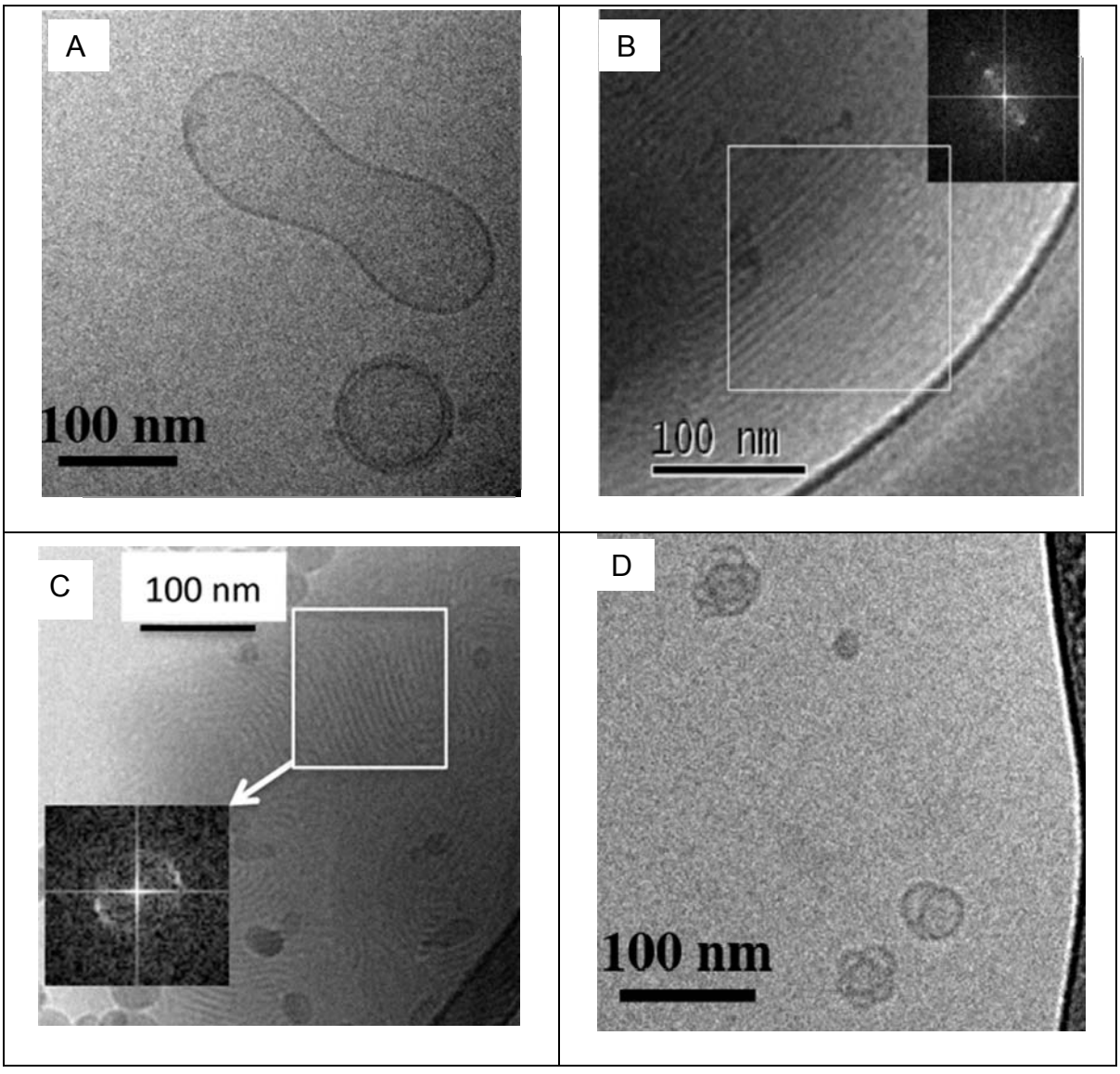

Figure 4-2. TEM micrographs of samples of varying lipid composition: (A, B, C) 5DPhPC:5DPhPE, and (D) 3DPhPC:7DPhPE. The white squares in B and C were Fast Fourier Transformed (FFT), resulting in the inserted FFT patterns.

The sample contained both unilamellar vesicles (Figure 4-2 A) and more densely-packed structures, which appear to be composed of close packed lipid bilayers, likely

discrete lamellar liquid crystalline phases (Figure 4-2 panels B and C). The repeat distance was calculated from the Fourier transform of selected parts of the image (Figure 4-2 C) and was found to be around 6.5 nm, which corresponds well to the proposed lamellar phase based on the height of a lipid bilayer. However, the specific phase of the liquid crystal cannot be determined solely from the micrographs. In Figure 4-2 D, a micrograph obtained from the 3DPhPC:7DPhPE sample is presented. In these samples, small flower-like, vesicles were observed and both the larger unilamellar vesicles and the densely-packed lipid bilayer aggregates were absent. For the sample consisting of pure DPhPE, no objects could be observed with the cryo-TEM technique.

DLS and NMR Diffusion

DLS and NMR diffusion were utilized to investigate the size of the lipid structures in aqueous solution. For DLS, the time-dependent fluctuation in the scattering intensity is observed. The scattering intensity is highly dependent on the size of the scattering entity which can cause larger objects to be overrepresented in the measured size distribution of a polydisperse sample. However, this overrepresentation can be corrected for by using a weighting function that transforms the mean intensity value to the mean number value. In Figure 4-3, both the intensity data and the adjusted data are presented as the sample's average effective diameter versus the lipid composition. As seen in the figure, the sizes of the aggregates' calculated diameters are independent of the lipid compositions ranging from pure DPhPC to 30% DPhPE. The samples' average effective diameters were approximately 100 nm (mean value weighted by the total number of object). Increasing the DPhPE relative molar concentration from 30% to 70%, caused a linear increase of the sample diameter to approximately 200 nm. Pure DPhPE samples had a relatively smaller diameter. In Figure 4-3, the aggregate sizes obtained

by NMR diffusion using D_m and $\langle D \rangle$ extracted from Equation 4-1 are also presented. The sizes measured by the NMR diffusion technique follow the same trend as the sizes measured by DLS. For the pure DPhPC and 7DPhPC:3DPhPE samples, smaller diameters were obtained by NMR diffusion in comparison to the results obtained by DLS. For the sample composed of 5DPhPC:5DPhPE, the two techniques gave sizes that were in good agreement. For higher concentrations of DPhPE, including pure DPhPE, the sample diameters obtained by NMR diffusion were larger than the number-averaged DLS sizes.

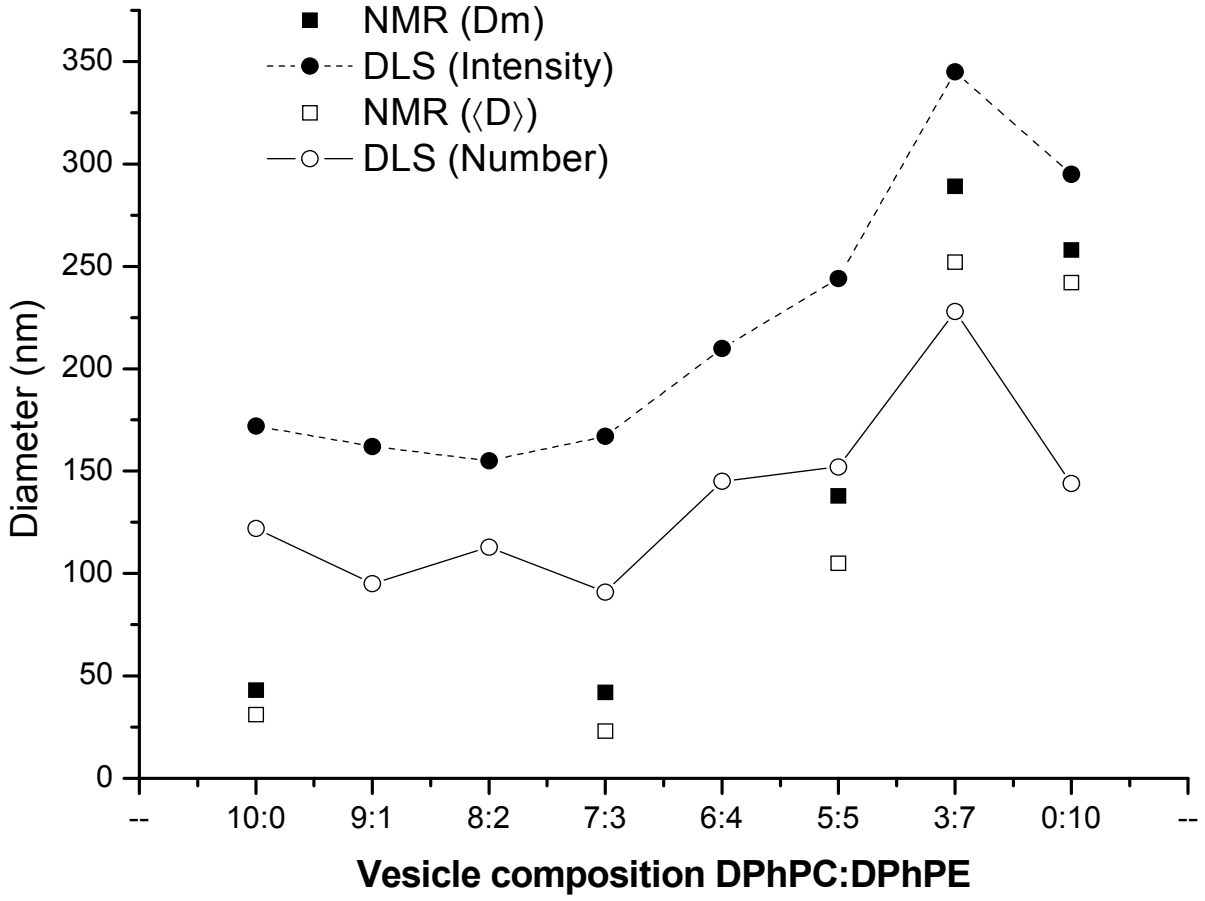

Figure 4-3. Average effective diameter as a function of lipid ratio. The sizes were obtained using DLS and NMR-diffusion and the lipid concentration was 0.2 g/l. The lines in the figure are only a guide to the eye.

Quartz Crystal Microbalance with Dissipation Monitoring (QCM-D)

Figure 4-4 shows the measured change in frequency and dissipation as a function of time that was recorded while two different concentrations of pure DPhPC vesicles interacted with a silica substrate.

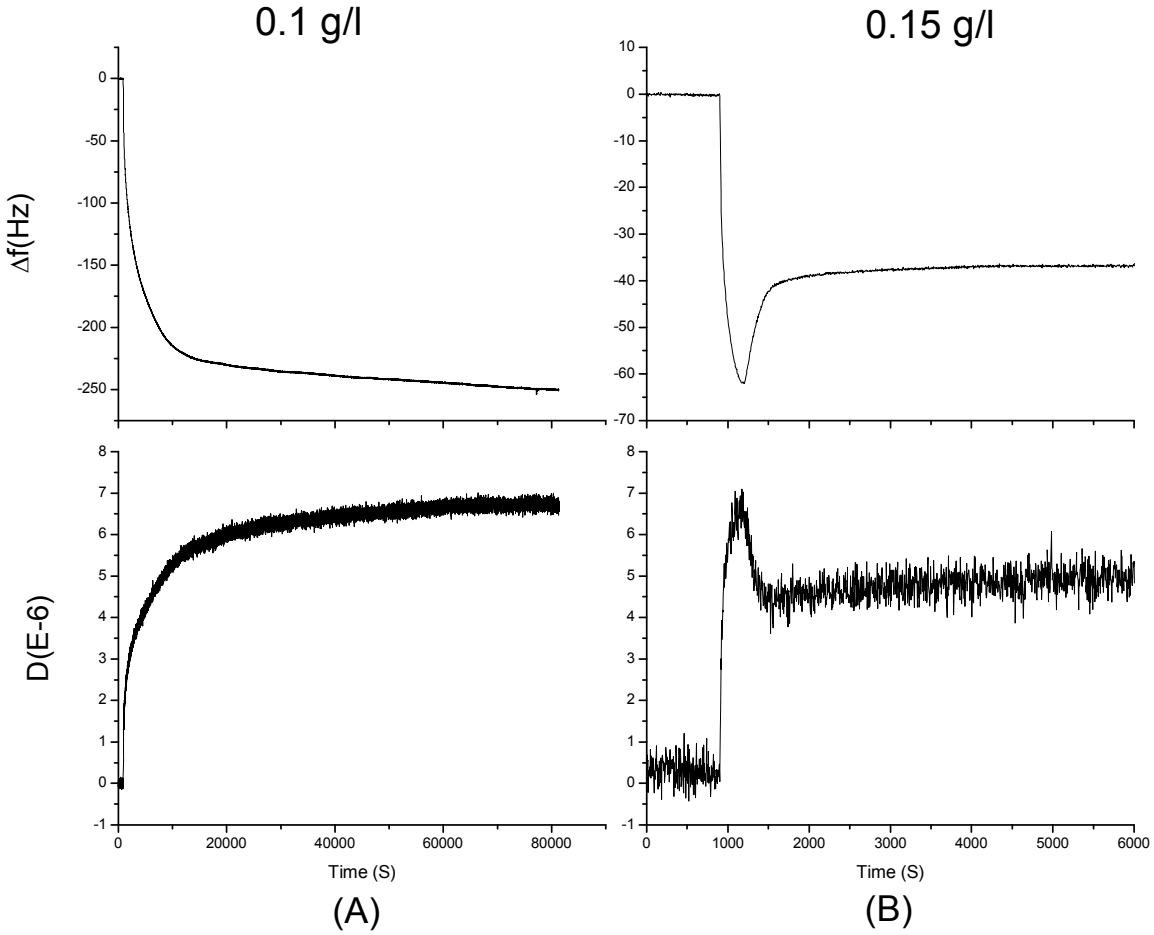

Figure 4-4. Changes in resonant frequency and dissipation versus time for adsorption of pure DPhPC vesicles onto silica substrates. (A) 0.1 g/l and (B) 0.15 g/l, The presented QCM-D data was recorded at the fifth overtone and renormalized such that $\triangle f = \triangle f_{n=5}/5$.

When the lipid concentration was relatively low, 0.1 g/l, a decrease in frequency together with an increase in dissipation over the course of time were observed as shown in Figure 4-4 A. The corresponding frequency shift indicates that vesicles were adsorbed on the silica surface, forming a highly viscoelastic film as evidenced by the

high energy dissipation. When the lipid concentration was increased to 0.15 g/l (Figure 4-5 B), the decrease in frequency change is initially the same as that observed for lower concentrations, but after ~1150 seconds the frequency starts to increase, indicating a decrease in adsorbed mass, followed by frequency stabilization (Figure 4-4 B). This adsorption behaviour is typical of vesicle fusion, where vesicles first adsorb on the surface until a critical concentration is attained and then rupture to form a solid-supported lipid bilayer.[90] When a vesicle ruptures, the hydrodynamically-coupled solvent in the vesicle's interior is released, resulting in an increased frequency (mass decrease) and a decreased dissipation (lower degree of viscoelasticity). The total frequency change was ~37 Hz, which corresponds to an adsorbed mass of 655 ng/cm^2 (according to equation 4-4). Assuming that a bilayer is formed, based on two-step vesicle fusion kinetics, a surface area per molecule of 43 Å^2 (Mw=846 D) results. However, this area is smaller than that of 77 Å^2, which was previously reported for DPhPC.[167]

Figure 4-5 shows the measured change in frequency and dissipation as a function of time that was recorded while various concentrations of pure DPhPC vesicles at various lipid concentrations interacted with a plasma-treated gold substrate. When the lipid concentration was low, 0.02 g/l, a decrease in the measured frequency together with an increase in dissipation over the course of time was observed (Figure 4-5 A). The corresponding frequency shift indicates that the vesicles adsorbed on the gold surface. When the lipid concentration was increased to 0.1 g/l, a more pronounced frequency decrease and dissipation increase as a function of time was observed (Figure 4-5 B). This indicates a higher concentration of adsorbed vesicles and a higher degree of film viscoelasticity (likely due to the increased vesicle surface coverage and the related

hydrodynamically-coupled solvent) in comparison to the 0.02 g/l sample. In Figure 4-5 C, the measured data obtained from a 0.15 g/l sample is shown. Here, the frequency decreases initially, followed by a frequency increase after ~1100 seconds, indicating a decrease in adsorbed mass. The total change in frequency was ~59 Hz, which corresponds to an adsorbed mass of 1044 ng/cm^2 (according to equation 4-4). Assuming that a bilayer is formed based on the characteristic two-step vesicle fusion kinetics, the result is a surface area per molecule of 27 Å^2, which is even smaller than the one obtained using the silica surface.

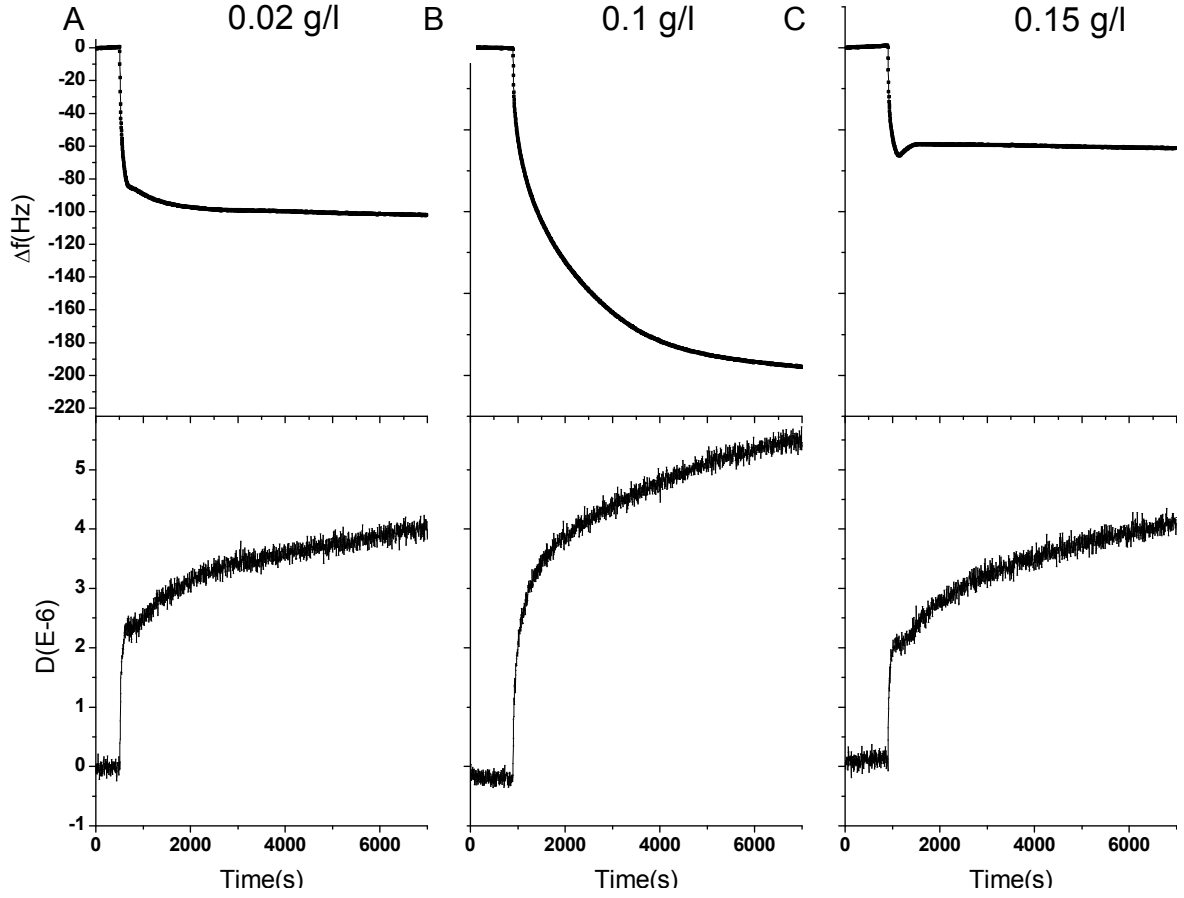

Figure 4-5. Changes in resonant frequency and dissipation versus time for the adsorption of pure DPhPC vesicles onto oxidized gold with lipid concentrations of (A) 0.02 g/l, (B) 0.1 g/l, and (C) 0.15 g/l. The data was recorded at the fifth overtone and renormalized such that $\triangle f = \triangle f_{n=5}/5$. For each concentration, the data are plotted on an identical scale.

It is important to note that the Sauerbrey equation used here to calculate the molecular surface areas is only valid for non-viscoelastic films, which is not the case in this situation. This can be seen in the dissipation curves (Figure 4-5 panels B and C), which show that the dissipation is relatively high even after the bilayer has formed, indicating either formation of a highly viscoelastic bilayer due to the unique structural features of phytanoyl lipids (see discussion) or incomplete bilayer formation such that intact, adsorbed vesicles coexist with ruptured vesicles. The QCM-D experimental results presented here were all obtained in buffer at pH 7.4. Experiments were also performed in pure water, which resulted in no vesicle adsorption or fusion regardless of lipid concentrations used. Furthermore, additional QCM-D measurements were performed on all of the aforementioned lipid compositions. Mixtures that had DPhPE lipid concentrations of less than 50% showed the same behaviour as for pure DPhPC. However, with increasing DPhPE concentration, no adsorption or vesicle fusion was observed, for the various lipid compositions used.

Atomic Force Microscopy (AFM)

AFM was performed on ultra smooth gold surfaces in the same buffer solution as that used for performing the QCM-D measurements. In Figure 4-6 A, an image of a pure gold surface without deposition of molecules on the surface is shown. As seen, the surface is smooth even on the nanometer length scale. In Figure 4-6 B, the same surface is shown two hours after the addition of a DPhPC vesicle solution at a concentration of 0.2 g/l. The surface is still smooth, however much less sharper images were obtained. This decreased sharpness is most probably due to the presence of a lipid bilayer on the gold surface, which would results in a viscoelastic surface that can be disturbed by the scanning probe.

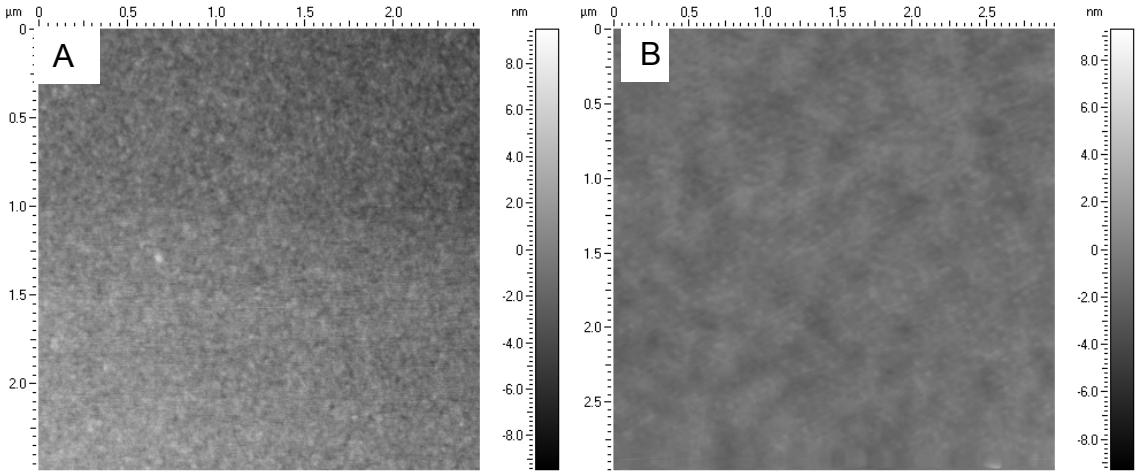

Figure 4-6. AFM images showing vesicle fusion on gold substrates. A) The pure gold surface (B) the same surface after vesicle addition and subsequent fusion, leading to solid-supported bilayer formation. The measurements were obtained in contact mode using a liquid cell.

Figure 4-7 shows both 2 dimensional and 3 dimensional renderings of AFM images, as well as a cross section analysis. These images were obtained two hours after addition of a 0.1 g/l vesicle solution.

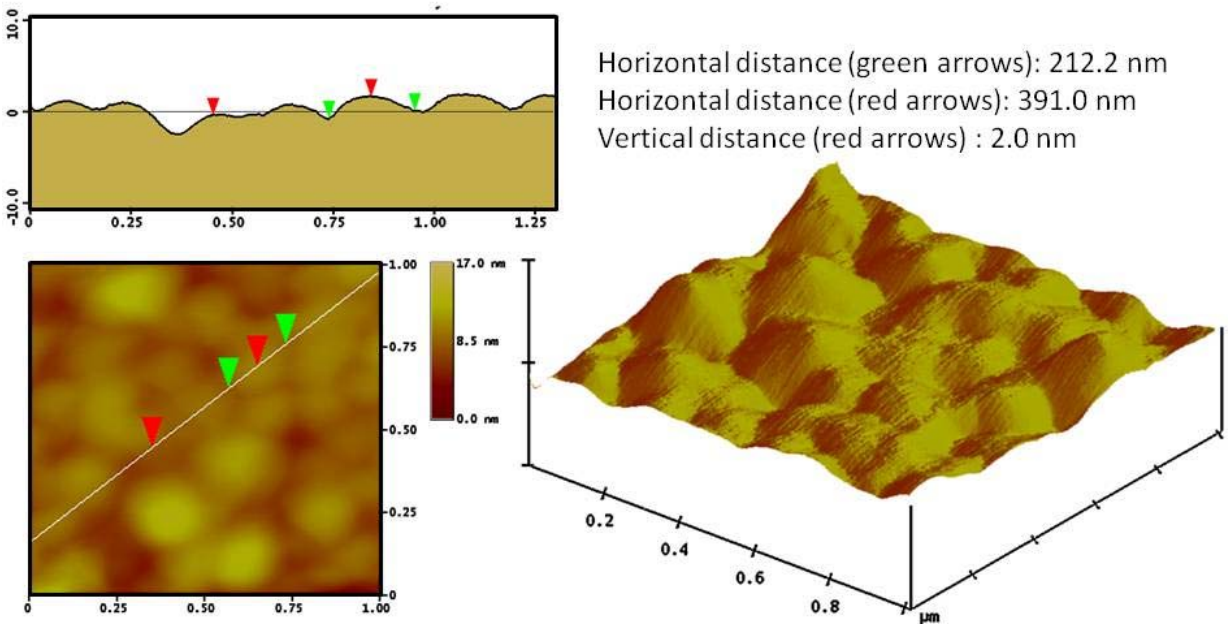

Figure 4-7. AFM images of pure DPhPC vesicles deposited on an ultra flat gold surface. The lipid concentration was ~0.1 g/l. The measurements were performed in contact mode using a liquid cell.

In the bottom left image in Figure 4-7, the surface is viewed from above and there are round objects that have diameters between 100-250 nm which is within expected range for adsorbed vesicles. Due to substrate-vesicle interactions, the adsorbed vesicles are not spherical but rather flattened in a pancake-like morphology, hence the larger diameters of these entities. These 3 dimensional features can be seen in the right figure, where a topographical image of the surface is presented. On the upper left, a cross section of the lower left figure is presented together with some relevant distances.

Discussion

In the present study, assemblies consisting of two phytanoyl lipids, 1,2-diphytanoyl-*sn*-glycero-3-phosphocholine (DPhPC) and 1,2-diphytanoyl-*sn*-glycero-3-phosphoethanolamine (DPhPE) in a polar environment were examined. From the results obtained by Cryo-TEM, DLS and NMR diffusion, it was determined that lipid compositions of single-component DPhPC and mixtures containing up to ~50% DPhPE form unilamellar vesicles, having sizes that are directly related, though not identical, to the membrane pore size of the polycarbonate membrane that was used for extrusion (~100 nm vesicle diameters vs. 80 nm membrane pore size). However, the vesicle sizes varied depending on the analytical technique used to measure them. For example, in the case of pure DPhPC vesicles, the diameters obtained were 122 nm (DLS), 43 nm (NMR-D), and 92 nm (Cryo-TEM). These differences in size are characteristic of using these different techniques and are due to the different physical properties that are analyzed with each technique. In the case of DLS and NMR-D the hydrodynamic radius is measured since they measure the free diffusion of particles. Even though the techniques give rise to different sizes for the same sample, the sizes follow an identical trend when the lipid ratio was varied. Cryo-TEM allows for a more direct method to

measure vesicle size. The technique, however, suffers from artifacts arising from the blotting process, which induces shearing on the sample. This shearing might affect the size and structure of the observed objects.[177] The specimen preparation technique might also result in objects that are forced closer to each other resulting in an apparent adhesion of imaged objects. This could for example be the reason why the pure DPhPC vesicles seem to be adhered to each other, even though DLS and NMR-D results show that the vesicles diffuse totally separate from one another.

The cryo-TEM technique, as with all microscopy techniques, suffers from poor statistics due to the low number of observed objects. At higher DPhPE concentrations, (>50%) both DLS and NMR revealed that the sizes of the measured objects increased. This was accompanied by an increase in size distribution, indicating a change in physical properties of the objects. There was further confirmation by cryo-TEM, with solutions containing 5DPhPC:5DPhPE, showing the appearance of several new structures in addition to unilamellar vesicles. These new structures were composed of lipid bilayers, which were less solvated in comparison to the vesicles, forming liquid crystalline structures of presumably hexagonal phase, even though this has not been confirmed in our studies. For the 3DPhPC:7DPhPE lipid compositions, only small flower-like vesicles were observed, although much larger objects were expected to be seen based on the results from the DLS and NMR-D measurements.

The absence of cryo-TEM images of the larger objects is likely due to the sample preparation process during which these larger objects may have been removed. These larger structures are likely similar to the dispersed liquid crystalline structures that were observed in the 5DPhPC:5DPhPE sample. Unilamellar vesicles were not observed in

the samples containing predominantly DPhPE, which would explain why our QCM-D results showed no vesicle adsorption with these lipid compositions. The seemingly small headgroup differences between these two lipids plays a role in the lipids' propensity to form or not form vesicles when in different mixtures. This difference significantly affects the critical packing parameter, resulting in a change of the lipid's spontaneous curvature. Also, the electrostatic energies are significantly different between the two head groups, with DPhPC having a much higher electrostatic energy.[35] As a consequence, the crystal to liquid crystalline transition temperature is lower for lipids with choline head-groups as compared to the amine head-groups. Studies performed on non-phytanoyl lipids with choline and ethanolamine head-groups, similar to investigations here, shows that a lamellar to reverse hexagonal phase transition occurs when the mixture contains more than 60% PE.[85, 178]

The QCM-D technique is an excellent tool to study vesicle adsorption and vesicle fusion since it reveals binding kinetics, calculates adsorbed film mass including hydrodynamically-coupled solvent, and provides viscoelastic information about the adsorbed film. In comparison to QCM-D studies performed on vesicles composed of straight chained lipids, phytanoyl lipids show slightly different behavior, especially as regards the analysis of dissipation. Usually, in the case of lipid bilayer formation, the dissipation increases when vesicles first adsorb to the surface but then decreases to near zero as vesicles rupture and the non-viscoelastic lipid bilayer forms.[90] In the case of phytanoyl lipids, the dissipation remains relatively high throughout the entire process, which has been observed in other studies for these types of lipids, performed on tethered supports.[99, 179] This result indicates that the bilayer formed has relatively high

viscoelastic character as compared to other bilayers, though the dissipation is still much less than that of an adsorbed vesicle film. Also, the final change in frequency after the vesicle fusion is larger than what has been obtained for DHPE, 37 Hz compared to 26 Hz.[90] In these investigations, the dissipation continues to be high even after the frequency has leveled out, indicating that the bilayer formed has significant viscoelastic character. A possible explanation for this finding could be a combination of high viscoelastic character of phytanoyl lipid bilayers, caused by the relatively high amounts of hydrodynamically-coupled solvent in the branched chains, together with incomplete bilayer formation. The branched chain structure of the lipids' hydrophobic tails leads to reduction of the conformational and wobbling motions of the alkyl chains, in contrast, the head groups do experience a higher degree of freedom and as a consequence, more solvent will be hydrodynamically-coupled around the lipid head groups, especially for DPhPC.[180] This increased bound water content together with the less dense packing of the hydrophobic tails will increase bilayer viscoelasticity, which could partly explain the QCM-D dissipation response. Despite the fact that phytanoyl membranes couple more solvent, excess chemical potential calculations have demonstrated that the lipid chain branching does not significantly change the partition of water through the hydrophobic part of the membrane.[167] Also, the alkyl branching inhibits the formation of cavities in the membrane, which could explain why the membranes have higher electrical resistances and low ion conduction.[167] The viscoelasticity of the formed bilayer could also be an explanation of the observations made using the AFM. When the lipid concentration was high enough resulting in lipid bilayer formation no sharp well resolved AFM micrographs could be obtained. This is something which is typical for AFM

investigations on low surfaces having low viscosity.[181] The QCM-D results showed that vesicle fusion was dependent on lipid concentration and the presence of ions, since no adsorption was observed in pure water. Even though the vesicle concentration is sufficient for full surface coverage, the concentration may not be great enough to cause vesicle fusion and bilayer formation. An excess of vesicles is needed to induce the bilayer formation, indicating that the interaction between the vesicles is essential. This phenomenon has been observed earlier for other lipid systems.[182] The AFM studies yielded results which are in agreement with observations made from the QCM-D data; that a relatively low lipid concentration results in vesicle adsorption and that there is a threshold in the lipid concentration when a bilayer starts to form, which would at approximately 0.15 g/l. The fact that the vesicles fused independently on the two tested surfaces, plasma-treated silica and plasma-treated gold is unusual. Vesicle fusion resulting in bilayer formation is often observed on silica surfaces but rarely on pure gold.[90] It is believed that the used plasma treatment, which reduced both of the surfaces' contact angles to ~6 degrees, played a major role in causing vesicle fusion to occur on the gold surface. Analysis of the AFM results and the resulting cross sectional calculations presented in Figure 4-7 indicate that the adsorbed vesicles appear to be flattened out and deformed. This vesicle deformation has been observed earlier as a result of vesicle-surface interactions and depends on both the surface and vesicle composition, among many other factors.[183]

Conclusions

In this study, it was demonstrated that the phytanoyl lipids, 1,2-diphytanoyl-*sn*-glycero-3-phosphocholine (DPhPC) and 1,2-diphytanoyl-*sn*-glycero-3-phosphoethanolamine (DPhPE) can be used to form supported lipid bilayers on

hydrophilic surfaces as well as at the liquid-air interface. DLS, NMR diffusion, and cryo-TEM showed that pure DPhPC and mixtures of DPhPC and DPhPE containing less than 50% of DPhPE formed unilamellar vesicles. These vesicles have the ability to fuse on hydrophilic surfaces of both plasma-treated gold and silica, forming solid-supported lipid bilayers as monitored by QCM-D and AFM. The bilayer formation, however, was concentration dependent and only initiated when the lipid concentration was above 0.15 g/l and only in buffer solution. The lipid bilayers formed had high viscoelasticities, based on the QCM-D dissipation measurements. This viscoelasticity is probably because of the ability of phytanoyl lipids to imbibe relatively high amounts of water or due to incomplete vesicle rupture and bilayer formation. No supported bilayers could be formed from solutions containing more than 50% DPhPE. As a whole, the results demonstrate the ability to form lipid bilayers of certain compositions of DPhPC and DPhPE at the solid-liquid and liquid-air interfaces.

CHAPTER 5
INCORPORATION OF RECOMBINANT BK_{CA} CHANNELS IN A TETHERED LIPID MEMBRANE AND FUNCTIONAL ANALYSIS

Introduction

High conductance calcium-activated potassium (BK_{Ca}) channels are found in most organisms where they regulate a large variety of physiological processes including smooth muscle tone, neurosecretion and hearing.[184-186] BK_{Ca} channels are typically gated by membrane depolarization and an increase in cytosolic Ca^{2+}, however, channel opening has been observed in the absence of Ca^{2+}. This observation suggests that calcium acts as a modulator to decrease the energy necessary for channel opening and that the BK_{Ca} channel is actually a voltage-dependent ion channel.[17] The Ca^{2+} bowl region of the channel, located intracellularly between the S9 and S10 segments (refer to Figure 1-3), contains an Asp-rich sequence motif (-QDDDDDP-) associated with Ca^{2+} binding and sensitivity.[41] The S4 segment of the BK_{Ca} channel is positively charged and forms part of the intrinsic voltage sensor of the channel, similar to that found in the other members of the voltage-dependent K^+ channel family.[37] The BK_{Ca} channel characteristic features are single-channel conductances ranging from 90 – 300 pS, and ionic currents which do not inactivate. Additionally, numerous peptide blockers from scorpion venom have been isolated and characterized and these elicit peculiar pharmacological effects and selective blockade of the channel.[187] These properties make BK_{Ca} channels ideal as candidates for biosensor development when incorporated in suitable membrane configurations.

Bilayer lipid membranes supported on solid substrates such as glass, metal and silica substrates have been used as models of biological membranes for fundamental studies of membrane dynamics and lipid-protein interactions.[188] Numerous studies have

been performed involving the incorporation of pore-forming peptides in supported lipid bilayers (SLBs) integrated to systems capable of rapid and reliable detection of analytes at the molecular level via stochastic sensing.[189-191] However, SLBs suffer the drawbacks of restricted fluidity and space limitations between the membrane and substrate. In most cases in SLBs, the membrane is separated from the substrate by a thin film of water of just about 10 - 20 Å, [73, 126] which compromises the lateral mobility and function of incorporated proteins.[94, 162, 192] Attempts to incorporate functional membrane proteins have been met with limited success due to denaturation, as a result of contact between extramembranous regions of proteins with the substrates.[77]

Tethered bilayer lipid membranes are lipid bilayers with the proximal layer coupled to the substrate by a covalently attached spacer group which provides a reservoir beneath the membrane.[193] These tethers have extremely high electrochemical sealing properties, comparable to those of natural membranes,[96] and therefore, allow electrical monitoring of the incorporation and function of channel proteins within the membrane. The tBLM can be characterized by surface sensitive techniques such as atomic force microscopy (AFM) and surface plasmon resonance spectroscopy (SPR).[85-87] When metal surfaces are used as substrates for tethering bilayer membranes, such as the commonly used technique of membrane tethering based on gold-sulfur interactions,[7, 93, 96] the substrate acts as an electrode and can therefore be used for making electrical measurements of ion channel currents. Like supported lipid bilayers, tBLMs have the advantage of enhanced resistance to mechanical and vibrational perturbation.[194]

Presently, most of the work done on the incorporation of pore-forming proteins in tethered bilayer membranes has involved only short peptides such as α-hemolysin[96, 113]

gramicidin[7, 195, 196] and valinomycin.[93] The relatively simple structures of these peptides tends to be limiting in terms of their sensing capacity. This, therefore, calls for studies to be performed on more complex proteins that have direct biological sensing capabilities.[99] BK_{Ca} channels have served as models for ion permeation, gating kinetics and pharmacology because of their robustness, inherently high conductance and relative ease of reconstitution from native membranes into lipid bilayers,[197, 198] making them ideal candidates for incorporation into tBLMs as stochastic sensors. Possible applications for biosensors based on transmembrane peptides and ion channels include the high throughput screening of drug candidates in the pharmaceutical industry, real-time environmental diagnostics, detection of heavy-metal contaminants in ground water, detection of biological warfare agents and many other possibilities.[96, 113] The ion channels to be incorporated into tBLMs can also be genetically re-engineered to develop sensor elements that are selectively sensitive to other different classes of compounds that they would naturally not detect.[112, 199]

For the studies presented here, recombinant BK_{Ca} ion channels were interfaced to a gold surface by fusing proteoliposomes containing reconstituted channels into tethered bilayer lipid membranes (tBLMs), which in turn were formed at multiple individual pixels of a microelectrode array device (MEA) illustrated in Figure 5-1. Single-channel activity recordings of the BK_{Ca} channels were performed using a modified patch clamp electrophysiology set-up, with electrodes from the sensor pad and probe pads on the MEA connected to an amplifier which processed current signals and gave a computer read-out. A silver and silver chloride electrode in a conventional patch clamp microelectrode pipette was used to measure currents from incorporated ion channels.

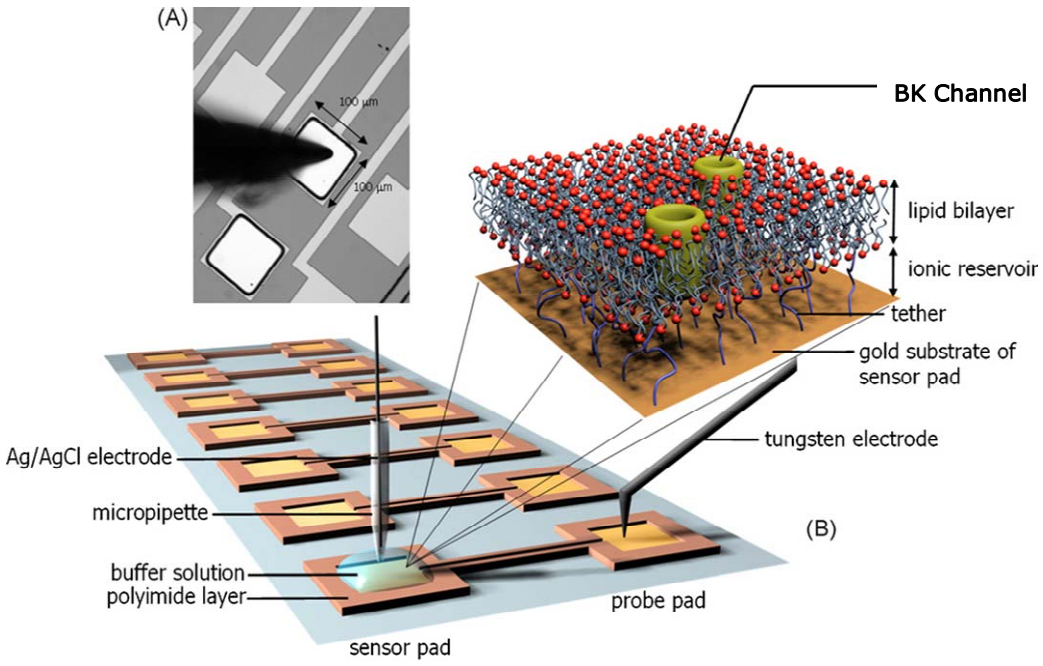

Figure 5-1. The tethered bilayer membrane on a microelectrode array device. A) Optical microscope image of the sensor pad showing pad dimensions of 100×100 µm^2 and tungsten electrode. B) The microelectrode array device. The graphics representing sensor pad show an incorporated channel in the tBLM. (Adapted from Keizer, H. M, *et al*. ChemBioChem 1246-1250 (2007)

One of the main advantages of bilayer membranes on solid supports, both tBLMs and SLBs, is that they can be easily characterized by surface-specific techniques in real-time. The process of the formation of the tBLM on the MEA was done in stages, the first of which was the deposition of the tethering moiety of the self-assembled monolayer 2,3-di-O-phytanyl-*sn*-glycerol-1-tetraethylene glycol-D,L-α-lipoic acid ester lipid (DPTL) by gold-sulfur interactions. This was followed by the formation of the bilayer from a mixture of the two archaeal lipids, 1,2-diphytanoyl-*sn*-glycero-3-phosphocholine (DPhPC) and 1,2-diphytanoyl-*sn*-glycero-3-phosphoethanolamine (DPhPE) in a 7:3 molar ratio to yield the complete tBLM. Finally to permit surface plasmon resonance (SPR) spectroscopy of the final configuration, the recombinant BK_{Ca} channel was inserted into a membrane tethered to a gold substrate that was not part of an MEA. The

SPR analysis showed that the observed channel activity was indeed as a result of gating events, and not membrane defects allowing current flow.

Because of the limited volume of the ionic reservoir in the sub-membrane space, we used a recombinant *mslo* BK_{Ca} channel with a C-terminal deletion after the S6 segment for incorporation into the tBLM. The truncation eliminated the bulky intracellular domain and the Ca^{2+} bowl region of the channel to allow better ionic flow within the reservoir and to maintain fluidity in the already densely packed reservoir region. Single-channel recordings were obtained within the experimental configuration described above and analysis of the pharmacological responses of the ion channels to externally applied tetraethylammonium (TEA) solutions was performed.

Materials and Methods

The Microelectrode Array (MEA) Device

The MEA device was fabricated by Daniel Fine in Dr. Ananth Dodabalapur's laboratory at the Microelectronics Research Center at the University of Texas at Austin, Austin, TX. The devices were fabricated on silicon wafers each containing 66 pixels. Each sensor pad was formed by evaporation of 3 nm of Ti on the silicon substrate followed by a 500 nm thick alloy of Au (60 %)/Pd (40%). A 200 nm thick layer of pure gold was then deposited on the alloy to form the surface of the pad, and a polyimide resist was photolithographically applied to define the pad size. The sensor and probe pads formed on the gold device were linked by a thin line of gold and electrically isolated from each other by the polyimide resist. Before tBLM formation, the device was rinsed with hexane, acetone, ethanol and water respectively, followed by UV/ozone treatment of the gold surface in a Harrick PDC-32 G plasma cleaner/sterilizer at high

radio-frequency power for 20 minutes under a flow of oxygen for oxidation, and for the removal of both chemical and organic contaminants.

Lipids

Archaea analogue phospholipids 1,2-diphytanoyl-*sn*-glycero-3-phosphocholine (DPhPC) and 1,2-diphytanoyl-*sn*-glycero-3-phosphoethanolamine (DPhPE) in chloroform were purchased from Avanti Polar Lipids Inc. (Alabaster, AL, USA), and were used without further purification. 2,3-di-*O*-phytanoyl-*sn*-glycerol-1-tetraethylene glycol-$_{D,L}$-α-lipoic acid ester (DPTL) was synthesized as described in literature.[101]

BK_{Ca} Channel

Plasmid DNA encoding mutant constructs of the C-terminal truncated BK_{Ca} channel with mRFP1 and histidine fusion tags was transcribed by the Ambion mMessage mMachine T7 Ultra kit. RNA was precipitated with LiCl, washed, and centrifuged in 70 % ethanol, dissolved in DEPC water and injected (46 nL per oocyte,~50 ng RNA) into defolliculated stage V or VI oocytes from *Xenopus laevis* (Xenopus Express, Florida, USA). Injected oocytes were maintained at 19 ˚C in ND-96 media (96 mM NaCl, 2 mM KCl, 1 mM $MgCl_2$, 10 mM HEPES, 1.8 mM $CaCl_2$, pH 7.4) enriched with sodium pyruvate (2.5 %), penicillin/streptomycin (1 %), and horse serum (5 %). Functional channel expression was verified by two-electrode voltage clamping (TEVC). Oocytes expressing the chimeric BK_{Ca} channels were rinsed in high K buffer (400 mM KCl, 5 mM PIPES, pH. 6.8) supplemented with 100 μM phenylmethylsulfonylfluoride, 1μM pepstatin, 1 μg/ml aprotinin, 1 μg/ml leupeptine, 1 μM p-aminobenzamidine and transferred to a 1 ml ground glass tissue grinder (Kontes Duall). After grinding, oocyte membrane extracts were stored at - 80 ˚C. Purification of the BK_{Ca} channels was performed by the use of immobilized metal ion affinity

chromatography as described in chapter 3 of this dissertation, followed by reconstitution by dialysis into liposomes formed from 7:3 DPhPC: DPhPE lipid mixtures. DLS and negative-staining TEM showed that the obtained proteoliposomes had diameters of 270±50 nm. A drop of pure lipid vesicle suspension was deposited, and incubated for >8 hours at 4 ˚C on the sensor pad containing a DPTL monolayer on the MEA device, to allow for vesicle fusion. A droplet of buffer solution (5.0 mm MOPS, 250 mm KCl, 0.1 mm $CaCl_2$) was applied to the sensor pad, and the bilayer quality was determined from membrane resistance. If a gigaohm resistance seal was obtained (~80% of trials) BK_{Ca} proteoliposomes were added to the sensor pad for single-channel analysis.

Electrophysiology

Recordings of single-channel activity were obtained using two electrodes. The active electrode, which was a conventional patch pipette containing an Ag/AgCl electrode and filled with a buffer solution (5mM MOPS, 250 mM KCl, 0.1 mM $CaCl_2$, pH 7.4), was inserted into a buffer solution droplet over the tBLM. The reference electrode consisted of a tungsten-tipped electrode that was positioned onto the probe pad that extended from the sensor pad. Both electrodes were connected to an Axon patch-clamp amplifier (Axopatch 200B, Molecular Devices Corporation, Union City, CA, USA). The signal was passed through a low-pass 5 kHz and digitized at a sampling rate of 50 kHz by using a Digidata 1322A (Molecular Devices Corporation).

Pharmacology

In the pharmacology measurements, stable control channel recordings were obtained before a drop of tetraethylammonium (TEA) in buffer solution (5.0 mm MOPS, 250 mm KCl, 0.1 mm $CaCl_2$) was added. Modulations of single channel currents in response to applied solutions of TEA were then recorded.

Lipid Vesicle Formation

Chloroform solutions of the lipids (50 mg/mL) were mixed to a 7:3 molar ratio (DPhPC/DPhPE) followed by rotary evaporation until a dry lipid film was obtained at the bottom of the vessel. The dry lipid film was then placed under vacuum in a dessicator overnight to eliminate any residual chloroform. The lipids were then lyophilized before hydration for 1 hour at 50 ˚C in buffer (5mM MOPS, 250 mM KCl, 0.1 mM $CaCl_2$, pH 7.4) to a final concentration of 2 mg/mL. After being cooled to room temperature the suspension was sonicated for 5 min, and extruded (21 passes) through a 100 nm polycarbonate membrane in a mini-extruder (Avanti Polar Lipids Inc.). The vesicle size profile was determined by the use of a dynamic light scattering (DLS) instrument (Brookhaven Instruments Corporation, Holtsville, New York, USA). Typically vesicle sizes of (140±30) nm were obtained as computed by the BI-DLSW Dynamic light scattering software.

Preparation of the Tethered Bilayer

The device was immersed into a DPTL-ethanol solution (0.3 mg/ml) overnight in a saturated ethanol environment (closed ethanol bath). The wafer was then rinsed with ethanol and millipure water. A drop of the lipid vesicle suspension was deposited on the DPTL treated sensor pad and left for >8 hours at 4 ˚C allowing for the vesicle to fuse therefore forming the tethered bilayer membrane. Prior to taking electrophysiological measurements a 5 µl droplet of buffer solution (5 mM MOPS, 250 mM KCl and 0.1 mM $CaCl_2$, pH 7.4) was applied to the treated sensor pads. Due to evaporation of water during the measurements, the droplet was regularly refreshed with pure water to keep a constant volume of the buffer.

Characterization of tBLM Formation and BK_{Ca} Membrane Insertion

The tBLM formation on gold substrates was investigated by surface plasmon resonance (SPR) enhanced ellipsometry and visualized by atomic force microscopy (AFM). The SPR instrument used was from Nanofilm technologie GmbH, Goettingen, Germany and for analysis of the kinetic fits, AnalysR software was used. Linearly plane-polarized light was directed through a 60˚ equilateral prism coupled to a gold coated glass slide via diodomethane oil as an index matching fluid in the Kretschmann configuration. The gold slide had a self-assembled monolayer of DPTL deposited on the surface by use of a similar methodology as on the MEA devices. Vesicles were injected into the flow-cell and the flow stopped for 30 minutes to 1 hour to allow for vesicle fusion to occur on the surface. The formation of the lipid bilayer was monitored by recording psi (Ψ) data versus time. Buffer solution (5 mM MOPS, 250 mM KCl and 0.1mM $CaCl_2$, pH 7.4) was flowed to remove free vesicles. A solution containing BK_{Ca} proteoliposomes was then flowed into the sample cell and upon stabilization of the SPR signal, more buffer solution was allowed to flow to remove any unincorporated proteoliposomes. Kinetic information associated with channel incorporation was then obtained.

Results

Membrane Insertion of BK_{Ca} Channels

The assembly of a tethered bilayer membrane on a gold substrate and subsequent incorporation of the BK_{Ca} channel involves three steps which include formation of the DPTL self-assembled monolayer, fusion of vesicles to form a tethered bilayer membrane and finally the membrane insertion of the BK_{Ca} channel. The process of the formation of a functionalized tBLM on the gold substrate was analyzed by SPR and the fit illustrated in Figure 5-2 was obtained.

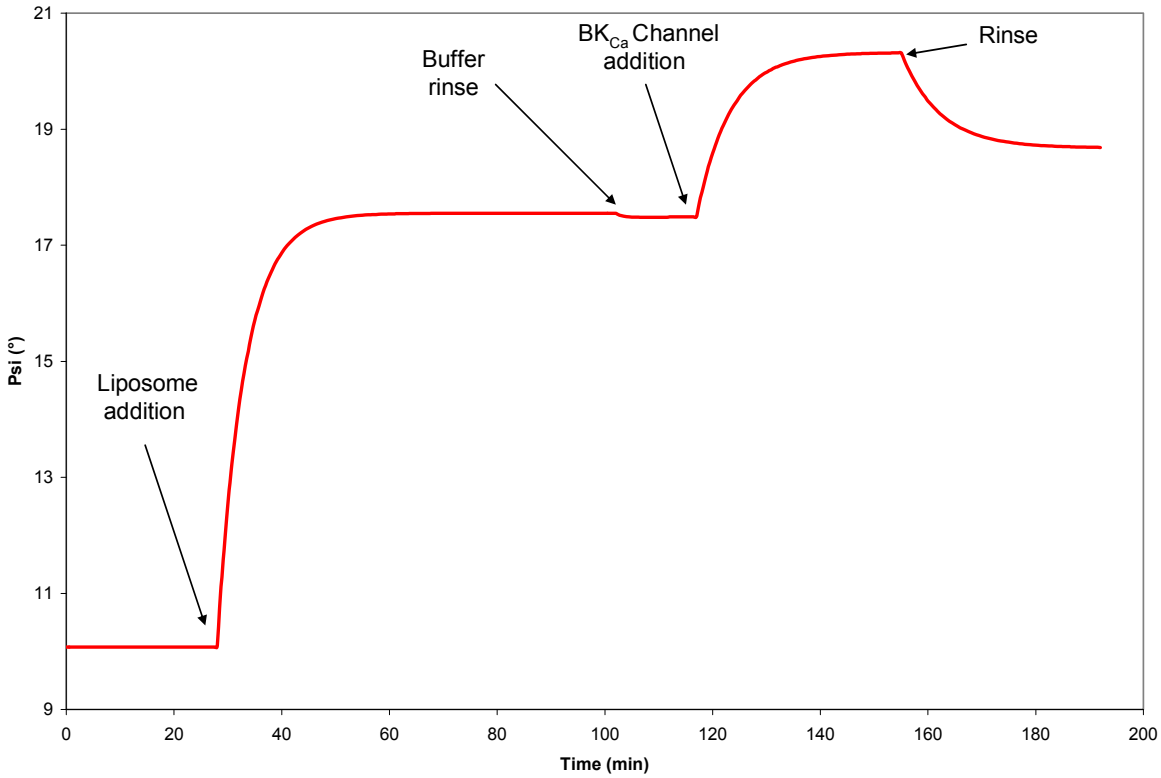

Figure 5-2. Fitted Kinetic data for incorporation of the BK_{Ca} Channel in the tBLM. The Y-axis shows the Ψ value and changes resulting in bilayer formation and incorporation of the channel. The X-axis shows the time-scale for the process.

The Y-axis shows the response in the SPR signal with changes occurring at the surface. Buffer solution was allowed to flow through the sample cell for ~30 min to establish a stable baseline signal. Liposomes prepared from 7/3 DPhPC: DPhPE lipid vesicles were then injected into the flow cell and the flow stopped for ~1 hour for vesicle fusion to occur on DPTL. A 7.5˚ change in the Ψ value was observed, corresponding to adhesion of vesicles followed by rupture to form a bilayer. Free vesicles were washed away leaving a tBLM; a minimal reduction in the Ψ value was observed. The SPR kinetic data, suggests that vesicle fusion to form a bilayer required about 1 hour for completion. The bilayer was rinsed, and judging by the stability of the SPR signal as can be observed in Figure 5-2 between 105 – 120 min it was clear that a stable membrane was formed. Proteoliposomes were injected in the flow cell leading to an increase in

thickness equivalent to 2.5 Ψ degrees. A final rinse resulted in 40 % reduction of the Ψ value as the channels that do not partition into the bilayer were washed off. Figure 5-3 illustrates the steps involved in tBLM formation and membrane insertion of channels.

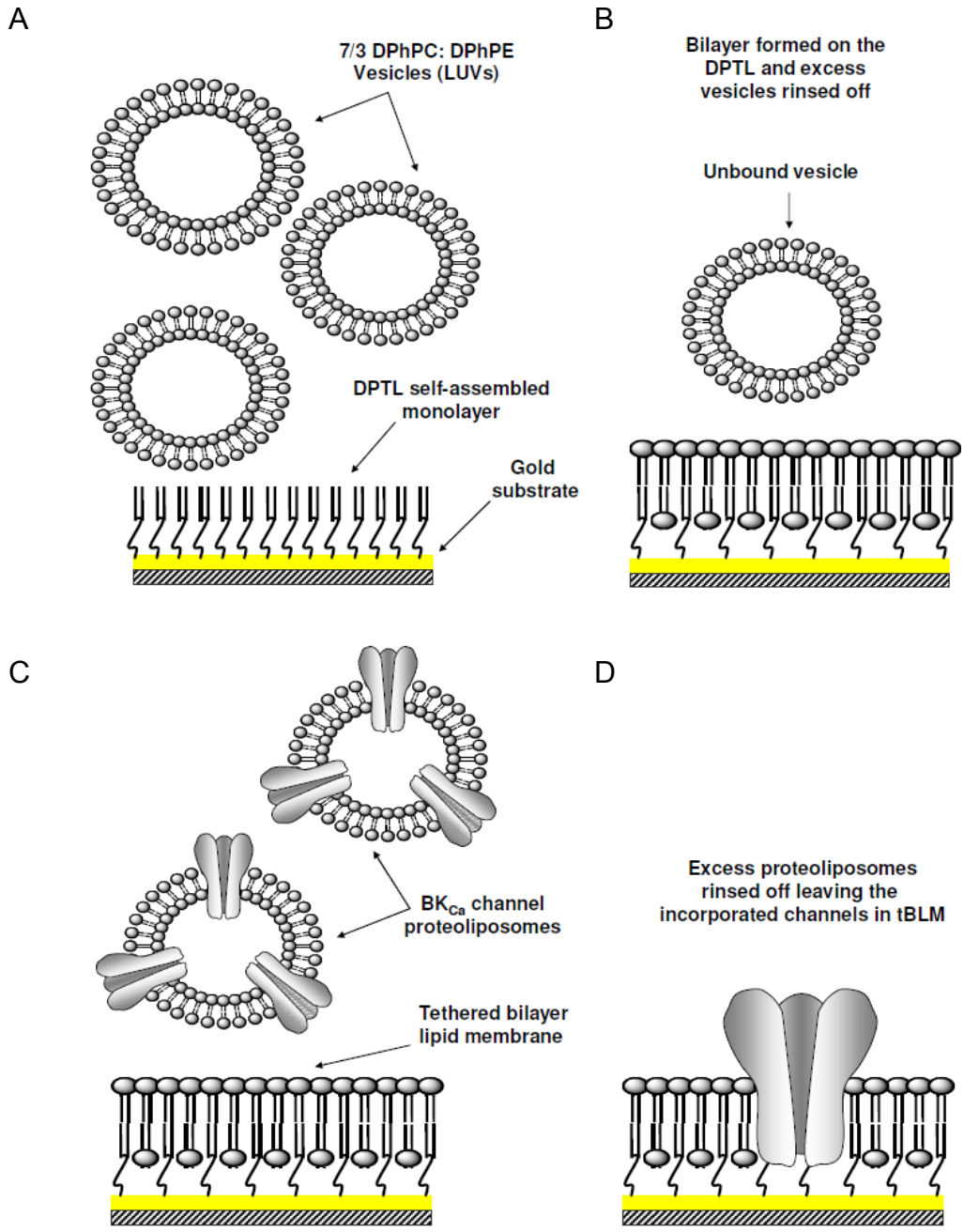

Figure 5-3. Schematic showing tBLM formation and incorporation of BK_{Ca} channels. A) Injection of vesicles on the SAM. B) Vesicle fusion to form tBLM and rinse of unbound vesicles. C) Addition of BK_{Ca} proteoliposomes on the tBLM. D) Incorporation of BK_{Ca} channels into tBLM.

Electrophysiology

In order to perform electrophysiology studies of ion channels within the tBLM, it is imperative that a stable, high electrically-resistant membrane be formed with resistances of ≥1 gigaohm (GΩ). Single-channel events are represented by unitary currents in the picoampere range and leakage currents between the recording electrode and ground had to be minimized. The tethering of the bilayer established an ionic reservoir that allowed the flow of ions across the membrane through the ion channel from the bulk solution above the membrane, to the reservoir below, and vice versa, in response to changes in transmembrane potential.

The SPR experiments above served as a control for tBLM formation and channel incorporation on the MEA. A drop of vesicle suspension was added on the MEA device, and after fusion of vesicles to form a bilayer over a period of 2 hours at room temperature, buffer solution (5 mM MOPS, 250 mM KCl, 0.1 mM $CaCl_2$, pH 7.4) was added to the sensor pad containing the tethered membrane. The limited size of the gold sensor pad surface (100×100 μm^2) and the electrical stability of the overlying lipid bilayer membrane made each pixel on the MEA sensitive enough to measure single ion-channel currents in the picoampere range. A comparison was made between the membrane resistance before and after BK_{Ca} channel incorporation into the tBLM. In both cases, the membrane resistance was above 1 GΩ therefore suitable for electrophysiological measurements. As shown in Figure 5-4, although changes in membrane potential generated ohmic changes in membrane potential consistent with the resistance of the membrane as a whole, no transient current steps consistent with single channel activity were recorded in the absence of BK_{Ca}. Figure 5-4 shows a stable trace recorded testing the bilayer membrane with different applied potentials.

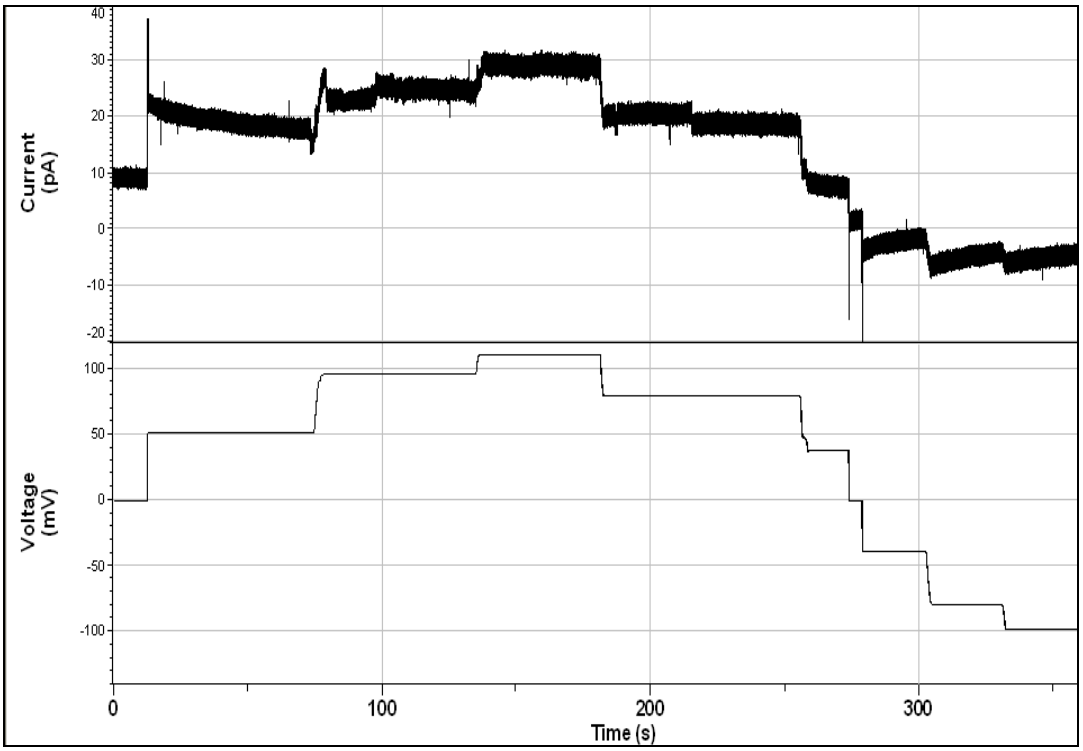

Figure 5-4. Recording from an electrically stable membrane formed by fusion of 7:3 DPhPC: DPhPE vesicles. The recording was done for approximately 6 minutes with applied voltages of between -100 mV to +120 mV.

Membrane potentials ranging from -100 mV to +120 mV were applied to the tBLM and stable traces were observed throughout the measurement duration. Pore-formation (electroporation) as a result of applied membrane potentials during electrophysiological experiments can complicate single-channel analysis. Electroporation is a phenomenon observed especially in bilayers supported at the air-water interface in experimental techniques with the tip-dip configuration. Within the tBLM system, stable traces were observed in several runs of experiments with giga-ohm seals ranging from 2.3 GΩ to 4.6 GΩ at applied potentials of 120 mV without evidence of membrane defects. The control recording in Figure 5-4 was obtained under recording conditions identical to those used during actual single-channel measurements. The tight sealing and electrical stability of the tBLM without evidence of leakage currents demonstrates that the system

is well suited for protein incorporation. Functional studies under a defined electric field are possible for inserted channel proteins and other pore-forming peptides within the tBLM. This experimental set-up therefore shows electrical properties similar to those of SLBs but with enhanced stability.

Single-Channel Analysis of the BK_{Ca} Channel

Proteoliposomes of the BK_{Ca} channel were incorporated into the tBLM and single-channel activity observed following changes in transmembrane potential. Fluctuations and single-channel records reflect the time course of gating steps. The single-channel activity exhibited by ion channels is a stochastic process; therefore, the order and duration of gating events are random variables. Statistical distributions were therefore employed to measure and quantify the parameters representative of gating events. The open and closed probabilities observed illustrated the voltage dependence of the channels. Figure 5-5 shows single channel activity of the chimeric mRFP1-tagged BK_{Ca} channel at applied membrane potentials of 120 mV.

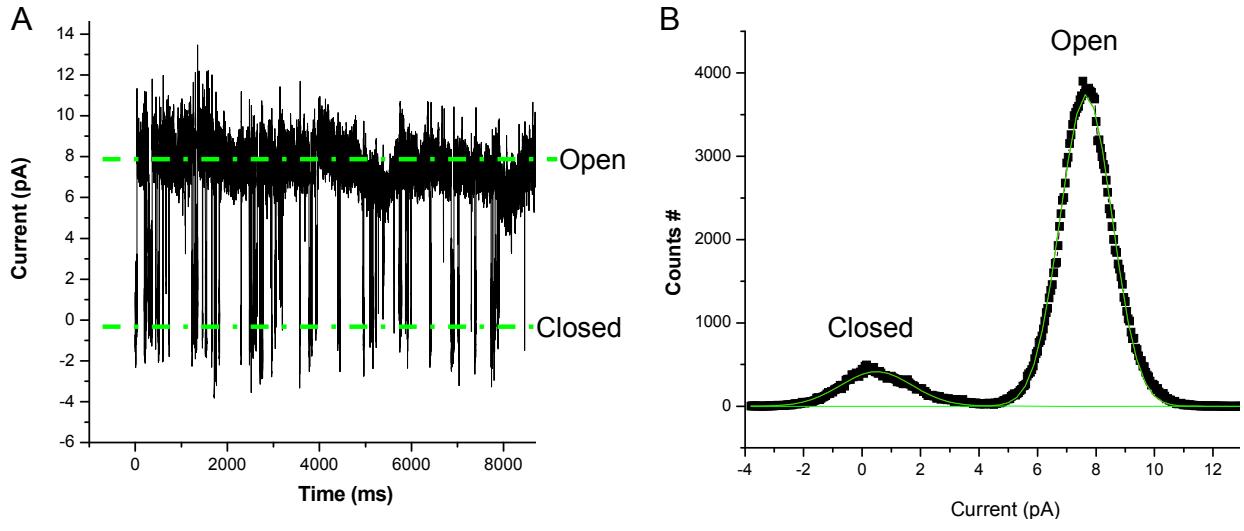

Figure 5-5. Single-channel activity of BK_{Ca} channels at 120 mV. A) Single-channel activity in the tBLM configuration. B) Histogram of open/close probabilities.

When potentials of +120 mV were applied, open and closed events were observed with current amplitudes of 8 pA upon normalization of the closed state to 0 pA as can be observed in Panel A of Figure 5-5. Single-channel histograms quantifying the number of events were fitted to a Gaussian distribution as can be observed in Figure 5-5 B and recombinant BK_{Ca} channels were found to be open ~89 % of the time at +120 mV. A reduction in applied potential resulted in a commensurate reduction in the open probability and vice versa; a characteristic property of voltage-dependent ion channels like the BK_{Ca} channel. For the experimental run represented by the trace in Figure 5-6 the applied potentials were reduced to 80 mV and open and closed events analyzed.

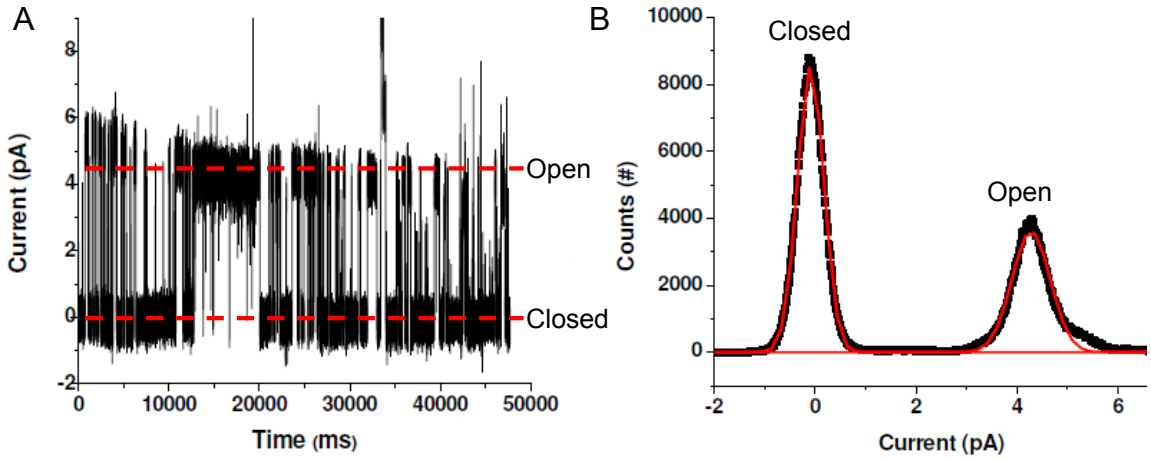

Figure 5-6. Single-channel activity of BK_{Ca} channel in tBLM at 80 mV applied voltage. A) A single-channel trace showing open/close events. B) Histogram showing the open/close probabilities at 80 mV.

After normalization of the closed state to 0 pA, the current amplitude in Figure 5-6 A is at the 4.5 pA level, corresponding to a reduction of ~ 43% in comparison to currents observed at applied potentials of +120 mV. Additionally, the open probability of the channel was reduced. From a total of approximately 9 $\times 10^3$ single-channel events, the open interval observed corresponds to ~ 3.8 $\times$ 10^3 events (29.6%) at this state, as can be observed in the Gaussian distribution fit illustrated in Figure 5-6 B.

The recordings of single-channel events observed in Figure 5-5 and Figure 5-6 demonstrate voltage dependence of the open probability of the BK_{Ca} channel. Single-channel recordings were also performed at negative voltages eliciting response of the BK_{Ca} channel with current amplitude exhibiting voltage dependence similar to that observed at positive potentials. The data in Figure 5-7 below shows fluctuation measurements of a single BK_{Ca} channel incorporated into the membrane with recordings obtained at applied potentials of -50 mV.

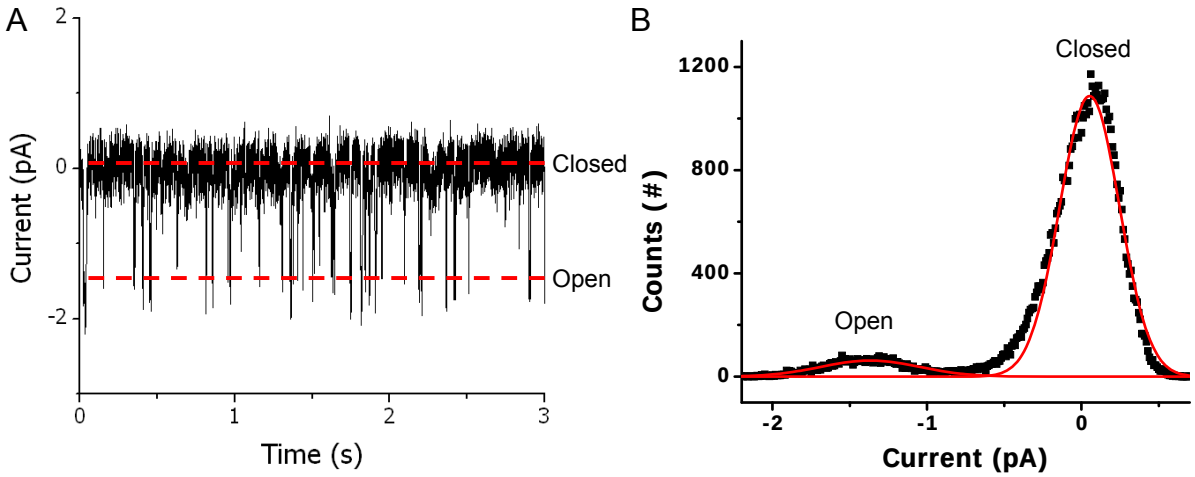

Figure 5-7. Single-channel activity of the BK_{Ca} channel in tBLM at – 50 mV applied potential. A) Single-channel open/close events. B) Open and closed probabilities.

There is a clear difference in the magnitude of open times at negative voltages in comparison to the experiments above run at +120 mV and + 80 mV. From panel B in Figure 5-7, it can also be noted that the number of open and shut events is significantly lower (1.2×10^3) in comparison to the counts of events during recordings performed at positive potentials (4×10^3 and 9×10^3). This observation is consistent with the space limitation within the hydrophilic volume of the sub-membrane region in the tethered bilayer membrane system resulting in a reduction in the volume of ions that can be contained in this region and available to traverse the channel at negative potentials. The

percentage of open time at applied potentials of -50 mV was ~10%. In all experimental recordings, the channels' responses to applied voltages consisted of unitary currents in the picoampere (pA) range and a time domain response at frequencies in the kilohertz (KHz) range, with the time-scale of channel openings in the millisecond range.

BK_{Ca} Channel Open Probability

The single-channel current histograms fitted to Gaussian distributions in Figure 5-5, Figure 5-6 and Figure 5-7 show a voltage dependence of the open probability. Being voltage dependent, the open probability of the BK_{Ca} channels could be fitted with a Boltzmann distribution by the equation below and represented in the Figure 5-8:

$$P_{open} = 1/(1 + \exp\{V_{1/2} - V)/k \quad (5\text{-}1)$$

Where P_{open} is the fraction of open channels, $V_{1/2}$ is the half-activation potential, k is the e-fold increase of the open probability.

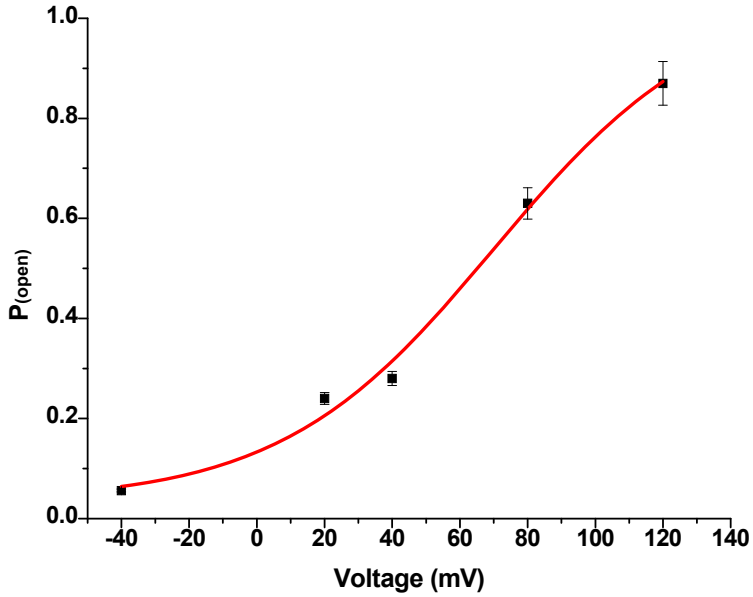

Figure 5-8. Open probability versus applied voltage fitted to a Boltzmann distribution, $P_{open} = 1/(1 + \exp\{V_{1/2} - V)/k$, where $V_{1/2} = 70.2 \pm 16.9$ mV and $k = 12 \pm 5$ mV.

The Boltzmann equation dictates the ratio of open to closed channels at equilibrium in terms of energy change, and explicitly gives the voltage dependence of

gating in the system.[1] The half-activation potential ($V_{1/2}$) observed here was 70.2 ± 16.9 mV representing approximately 85 mV of a shift compared to that observed in native membranes where $V_{1/2}$ values of -19 mV were measured.[200] The e-fold increase of the open probability k = 12 ± 5 mV is comparable to the k = 10 – 15 mV obtained for channels in native membranes under comparable conditions.[38] Event detection was performed by the half-amplitude threshold method and curves fitted for the investigation of channel kinetics and measurement of amplitudes. When fitted with three exponentials, the open dwell-time distribution ($V_{applied}$ = 100 mV) resulted in the lifetimes, $\tau_{o,1}$ = 0.6, $\tau_{o,2}$ = 7.5 and $\tau_{o,3}$ = 12. The closed state fitted with three exponentials yielded lifetimes of $\tau_{c,1}$ = 0.9, $\tau_{c,2}$ = 4.2 and $\tau_{c,3}$ = 56 ms as determined by Clampfit 9.1 data analysis software. The lifetimes for the mRFP1-BK_{Ca} channel constructs all fell within the millisecond (ms) time range. Figure 5-9 illustrates the logarithm histograms of square root ordinates that bin dwell times of all intervals and the fitted lifetimes from three exponentials.

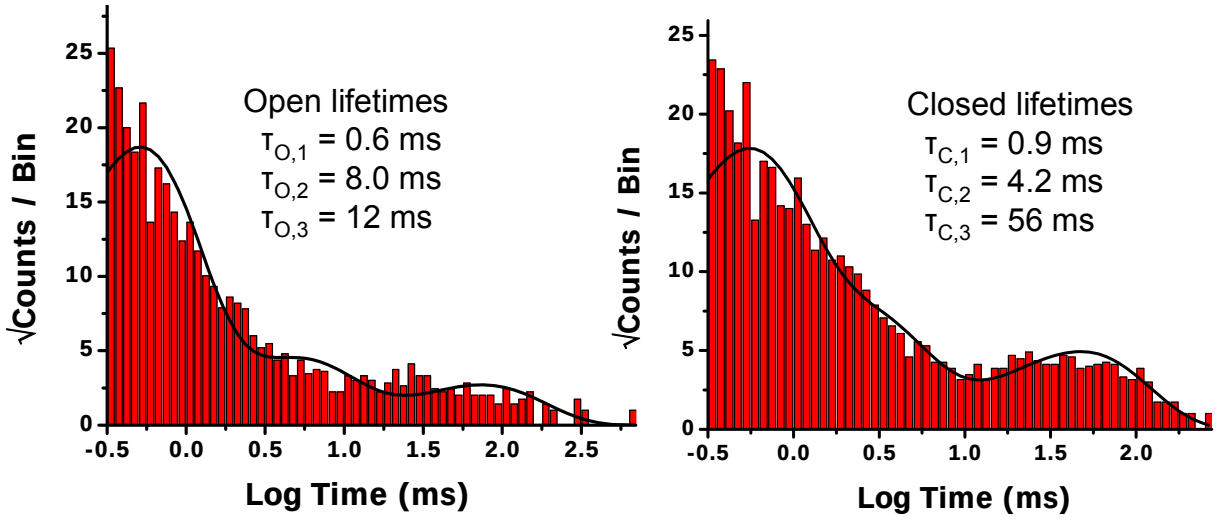

Figure 5-9. Logarithm histogram of square root ordinate that bins dwell-times of all intervals and fitted lifetimes from three exponentials.

BK_{Ca} Conductance

Among the major characteristic electrical properties of the BK_{Ca} channel is the large conductance of 90-300 pS in 100 mM symmetrical K^+.[17] The slope of the linear fit of the *I-V* curve in Figure 5-10 represents the conductance of the BK_{Ca} channel.

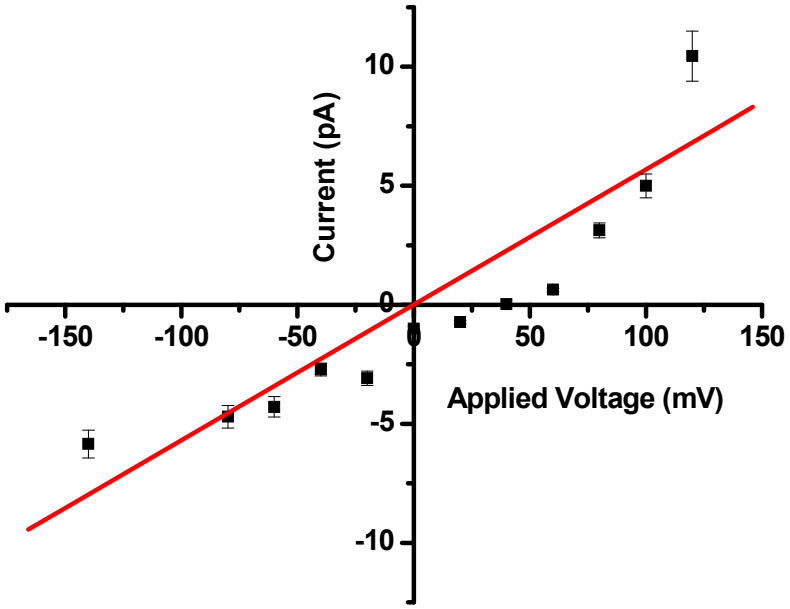

Figure 5-10. Current-voltage relationship for the BK_{Ca} channel. The data in the figure was obtained from five experiments and the straight line is the linear fit through origin.

The data reflects the apparent non-linearity of the current-voltage relation in the channel as opposed to the perfectly linear slope expected from the Ohm's law. The curvature observed in this case likely stems from the asymmetry in concentrations of bathing ions which would explain differences in ion flow between large positive voltages and large negative voltages through the BK_{Ca} channel incorporated in the tBLM. The current-voltage relationship in Figure 5-10 illustrates the linear function of the BK_{Ca} channel current amplitude with applied potential. Similar experimental runs with different membrane resistances (seals) were fitted and the Ohm's law used to calculate

conductance. Calculations of this data using the Ohm's law yield a unitary conductance value of ~ 50 pS which shows an apparent reproducibility over similar repeated experimental runs. The apparent mean conductance (n = 5) after fitting similar experiments from different seal resistances was 39 ± 2 pS, a value which is considerably lower than the conductance typically obtained from the wild type full-length BK_{Ca} channel in other planar systems.[200] The unitary conductance observed here for the chimeric BK_{Ca} channel was ~ 40 % greater than the mean conductance, with the discrepancy comparable to that observed in patch clamped ion channels.[201]

Pharmacology

Blockers of the BK_{Ca} channel have long been used as experimental tools for elucidating structural properties of the channel and for probing the mechanisms of their action under various physiological conditions.[202, 203] It is generally accepted that in selective ion channels, ions must interact with specific chemical sites which are responsible for the bias in the permeation of some ions and not others. Some of the important sites for ion interaction are energy wells, where ions may bind stably, or energy barriers which are points of maximum resistance to ion passage.[204] All channel blockers tend to have a common mechanism of action whereby they completely obstruct channel current for a short duration of time. The tetraethylammonium (TEA^+) ion belongs to a group of compounds known as quaternary ammoniums (QAs) which have been known to block K^+ conductance in voltage-gated and inward rectifying potassium channels by binding to two distinct sites which are accessible from the intracellular and extracellular space.[205-207] For studies of the response of the BK_{Ca} channel in a tBLM to tetraethylammonium, solutions with various concentrations of TEA were used and observations of electrophysiological responses made. Representative

data are documented in Figure 5-11 below, of the control current traces in the absence of TEA, and the response obtained after applying solutions of TEA of different concentrations (100 μM, 250 μM and 500 μM). Membrane potentials of 100 mV were applied for each experimental run.

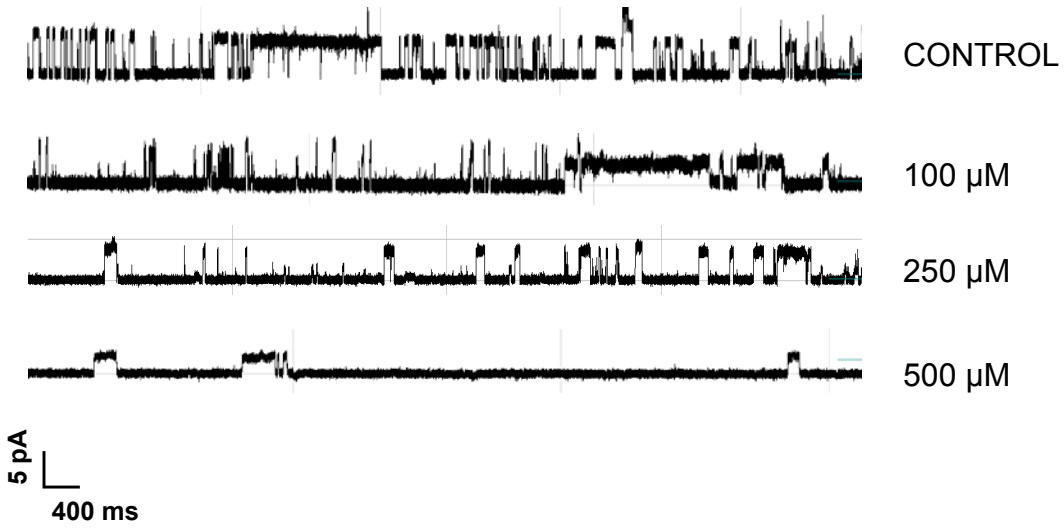

Figure 5-11. Single channel traces of channels at 100 mV applied voltage under different concentrations of TEA solutions. The control experiment had plain buffer without TEA and the others had TEA at 100 μM, 250 μM and 500 μM as shown on the legend.

Three categories of channel blockers can be described based of the appearance of single-channel recordings that they elicit. Slow blockers produce clearly resolved interruptions to channel opening that closely resemble the closing of channels, intermediate blockers produce rapid fluctuations in current that are too brief to resolve as individual events, and fast blockers produce frequent, extremely brief interruption of channel current that can only be detected as an apparent reduction in the level of open channel current.[204] From the results documented here after repeated experiments, it is clear that reconstituted BK_{Ca} channels in tBLMs demonstrate typical decrease of current amplitude upon the addition of micromolar and millimolar concentrations of

tetraethylammonium solutions. These results correspond to the known characteristics of TEA which exhibits fast kinetics therefore demonstrates blockade evident by an apparent reduction in open current amplitudes as in Figure 5-11. A dose-response curve was plotted to represent the relationship between the percentage block of the mRFP1-tagged BK_{Ca} channel by TEA versus the concentrations of applied solutions of TEA as illustrated in Figure 5-12.

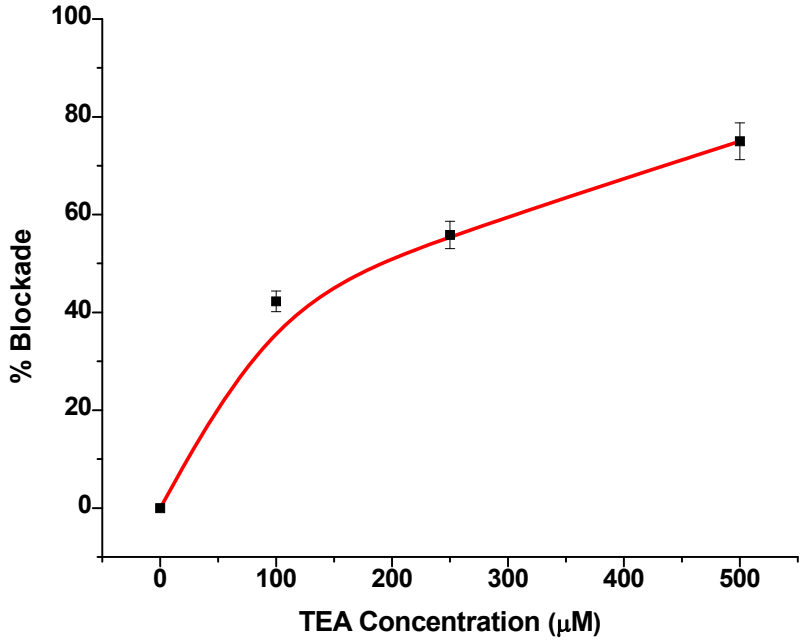

Figure 5-12. Dose-response curve of the BK_{Ca} channel mutant. Plot of percentage block of the BK_{Ca} channel versus concentration of TEA fitted to the Hill equation (solid line).

Response of TEA block was plotted in a dose-response curve and fitted to the Hill equation:

$$\%\text{Block} = \left(1 + \left(\frac{K_D}{[TEA]}\right)^N\right) * 100\% \qquad (5\text{-}2)$$

The half-activation concentration $K_{1/2}$ at 100 mV of applied membrane potential was determined to be 60 ± 10 μM (n= 3) which is lower than the half-activation concentration for TEA of $K_{1/2}$ = 158 μM determined for the BK_{Ca} channel under patch-clamp conditions.[200] The location of the TEA binding site relative to the tBLM and hence

the apparent orientation of the channel in the membrane can be inferred from the voltage dependence of block. Voltage-dependence of blockade of channels at applied potentials of 120 mV, 95 mV, and 80 mV in 500 µM TEA solutions was investigated. Figure 5-13 shows the voltage-dependence of TEA block.

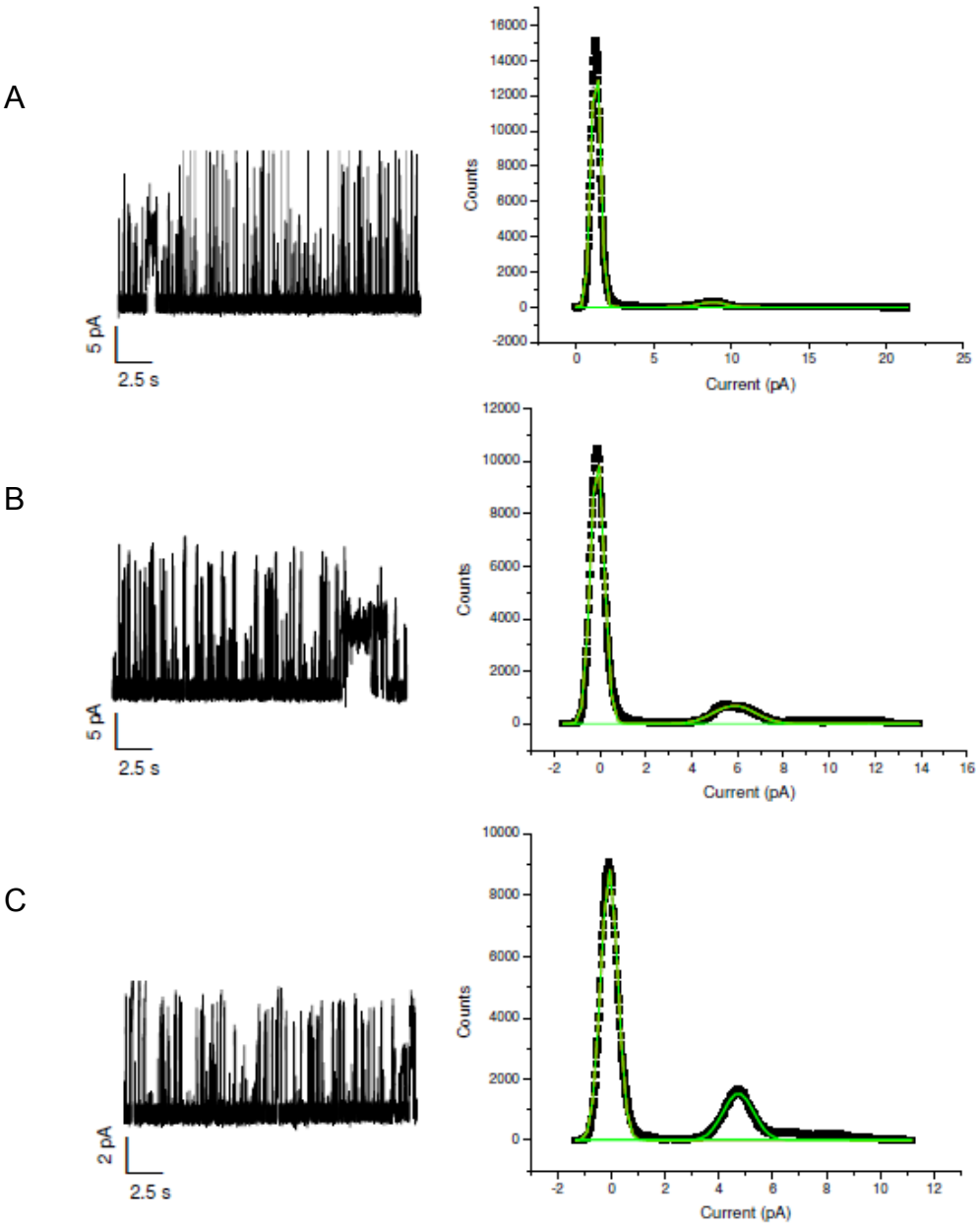

Figure 5-13. Voltage-dependence of blockade by 500 µM tetraethylammonium (TEA). A) Block by TEA at 120 mV with a current amplitude of 8.5 pA. B) Block by TEA at 95 mV and current amplitude of 6 pA. C) Block by TEA at 80 mV with current amplitude of 4.5 pA.

When membrane potentials of 120 mV were applied on the tBLM, current amplitudes corresponded to levels of approximately 8.5 pA. At membrane potentials of 95 mV the current amplitude was 6 pA, while at 80 mV the current amplitude was approximately 4.5 pA (Figure 5-13). The observed voltage dependence of blockade is associated with an internal TEA binding site, since external TEA block would usually show almost no voltage dependence.[208] Tetraethylammonium ions do not partition through the membrane and any elicited responses observed are strictly as a result of antagonist bound in the respective site of application, in this case internally on an inside-out BK_{Ca} channel. Evidence of an internal binding site being responsible for the pharmacological responses observed here suggests that the mutant BK_{Ca} channel was incorporated into the tBLM in the inside-out configuration; that is, with the C-terminal region oriented towards the external bulk solution and the N-terminus oriented proximal to the gold substrate within the tethered domain constituting the ionic reservoir beneath the membrane.

Discussion

The results in this chapter detail the incorporation of recombinant BK_{Ca} channels into tethered bilayer lipid membranes on microelectrode array devices and the subsequent functional characterization in these novel membrane systems. The BK_{Ca} channels under study here had a C-terminal deletion just after the S6 segment and an mRFP1 fluorescent tag attached for purposes of tracking expression and determining the configuration of the channel within the membrane. A histidine tag was added to facilitate purification, as discussed in great detail in Chapter 2 of this dissertation. Control experiments using the surface plasmon resonance spectroscopy techniques were performed to demonstrate the viability of the incorporation of channel proteins in

microelectronic devices. A modified patch clamp electrophysiology technique was used to perform single-channel recordings of the channels in the tBLM.

The findings in this study indicate that tethered bilayer membranes were successfully formed on the MEA devices by fusion of DPhPC: DPhPE vesicles on the DPTL self-assembled monolayer and recombinant BK_{Ca} channels incorporated in the tBLM as evidenced by SPR kinetic experimental results. The bilayer membranes formed were electrically stable with resistances in the gigaohm range, therefore suitable for electrophysiological measurements. Functional analysis probed by measurements of single-channel activity in the tBLM system showed that for the most part, the recombinant BK_{Ca} channel had electrical properties that were comparable to those observed in the wild-type (full length) BK_{Ca} channel. The channel also exhibited fast kinetics and lifetimes in the microsecond time-scale as observed in similar channels studied under patch clamp techniques.[38] However, analysis of the recorded data showed a significant reduction in the conductance of this channel in the tBLM in comparison to published data obtained using other measurement configurations. The C-terminal deletions of the recombinant BK_{Ca} channel and the attachment of mRFP1 and histidine tags are ruled out as possible causes for this sub-optimal conductance because similar conductance ranges of 35 pS – 50 pS have been observed in wild-type BK_{Ca} channels in the tBLM system.[99] Additionally, in Chapter 3 of this study, the conductance calculated from macroscopic currents obtained by TEVC of oocytes expressing mRFP1-tagged BK_{Ca} channels were ~ 129 pS, well within the typical range (90 – 300 pS) expected for BK_{Ca} channels.

Incidentally, the mechanosensitive channel of large conductance (MscL) and the synthetic ion channel based on the pore-lining domain of the nicotinic acetylcholine receptor (nAChR) of *Topedo californica*, the M2δ channel, studied independently in our laboratory under the same tBLM model membrane system also showed significantly lower conductances than observed in under patch clamp and whole cell systems.[99,97] The exception to this trend was observed in gramicidin (gA), a 2 kDa linear pentadecapeptide consisting of 15 hydrophobic alternating D,L-amino acids known to induce a high permeability for small monovalent cations in natural and artificial lipid membranes.[160] Within the tBLM, the four ion channels, recombinant and wild type BK_{Ca}, M2δ and MscL exhibited conductances that were between 3 times lower to an order of magnitude lower than those observed in patch clamp or whole cell measurement configurations, while the gramicidin (gA) channel had comparable conductance ranges in the tBLM relative to other measurement configurations, the data shown in Table 5-1.

There is an apparent correlation between the relative sizes of the ion channels incorporated into the tBLM and their conductances as calculated from the Ohm's law based on obtained data. The full-length BK_{Ca} channel and the C-terminally deleted recombinant BK_{Ca} channel with mRFP1 and histidine fusion tags have molecular weights of 120 kDa and 70 kDa respectively.[209] The native *E. coli* MscL channel has a molecular weight of 60-80 kDa and monomeric molecular weight of 15 kDa while the M2δ ion channel with a molecular weight of 65 kDa.[210, 211] These four ion channels have much higher molecular weights than the gramicidin (gA) channel and all of them have relatively bulky domains extending both intracellularly and extracellularly which increases on the packing dynamics in the reservoir region below the membrane

subsequent to incorporation in the tBLM. These structural aspects may well be responsible for the observed low conductances in the channels with high molecular weights. The ionic reservoir region within the tethers in the tBLM is known to be densely packed and with a higher viscosity than the bulk solution above the membrane.[93]

Table 5-1. Comparison of the different ion channels incorporated in the tBLM and their molecular weights

Ion Channel	Conductance (pS) (Literature)	Conductance (pS) (tBLM)	Molecular Weight (kDa) (Literature)
BK_{Ca} Channel	90 – 300	30 – 50 [99]	120 kDa [99]
MscL Channel	100 – 3000 [212, 213]	50 – 300 [97]	17 kDa [213]
M2δ	15 – 45 [214]	13 – 15 [99]	15 kDa [214]
Gramicidin (gA)	20 – 90 [88, 215, 216]	50 – 90 [160]	2 kDa [102]

The additional volume within this region as a result of the incorporation of the bulky ion channels limits ionic mobility even further and prevents the free flow of ions in both directions. Because the gramicidin (gA) channel is much smaller, and has a significantly lower molecular weight in comparison to the other three channels, it does not affect ionic mobility, hence its conductance compares favorably with values obtained from experiments done using conventional patch clamp setups.

In previous work performed in the Duran laboratory,[99] the BK_{Ca} mutant construct studied here was inserted into the tBLM directly from *Xenopus laevis* oocyte membrane vesicles, and therefore differs from the configuration examined here, in terms of the immediate lipid environment of the channel protein: native lipids in the former case and phytanoyl model membranes in the latter. The results show that the purified mRFP1-tagged BK_{Ca} channel construct studied in the tBLM showed electrical properties comparable to channels in native membranes within this measurement configuration. Analysis of open probabilities showed that the BK_{Ca} channel in native membranes had a

half-activation potential of 69 ± 5 mV while the mutant construct had a half-activation potential of 70.2 ± 16.9 mV. Both channels had lifetimes in the millisecond range and pharmacological profiles that were statistically indistinguishable. BK_{Ca} channels in native membranes and the mutant constructs had mean conductances of ~ 40 pS, both being at least 55 % less that expected for BK_{Ca} channels studied by patch clamping.[27, 200]

These similarities in electrical properties are rather intriguing considering the distinct differences in composition between native membranes and the model membrane system (tBLM). The phytanoyl lipids used for preparation of model membranes in this study constituted 70% phosphatidylcholine (PC) and 30 % phosphatidylethanolamine (PE). On the other hand, the percentage of total phospholipids in *X. laevis* oocyte membranes includes 65 % PC and 19 % PE, while the rest is composed of phosphatidyl inositol (PI), phosphatidyl serine (PS), sphingomyelin and cholesterol.[172] A possible explanation for similarities in electrical properties between these channels in two contrasting lipid environments would be because of the nature of the phytanoyl lipids used in the model membranes. Phytanoyl lipids have branched, saturated acyl chains that induce membrane packing dynamics similar to those observed when cholesterol molecules are added to lipid bilayers.[167] Because native *X. laevis* oocyte membranes have some cholesterol, it is likely that channels in native membranes and phytanoyl model membranes would show similar functional properties.

The characteristics of the reservoir within the tBLM and its effects on the electrical properties of the membrane possibly account for the reduced conductance of incorporated BK_{Ca} channels. Of great significance is the interfacial capacitance at the gold substrate. The use of tetraethylene glycol chains as tethering moieties for lipid

bilayer membranes to gold surfaces results in a polar layer between the membrane and gold surface which may sequester ions and act as a reservoir for ions translocated across the tBLM.[102] The gramicidin (gA) channel exhibits its known conductance unlike the other bulkier channels despite the effects of the interfacial capacitance as shown in Table 5-1. This is so because, unlike with BK_{Ca} ion channels, the ionic conduction of gA channels is not strongly dependent on membrane potential but is nonlinearly dependent on concentration, therefore, the mobility and density of the ions within the reservoir can directly limit the ion flux through the gramicidin channel.[217, 218] Because the ionic concentration of buffer solutions used is high, the conductance of gA in the tBLM remains unaffected.

A possible approach to be considered in order to correct the anomaly observed as regards conductance of BK_{Ca} ion channels in the tBLM would be to experiment with different types and lengths of polar tethers for the membrane. The conductivity of the channels to various ion types depends on the type of tether used for anchoring the membrane to the gold substrate, which in turn affects the region in the reservoir which is in close proximity to the gold surface and would help maintain the ionic reservoir properties to mimic those of the bulk electrolyte solution as much as possible.

Conclusions

In this chapter, proteoliposomes containing BK_{Ca} channels were fused to a tethered bilayer lipid membrane and functional analysis of incorporated channels performed. Control experiments showed the viability of incorporation of channels in this model membrane system and functional studies showed typical results as far as the electrical properties of the channels are concerned albeit with a deviation in expected conductance. The results highlighting the function of BK_{Ca} channels in a tBLM are in

good agreement with data obtained using other measurement configurations such as whole-cell and other planar patch-clamp systems. Lifetime and kinetic studies of the channel are comparable to those obtained and documented elsewhere and these suggest that the BK_{Ca} channel in the tBLM functions as expected and is suitable for any envisaged applications that would require a solid supported receptor. However, further studies are required to improve the system and provide a close mimic as possible to the natural membrane by altering the tethering units to yield a reservoir environment similar to the bulk electrolyte solution above the tethered membrane.

Pharmacological studies performed on the channel in the tBLM focused on probing the response to micromolar concentrations of tetraethylammonium show that the mRFP1 tagged BK_{Ca} channel within this configuration is as sensitive to TEA as those channels in native membranes studied using conventional patch clamp techniques. Furthermore, response to TEA also reveals the apparent preferred orientation of the channel in the tBLM with signals recorded showing characteristic features of an “inside-out” BK_{Ca} channel evidenced by the voltage dependence of TEA blockade. It is clear that besides possibly influencing the orientation of the recombinant BK_{Ca} channel in the tBLM, the mRFP1 and histidine fusion tags do not compromise the activity of the channels incorporated in the tBLM. Such mutant channels can therefore be modified to detect an even greater variety of chemical analytes and purified for incorporation in these novel model membrane systems for numerous applications limited only by imagination.

CHAPTER 6
VOLTAGE-INDUCED GATING OF THE MECHANOSENSITIVE CHANNEL OF LARGE CONDUCTANCE (MSCL) IN TETHERED BILAYER LIPID MEMBRANES

Introduction

Mechanosensitive channels (MS channels) are pore-forming proteins found in prokaryotic and eukaryotic cell membranes where they open for ion conduction in response to mechanical stress. MS channels react to mechanical stimuli triggering a shift in equilibrium from a closed to open conformation of the protein.[97] Stimulation of MS channels is responsible for physiological processes such as pain sensation, micturition, touch, hearing, salt and fluid balance, and turgor pressure changes in cells.[219] MS channels can generally be classified based on conductance into three categories, the 3 pS mechanosensitive channel of large conductance (MscL), and two smaller conducting MS channels, the mechanosensitive channel of small conductance, MscS (~1 nS), and the MS channel of mini conductance, MscM (0.3 nS). The most studied MS protein is the *Escherichia coli* MscL which typically serves as the model system for mechanosensory transductions.

The E. coli MscL Structure and Function

When a bacterial cell is exposed to hypo-osmotic conditions, MscL senses the tension in the membrane causing it to open a conducting pore releasing osmolytes. MscL opening therefore allows the channel to serve as an “emergency release valve” preventing membrane rupture during an osmotic downshock.[123, 220, 221] X-ray crystallography with a resolution of 3.5 Å by the Douglas Rees’s group revealed the MS channel from *M. tuberculosis* to be a 17 kDa homopentamer with a width of approximately 50 Å in the plane of the membrane and a height of 85 Å. Furthermore, MscL was demonstrated to have two transmembrane domains (TM1 and TM2) joined

by a periplasmic loop and bearing cytoplasmic N and C termini.[222-224] Figure 6-1 shows the crystal structure of the MscL from *M. tuberculosis* adopted from the protein data bank showing the N and C termini and the transmembrane domain.

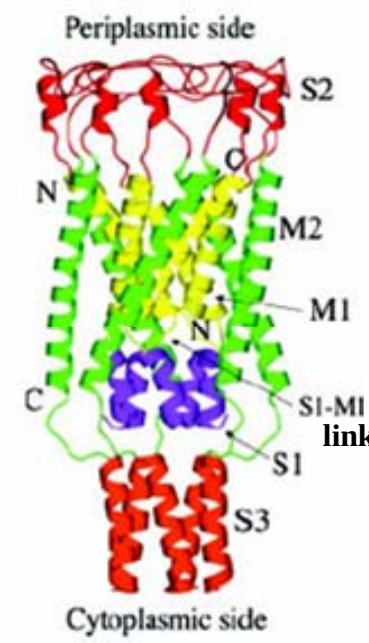

Figure 6-1. Crystal structure of MscL from M. tuberculosis adopted from the protein data bank (PDB) showing the two transmembrane domains and positions of the N and C termini.

The TM1 from each peptide forms the 30-40 Å pore in response to tension in the membrane bilayer, releasing ions and other solutes from the cytoplasm while the TM2 domain faces the lipid membrane.[222]

Gating in the MscL

Bacterial MS channels gate by sensing tension in the membrane independent of other proteins or artifacts allowing them to serve as a "simple", easy-to-gate molecular model for functional studies. The structural changes that occur during gating are not known, but the crystal structure of a nearly closed state of the *M. tuberculosis* homologue and computer simulations have resulted in models for the protein in its

closed and open state.[213, 225-227] Mutagenesis studies have indicated that the periplasmic loop plays the role of a torsional spring, inhibiting the channel from gating under non-osmotic conditions.[228] The role and conformation of the two cytoplasmic domains, the N-terminal and the C-terminal during gating are not well understood. However, the C-terminal region consists of a linker area starting just after TM2, and the α-helical bundle termed S3-bundle which is involved in conformational changes during gating. A detailed evaluation of the S3-α-helical bundle obtained from the crystal structure revealed a conformation in which the hydrophobic side-chains were exposed outside the S3 helix with the hydrophilic and charged side-chains packed inside the bundle.

Gating of MscL has been successfully achieved using patch clamping techniques using a pressure stimulus to induce tension in the membrane.[97, 229] Although gating has been shown to be voltage dependent,[97, 229] the amount of voltage required to induce a gating membrane tension (~300 mV) is not practically achievable under normal patch clamp conditions without causing membrane defects, thus gating of the channel solely by voltage-induced membrane tension had not been previously reported.

Presented here is the novel technique utilizing tethered bilayer lipid membranes (tBLM) to measure single channel activity of the MscL channel. The tBLM is part of an engineered microelectronic array chip and is the same system used for incorporation and functional analysis of BK_{Ca} channels in Chapter 5 of this dissertation and illustrated in Figure 5-1. The tethers work as stabilizing anchors and serve as spacers to the underlying gold surface thereby forming an ionic reservoir allowing for ionic flow through the channel. The tBLM system here is also assembled using the phytanoyl lipids 1,2-

diphytanoyl-*sn*-glycero-3-phosphocholine (DPhPC) and 1,2-diphytanoyl-*sn*-glycero-3-phosphoethanolamine (DPhPE) illustrated in Figure 1-12 of this dissertation. Phytanoyl lipids have branched acyl chains that have been demonstrated to confer electrical stability to the membrane, and have been used in previous investigations for electrophysiological studies where a membrane with stability to mechanical shocks and vibrations is desirable. The work in this chapter represents analysis of MscL channel activity for the first time in a supported bilayer membrane.

Materials and Methods

Lipids and Chemicals

Archaea analogue phospholipids 1,2-diphytanoyl-*sn*-glycero-3-phosphocholine (DPhPC) and 1,2-diphytanoyl-*sn*-glycero-3-phosphoethanolamine (DPhPE) in chloroform were purchased from Avanti Polar Lipids Inc. (Alabaster, AL, USA), and were used without further purification. 2,3-di-*O*-phytanoyl-*sn*-glycerol-1-tetraethylene glycol-$_{D,L}$-α-lipoic acid ester (DPTL) was synthesized as described in literature and supplied by a project collaborator.[101] Morpholinopropanesulfonic acid (MOPS) (>99.5%, Fluka, ultra grade). Potassium chloride (certified ACS grade), calcium chloride (certified grade) and potassium hydroxide (ACS certified grade) were purchased form Fisher Scientific and used as received.

The Microelectrode Array Device

The microelectrode array device was fabricated by Daniel Fine in Dr. Ananth Dodabalapur's laboratory at the Microelectronics Research Center at the University of Texas at Austin, Austin, TX. The fabrication of the MEA devices was on silicon wafers each of which contained 66 pixels. Each sensor pad was formed by evaporation of 3 nm of Ti on the silicon substrate followed by a 500 nm thick alloy of Au (60 %)/Pd (40%). A

200 nm thick layer of pure gold was then deposited on top of the alloy to form the surface of the pad, and a polyimide resist was photolithographically applied to define the pad size. The sensor and probe pads formed on the gold device were linked by a thin line of gold and were electrically isolated from each other by the polyimide resist. Before the formation of the tBLM, the device was rinsed with hexane, acetone, ethanol and water respectively. This was followed by UV/ozone treatment of the gold surface in a Harrick PDC-32 G plasma cleaner/sterilizer at high radio-frequency power for 20 minutes under a flow of oxygen for oxidation, and for the removal of both chemical and organic contaminants.

MscL Isolation and Purification

Expression and purification of the MscL was done in Dr. Paul Blount's laboratory at the University of Texas Southwestern Medical Center. In order to isolate and purify MscL, the protein is first generated with a C- terminal 6His-tag and expressed in the mscL-null strain PB104 using the pET21a expression vector. The pET vector is able to mass-produce proteins due to its T7-promoter site that binds T7 RNA polymerase and promotes transcription of the target protein. Secondly, cells were grown to an OD of about 0.6 and induced with 1mM IPTG for 1 hour at 37°C. The cells were then centrifuged at 4000 rpm and the pellets were re-suspended in 40 ml of base buffer (10 mM NaPi and 300 mM pH 8.0) and 100 µL of protease inhibitor cocktail (His-tag Protease Inhibitor from Sigma) was added to prevent the denaturing of the proteins. A few crystals of DNase and lysozyme was added and allowed to mix for 45 minutes. The samples were then disrupted by French pressing at 16K PSI at 4°C and membrane fractions were separated and resuspended in extraction buffer (50 mM Na_2HPO_4/NaH_2PO_4, pH 8.0, 300 mM NaCl, 20 mM imidazole plus 2% (v/v) Triton X-

100).[202] The resulting suspension was incubated with 500 µL of pre-equilibrated with extraction buffer Ni-NTA agarose (Qiagen) for 30 min at room temp to bind the proteins. To prepare for the protein purification by affinity chromatography, the NTA-agarose matrix was loaded into a 10 cm column with the protein bound. The column was washed with 10 mL of extraction buffer in the presence of 50mM of imidazole and 1% Triton X-100. Proteins were then eluted in 1.5 mL extraction buffer with 200mM imidazole and 0.2% Triton X-100. They were lastly analyzed by SDS-Page gel for purity and stored at -80°C by flash freezing.

Preparation of the Tethered Bilayer

The device was submersed into a DPTL–ethanol solution (0.3 mg/mL) and left overnight in a saturated ethanol environment (closed ethanol bath). The wafer was then rinsed with ethanol. A chloroform solution (2 mg/mL) containing DPhPC:DPhPE 7:3 molar percentage was mixed and the solvents were evaporated under vacuum and hydrated in 1mL of water and heated at 50 ◦C until a clear solution was obtained (ca. 1 hour). After cooling to room temperature the suspension was sonicated for 5 min, followed by filtration through a 0.45 µm filter. The vesicle size was determined by dynamic light scattering (DLS) instrument using a 90 Plus/BI-MAS detector with a BI 9000AT digital correlator (Brookhaven Inc.). Typically vesicle diameters of 150±50 nm were obtained. A drop of the vesicle solution was deposited on the DPTL treated sensor pad and left for >8 hours at 4 ◦C allowing for the vesicle to fuse and form the tethered bilayer. Prior to the electrophysiology examinations a drop (5 µL) of buffer solution (5 mM MOPS, 250 mM KCl and 0.1 mM $CaCl_2$, titrated to pH 7.4 using KOH) was applied to the treated sensor pads.

Electrophysiology

Recordings of single channel activity were obtained using two different types of electrodes. The active electrode, which was inserted into the buffer drop over the tBLM was a conventional patch pipette containing an Ag/AgCl electrode and filled with buffer solution. The reference electrode consisted of a tungsten-tipped electrode that was positioned onto the probe pad that extended from the sensor pad. Both electrodes were connected to an Axon Patch-Clamp amplifier (Axopatch 200B Molecular Devices Corporation, Union City, CA). The signal was passed through a low-pass 5 kHz filter and digitized at a sampling rate of 20 kHz using a Digidata 1322A (Molecular Devices Corporation). After a giga-seal was obtained, 2 μL of the protein solution was added for MscL incorporation into the tBLM and subsequent single channel analysis.

Results and Discussion

The detection of single channel activity, represented by currents in the picoampere (pA) range, requires a high signal-to-noise ratio. As a consequence, low leakage current in the pathway between the two electrodes is a necessity. This requires a stable and low conducting lipid membrane having an electrical resistance in the gigaohm (GΩ) range. In this study, the resistance between the two pure gold pads connected to the two electrodes ranged from 1.5 GΩ to approximately 17 GΩ. Figure 6-2 shows a plot of current as a function of applied voltage for one of the obtained membrane seals prior to incorporation of the MscL channel for functional studies. The particular presented seal had a resistance of 11 GΩ as calculated from the Ohm's law:

$$V = IR \text{ and } R = V/I \qquad (6\text{-}1)$$

Where V is the applied voltage, I is the current and R is the resistance.

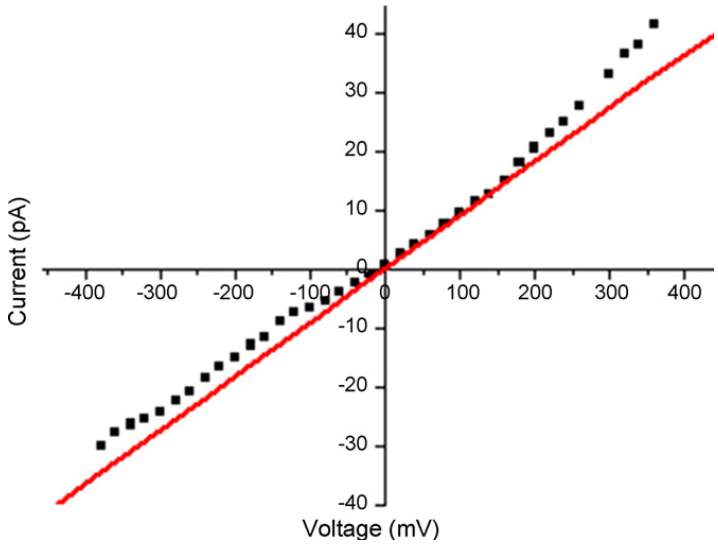

Figure 6-2. Current plotted against the applied voltage of a giga-seal. The solid line is a linear fit forced through origin.

Figure 6-3 below illustrates a trace of a stable bilayer formed by the 70PC/30PE lipid composition within the tBLM. The calculated resistance is 4.08 GΩ, and the applied voltage is 300 mV. The duration of recording as can be observed from the trace is over a 10 minute time scale with no evidence of membrane defects or membrane instability.

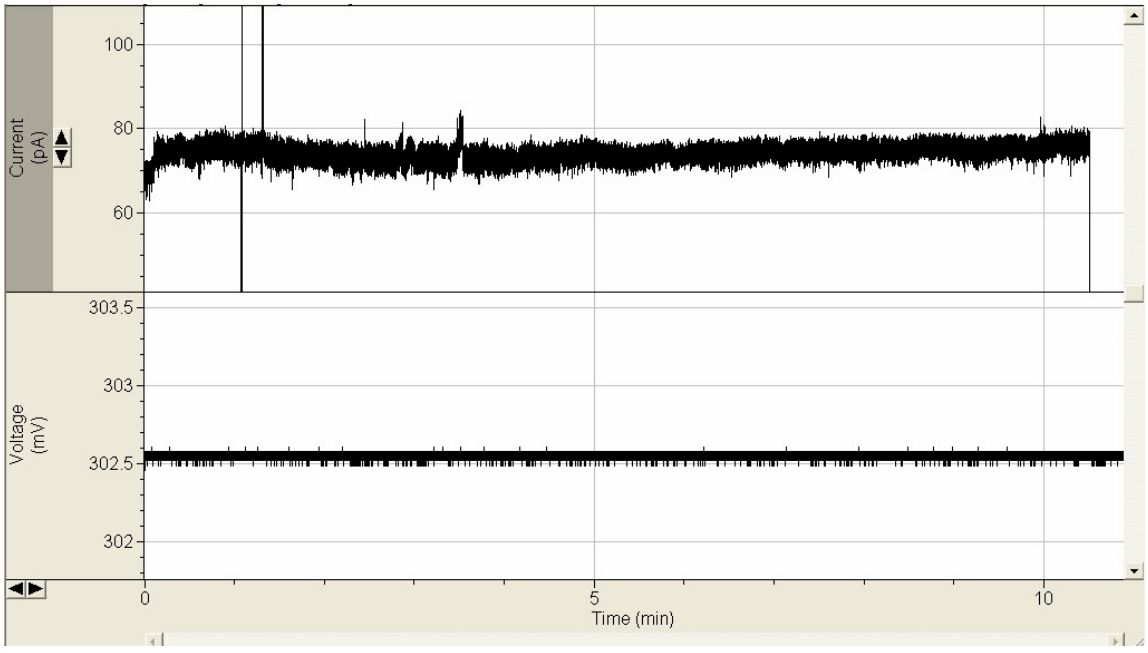

Figure 6-3. A stable trace recorded from a 7:3 DPhPC/DPhPE bilayer membrane over a duration of 10 minutes.

MscL channels were incorporated into stable tBLMs and single channel activity recorded. In Figure 6-4 typical current traces obtained from the wildtype MscL are shown. These recordings were obtained at 300mV, which was the voltage-gating threshold, i.e. no signals were observed at lower potentials for the MscL.

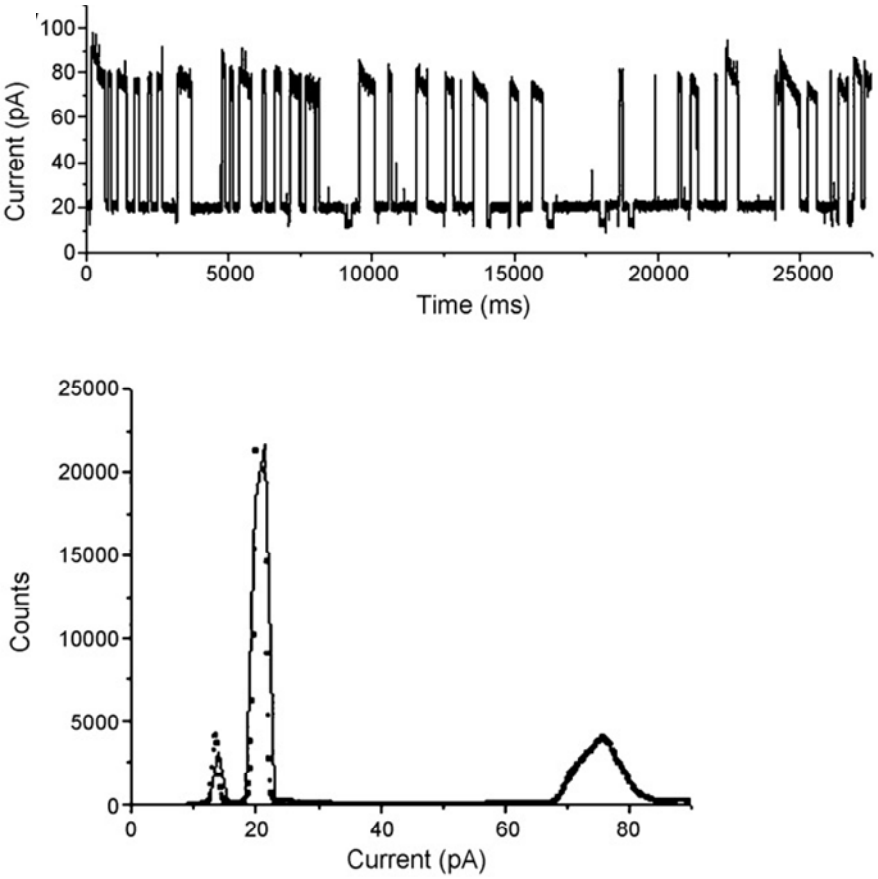

Figure 6-4. Single channel behavior of MscL presented as measured current at an applied transmembrane potential of + 300 mV. (A) The trace shows the activity of one MscL channel having two conductivity states and it current distributions.

The trace in Figure 6-4 shows two distinct conductivity levels for the incorporated MscL channel: a lower current level corresponding to a unitary conductance of ~23 pS ((21–14) pA/0.3 V) and a higher current level corresponding to a unitary conductance of ~203 pS ((75–14) Pa/0.3 V). The success rate of achieving stable GΩ seals was ca. 60% and the lifetimes (generally due to loss of seal) varied between a few seconds up

to 1.5 hours, depending on the applied voltage in these unoptimized experiments. The lower conductance was not always present as seen in Figure 6-5 below which is from a recording of single channel activity under identical conditions as those for the experiment that yielded the data in Figure 6-4.

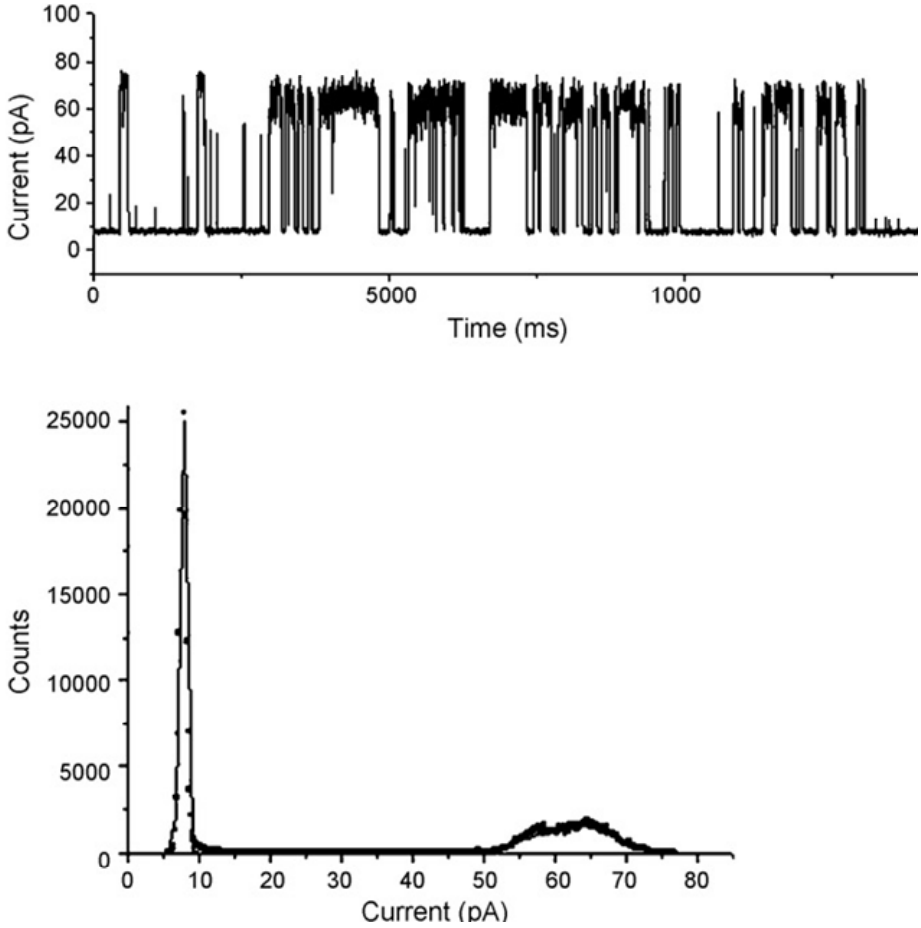

Figure 6-5. A trace for one MscL showing only one conductivity state and B) its current distributions.

The conductance of the MscL observed here under a tethered bilayer membrane (tBLM) system was 0.2 nS which is lower in comparison to 3 nS reported in the literature under patch clamp conditions. The reason for this is not very clear, however, the characteristics of the ionic reservoir in the sub-membrane space are believed to contribute to this atypical conductance. Another possible explanation for this sub-

optimal conductance could be the lack of an external pressure to induce gating. In the reservoir the ion mobility is decreased due to the lack of space, presence of tethers, and the low ionic concentration in comparison to that in the free buffer on the opposite side of the membrane.[102] However, this concentration difference is not believed to be large enough to induce much of an osmotic pressure. This is based upon earlier findings made using gramicidin A, in which the observed conductance was the same on the device as when utilizing tip dipping, a more conventional measuring technique in electrophysiology.[160] Furthermore, the lipid environment hosting the protein is also crucial, which also can be a reason for the low observed conductivity. The tethers that decouple the tBLM from the substrate also form a somewhat different composition in the lower leaflet of the membrane compared to the upper one.

The lifetime distributions determined from probability density functions displayed fast kinetics with the channels open for $\tau 1$ = 0.64 ms, $\tau 2$ = 1.17 ms and $\tau 3$ = 2.31 ms (n = 4), which are comparable with values found in literature when patch clamping methods were utilized.[221] As given by the Maxwell stress tensor, an electrical field applied over a lipid bilayer induces a perpendicular stress in the membrane. This stress can be viewed as an increase in membrane area and can cause changes in the curvature in a phenomenon referred to as flexoelectricity that has been demonstrated in both lipid bilayers[230] and cell membranes.[147] In the present work, an electrical field induced membrane stress (σ) strong enough to trigger an opening of the MscL channel was observed. According to Needham and Hochmuth the tension as a function of the transmembrane potential (V) can be expressed as:

$$\sigma = \varepsilon\varepsilon_0 d\,(2/d_e^2)\,V^2 \qquad (6\text{-}2)$$

where ε is the dielectric constant of the surrounding medium (typically ca. 60), ε_0 is the permittivity of free space, d is the bilayer thickness (~4 nm), and d_e is the dielectric thickness (~3 nm).[231]

The thicknesses are derived from capacitance measurements on similar lipids.[64] The membrane tension needed to gate the MscL ion channel, in a lipid environment, as used in this work, has been shown to be approximately 12 dyne/cm, which has been derived from pressure-induced stretching of the bilayer.[97] According to Equation 6-1 this tension corresponds to a transmembrane potential of ~300mV, which is in very good agreement with our findings, that is, no signals were observed for voltages below 300mV. This strongly suggests that the gating of the MscL is tension dependent. Precautions were taken during this study to avoid true electroporation of the membrane. A stable giga-seal was always obtained before the addition of the protein and no signals were detected before the MscL addition. The seal was stable at 300mV for approximately 1.5 hours.

Conclusions

In conclusion, a novel approach that examines a functional mechanosensitive channel reconstituted on a tethered membrane surface has been developed. The channel was gated upon the application of potential, which according to calculations give rise to a stress on the lipid bilayer similar to pressure-induced tensions. This strengthens the fact that the MscL ion channel is gated in response to stress in the lipid membrane as opposed to pressure across it. Furthermore, these findings show the possibility of using MscL as a release valve for engineered membrane devices; one step closer to mimicking the true function of the living cell.

CHAPTER 7
CONCLUSION AND FUTURE DIRECTIONS

The long term objective of this project was to develop a biosensor based on the BK_{Ca} channel for the detection of chemical and biological analytes. Several parameters needed to be considered to achieve the goal of incorporating channels within bilayer lipid membranes and realize functional activity. Foremost, the bilayer lipid membrane had to exhibit the appropriate resistances required for electrical studies of incorporated ion channels and be stable to mechanical shocks and vibrations. Additionally, the bilayer membrane had to have curvature that would allow optimal insertion of the channel in the correct functional conformation within a system capable of converting the biological events of gating into measurable and recordable electrical signals. In order to demonstrate the potential for the detection of analytes by this system, it was imperative that we obtain pharmacological responses of incorporated BK_{Ca} channels to known antagonists. Investigations were organized into specific goals that would collectively build up to the overall objective.

The first step was to obtain channels and this was achieved through heterologous expression of the *mslo* mouse gene encoding for the BK_{Ca} channel. For the expression system, *Xenopus laevis* oocytes were found to be convenient and channels were expressed on the membranes of these oocytes. A mutant construct of the BK_{Ca} channel with a truncation of the C-terminus was expressed because of the potential difficulty of inserting the full-length channel with a bulky intracellular domain into a tethered bilayer membrane. We developed an affinity chromatography purification protocol to isolate the channels from other solubilized membrane components that would potentially perturb functional activity upon insertion in synthetic membranes. The properties of non-native

lipids underlie the success of reconstitution of purified channels into vesicles and formation of tethered bilayer membranes. Among the characteristics of lipids critical for our applications would be curvature, membrane packing dynamics and the propensity to form bilayers on solid substrates. We used atomic force microscopy (AFM) and quartz crystal microbalance with dissipation monitoring (QCM-D) to investigate the kinetics of lipid fusion for the formation of bilayers on solid substrates. Among the different concentrations of the phytanoyl lipids DPhPC and DPhPE studied for their ability to form bilayers on gold and silica substrates, a minimum concentration of 0.15 g/ml was found to be the threshold concentration required for fusion on solid substrates. A number of compositions of the two phytanyl lipids were also studied to determine the most suitable combination required for the formation of stable bilayers, and 7/3 DPhPC:DPhPE was most ideal. A size analysis of vesicles extruded through polycarbonate membranes of varied pore sizes was performed by dynamic light scattering and a comparison was done by NMR. Imaging by cryogenic transmission electron microscopy was used to give an idea of the structural morphology of the vesicles. Purified BK_{Ca} channels were reconstituted in vesicles of DPhPC: DPhPE in a 7:3 molar ratio through a dialysis procedure and then fused on self-assembled monolayers of DPTL deposited on microchip devices.

Numerous studies have been done on pore-forming peptides incorporated in tethered bilayer membranes; however, all of the studies have involved use of simple peptides which cannot not give qualitative pharmacological data as ion channels would. Besides offering the advantage of yielding pharmacological responses, ion channels also exhibit characteristic stochastic signatures, in contrast to pores, and are therefore

natural biological sensing units. The studies documented here represent the first successful incorporation of a functional ion channel within a tethered bilayer lipid membrane environment. The incorporation of the BK_{Ca} channel within the tBLM was confirmed by surface plasmon resonance-enhanced ellipsometry and functional studies were performed by use of a modified patch clamp electrophysiology technique.

The gold surface on the microchip device that serves as a substrate for tethering of the bilayer membrane allows the study of surface molecules under a defined electric field, therefore is ideal for investigations of field sensitive processes such as ion translocation through tBLM incorporated channels. Demonstration of a response to activators, blockers or modulators by ion channels is a major milestone towards realizing the goal of developing a biosensor. Quaternary ammonium compounds have been shown to block potassium channels therefore; we used derivatives of tetraethylammonium (TEA) to investigate modulation of BK_{Ca} channel activity within the tBLM. Being an open channel blocker with differences in stochastic signals depending on whether internally or externally applied, TEA responses by the BK_{Ca} channel gave insight on channel orientation within the membrane.

Future experimental work can be focused on the application of selective BK_{Ca} channel blockers such as iberiotoxin (IbTX) and monitoring subsequent current modulations through channels in the tethered bilayer membrane system. Such a step would go a long way in demonstrating the potential of this system as a biosensor for specific target molecules. The beauty about biological sensing elements such as ion channels is the ability to re-engineer them and create novel binding sites for a variety of agents they would naturally not respond to. Biochemical modifications can be made to

channels at locations that would alter normal function, thereby producing defined changes to stochastic signatures and allow detection to a high level of specificity.

The electrical properties of BK_{Ca} channels in the tBLM showed a deviation from those observed under other measurement configurations such as patch clamping. These deviations could be attributed to a few factors relating to both the truncated channel as well as the experimental set-up. Piskorowski and his co-workers performed studies of truncated BK_{Ca} channels and recorded currents that were modulated by alterations in calcium concentrations, however, they noted that the kinetics of channel opening were altered to some degree. The observation they made regarding variation in electrical properties of channels due to truncation of the C-terminus as well as the differences in experimental configurations could partly explain why our results show a deviation from studies under the patch clamp configuration. It is also possible that the differences between our results and those documented in literature stem from the lipid environment within which reconstitution is done and bilayers formed for our investigations.

Synthetic phytanoyl lipids DPhPC and DPhPE which are derivatives of archaeal lipids were used for formation of vesicles and bilayer membranes. Despite the ubiquity of BK_{Ca} channel distribution in most living organisms, these channels are not found in bacteria and the unique membrane packing dynamics and fluidity of phytanoyl lipids could have conformational implications to proteins that are inserted in membranes formed of such lipids. These conformational implications might be responsible for differences in electrical properties between channels in the tBLM system in this study, and those channels that are reconstituted in eukaryotic lipid membranes. Among the

electrical properties that show a deviation from literature values would be conductance. Conductances of BK_{Ca} channels in the tBLM were found to be approximately 40 pS, nearly an order of magnitude lower than the 300 pS recorded under patch clamp conditions. The same pattern was observed during investigations performed and documented in Chapter 6 of this study involving the incorporation of the mechanosensitive channel of large conductance (MscL), which had recordings of 300 pS in the tBLM system, compared to 3 nS recorded under patch clamp conditions, an order of magnitude higher. The interesting observation made here points to the molecular sizes of the channels incorporated in the tBLM as being responsible for the recording of anomalously lower conductances than expected. The conclusion regarding the molecular weights of incorporated channels explaining the atypical conductance is further supported by observations of normal conductance levels in the gramicidin (gA) peptides inserted in tBLMs. The gramicidin channel is comparably a very small peptide when contrasted against true ion channels like the BK_{Ca} channel or the MscL channel. Apparently, high molecular weight ion channels compromise on the volume of the sub-membrane space of the tBLM which is already densely packed with DPTL tethering units, hence limiting ion mobility critical for maintaining free ionic flow hence normal conductance levels.

Future work could involve changes to the overall configuration of the tBLM system which exhibits asymmetry between the viscosity of the ionic reservoir below the membrane and the bulk solution above the tBLM that collectively would affect conductance. On-going work targeted at improving the tBLM system, in particular the thiol-modified tethering unit, for the last few years by Wolfgang Knoll and Ingo Koepper

has resulted in advances in tBLM properties and the movement of ions in this region.[100, 148, 232-236] Among possibilities explored include increasing the volume of the sub-membrane space by synthesis of longer tethering units with the goal of increasing the fluidity of the ionic reservoir within the tBLM system.[236] Additionally, Knoll and co-workers combined polymer supported bilayer and the tethered bilayer to create the polymer-tethered lipid bilayer system on modified substrates.[148] This alternative membrane configuration significantly increased the decoupling of the membrane from the metal substrate hence improved the fluidity in the ionic reservoir.

Further improvements of the measurement configuration could be considered towards improving the system. In the present tBLM system, there is an interfacial capacitance associated with the membrane and the solution interfaces above and below the bilayer, as well as resistance in the bulk solution and within the membrane. An alternative equivalent circuit model which would allow for a more accurate account of the actual transmembrane potential within the tBLM system could be considered for study of electrical properties of ion channels. Nonetheless, the system studied in this work demonstrates the potential of using purified BK_{Ca} channels incorporated within a tBLM successfully for biosensor applications.

APPENDIX A
DYNAMIC LIGHT SCATTERING ANALYSIS OF TEMPERATURE EFFECTS ON SIZES OF PHYTANOYL LIPID VESICLES OF DIFFERENT MIXTURES

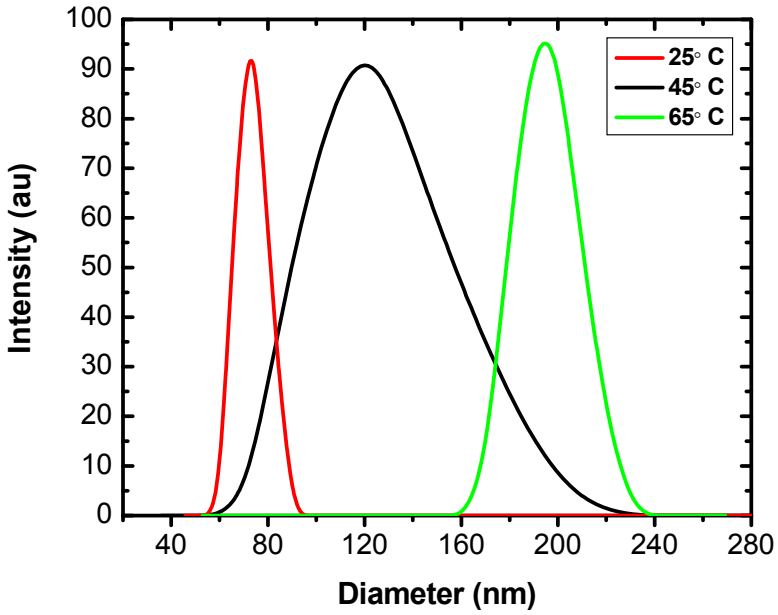

Figure A-1. Diameters of 100 % DPhPC vesicles at 25˚C, 45˚C and 65˚C as a function of intensity of scattered light.

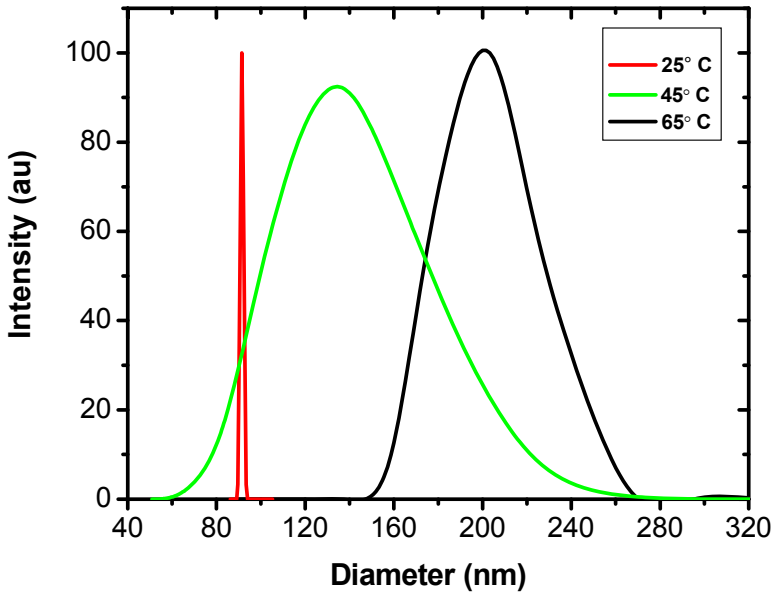

Figure A-2. Diameters of vesicles of DPhPC: DPhPE lipid mixtures at a 7:3 molar ratio at 25˚C, 45˚C and 65˚C as a function of intensity of scattered light.

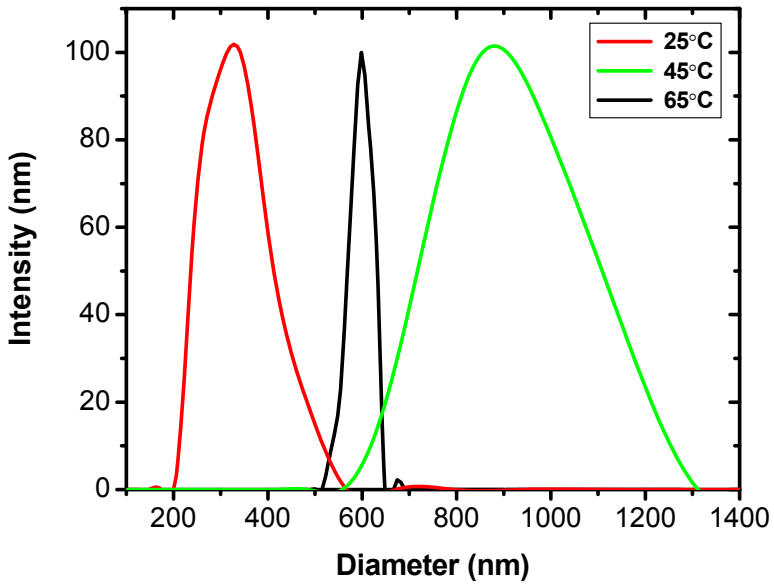

Figure A-3. Diameters of vesicles of DPhPC: DPhPE lipid mixtures at a 5:5 molar ratio at 25˚C, 45˚C and 65˚C as a function of intensity of scattered light.

APPENDIX B
X-RAY PHOTOELECTRON SPECTROSCOPY USED FOR SURFACE ANALYSIS OF PLASMA-TREATED GOLD

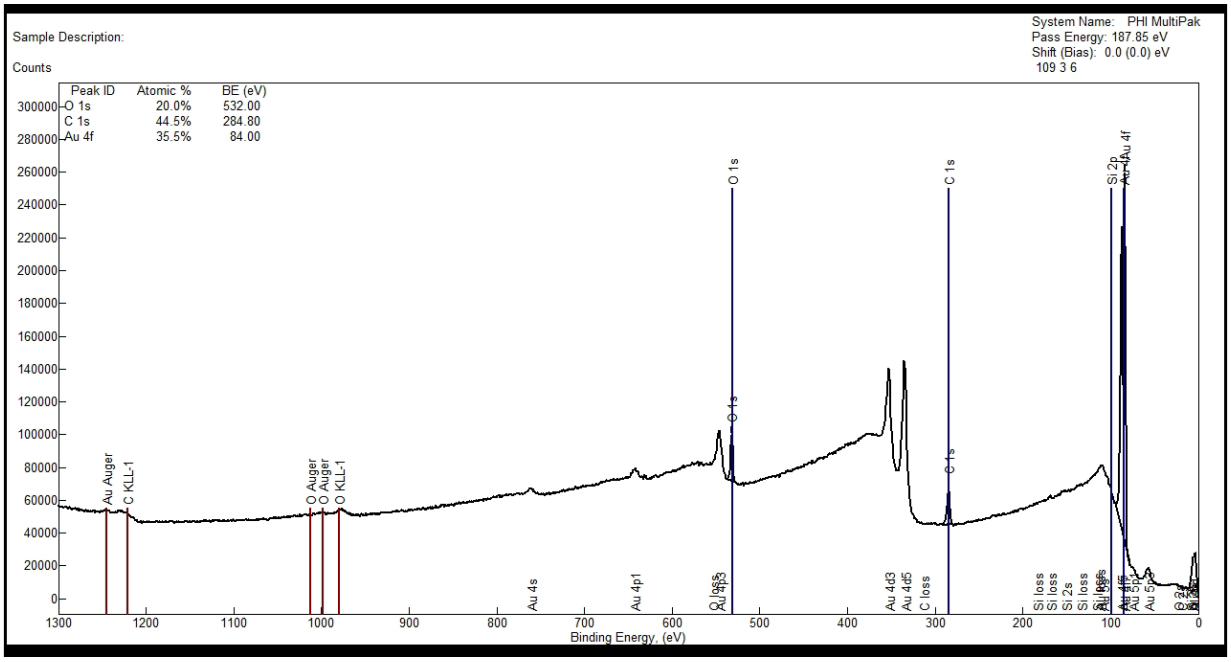

Figure B-1. XPS results showing gold, oxygen and carbon as the only elements present on plasma-treated gold.

APPENDIX C
DNA AND AMINO ACID SEQUENCES OF PROTEINS

Table C-1. Full Length *mslo* Amino Acid Sequences (BK_{Ca} Channel)

1	MELEHPKSPP	YPSSSSSSSS	SSVHEPKMDA	LIIPVTMEVP	CDSRGQRMWW
51	AFLASSMVTF	FGGLFIILLW	RTLKYLWTVC	CHCGGKTKEA	QKINNGSSQA
101	DGTLKPVDEK	EEVVAAEVGW	MTSVKDWAGV	MISAQTLTGR	VLVVLVFALS
151	IGALVIYFID	SSNPIESCQN	FYKDFTLQID	MAFNVFFLLY	FGLRFIAAND
201	KLWFWLEVNS	VVDFFTVPPV	FVSVYLNRSW	LGLRFLRALR	LIQFSEILQF
251	LNILKTSNSI	KLVNLLSIFI	STWLTAAGFI	HLVENSGDPW	ENFQNNQALT
301	YWECVYLLMV	TMSTVGYGDV	YAKTTLGRLF	MVFFILGGLA	MFASYVPEII
351	ELIGNRKKYG	GSYSAVSGRK	HIVVCGHITL	ESVSNFLKDF	LHKDRDDVNV
401	EIVFLHNISP	NLELEALFKR	HFTQVEFYQG	SVLNPHDLAR	VKIESADACL
451	ILANKYCADP	DAEDASNIMR	VISIKNYHPK	IRIITQMLQY	HNKAHLLNIP
501	SWNWKEGDDA	ICLAELKLGF	IAQSCLAQGL	STMLANLFSM	RSFIKIEEDT
551	WQKYYLEGVS	NEMYTEYLSS	AFVGLSFPTV	CELCFVKLKL	LMIAIEYKSA
601	NRESRILINP	GNHLKIQEGT	LGFFIASDAK	EVKRAFFYCK	ACHDDVTDPK
651	RIKKCGCRRL	IYFEDEQPPT	LSPKKKQRNG	GMRNSPNTSP	KLMRHDPLLI
701	PGNDQIDNMD	SNVKKYDSTG	MFHWCAPKEI	EKVILTRSEA	AMTVLSGHVV
751	VCIFGDVSSA	LIGLRNLVMP	LRASNFHYHE	LKHIVFVGSI	EYLKREWETL
801	HNFPKVSILP	GTPLSRADLR	AVNINLCDMC	VILSANQNNI	DDTSLQDKEC
851	ILASLNIKSM	QFDDSIGVLQ	ANSQGFTPPG	MDRSSPDNSP	VHGMLRQPSI
901	TTGVNIPIIT	ELVNDTNVQF	LDQDDDDDPD	TELYLTQPFA	CGTAFAVSVL
951	DSLMSATYFN	DNILTLIRTL	VTGGATPELE	ALIAEENALR	GGYSTPQTLA
1001	NRDRCRVAQL	ALLDGPFADL	GDGGCYGDLF	CKALKTYNML	CFGIYRLRDA
1051	HLSTPSQCTK	RYVITNPPYE	FELVPTDLIF	CLMQFDHNAG	QSRASLSHSS
1101	HSSQSSSKKS	SSVHSIPSTA	NRPNRPKSRE	SRDKQNATRM	TRMGQAEKKW
1151	FTDEPDNAYP	RNIQIKPMST	HMANQINQYK	STSSLIPPIR	EVEDEC

Table C-2. Truncated BK_{Ca} Channel at position 335 with 12 additional residues coded for at the C-terminus to introduce a stop codon

1	MELEHPKSPP	YPSSSSSSSS	SSVHEPKMDA	LIIPVTMEVP	CDSRGQRMWW
51	AFLASSMVTF	FGGLFIILLW	RTLKYLWTVC	CHCGGKTKEA	QKINNGSSQA
101	DGTLKPVDEK	EEVVAAEVGW	MTSVKDWAGV	MISAQTLTGR	VLVVLVFALS
151	IGALVIYFID	SSNPIESCQN	FYKDFTLQID	MAFNVFFLLY	FGLRFIAAND
201	KLWFWLEVNS	VVDFFTVPPV	FVSVYLNRSW	LGLRFLRALR	LIQFSEILQF
251	LNILKTSNSI	KLVNLLSIFI	STWLTAAGFI	HLVENSGDPW	ENFQNNQALT
301	YWECVYLLMV	TMSTVGYGDV	YAKTTLGRLF	MVFFIALRTP	RRPELFF

Table C-3. Red fluorescent protein (mRFP1) DNA and protein sequences

DNA	ATGGCCTCCT CCGAGGACGT CATCAAGGAG TTCATGCGCT TCAAGGTGCG CATGGAGGGC TCCGTGAACG GCCACGAGTT CGAGATCGAG GGCGAGGGCG AGGGCCGCCC CTACGAGGGC ACCCAGACCG CCAAGCTGAA GGTGACCAAG GGCGGCCCCC TGCCCTTCGC CTGGGACATC CTGTCCCCTC AGTTCCAGTA CGGCTCCAAG GCCTACGTGA AGCACCCCGC CGACATCCCC GACTACTTGA AGCTGTCCTT CCCCGAGGGC TTCAAGTGGG AGCGCGTGAT GAACTTCGAG GACGGCGGCG TGGTGACCGT GACCCAGGAC TCCTCCCTGC AGGACGGCGA GTTCATCTAC AAGGTGAAGC TGCGCGGCAC CAACTTCCCC TCCGACGGCC CCGTAATGCA GAAGAAGACC ATGGGCTGGG AGGCCTCCAC CGAGCGGATG TACCCCGAGG ACGGCGCCCT GAAGGGCGAG ATCAAGATGA GGCTGAAGCT GAAGGACGGC GGCCACTACG ACGCCGAGGT CAAGACCACC TACATGGCCA AGAAGCCCGT GCAGCTGCCC GGCGCCTACA AGACCGACAT CAAGCTGGAC ATCACCTCCC ACAACGAGGA CTACACCATC GTGGAACAGT ACGAGCGCGC CGAGGGCCGC CACTCCACCG GCGCCTAA
PROTEIN	MASSEDVIKE FMRFKVRMEG SVNGHEFEIE GEGEGRPYEG TQTAKLKVTK GGPLPFAWDI LSPQFQYGSK AYVKHPADIP DYLKLSFPEG FKWERVMNFE DGGVVTVTQD SSLQDGEFIY KVKLRGTNFP SDGPVMQKKT MGWEASTERM YPEDGALKGE IKMRLKLKDG GHYDAEVKTT YMAKKPVQLP GAYKTDIKLD ITSHNEDYTI VEQYERAEGR HSTGA

Table C-5. E. coli Mechanosensitive Channel of Large Conductance (MscL) DNA sequences

```
1   TATGGTTGTC GGCTTCATAG GGAGAATAAC ATGAGCATTA TTAAAGAATT
51  TCGCGAATTT GCGATGCGCG GGAACGTGGT GGATTTGGCG GTGGGTGTCA
101 TTATCGGTGC GGCATTCGGG AAGATTGTCT CTTCACTGGT TGCCGATATC
151 ATCATGCCTC CTCTGGGCTT ATTAATTGGC GGGATCGATT TTAAACAGTT
201 TGCTGTCACG CTACGCGATG CGCAGGGGGA TATCCCTGCT GTTGTGATGC
251 ATTACGGTGT CTTCATTCAA AACGTCTTTG ATTTTCTGAT TGTGGCCTTT
301 GCCATCTTTA TGGCGATTAA GCTAATCAAC AAACTGAATC GGAAAAAAGA
351 AGAACCAGCA GCCGCACCTG CACCAACTAA AGAAGAAGTA TTACTGACAG
401 AAATTCGTGA TTTGCTGAAA GAGCAGAATA ACCGCTCTTA ACAAGCGCCT
451 GAAAGCAGAA GACCAGTGGT AAAAAAGTGA TTTACTTTCT TGCCACTGGC
501 CTCCCAGTTC CCCCGATTGC CATG
```

Table C-4. E. coli Mechanosensitive Channel of Large Conductance (MscL) amino acid sequences

```
1   MSIIKEFREF AMRGNVVDLA VGVIIGAAFG KIVSSLVADI IMPPLGLLIG
51  GIDFKQFAVT LRDAQGDIPA VVMHYGVFIQ NVFDFLIVAF AIFMAIKLIN
101 KLNRKKEEPA AAPAPTKEEV LLTEIRDLLK EQNNRS
```

APPENDIX D
PLASMID MAP FOR THE PCDNAOX AND "MSLO" GENE INSERTS

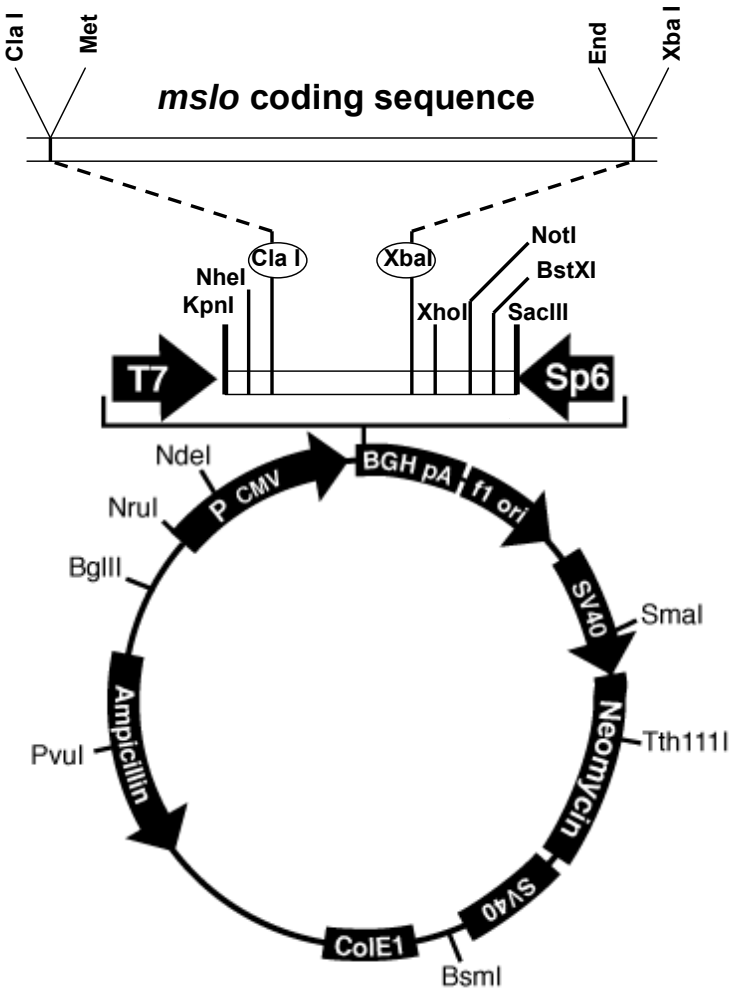

Figure D-1. Map for the pCDNAOX plasmid containing the *mslo* BK_{Ca} channel gene insert and the restriction sites.

LIST OF REFERENCES

1. Hille, B. *Ion Channels of Excitable Membranes* (Sinauer, Sunderland, Massachusetts, USA, 2001).

2. Willumsen, N. J. et al. High throughput electrophysiology: new perspectives for ion channel drug discovery. *Receptors and channels* **9**, 3-12 (2003).

3. Owen, D. & Silverthorne, A. Channeling drug discovery. Current trends in ion channel drug discovery research. *Drug Discovery World* **53**, 48-61 (2002).

4. Ashcroft, F. M. *Ion Channels and Disease - Channelopathies* (Academic Press, San. Diego CA, USA, 2000).

5. Steizle, M., Weismuller, G. & Sackmann, E. On the application of supported bilayers as receptive layers for biosensors with electrical detection. *J. Phys. Chem.* **97**, 2974-2981 (1993).

6. Reiken, S. R. et al. Bispecific antibody modification of nicotinic acetylcholine receptors for biosensing. *Biosensors and Bioelectronics* **111**, 99-102 (1996).

7. Cornell, B. A. et al. A biosensor that uses ion-channel switches. *Nature* **387**, 580–583 (1997).

8. Neher, E. & Sakmann, B. Single-channel currents recorded from membrane of denervated from muscle fibres. *Nature* **260**, 799-802 (1976).

9. Salkoff, L., Butler, A., Ferreira, G., Santi, C. M. & Wei, A. High conductance Potassium Channels of the Slo Family. *Nature Reviews Neurosci.* **5**, 921-931 (2006).

10. Miller, C. An overview of the potassium channel family. *Genome Biol.* **1**,0004 (2000).

11. Papazian, D. M., Schwarz, T. L., Tempel, B. L., Jan, Y. N. & Jan, Y. L. Cloning of genomic and complementary DNA from Shaker, a putative potassium channel gene from Drosophila. *Science* **237**, 749-753 (1987).

12. Ho, K. et al. Cloning and expression of an inwardly rectifying ATP-regulated potassium channel. *Nature* **362**, 31-38 (1993).

13. Heginbotham, L., Lu, Z., Abramson, T., MacKinnon, R. & Mutations in the K+ channel signature sequence. *Biophys J.* **66**, 1061-1067 (1994).

14. Pongs, O. et al. Shaker encodes a family of putative potassium channel proteins in the nervous system of Drosophila. *EMBO J.* **7**, 1087-1096 (1988).

15. Hille, B. & Schwarz, W. Potassium channels as multi-ion single-file pores. *J. Gen Physiol.* **72**, 409-442 (1978).

16. Gouaux, E. & Mackinnon, R. Principles of selective ion transport in channels and pumps. *Science* **310**, 1461-1465 (2005).

17. Orio, P., Rojas, P., Ferreira, G. & Latorre, R. New guises for an old channel: maxik channel beta subunits. *News Physiol. Sci.* **17**, 156-161 (2002).

18. Marty, A. Ca-dependent K channels with large unitary conductance in chromaffin cell membranes. *Nature* **291**, 497-500 (1981).

19. Park, Y. B. Ion selectivity and gating of small conductance calcium-activated potassium channels in cultured rat adrenal chromaffin cells. *J. Physiol. (Lond.)* **481**, 555-570 (1994).

20. Blatz, A. L. & Magleby, K. L. Correcting single channel data for missed events. *Biophys. J.* **49**, 967-980 (1986).

21. Logsdon, N. J., Kang, J., Togo, J. A., Christian, E. P. & Aiyar, J. A novel gene, hKCa4, encodes the calcium-activated potassium channel in human T lymphocytes. *J. Biol. Chem.* **272**, 32723– 32726 (1997).

22. Ishii, T. M. et al. A human intermediate conductance calcium-activated potassium channel. *Proc Natl Acad Sci USA* **94**, 11651–11656 (1997).

23. Adelman, J. P. et al. Calcium-activated potassium channels expressed from cloned complementary DNAs *Neuron* **9**, 209−216 (1992).

24. Atkinson, N. S., Robertson, G. A. & Ganetzky, B. A component of calcium-activated potassium channels encoded by the Drosophila slo locus. *Science* **253**, 551-555 (1991).

25. Meera, P., Wallner, M., Song, M. & Toro, L. Large conductance voltage- and calcium-dependent K+ channel, a distinct member of voltage-dependent ion channels with seven N-terminal transmembrane segments (S0-S6), an extracellular N terminus, and an intracellular (S9-S10) C terminus. *Proc Natl Acad Sci USA* **94**, 14066-14071 (1977).

26. Wallner, M., Meera, P. & Toro, L. Determinant for beta-subunit regulation in high-conductance voltage-activated and Ca(2+)-sensitive K+channels: an additional transmembrane region at the N terminus. *Proc Natl Acad Sci USA* **93**, 14922–14927 (1996).

27. Toro, L., Wallner, M., Meera, P. & Tanaka, Y. Maxi-K(Ca), a unique member of the voltage-gated K channel superfamily. *News Physiol Sci* **13**, 112-117 (1998).

28. Knaus, H. G. et al. Primary sequence and immunological characterization of beta-subunit of high conductance Ca(2+)-activated K+channel from smooth muscle. *J. Biol. Chem.* **269**, 17274– 17278 (1994).

29. Knaus, H. G. et al. Tremorgenic indole alkaloids potently inhibit smooth muscle high-conductance calcium-activated potassium channels. *Biochemistry* **33**, 5819–5828 (1994).

30. Jiang, Y., Pico, A., Cadene, M., Chait, B. T. & MacKinnon, R. Structure of the RCK domain from the E. coli K+ channel and demonstration of its presence in the human BK channel. *Neuron* **29**, 593-601 (2001).

31. Wei, A., Solaro, C., Lingle, C. & Salkoff, L. Calcium sensitivity of BK-type KCa channels determined by a separable domain. *Neuron* **13**, 671-681 (1994).

32. Stefani, E. et al. Voltage-controlled gating in a large conductance Ca2+-sensitive K+ channel (hslo). *Proc Natl Acad Sci USA* **94**, 5427– 5431 (1997).

33. Bezanilla, F., Perozo, E., Papazian, D. M. & Stefani, E. Molecular basis of gating charge immobilization in Shaker potassium channels. *Science* **254**, 679– 683 (1991).

34. Cui, J., Cox, D. H. & Aldrich, R. W. Intrinsic voltage dependance and calcium regulation of mslo large conductance calcium-activated K+ channels. *J. Gen. Physiol.* **109**, 647-673 (1997).

35. Latorre, R., Oberhauser, A., Labarca, P. & Alvarez, O. Varieties of calcium-activated potassium channels. *Ann. Rev. Physiol.* **51**, 385-399 (1989).

36. Pallotta, B. S. N-bromoacetamide removes a calcium-dependent component of channel opening from calcium-activated potassium channels in rat skeletal muscle. *J. Gen. Physiol.* **86**, 601-611 (1985).

37. Papazian, D. M., Timpe, L. C., Jan, Y. N. & Jan, Y. L. Alteration of voltage-dependence of shaker potassium channels by mutations in the S4 sequence. *Nature* **349**, 305-310 (1991).

38. Rothberg, B. S. Allosteric modulationof ion channels: the case of maxi-k. *Sci STKE* **2004** (2004).

39. Tian, L., Coghill, L. S., MacDonald, S. H., Armstrong, D. L. & Shipston, M. J. Leucine zipper domain targets cAMP-dependent protein kinase to mammalian BK channels. *J. Biol. Chem.* **278**, 8669– 8677 (2003).

40. Wei, A., Jegla, T. & Salkoff, L. Eight potassium channel families revealed by the C. elegans genome project. *Neuropharmacology* **35**, 805-829 (1996).

41. Schreiber, M. & Salkoff, L. A novel calcium-sensing domain in the BK channel. *Biophys. J.* **73**, 1355– 1363 (1997).

42. Xia, X. M., Zeng, X. & Lingle, C. J. Multiple regulatory sites in largeconductance calcium-activated potassium channels. *Nature* **418**, 880-884 (2002).

43. Piskorowski, R. & Aldrich, R. W. Calcium activation of BK(Ca) potassium channels lacking the calcium bowl and RCK domains. *Nature* **420**, 499-502 (2002).

44. Knaus, H. et al. Characterization of Tissue-expressed α-Subunits of the High Conductance Calcium-activated Potassium Channel. *Journal of Biological Chemistry* **270**, 22434-22439 (1995).

45. Jin, P., Weiger, T. M. & Levitan, I. B. Reciprocal modulation between the alpha and beta 4 subunits of hSlo calcium-dependent potassium channels. *J. Biol. Chem.* **277**, 43724– 43729 (2002).

46. Zeng, X. H., Xia, X. M. & Lingle, C. J. Redox-sensitive extracellular gates formed by auxiliary beta subunits of calcium-activated potassium channels. *Nat. Struct. Biol.* **10**, 448-454 (2003).

47. Jin, P., Weiger, T. M., Wu, Y. & Levitan, I. B. Phosphorylation dependent functional coupling of hSlo calcium-dependent potassium channel and its beta 4 subunit. *J. Biol. Chem.* **277**, 10014–10020 (2002).

48. Egan, T. M., Dagan, D. & Levitan, I. B. Properties and modulation of a calcium-activated potassium channel in rat olfactory bulb neurons. *J. Neurophysiol.* **69**, 1433– 1442 (1993).

49. Galvez, A. et al. Purification and characterization of a unique, potent, peptidyl probe for the high conductance calcium-activated potassium channel from venom of the scorpion Buthus tamulus. *J. Biol. Chem.* **265**, 11083–11090 (1990).

50. Giangiacomo, K. M., Garcia, M. L. & McManus, O. B. Mechanism of iberiotoxin block of the large-conductance calcium- activated potassium channel from bovine aortic smooth muscle. *Biochemistry* **31**, 6719–6727 (1992).

51. Candia, S., Garcia, M. L. & Latorre, R. Mode of action of iberiotoxin, a potent blocker of the large conductance Ca2+-activated K+ channel. *Biophys. J.* **63**, 583-590 (1992).

52. Kaczorowski, G. J., Knaus, H.-G., Leonard, R. J., McManus, O. B. & Garcia, M. L. High-conductance calcium-activated potassium channels; Structure, pharmacology, and function. *J. Bioenergetics & Biomembranes* **28**, 255-267 (1996).

53. Blatz, A. L. & Magleby, K. L. Calcium-activated potassium channels. *Trends in Neurosciences* **10**, 463-467 (1987).

54. Yellen, G. Voltage gated potassium channels and their relatives. *Nature* **419**, 35-42 (2002).

55. Tristani-Firouzi, M., Chen, J. & Sanguinetti, M. C. Interactions between S4-S5 linker and S6 transmembrane domain modulate gating of HERG K+ channels. *J. Biol. Chem.* **277**, 18994-19000 (2002).

56. Doyle, D. A. et al. The structure of the potassium channel: molecular basis of K+ conduction and selectivity. *Science* **280**, 69-76 (1998).

57. Zagotta, W. N., Hoshi, T. & Aldrich, R. W. Restoration of inactivation in mutants of Shaker potassium channels by a peptide derived from ShB. *Science* **250**, 568-571 (1990).

58. Hoshi, T., Zagotta, W. N. & Aldrich, R. W. Biophysical and molecular mechanisms of Shaker potassium channel inactivation. *Science* **250**, 533-538 (1990).

59. Yellen, G. The moving parts of voltage-gated ion channels. *Quart. Rev. Biophys.* **31**, 239-295 (1998).

60. Opekarová, M. & Tanner, W. Specific lipid requirements of membrane proteins--a putative bottleneck in heterologous expression. *Biochim Biophys Acta - Biomembranes* **1610**, 11-22 (2003).

61. Findlay, H. E. & Booth, P. J. The biological significance of lipid–protein interactions. *J. Phys. Condens. Matter* **18**, 1281-1291 (2006).

62. Vilayaveeti, F. I., Zhou, Y. & MacKinnon, R. Lipids in the structure, folding and function of the KcsA K+ channel. *Biochemistry* **41**, 10771-10777 (2002).

63. Fernandis, A. Z. & Wenk, M. R. Membrane lipids as signaling molecules. *Current opinion in lipidology* **18**, 121-128 (2007).

64. Simons, K. & Toomre, D. Lipid rafts and signal transduction. *Nat. Rev. Mol. Cell. Biol.* **1**, 31-39 (2000).

65. Yeagle, P. L., 822 (1985) 267-287. Cholesterol and the cell membrane. *Biochimica et Biophysica Acta (BBA) - Reviews on Biomembranes* **822**, 267-287 (1985).

66. Gennis, R. *Biomembranes: Molecular structure and function* (Springer-Verlag New York Inc., New York, 1989).

67. Schleifer, K. H. & Stackenbrandt, E. Molecular systematics of prokaryotes. *Ann. Rev. Microbiol.* **37**, 143-187 (1983).

68. Silvius, J. R. Role of cholesterol in lipid raft formation: lessons from lipid model systems. *Biochim Biophys Acta* **1610**, 174-183 (2003).

69. Yeagle, P. *Structure of Biological Membranes* (CRC, New York, 2005).

70. Nelson, L. & Cox, M. M. *Lehniger Principles of Biochemistry* (Sara Tenney, New York, 2005).

71. Madden, T. D. Current concepts in membrane protein reconstitution. *Chem. Phys. Lipids* **40**, 207-222 (1986).

72. Chan, Y.-H. M. & Boxer, S. G. Model membrane systems and their applications *Current Opinion in Chemical Biology* **11**, 1-7 (2007).

73. Tamm, L. K. & McConnell, H. M. Supported phospholipid bilayers. *Biophys J.* **47**, 105-113 (1985).

74. Cremer, P. S. & Boxer, S. Formation and Spreading of Lipid Bilayers on Glass Surfaces. *J. Phys. Chem. B.* **103**, 2554-2559 (1999).

75. Israelachvili, J. *Intermolecular and Surface Forces* (Academic Press, New York, 1991).

76. Parsegian, V. A. Long range physical forces in the biological milieu. *Annu. Rev. Biophys. Bioeng.* **2**, 221-225 (1973).

77. Sackmann, E. Supported membranes: Scientific and practical applications. *Science* **271**, 43-48 (1996).

78. Miller, C., Cuendet, P. & Grätzel, M. K+ sensitive bilayer supporting electrodes. *J. Electroanal. Chem.* **278**, 175-192 (1990).

79. McConnell, H. M., Watts, T. H., Weis, R. M. & Brian, A. A. Supported planar membranes in studies of cell-cell recognition in the immune system. *Biochim Biophys Acta.* **864**, 95-106 (1986).

80. Elender, G., Kühner, M. & Sackmann, E. Functionalisation of Si/SiO2 and glass surfaces with ultrathin dextran films and deposition of lipid bilayers. *Biosens. Bioelectron.* **11**, 565-577 (1996).

81. Ariga, k. & Okahata, Y. Polymerized monolayers of single-, double-, and triple-chain silane amphiphiles and permeation control through the monolayer-immobilized porous glass plate in an aqueous solution. *J. Am. Chem. Soc.* **111**, 5618-5622 (1989).

82. Fare, T. L. Electrical characterization of dipalmitoylphosphatidylethanolamine and cadmium stearate films on platinum surfaces in aqueous solutions. *Langmuir* **6**, 1172-1179 (1990).

83. Stelzle, M. & Sackmann, E. Sensitive detection of protein adsorption to supported lipid bilayers by frequency-dependent capacitance measurements and microelectrophoresis. *Biochim. Biophys. Acta* **981**, 135-142 (1989).

84. Nikolelis, D. P., Siontorou, C. G., Krull, U. J. & Katrivanos, P. L. Ammonium Ion Minisensors from Self-Assembled Bilayer Lipid Membranes Using Gramicidin as an Ionophore. Modulation of Ammonium Selectivity by Platelet-Activating Factor. *Anal. Chem.* **68**, 1735-1741 (1996).

85. Shao, Z., Mou, J., Czajkowsky, J., Yang, J. & Yuan, J.-Y. Biological atomic force microscopy: what is achieved and what is needed. *Adv. Phys.* **45**, 1-86 (1996).

86. Kung, L. A., Kam, L., Hovis, J. S. & Boxer, S. G. Patterning Hybrid Surfaces of Proteins and Supported Lipid Bilayers. *Langmuir* **16**, 6773-6776 (2000).

87. Knoll, W. Interfaces and thin films as seen by bound electromagnetic waves. *Annu. Rev. Phys. Chem.* **49**, 569-638 (1998).

88. Richter, R. P., Bérat, R. & Brisson., A. R. The formation of solid-supported lipid bilayers - an integrated view. *Langmuir* **22**, 3497-3505 (2006).

89. Zhdanov, V. P. & Kasemo, B. Comments on Rupture of Adsorbed Vesicles. *Langmuir* **17**, 3518-3521 (2001).

90. Zhdanov, V. P., Keller, C. A., Glasmastar, K. & Kasemo, B. Simulation of adsorption kinetics of lipid vesicles. *J. Chem. Phys.* **84**, 5443-5446 (2000).

91. Tanaka, M. & Sackmann, E. Polymer supported membranes as models of the cell surface. *Nature* **437**, 656-663 (2005).

92. Kiessling, V., Crane, J. M. & Tamm, L. K. Transbilayer effects of raft-like lipid domains in asymmetric planar bilayers measured by single molecule tracking. *Biophys. J.* **91**, 3313-3326 (2006).

93. Raguse, B. et al. Tethered Lipid Bilayer Membranes: Formation and Ionic Reservoir Characterization. *Langmuir* **14**, 648-659 (1998).

94. Salafsky, J., Groves, J. T. & Boxer, S. G. Architecture and function of membrane proteins in supported bilayers: a study with photosynthetic reactive centers. *Biochemistry* **35**, 14773-14781 (1996).

95. Wagner, M. L. & Tamm, L. K. Tethered Polymer-Supported Planar Lipid Bilayers for Reconstitution of Integral Membrane Proteins: Silane-Poly(ethylene glycol)-Lipid as a Cushion and Covalent Linker. *Biophys. J.* **79**, 1400-1414 (2000).

96. Vockenroth, I. K., Atanasova, P. P., Toby, A., Jenkins, A. & Köper, I. Incorporation of α-Hemolysin in Different Tethered Bilayer Lipid Membrane Architectures. *Langmuir* **24**, 496-502 (2008).

97. Andersson, M. et al. Voltage-induced gating of the mechanosensitive MscL ion channel reconstituted in a tethered lipid bilayer membrane. *Biosensors and Bioelectronics* **23**, 919-923 (2008).

98. Andersson, M. et al. Detection of single ion channel activity on a chip using tethered bilayer membranes. *Langmuir* **23**, 2924-2927 (2007).

99. Keizer, H. M. et al. Functional Ion Channels in Tethered Bilayer Membranes—Implications for Biosensors. *ChemBioChem* **8**, 1246-1250 (2007).

100. Knoll, W. Functional tethered lipid bilayers. *Reviews in Molecular Biotechnology* **74**, 137-158 (2000).

101. Schiller, S. M., Naumann, R., Lovejoy, K., Kunz, H. & Knoll, W. Archaea Analogue Thiolipids for Tethered Bilayer Lipid Membranes on Ultrasmooth Gold Surfaces. *Angew. Chem., Int. Ed.* **42**, 208-211 (2003).

102. Krishna, G., Schulte, J., Cornell, B. A., Pace, R. & Osman, P. Tethered bilayer membranes containing ionic reservoirs: Selectivity and conductance. *Langmuir* **19**, 2294-2305 (2003).

103. Dubois, L. H. & Nuzzo, R. G. Synthesis, Structure, and Properties of Model Organic Surfaces. *Annual Review of Physical Chemistry* **43**, 437-463 (1992).

104. Woese, C. R. & Fox, G. E. Phylogenetic structure of the prokaryotic domain: the primary kingdoms. *Proc Natl Acad Sci USA* **74**, 5088–5090 (1977).

105. Sten-Knudsen, O. *Passive transport processes in membrane transport in biology* (Springer-Verlag, New York, 1978).

106. Tien, H. T. & Ottova-Leitmannova. *Planar lipid bilayers (BLMs) and their applications* (Elsevier, Amsterdam, 2003).

107. Cole, K. S. *Membranes, ions and impulses: A chapter of classical biophysics* (University of California Press, Berkeley, 1968).

108. Almers, W. Gating currents and charge movements in excitable membranes. *Rev. Physiol. Biochem. Pharmacol.* **82**, 96-190 (1978).

109. Coronado, R. & Latorre, R. Phospholipid bilayers made from monolayers on patch-clamp pipettes. *Biophys. J.* **43**, 231-236 (1983).

110. Wiegand, G., Arribas-Layton, N., Hillebrandt, H., Sackmann, E. & P. Wagner. Electrical properties of supported lipid bilayer membranes. *J. Phys. Chem. B.* **106**, 4245-4254 (2002).

111. Hladky, S. B. & Haydon, D. A. Discreteness of conductance change in bimolecular lipid membranes in the presence of certain antibiotics. *Nature* **225**, 451-453 (1970).

112. Bayley, H., Braha, O. & Gu, L.-Q. Stochastic sensing with protein pores. *Adv. Mater.* **12**, 139-142 (2000).

113. Bayley, H. & Cremer, P. S. Stochastic sensors inspired by biology. *Nature* **413**, 226-230 (2001).

114. Kodadek, T. Protein microarrays: prospects and problems. *Chem Biol.* **8**, 105-115 (2001).

115. Gurdon, J. B., Lane, C. D., Woodland, H. R. & Marbaix, G. Use of frog eggs and oocytes for the study of messenger RNA and its translation in living cells. *Nature (Land.)* **233**, 177-182 (1971).

116. Vargo, M. A. & Colman, R. F. Heterodimers of wild-type and subunit interface mutant enzymes of glutathione S-transferase A1–1: Interactive or independent active sites? *Protein Sci.* **13**, 1586-1593 (2004).

117. Hochuli, E., Dobeli, H. & Struber, A. New metal chelate adsorbents selective for proteins and peptides containing neighbouring histidine residues. *J. Chromatogr.* **411**, 177-184 (1987).

118. Hochuli, E., Banworth, W., Dobeli, H., Gentz, R. & Struber, A. Genetic approach to facilitate purification of recombinant proteins with a novel metal chelate adsorbent. *BioTechnol*. **6**, 1321-1325 (1988).

119. Sakmann, B. & Neher, E. *Single-channel recording* (Plenum Press, New York, 1995).

120. Subrahmanyam, S., Piletsky, S. & Turner, A. Application Natural Receptors in Sensors and Assays. *Anal. Chem.* **74**, 3942-3951 (2002).

121. Delcour, A. H., Martinac, B., Adler, J. & Kung, C. Modified Reconstitution Method Used in Patch-Clamp Studies of Escherichia-Coli Ion Channels. *Biophys. J.* **56**, 631-636 (1989).

122. MacKinnon, R. Potassium Chanels and Atomic Basis of Selective Ion Conduction. *Angewandte Chemie* **43**, 4265-4277 (2004).

123. Sukharev, S. I., Blount, P., Martinac, B. & Kung, C. Mechanosensitive channels of Escherichia coli: The MscL gene, protein, and activities. *Annual Review of Physiology* **59**, 633-657 (1997).

124. Chu, B. *Laser Light Scattering* (Academic Press, Inc, San Diego, 1991).

125. Precision Deconvolve[32] *User Manual* (2003).

126. Johnson, S. J. et al. Structure of an adsorbed dimyristoylphosphatidylcholine bilayer measured with specular reflection of neutrons. *Biophys. J.* **52**, 289-294 (1991).

127. Ebenstein, Y., E. *Nano Letters* **2**, 945-950 (2002).

128. Digital Instruments, *User manual* (2000).

129. Ikeda, S. R., Soler, F., Zuhlke, R. D., Joho, R. H. & Lewis, L. D. Heterologous expression of the human potassium channel Kv2.1 in clonal mammalian cells by direct cytoplasmic microinjection of cRNA. *Pflügers Archiv* **422**, 201-203 (1992).

130. Capecchi, M. R. High efficiency transformation by direct microinjection of DNA into cultured mammalian cells. *Cell* **22**, 479-488 (1980).

131. Kamb, A., Korenbrot, J. I. & Kitajewski, J. Expression of ion channels in cultured cells using baculovirus. *Methods in Enzymology* **207**, 423-431 (1992).

132. Fulita, N. et al. Biosynthesis of the Torpedo californica acetylcholine receptor a subunit in yeast. *Science* **231**, 1284-1289 (1986).

133. King, K., Dohlman, H. G., Thorner, J., Caron, M. G. & Lefkowitz, R. J. Control of yeast mating signal transduction by a mammalian beta 2-adrenergic receptor and Gs alpha subunit. *Science* **250**, 121-123 (1990).

134. Strosberg, A. D. & Marullo, S. Functional expression of receptors in microorganisms. *Trends Pharmacol. Sci.* **13**, 95-98 (1992).

135. Barthel, F. et al. Gene regulation analysis by lipopolyamine-mediated DNA transfer in primary neurons. *Methods in Neuroscience* **9**, 292-312 (1992).

136. Holt, C. E., Garlick, N. & Cornel, E. Lipofection of cDNAs in the embryonic verterbrae central nervous system. *Neuron* **4**, 203-214 (1990).

137. Bianchi, L. & Driscoll, M. *Heterologous expression of C. elegans ion channels in Xenopus oocytes* (Wormbook, ed. The C. elegans Research Community, 2006).

138. Campbell, R. E. et al. A monomeric red fluorescent protein. *PNAS* **99**, 7877-7882 (2002).

139. Bevis, B. J. & Glick, B. S. Rapidly maturing variants of the Discosoma red fluorescent protein (DsRed). *Nature Biotechnology* **20**, 83-87 (2002).

140. Ohlendieck, K. *Protein Purification Protocols* (Humana Press, New Jersey, 2008).

141. Kusaka, I. & Kanai, K. Purification and Characterization of Alanine Carrier Isolated from H-Proteins of Bacillus subtilis. *European Journal of Biochemistry*, **83**, 307 - 311 (1978).

142. Riepl, R. & Vidaver, G. A. Effects of Triton X-100 Treatments on the Composition and Activities of Membrane Vesicles from Pegion Erythrocytes. *Biochimica et Biophysica Acta* **507**, 94 -106 (1978).

143. Mimms, L. T., Zampighi, G., Nozaki, Y., Tanford, C. & Reynolds, J. A. Phospholipid vesicle formation and transmembrane protein incorporation using octyl glucoside. *Biochemistry* **20**, 833–845 (1981).

144. DiChiara, T. J. & Reinhart, P. H. Distinct effects of Ca2+ and voltage on the activation and deactivation of cloned Ca2+-activated K+ channels. *J. Physiol. (Lond.)* **489**, 403-418 (1995).

145. Ausubel, F. M. et al. *Current Protocols in Molecular Biology* (Wiley Interscience, New York, New York, 1988).

146. Krause, J. D., Foster, C. D. & Reinhart, P. H. Xenopus laevis oocytes contain endogenous large conductance Calcium-activated potassium channels. *Neuropharmacology* **35**, 1017-1022 (1996).

147. Zhang, Y. L., Dunlop, J. & Dalziel, J. E. Recombinant human voltage-gated sodium channels are pharmacologically functional in planar lipid bilayers. *Biosensors and Bioelectronics* **22**, 1006-1012 (2007).

148. Lu, L., Montrose-Rafizadeh, C., Hwang, T.-C. & Guggino, W. B. A delayed rectifier potassium current in Xenopus oocytes. *Biophys. J.* **57**, 1117-1123 (1990).

149. Methfessel, C. et al. Patch clamp measurements on Xenopus laevis oocytes: Currents through endogenous channels and implanted acetylcholine receptor and sodium channels. *Pflugers Arch.* **407**, 577-588 (1996).

150. Witzmann, F., Jarnot, B. & Parker, D. Dodecyl maltoside detergent improves resolution of hepatic membrane proteins in two-dimensional gels. *Electrophoresis* **9**, 687-688 (1991).

151. Bernajee, P. Differential solubilization of lipids along with membrane proteins by different classes of detergents. *Chem. Phys. Lipids* **77**, 65-78 (1995).

152. Sumikawa, K. & Miledi, R. Assembly and N-glycosylation of all ACh receptor subunits are required for their efficient insertion into plasma membranes. *Molec. Brain Res.* **5**, 183-192 (1989).

153. Sumikawa, K., Parker, I. & Miledi, R. Effect of tunicamicyn on the expression of functional brain neurotransmitter receptors and voltage-operated channels in Xenopus oocytes. *Molec. Brain Res.* **4**, 191-199 (1988).

154. Sigel, E. Properties of single sodium channels translated by Xenopus oocytes after injection with messenger ribonucleic acid. *J. Physiol., Lond.* **386**, 73-90 (1987).

155. Wheatley, M. & Hawtin, S. R. Glycosylation of G-protein-coupled receptors for hormones central to normal reproductive functioning: its occurence and role. *Human Reproduction Update* **5**, 356-364 (1999).

156. Rigaud, J.-L. & Lévy, D. Reconstitution of membrane proteins into liposomes. *Methods in enzymology* **372**, 65-86 (2003).

157. Berquand, A., Mingeot-Leclercq, M. P. & Dufrene, Y. F. Real-time imaging of drug-membrane interactions by atomic force microscopy. *Biochim. Biophys. Acta, Biomembr.* **1664**, 198-205 (2004).

158. Deshayes, S., Morris, M. C., Divita, G. & Heitz, F. Interactions of amphipathic carrier peptides with membrane components in relation with their ability to deliver therapeutics. *J. Pept. Sci.* **12**, 758-765 (2006).

159. Rodrigues, C., Gameiro, P., Reis, S., Lima, J. L. & Castro, B. d. Derivative spectrophotometry as a tool for the determination of drug partition coefficients in water/dimyristoyl-L-alpha-phosphatidylglycerol (DMPG) liposomes. *Biophys. Chem.* **94**, 97-106 (2001).

160. Andersson, M. et al. Detection of single ion channel activity on a chip using tethered bilayer membranes. *Langmuir* **23**, 2924-2927 (2007).

161. Tamm, L. K. & Kalb, E. *Microspectrofluorometry on supported planar membranes* (John Wiley and Sons, New York, 1993).

162. Poglitsch, C. L., Sumner, M. T. & Thompson, N. L. Binding of IgG to MoFc gamma RII purified and reconstituted into supported planar membranes as measured by total internal reflection fluorescence microscopy. *Biochemistry* **30**, 6662-6671 (1991).

163. Silvestro, L. & Axelsen, P. H. Infrared spectroscopy of supported lipid monolayer, bilayer and multibilayer membranes. *Chem. Phys. Lipids* **96**, 69-80 (1998).

164. Tamm, L. K. & Tatulian, S. A. Infrared spectroscopy of proteins and peptides in lipid bilayers. *Q. Rev. Biophys.* **30**, 365-429 (1997).

165. Kagawa, Y. Energy transducing proteins in thermophilic biomembranes. *J. Memb. Biol.* **55**, 1-8 (1980).

166. Driessen, A. J. M., Vossenberg, J. L. & Konings, W. N. Membrane composition and ion-permeability in extremophiles. *FEMS Microbiol. Rev.* **18**, 139-148 (1996).

167. Shinoda, W., Mikami, M., Baba, T. & Hato, M. Dynamics of a highly branched lipid bilayer: a molecular dynamics study. *Chem. Phys. Lett.* **390**, 35–40 (2004).

168. Hsieh, C.-H., Sue, S.-C., Lyu, P.-C. & Wu, W.-G. Membrane packing geometry of diphytanyolphosphatidylcholine is highly sensitive to hydration: Phospholipid polymorphism induced by molecular rearrangement in the headgroup region. *Biophys. J.* **73**, 870-877 (1997).

169. Atanasov, V. et al. Membrane on a Chip. A functional tethered lipid bilayer membrane on silicon oxide surfaces. *Biophys. J.* **89**, 1780-1788 (2005).

170. Naumann, R. et al. Tethered lipid Bilayers on ultraflat gold surfaces. *Langmuir* **19**, 5435-5443 (2003).

171. Suzuki, H., Tabata, K. V., Noji, H. & Takeuchi, S. Highly reproducible method of planar lipid bilayer reconstitution in polymethyl methacrylate microfluidic chip. *Langmuir* **22**, 1937-1942 (2006).

172. Santiago, J. et al. Probing the effects of membrane cholesterol in the Torpedo californica acetylcholine receptor and the novel lipid-exposed mutation alpha C418W in Xenopus oocytes. *J. Biol. Chem.* **276**, 46523-46532 (2001).

173. Gustafsson, J., Oradd, G., Nyden, M., Hansson, P. & Almgren, M. Defective lamellar phases and micellar polymorphism in mixtures of glycerol monooleate and cetyltrimethylammonium bromide in aqueous solution. *Langmuir* **14**, 4987-4996 (1998).

174. Provencher, S. W. CONTIN - A general-purpose constrained regularization program for inverting noisy linear algebraic and integral equations. *Comput. Phys. Commun.* **27**, 229-242 (1982).

175. Provencher, S. W. A constrained regularization program for inverting data represented by linear algebraic or integral equations. *Comput. Phys. Commun.* **27**, 213-227 (1982).

176. Einstein, A. *Investigations on the theory of Brownian movement.* (Dover Publications Inc. USA 1956).

177. Danino, D., Talmon, Y. & Zana, R. Cryo-TEM of thread-like micelles: on-the-grid microstructural transformations induced during specimen preparation. *Colloid Surf. A-Physicochem. Eng. Asp.* **169**, 67-73 (2000).

178. Rand, R. P. & Fuller, N. L. Structural dimensions and their changes in a reentrant hexagonal-lamellar transition of phospholipids. *Biophys. J.* **66**, 2127-2138 (1994).

179. Naumann, R. et al. Tethered lipid Bilayers on ultraflat gold surfaces. *Langmuir* **19**, 5435-5443 (2003).

180. Gauger, D. R., Binder, H., Vogel, A., Selle, C. & Pohle, W. Comparative FTIR-spectroscopic studies of the hydration of diphytanoylphosphatidylcholine and -ethanolamine. *J. Mol. Struct.* **614**, 211-220 (2002).

181. Scott, W. W. & Bhushan, B. *4th International Conference on Scanning Probe Microscopy, Sensors and Nanostructures* (Elsevier Science, Las Vegas, Nv, 2002).

182. Seantier, B., Breffa, C., Felix, O. & Decher, G. Dissipation-enhanced quartz crystal microbalance studies on the experimental parameters controlling the formation of supported lipid bilayers. *J. Chem. Phys.* **109**, 21755-21765 (2005).

183. Reviakine, I. & Brisson, A. Formation of supported phospholipid bilayers from unilamellar vesicles investigated by atomic force microscopy. *Langmuir* **16**, 1806-1815 (2000).

184. Brenner, R. et al. Vasoregulation by the beta1 subunit of the calcium-activated potassium (BK) channel. *Nature* **407**, 870-876 (2000).

185. Ramanathan, K. & Fuchs, P. A. Modeling hair cell tuning by expression gradients of potassium channel beta subunits. *Biophys. J*. **82**, 64-75 (2002).

186. Robitaille, R., Garcia, M. L., Kaczorowski, G. J. & Charlton, M. P. Functional colocalization of calcium and calcium-gated potassium channels in control of transmitter release. *Neuron* **11**, 645-655 (1993).

187. Gao, Y.-D. & Garcia, M. L. Interaction of Agitoxin2, Charybdotoxin and Iberiotoxin with Potassium Channels: Selectivity between cause blockade of the channel Voltage-gated and Maxi-K channels. *Proteins: structure function and genetics* **52**, 146-154 (2003).

188. Terrettaz, S., Mayer, M. & Vogel, H. Highly electrically insulating tethered lipid bilayers for probing the function of ion channel proteins. *Langmuir* **19**, 5567-5569 (2003).

189. Steinem, C., Janshoff, A., Ulrich, W. P., Sieber, M. & Galla, H. J. Impedance analysis of supported lipid bilayer membranes: a scrutiny of different preparation techniques. *Biochim Biophys Acta.* **1279**, 169-180 (1996).

190. Vallejo, A. E. & Gervasi, C. A. Impedance analysis of ion transport through gramicidin channels in supported lipid bilayers. *Bioelectrochemistry* **57**, 1-7 (2002).

191. Schuster, B., Pum, D., Braha, O., Bayley, H. & Sleytr, U. B. Self-assembled alpha-haemolysin pores in an S-layer supported lipid bilayer. *Biochim. Biophys. Acta.* **1370**, 280-288 (1998).

192. Hinterdorfer, P., Baber, G. & Tamm, L. K. Reconstitution of Membrane Fusion Sites. *J. Biol. Chem.* **269**, 20360-20368 (1994).

193. Atanasov, V., Atanasova, P. P., Vockenroth, I. K., Knorr, N. & Koper, I. A molecular toolkit for highly insulating tethered bilayer lipid membranes on various substrates. *Bioconjugate Chem*. **17**, 631-637 (2006).

194. Tien, H. T. *Bilayer Lipid Membranes (BLM): Theory and Practice. The Quarterly Review of Biology* (Elsevier, Amsterdam 1976).

195. Woodhouse, G. E., King, L. G., Wieczorek, L. & Cornell, B. A. Kinetics of the competitive response of receptors immobilized to ion-channels which have been incorporated into a tethered bilayer. *Faraday Discuss*. **111**, 247-258 (1998).

196. Schmidt, E. K. et al. Incorporation of the acetylcholine receptor dimer from Torpedo californica in a peptide supported lipid membrane investigated by surface plasmon and fluorescence spectroscopy. *Biosensors & Bioelectronics* **13**, 585-591 (1998).

197. Horrigan, F. T. & Aldrich, R. W. Coupling between voltage sensor activation, Ca2+ binding and channel opening in large conductance (BK) potassium channels. *J. Gen. Physiol.* **120**, 267-305 (2002).

198. Magleby, K. L. Gating mechanism of BK (Slo1) channels: so near, yet so far. *J Gen Physiol.* **121**, 81-96 (2003).

199. Braha, O. et al. Designed protein pores as components for biosensors. *Chem Biol.* **7**, 497-505 (1997).

200. Pérez, G., Lagrutta, A., Adelman, J. P. & Toro, L. Reconstitution of expressed BKCa channels from Xenopus oocytes to lipid bilayers. *Biophys. J.* **66**, 1022-1027 (1994).

201. Fenwick, E. M., Marty, A. & Neher, E. Sodium and calcium channels in bovine chromaffin cells. *J. Physiol. (Lond.)* **331**, 599-635 (1982).

202. Liu, A. L. *Advances in Planar Lipid Bilayers and Liposomes* (Elsevier, London, 2006).

203. Hanner, M. et al. The beta subunit of the high conductance calcium-activated potassium channel. Identification of residues involved in charybdotoxin block. *J. Biol. Chem.* **273**, 16289-16296 (1998).

204. Yellen, G. Ionic permeation and blockade in calcium-activated K+ channels of bovine chromaffin cells. *J. Gen. Physiol.* **84**, 157-186 (1984).

205. Stanfield, P. R. Tetraethylammonium ions and the potassium permeability of excitable cells. *Rev. Physiol. Biochem. Pharmacol.* **97**, 1-67 (1983).

206. Mackinnon, R. & Yellen, G. Mutations affecting TEA blockade and ion permeation in voltage-activated K+ channels. *Science (Washington D.C.)* **250**, 276-279 (1990).

207. Naumann, R. et al. Tethered lipid bilayer on ultraflat gold surface. *Langmuir* **19**, 5435-5443 (2003).

208. Taglialatela, M. et al. Patterns of internal and external tetraethylammonium block in four homologous K+ channels. *Molecular Pharmacology* **40**, 299-307 (1991).

209. Garcia-Calvo, M. et al. Purification and reconstitution of the high-conductance, calcium-activated potassium channel from tracheal smooth muscle. *Journal of Biological Chemistry* **269**, 676-682 (1994).

210. Hase, C. C., Alexander C. Le Dain & Martinac, B. Purification and Functional Reconstitution of the Recombinant Large Mechanosensitive Ion Channel (MscL) of Escherichia coli. *J. Biol. Chem.* **270**, 18329-18334 (1995).

211. Stroud, R., McCarthy, M. & Shuster, M. Nicotinic acetylcholine receptor superfamily of ligand-gated ion channels. *Biochemistry* **29**, 11009-11023 (1990).

212. Blount, P., Sukharev, S. I., Schroeder, M. J., Nagle, S. K. & Kung, C. Single residue substitutions that change the gating properties of a mechanosensitive channel in Escherichia coli. *Proceedings of the National Academy of Sciences of the United States of America* **93**, 11652-11657 (1996).

213. Chang, G., Spencer, R. H., Lee, A. T., Barclay, M. T. & Rees, D. C. (1998) Structure of the MscL homolog from Mycobacterium tuberculosis: A gated mechanosensitive ion channel. *Science* **282**, 2220-2226. (1998).

214. Montal, M. O., Iwamoto, T., Tomich, J. & Montal, M. Design, synthesis and functional characterization of a pentameric channel protein that mimics the presumed pore structure of the nicotinic cholinergic receptor. *Federation of European Biochemical Societies* **320**, 261-266 (1993).

215. Goennenwein, S., Tanaka, M., Hu, B., Moroder, L. & Sackmann, E. Functional Incorporation of Integrins into Solid Supported Membranes on Ultrathin Films of Cellulose: Impact on Adhesion. *Biophys. J.* **85**, 646-655 (2003).

216. Matsuno, Y., Osono, C., Hirano, A. & Sugawara, M. Single-Channel Recordings of Gramicidin at Agarose-Supported Bilayer lipid Membranes formed by the Tip-Dip and Painting Method. *Analytical Sciences* **20**, 1217-1221 (2004).

217. Hianik, T., Passechnik, V. I., Paltauf, F. & Hermetter, A. Nonlinearity of current-voltage characteristics of the gramicidin channel and structure of the gramicidin molecule. *Bioelectrochem.Bioenerg.* **34**, 61-68 (1994).

218. Koeppe, R. E. & Andersen, O. A. Engineering the Gramicidin Channel. *Annu. Rev. Biophys. Biomol. Struct.* **25**, 231-258 (1996).

219. Hamill, P. O. & Martinac, B. Molecular basis of mechanotransduction in living cells. *Physiological Reviews* **81**, 685-740 (2001).

220. Blount, P., Shroeder, M. J. & Kung, C. Mutations in MscL, a bacterial mechanosensitive channel, can change the cellular response to osmotic stress. *Biophysical Journal* **74**, A239-a239 (1998).

221. Blount, P., Sukharev, S. I., Moe, P. C., Nagle, S. K. & Kung, C. Towards an understanding of the structural and functional properties of MscL, a mechanosensitive channel in bacteria. *Biology of the Cell* **87**, 1-8 (1996).

222. Cruickshank, C. C., Minchin, R. F., LeDain, A. C. & Martinac, B. Estimation of the pore size of the large-conductance mechanosensitive ion channel of Escherichia coli. *Biophysical Journal* **73**, 1925-1931 (1997).

223. Kung, C. & Blount, P. Channels in microbes: so many holes to fill. *Molecular Microbiology* **53**, 373-380 (2004).

224. Martinac, B., Buechner, M., Delcour, A. H., Adler, J. & Kung, C. Pressure-Sensitive Ion Channel in Escherichia-Coli. *Proceedings of the National Academy of Sciences of the United States of America* **84**, 2297-2301 (1987).

225. Bartlett, J. L., Levin, G. & Blount, P. An in vivo assay identifies changes in residue accessibility on mechanosensitive channel gating. *Proceedings of the National Academy of Sciences of the United States of America* **101**, 10161-10165 (2004).

226. Iscla, I., Levin, G., Wray, R., Reynolds, R. & Blount, P. Defining the physical gate of a mechanosensitive channel, MscL, by engineering metal-binding sites. *Biophysical Journal* **87**, 3172-3180 (2004).

227. Levin, G. & Blount, P. Cysteine scanning of MscL transmembrane domains reveals residues critical for mechanosensitive channel gating. *Biophysical Journal* **86**, 2862-2870 (2004).

228. Ou, X. R., Blount, P., Hoffman, R. J. & Kung, C. One face of a transmembrane helix is crucial in mechanosensitive channel gating. *Proceedings of the National Academy of Sciences of the United States of America* **95**, 11471-11475 (1998).

229. Blount, P. & Moe, P. C. Bacterial mechanosensitive channels: integrating physiology, structure and function. *Trends in Microbiology* **7**, 420-424 (1999).

230. Todorov, A., Petrov, A. G. & Fendler, J. H. Flexoelectricity of charged and dipolar bilayer lipid membranes studied by stroboscopic interferometry. *Langmuir* **10**, 2344-2350 (1994).

231. Needham, D. & Hochmuth, R. M. Electro-Mechanical Permeabilization of Lipid Vesicles - Role of Membrane Tension and Compressibility. *Biophysical Journal* **55**, 1001-1009 (1989).

232. Nauman, C. A. et al. The polymer-supported phospholipid bilayer: tethering as a new approach to substrate-membrane stabilization. *Biomacromolecules* **3**, 27-35 (2002).

233. Schiller, S. M., Naumann, R., Lovejoy, K., Kunz, H. & Knoll, W. Archaea Analogue Thiolipids for Tethered Bilayer Lipid Membranes on Ultrasmooth Gold Surfaces. *Angewandte Chemie International Edition* **42**, 208-211 (2003).

234. Knoll, W., Koper, I., Naumann, R., Schiller, S. & Duran, R. S. Functional tethered bimolecular lipid membranes. Abstracts of Papers of the American Chemical Society 227, U853-U853 (2004).

235. Breffa, C. *Chemistry 150* (Max Planck Institut fur Polymerforschung and Johannes Gutenberg Universitat Mainz, Geboren, 2005).

236. He, L. et al. Tethered Bilayer Lipid Membranes Based on Monolayers of Thiolipids Mixed with a Complementary Dilution Molecule. 1. Incorporation of Channel Peptides. *Langmuir* **21**, 11666-11672 (2005).

BIOGRAPHICAL SKETCH

George Okeyo was born in Nairobi, Kenya. He graduated from the University of Nairobi in November 1998 with his B.S. degree having majored in chemistry with a minor in botany. He then worked as a pharmaceutical representative and later as Regional sales manager for Bristol-Myers Squibb in Western Kenya. He proceeded on to graduate school enrolling in the chemistry graduate program at the University of Florida in January 2005, working under the direction of Dr. Randolph Duran. He later worked under the direction of Dr. Gail Fanucci.